



UNIVERSITY OF  
BIRMINGHAM

**PARTICLE MATTER EMISSION CONTROL AND RELATED  
ISSUES FOR DIESEL ENGINES**

by

**Jun Zhang**

**A thesis submitted to  
The University of Birmingham  
for the degree of  
DOCTOR OF PHILOSOPHY**

**School of Mechanical Engineering  
The University of Birmingham  
November 2010**

**UNIVERSITY OF  
BIRMINGHAM**

**University of Birmingham Research Archive**

**e-theses repository**

This unpublished thesis/dissertation is copyright of the author and/or third parties. The intellectual property rights of the author or third parties in respect of this work are as defined by The Copyright Designs and Patents Act 1988 or as modified by any successor legislation.

Any use made of information contained in this thesis/dissertation must be in accordance with that legislation and must be properly acknowledged. Further distribution or reproduction in any format is prohibited without the permission of the copyright holder.

## **ABSTRACT**

The particulate matter is probably one of the most critical issues of the diesel engine emissions. After years of research, people begin to understand it further, with respect to its impact on the environment and human health, its formation mechanism inside and outside the diesel engine, and most importantly, the methods to control its formation.

This study has focused on the particulate matter emission control in diesel engines. It started with the application of two closely coupled Diesel Particle Filters (DPFs), consisting of an assistant DPF and a main standard honeycomb DPF, to replace the standard Diesel Oxidation Catalyst (DOC) + DPF system, commonly applied on diesel engines these days. This new after-treatment system showed a great potential to be adopted in the future, not only for the tighter emission regulations but also for the great cost reduction of the total after-treatment system by the reduction of the main DPF's size and weight and more options of other cheaper materials. The back pressure problem revealed in the experiment was then studied through a one dimensional model simulation and its influence to the engine performance was discussed.

Fuel injection parameters which are related with the engine performance and emissions were also investigated in the study. After careful calibrations, a single injection induced Partially Charge Compression Ignition (PCCI) combustion was achieved, in which mode, NO<sub>x</sub> and smoke emissions were reduced by more than 80% compared with using the normal multiple injections.

Following that, the non-volatile particulate emissions under the pilot injection's impacts were studied and the key parameters of the pilot control such as fuel quantity and

injection timing were examined. The particulate number concentrations and size distributions were investigated under different engine operation conditions and the results illustrated how a pilot injection alongside a main injection could influence particulates and what these effects were closely related to.

The research continued with the investigation of bio-fuels on the particle emission reduction, when 10% alternative diesel fuel blends (Rapeseed Methyl Ester (RME) and Gas-to-Liquid (GTL)) were used. They indicated that without any modification to the engine, adding selected alternative fuels, even at a low percentage, could result in a noticeable reduction of the particle numbers, both in the total and the non-volatile parts; however, the number of nucleation mode particles could increase in certain cases. It was also revealed that the engine suffered very high numbers of the nucleation mode particulates during warming up.

## **ACKNOWLEDGEMENTS**

I would like to thank my supervisor Professor Hongming Xu for his guidance and encouragement throughout all my study. I thank my associate supervisor Professor Miroslaw Lech Wyszynski and also Dr Athanasios Tsolakis for their helpful suggestions.

I would also like to express my gratitude to Thomas Gardiner from Jaguar Land Rover (JLR) for his technical support towards the research project, Sathaporn Chupeng for his kind help during my first year of study, Haiwen Song and Phil Price from Ford Motor Company Limited and Roger Cracknell from Shell Global Solutions UK for their technical advice.

I acknowledge Dr Guohong Tian, Dr Mingshan Wei, and Dr Shaohua Zhong for their great help during my study, Dr Rizalman Mamat for his valuable discussions during my Wave model development, Dr Hanshan Dong from the Department of Materials and Metallurgy for his kind supply of the furnace for the DPF regeneration.

A special thank goes to my friends and colleagues in the FPS group: Yanfei Li, Haiying Li, Fan Zhang, He Ma, Xuesong Wu, Paul Rounce, Ritchie Daniel, Nik Rosli Abdullah for their great support to my study as well as my social life.

*I wish to dedicate this thesis  
to my families and friends  
for their love and great supports along the way*

## TABLE OF CONTENTS

<b>CHAPTER 1 INTRODUCTION.....</b>	<b>26</b>
1.1    Background.....	26
1.1.1    Diesel Engine Combustion.....	27
1.1.2    Diesel Engine Emissions.....	27
1.1.3    Overview of the Diesel Engine Emission Regulation and Controls..	29
1.1.4    The Diesel Engine After-treatment System .....	31
1.1.5    New Fuels and Their Blends .....	32
1.1.6    New Fuel Injection and Combustion Strategies .....	33
1.2    Objectives and Approaches.....	34
1.3    Thesis Outline.....	34
<b>CHAPTER 2 LITERATURE REVIEW.....</b>	<b>36</b>
2.1    Engine Emission Toxicity and Regulations .....	36
2.1.1    The Toxicity of the Engine Emissions .....	37
2.1.2    Global Automotive Emission Regulations.....	38
2.2    Particulates.....	39
2.2.1    The Mechanism of Engine Particulate Formation .....	41
2.2.2    Particulate Measurement .....	43
2.2.3    Diesel Engine Particulates .....	45
2.3    Diesel Particulate Filter (DPF).....	47
2.3.1    DPF Regeneration .....	48
2.3.2    New DPF Configuration and Materials .....	49
2.4    New Injection Strategies for Diesel Engines .....	51

2.4.1	Multiple Injection Strategies .....	52
2.4.2	Exhaust Gas Recirculation (EGR).....	53
2.4.3	LTC, HCCI and PCCI Combustion.....	54
2.5	Alternative Fuels for Diesel Engines .....	56
2.5.1	Biodiesel .....	56
2.5.2	Gas to Liquid (GTL) Diesel .....	59
2.5.3	Combined Alternative Fuels with New Injection Strategies .....	61
2.6	Summary.....	62
<b>CHAPTER 3</b>	<b>RESEARCH METHODOLOGY.....</b>	<b>63</b>
3.1	Engine and Instrumentation.....	64
3.1.1	Engine.....	64
3.1.2	Engine Start and Control System .....	65
3.1.3	Dynamometer.....	68
3.1.4	Dynamometer Control System .....	70
3.1.5	In-cylinder Pressure Data Acquisition .....	74
3.1.6	Temperature and Pressure Measurement .....	77
3.1.7	The Fuel and the Fuelling System .....	79
3.1.8	Cooling System .....	80
3.2	Exhaust Measurement.....	81
3.2.1	Engine Exhaust Gas Emissions .....	81
3.2.2	Engine Smoke Emissions .....	82
3.2.3	Engine Emission Particulate Number Size Distribution .....	83
3.2.4	Diluter .....	85
3.2.5	Scanning Electron Microscope (SEM).....	87

3.3	DPF Regeneration.....	88
3.3.1	Furnace .....	88
3.3.2	Arvin Meritor Vaporizer .....	88
3.4	One Dimensional Engine Model .....	90
3.4.1	Woschini Model .....	90
3.4.2	Diesel Wiebe Model .....	92
3.5	Experimental Data Uncertainties Analysis .....	94
3.6	Summary.....	95

<b>CHAPTER 4</b>	<b>APPLICATION OF TWO CLOSELY COUPLED DPFS AS THE DIESEL ENGINE AFTER-TREATMENT SYSTEM .....</b>	<b>96</b>
4.1	Problems and Possible Solutions to the Current After-treatment System....	96
4.1.1	Cost and Installation.....	97
4.1.2	Concept of Solutions to the Problems .....	98
4.1.3	Research objective.....	98
4.2	Engine Test Modes and Procedures.....	98
4.3	Pressure Drop along the Two Different After-treatment Systems.....	101
4.3.1	Transient test A.....	101
4.3.2	Transient test B.....	104
4.3.3	Steady State Test.....	106
4.4	Emissions along the Two Different After-treatment Systems.....	107
4.4.1	Gaseous Emissions.....	107
4.4.2	Smoke Emissions.....	108
4.4.3	PM Characteristics.....	109
4.5	Impact of the Exhaust Back Pressure on the Engine Performance .....	112

4.5.1	One Dimensional Diesel Engine Model Set up .....	112
4.5.2	Model Validation.....	115
4.5.3	Model Application.....	116
4.6	Summary.....	119
<b>CHAPTER 5</b>	<b>PM CHARACTERISTICS WITH SINGLE INJECTIONS.....</b>	<b>122</b>
5.1	Fuel Injection Impact on the Engine Performance and Emissions.....	122
5.1.1	Fuel Injection Parameters.....	123
5.1.2	Engine Test Modes.....	124
5.1.3	Main Injection Timing.....	124
5.1.4	EGR.....	127
5.1.5	Injection Pressure.....	129
5.2	Single Injections VS Multiple Injections.....	131
5.3	PCCI Combustion with Single Injections .....	137
5.4	Summary .....	142
<b>CHAPTER 6</b>	<b>PM CHARACTERISTICS WITH PILOT INJECTIONS.....</b>	<b>144</b>
6.1	Multiple Injections.....	144
6.1.1	Pilot Injection .....	145
6.1.2	Research Objective .....	146
6.2	Engine Test Modes and Procedures .....	146
6.3	Effects of Pilot Injections on PM Emissions .....	148
6.3.1	Effect of Pilot Fuel Quantity .....	148
6.3.2	Effect of Pilot Injection Timing .....	155
6.3.3	Restrictions of the Pilot Injection Parameters .....	161

6.4	Summary .....	163
<b>CHAPTER 7 PM CHARACTERISTICS WITH ALTERNATIVE FUEL BLENDS165</b>		
7.1	Biodiesel and GTL Diesel Blends.....	165
7.1.1	Benefits and Blending Ratio.....	165
7.1.2	Research Objective.....	167
7.2	Engine Test Modes and Procedures.....	167
7.3	PM Number and Size Distribution from Diesel, RME10 and GTL10.....	169
7.3.1	PM Number Concentration .....	169
7.3.2	PM Mean Diameter .....	170
7.3.3	PM Size and Distribution .....	171
7.3.4	Non-volatile Particulates .....	175
7.3.5	In-cylinder Pressure and Heat Release.....	177
7.4	PM Mass and Morphology from Diesel, RME10 and GTL10.....	180
7.4.1	PM Mass.....	180
7.4.2	PM Morphology .....	181
7.5	Non-volatile PM Characteristics during Warm-up from a Cold Start.....	183
7.5.1	Number Weighted Size Distribution .....	184
7.5.2	Surface Area Weighted Size Distribution .....	185
7.5.3	Mass Weighted Size Distribution .....	186
7.6	Gaseous Emissions from Diesel, RME10 and GTL10.....	186
7.6.1	Emissions of NO <sub>x</sub> .....	186
7.6.2	Emissions of THC and CO .....	188
7.6.3	Emissions of CO <sub>2</sub> .....	189
7.7	Discussion and Summary.....	190

7.7.1	The Reliability of Thermo Dilution .....	190
7.7.2	Summary .....	191
<b>CHAPTER 8</b>	<b>CONCLUSIONS AND FUTURE WORK</b> .....	<b>193</b>
8.1	Conclusion Remarks.....	193
8.1.1	The After-treatment system.....	193
8.1.2	Single Injections .....	194
8.1.3	Multiple Injections .....	194
8.1.4	Alternative Fuels .....	194
8.2	Future Work.....	195
8.2.1	DPF on Particulate Trapping under Transient Mode .....	195
8.2.2	One Dimensional Emission Model .....	195
8.2.3	PCCI and HCCI .....	196
8.2.4	Portion of Alternative and Engine Map Optimisation for Biodiesel Blends .....	196
8.2.5	Particulate measurement .....	196
8.2.6	Particulate Chemical Composition .....	197
<b>APPENDIX A. RESEARCH METHODOLOGY</b> .....	<b>198</b>	
<b>APPENDIX B. APPLICATION OF TWO CLOSELY COUPLED DPFS AS THE DIESEL ENGINE AFTERTREATMENT SYSTEM</b> .....	<b>203</b>	
<b>APPENDIX C. PM CHARACTERISTICS WITH PILOT INJECTIONS</b> .....	<b>205</b>	
<b>LIST OF REFERENCES</b> .....	<b>207</b>	

## LIST OF ABBREVIATIONS

ADPF	Assistant diesel particulate filter
AI	Analogue input
bsfc	Brake specific fuel consumption
BMEP	Brake mean effective pressure
BTDC	Before top dead center
BTL	Biomass to liquid
C <sub>1</sub>	Dimensionless quantity
CA	Crank angle
CAN	Control area network
CF	Calibration factor
CI	Compression ignition
CLD	Chemiluminescence
CO	Carbon monoxide
CO <sub>2</sub>	Carbon dioxide
CPC	Condensation particle counter
CVS	Constant volume sampling
d*	Kelvin diameter
DAQ	Data acquisition
DC	Direct current
DI	Direct injection
DMA	Differential mobility analyser
DMS	Differential mobility spectrometer
DOC	Diesel oxidation catalyst
DR	Dilution ratio
DPF	Diesel particulate filter
EC	Electrostatic classifier
ECU	Electronic control unit
EEPS	Engine exhaust particle sizer
EGR	Exhaust gas recirculation
ELPI	Electrical low pressure impactor
EPA	Environment protection agency
EPAct	Energy policy act
FID	Flame ionization detection
FS	Full scale
FSN	Filter smoke number
GTL	Gas to liquid
H <sub>2</sub>	Hydrogen
HC	Hydrocarbon
HCCI	Homogeneous charge compression ignition
HR	Heat release
HRR	Heat release rate
LD	Light duty
LIVC	Late intake valve closing
LNT	Lean NO <sub>x</sub> trap

LTC	Low temperature combustion
M	Molecular weight
MPD	Magneto-pneumatic detection
MVEG	Motor vehicle emission group – 11 second variation to European Driving cycle
N	Atomic nitrogen
N <sub>2</sub>	Molecular nitrogen
N <sub>2</sub> O	Nitrogen dioxide
NDIR	Non-dispersive infrared
NI	National instrument
NO	Nitric oxide
NO <sub>2</sub>	Nitrogen dioxide
NO <sub>x</sub>	Nitrogen oxides
O <sub>2</sub>	Oxygen
OC	Organic carbon
OH	Hydroxyl
p	Instantaneous cylinder pressure
PAH	Polycyclic aromatic hydrocarbon
PB	Paper blackening
PCCI/PCI	Partially charge compression ignition
Pd	Palladium
p <sub>f</sub>	Premixed fuel fraction
PM	Particulate matter
P <sub>max</sub>	Maximum in-cylinder pressure
PMP	Particulate measurement programme
PN	Particle number
ppm	Part per million
P <sub>r</sub>	Reference pressure
PRT	Platinum resistance thermometer
p <sub>s</sub>	Saturation vapor pressure at a given temperature
Pt	Platinum
Q	Heat flow
R	Universal gas constant
RME	Rapeseed methyl ester
SCR	Selective catalytic reduction
SEM	Scanning electron microscope
SI	Spark ignition
SiC	Silicon carbide
SOI	Start of injection
SOF	Soluble organic fraction
T	Absolute temperature
T <sub>c</sub> <sup>0</sup>	Initial cylinder temperature
T <sub>c</sub> <sup>n</sup>	Current cylinder temperature
THC	Total hydrocarbon
TDC	Top dead centre
T <sub>r</sub>	Reference temperature
ULSD	Ultra-low sulfur diesel
USB	Universal serial bus

$V$	Instantaneous volume of the engine cylinder
$V_c$	Clearance volume
$V_d$	Displacement
VGT	Variable geometry turbocharger
$V_m$	Mean piston speed
VOF	Volatile organic fraction
$V_r$	Reference volume
$V_s$	Swirl velocity
$W$	Accumulative mass fraction burned
$\sigma$	Surface tension
$\rho$	Density
$\gamma$	Ratio of specific heats
$\Delta\theta$	Time step size in degrees
$\Delta\theta_{\text{delay}}$	Ignition delay
$\theta_0$	Beginning of the ignition delay interval
$\theta_b$	Start of combustion
$\Phi$	Equivalence ratio

## LIST OF FIGURE ILLUSTRATIONS

<b>Figure 1.1</b> Typical diesel engine combustion heat release (Heywood 1988).....	27
<b>Figure 2.1</b> Typical particle size and distribution from combustion engines (Kittelson 1997).....	40
<b>Figure 2.2</b> Schematic view of flow pattern through a channel of a wall flow DPF, showing pressure loss components (Konstandopoulos et al. 2001).....	47
<b>Figure 2.3</b> Common rail system (Denso Australia 2010) .....	51
<b>Figure 2.4</b> Concepts of PCCI (PCI) and HCCI combustion (Okude et al. 2004) .....	55
<b>Figure 2.5</b> Schematic of biodiesel production path (Alternative Fuels & Advanced Vehicle Data Center 2010).....	57
<b>Figure 2.6</b> Biodiesel Supply and Consumption (US Energy Information Administration 2009).....	58
<b>Figure 2.7</b> The EU biodiesel industry (European Biodiesel Board 2010) .....	58
<b>Figure 2.8</b> GTL process using the Fischer Tropsch method (Dexcel 2008) .....	60
<b>Figure 3.1</b> The Ford Puma diesel engine test cell.....	63
<b>Figure 3.2</b> Engine characteristics graph.....	65
<b>Figure 3.3</b> Engine's starting system.....	65
<b>Figure 3.4</b> How the control system works with ECU files.....	66
<b>Figure 3.5</b> The interface of the ATI engine control system.....	67
<b>Figure 3.6</b> Overall dynamometer dimensions (mm) .....	68
<b>Figure 3.7</b> Dynamometer power curve (mm) .....	69
<b>Figure 3.8</b> NDE Clarke drive shaft.....	69

<b>Figure 3.9</b> (a) The dimension of the adaptor for the dynamometer end; (b) the dimension of the adaptor for the dynamometer end.....	70
<b>Figure 3.10</b> The CADET system.....	71
<b>Figure 3.11</b> The sketch of the throttle actuator (supplied by CP Engineering) .....	72
<b>Figure 3.12</b> Control unit LSG 2000.....	72
<b>Figure 3.13</b> (a) actuator (b) actuator control.....	73
<b>Figure 3.14</b> (a) Kistler pressure sensor (b) Charge amplifier.....	74
<b>Figure 3.15</b> Pressure measurement of the charge amplifier with/without drift compensation.....	75
<b>Figure 3.16</b> Layout of the engine test system.....	78
<b>Figure 3.17</b> Schematic Diagram of the EC.....	84
<b>Figure 3.18</b> Thermo Dilution (Kasper 2004) .....	87
<b>Figure 3.19</b> The ZS-ArM vaporizer system.....	88
<b>Figure 3.20</b> The ECU.....	89
<b>Figure 3.21</b> Diesel Wiebe function in WaveBuild.....	92
<b>Figure 4.1</b> DPF weight gaining with ADPF and DOC.....	101
<b>Figure 4.2</b> DPF pressure drop (a) for one test (18 hours), (b) details under three engine cycles.....	102
<b>Figure 4.3</b> ADPF/DOC pressure drop.....	103
<b>Figure 4.4</b> Transient Test B test result.....	104
<b>Figure 4.5</b> DPF pressure drop when coupled with APDF and DOC.....	104
<b>Figure 4.6</b> ADPF/DOC pressure drops (a) for one test (6 hours), (b) details under eight mode cycles.....	105

<b>Figure 4.7</b> Pressure drop of ADPF and DOC over varied engine torque (speed 2000 rpm, torque 5 Nm/15 Nm/60 Nm/90 Nm/150 Nm/200 Nm) .....	106
<b>Figure 4.8</b> Pressure drops of DOC, SC and DPF for each engine mode.....	107
<b>Figure 4.9</b> (a) Engine gas emissions of CO, NOx and THC (b) gaseous emission reduction efficiencies of ADPF and DOC for each engine mode (ppm = part per million).....	107
<b>Figure 4.10</b> 3-D map for engine speed, load and smoke level for each mode.....	108
<b>Figure 4.11</b> (a) Smoke level of the engine modes; (b) Smoke reduction efficiencies of ADPF and DOC for each engine mode.....	109
<b>Figure 4.12</b> (a) Particle total concentration along the after-treatment system (1200 rpm,30 Nm); (b) particle total concentration along the after-treatment system (1200 rpm, 60 Nm).....	110
<b>Figure 4.13</b> (a) Particle mean diameter along the after-treatment system (1200 rpm, 30 Nm); (b) particle mean diameter along the after-treatment system (1200 rpm, 60 Nm) ...	110
<b>Figure 4.14</b> Particle size and distribution (a) along the DOC+DPF system (1200 rpm, 30 Nm); (b) along the ADPF+DPF system (1200 rpm, 30 Nm); (c) along the DOC+DPF system (1200 rpm, 60 Nm); (d) along the ADPF+DPF system (1200 rpm, 60 Nm).111	
<b>Figure 4.15</b> WaveBuild of the I4 diesel engine.....	113
<b>Figure 4.16</b> Engine general panel in WaveBuild.....	114
<b>Figure 4.17</b> Experimental and simulated (a) air flow, (b) torque, (c) power, (d) sfc. (blue curve=experiment, red curve=simulation) .....	115
<b>Figure 4.18</b> WaveBuild of the I4 diesel engine with back pressure simulation.....	116
<b>Figure 4.19</b> Experimental and simulated (a) air flow, (b) torque, (c) power, (d) sfc. ( blue curve=experiment, red curve=simulation) .....	117

<b>Figure 4.20</b> Simulation of engine performance with increased DPF clog (c) exhaust pressure and temperature, (b) air flow and boost, (c) brake torque and power, (d) bsfc.....	118
<b>Figure 5.1</b> (a) In-cylinder pressure and heat release (CAD= crank angle degree) (b) ignition delay (c) Pmax with different main SOIs.....	125
<b>Figure 5.2</b> Smoke and NOx trade-off using different main SOI.....	126
<b>Figure 5.3</b> (a) CO and THC emissions (b) CO <sub>2</sub> /O <sub>2</sub> trade-off using different main SOI.....	127
<b>Figure 5.4</b> (a) In-cylinder pressure and heat release (b) ignition delay (c) Pmax with different EGR.....	128
<b>Figure 5.5</b> Smoke and NOx trade-off using different EGR.....	129
<b>Figure 5.6</b> (a) CO and THC emissions (b) CO <sub>2</sub> /O <sub>2</sub> trade-off using different EGR.....	129
<b>Figure 5.7</b> (a) In-cylinder pressure and heat release (b) ignition delay (c) Pmax with different injection pressures.....	130
<b>Figure 5.8</b> Smoke and NOx trade-off using different injection pressure.....	130
<b>Figure 5.9</b> (a) CO and THC emissions (b) CO <sub>2</sub> /O <sub>2</sub> trade-off using different injection pressure.....	131
<b>Figure 5.10</b> In-cylinder pressure and heat release with single and multiple injections (a) idle mode (b) medium mode (c) high mode.....	132
<b>Figure 5.11</b> (a) P <sub>rate</sub> ; (b) smoke and NOx emissions with and without pilot injection.....	133
<b>Figure 5.12</b> The total particle number and mean diameter with single and multiple injection: (a) total particle concentration; (b) particle mean diameter.....	134
<b>Figure 5.13</b> Particle size and distribution with single and multiple injection (a) idle mode (800 rpm, 0.68 bar BMEP); (b) medium speed/load mode (1800 rpm, 5.2 bar BMEP); (c) high speed/load mode (2500 rpm, 7.0 bar BMEP) .....	135
<b>Figure 5.14</b> Gaseous emissions with single and multiple injections: (a) THC, (b) CO.....	136

<b>Figure 5.15</b> (a) Smoke and NO <sub>x</sub> emissions (b) particulate concentration (c) particle mean diameter of the engine modes.....	138
<b>Figure 5.16</b> Particle size distribution of the base mode, Mode 2, Mode 5 and Mode 8.....	139
<b>Figure 5.17</b> (a) In-cylinder pressure, heat release and fuel injection time (b) combustion duration of the base mode, Mode 2 and Mode 8.....	140
<b>Figure 5.18</b> (a) Ignition delay and fuel mixing time after the injection finished (b) P <sub>max</sub> and P <sub>rate</sub> of the base mode, Mode 2 and Mode 8.....	140
<b>Figure 5.19</b> (a) CO and THC emissions (b) CO <sub>2</sub> /O <sub>2</sub> trade-off of the single injection PCCI test.....	141
<b>Figure 6.1</b> Sketch of a typical injection.....	145
<b>Figure 6.2</b> HRR premix: index of the heat release during the premixed combustion.....	147
<b>Figure 6.3</b> In-cylinder pressure and heat release with different pilot fuel quantity (a) Mode 1 (b) Mode 2 (c) Mode 3.....	149
<b>Figure 6.4</b> Total particulate numbers with different pilot fuel quantities (base mode) .....	150
<b>Figure 6.5</b> (a) Premixed-controlled main combustion duration and heat release (base mode); (b) Prate under different pilot fuel quantities.....	151
<b>Figure 6.6</b> (a) AHR <sub>50</sub> (b) EOC and main SOC under different pilot fuel quantities.....	151
<b>Figure 6.7</b> Total particulate numbers with different pilot fuel quantities (base mode) .....	152
<b>Figure 6.8</b> Mean particulate diameters with different pilot fuel quantities (base mode) .....	152
<b>Figure 6.9</b> Particulate size distributions with different pilot fuel quantities (base mode) ...	153
<b>Figure 6.10</b> Nucleation mode particles (a) concentration, (b) mean diameter with different pilot fuel quantities (base mode) .....	154

<b>Figure 6.11</b> Accumulation mode particle (a) concentration, (b) mean diameter with different pilot fuel quantities (base mode) .....	155
<b>Figure 6.12</b> In-cylinder pressure and heat release with different pilot injection timing (1.5 mm <sup>3</sup> /stroke) (a) Mode 1 (b) Mode 2 (c) Mode 3.....	156
<b>Figure 6.13</b> (a) Premixed-controlled main combustion duration and heat release (base mode); (b) P <sub>rate</sub> under different pilot fuel injection timing.....	157
<b>Figure 6.14</b> (a) AHR <sub>50</sub> (b) EOC and main SOC under different pilot fuel injection timing..	157
<b>Figure 6.15</b> Total particulate numbers with different pilot fuel injection timings (1.5 mm <sup>3</sup> /stroke).....	158
<b>Figure 6.16</b> Particulate mean diameter with different pilot fuel injection timings (1.5 mm <sup>3</sup> /stroke).....	158
<b>Figure 6.17</b> Particulate size distributions with different pilot fuel injection timings (1.5 mm <sup>3</sup> /stroke) .....	159
<b>Figure 6.18</b> Nucleation mode particles (a) concentration, (b) mean diameter with different pilot fuel injection timings (1.5 mm <sup>3</sup> /stroke).....	160
<b>Figure 6.19</b> Accumulation mode particles (a) concentration, (b) mean diameter with different pilot fuel injection timings (1.5 mm <sup>3</sup> /stroke) .....	161
<b>Figure 6.20</b> Total particulate numbers with different pilot fuel quantity and injection timings (a) Mode 1 (b) Mode 2 (c) Mode 3.....	162
<b>Figure 6.21</b> (a) Heat release and (b) total concentration of Mode 1 with 3 mm <sup>3</sup> /stroke pilot injection at 29 °BTDC.....	163
<b>Figure 7.1</b> Exhaust particulate number concentrations (total) .....	169
<b>Figure 7.2</b> Particle mean diameter.....	171
<b>Figure 7.3</b> Number weighted particle size distributions at 800 rpm (total) .....	171

<b>Figure 7.4</b> Number weighted size distributions at 1800 rpm (total) .....	172
<b>Figure 7.5</b> Number weighted size distributions at 3100 rpm: (a) Mode 6 (b) Mode 7 (c) Mode 8 (d) load increased from Mode 6 to Mode 8.....	173
<b>Figure 7.6</b> Number weighted size distributions at 1800 rpm with different EGR: (a) EGR valve opening 31% (b) EGR valve opening 15% (c) No EGR (total).....	174
<b>Figure 7.7</b> Exhaust particulate number concentrations (non-volatiles) .....	175
<b>Figure 7.8</b> Non-volatile particle mean diameter.....	176
<b>Figure 7.9</b> Non-volatiles' number weighted particle size distributions at (a) 800 rpm; (b) 1800 rpm; (a) 3100 rpm.....	176
<b>Figure 7.10</b> In-cylinder pressure and heat release for (a) Mode 1 (800 rpm,2.1 Nm); (b) Mode 2 (1800 rpm,30 Nm); (c) Mode 5 (1800 rpm,134 Nm); (d) Mode 6 (3100 rpm,35 Nm).....	177
<b>Figure 7.11</b> (a) Prate (b) exhaust temperature.....	178
<b>Figure 7.12</b> (a) Main start of combustion (SOC) and the end of combustion; (b) AHR <sub>50</sub> ....	179
<b>Figure 7.13</b> Premixed-controlled main combustion duration and heat release.....	180
<b>Figure 7.14</b> (a) FSN (b) NO <sub>x</sub> concentration (c) smoke and NO <sub>x</sub> trade off for different EGR.....	180
<b>Figure 7.15</b> Particle morphology (captured under engine mode of 1800 rpm, 30 Nm): (a) Diesel magnification of 10000; (b) Diesel magnification of 65000; (c) RME 10 magnification of 10000; (d) RME magnification of 65000; (e) GTL10 magnification of 10000; (f) GTL10 magnification of 65000.....	182
<b>Figure 7.16</b> Engine temperatures during the idling warming up.....	183
<b>Figure 7.17</b> Number weighted size distribution during the warming up (non-volatiles).....	184

<b>Figure 7.18</b> Surface area weighted size distribution during the idling warming up (non-volatiles).....	185
<b>Figure 7.19</b> Mass weighted size distribution during the idling warming up (non-volatiles)..	86
<b>Figure 7.20</b> NO <sub>x</sub> emissions.....	187
<b>Figure 7.21</b> NO/NO <sub>x</sub> emissions.....	188
<b>Figure 7.22</b> THC emissions.....	188
<b>Figure 7.23</b> CO emissions.....	188
<b>Figure 7.24</b> CO <sub>2</sub> emissions.....	189
<b>Figure 7.25</b> O <sub>2</sub> emissions.....	189
<b>Figure A1</b> Throttle actuator performance graph.....	198
<b>Figure A2</b> TCK-4 thermocouple amplifier dimension.....	200
<b>Figure A3</b> PCI 6251 pin out.....	201
<b>Figure A4</b> USB 6218 pin out.....	202
<b>Figure A5</b> Thermo-valve piping diagram.....	202
<b>Figure B1</b> Compressor map.....	203
<b>Figure B2</b> Turbine map.....	204

## LIST OF TABLES

<b>Table 1.1</b> European emission standards for diesel light commercial vehicles $\leq 1305 \text{ kg}$ (Category N1 - I), g/km(a).....	30
<b>Table 3.1</b> Engine specifications.....	64
<b>Table 3.2</b> Actuator specification.....	73
<b>Table 3.3</b> Kistler pressure sensor specification.....	74
<b>Table 3.4</b> Shaft encoder specification.....	75
<b>Table 3.5</b> PCI-6251 National Instrument card specification.....	76
<b>Table 3.6</b> USB-6218 National Instrument card specification.....	79
<b>Table 3.7</b> Test fuel properties.....	79
<b>Table 3.8</b> Horiba MEXA-7100 DEGR component specifications.....	81
<b>Table 3.9</b> AVL smoke meter specifications.....	83
<b>Table 3.10</b> Jeol JSM-7000F FE SEM specification.....	87
<b>Table 4.1</b> Engine mode for transient test A.....	99
<b>Table 4.2</b> Engine mode for transient test B .....	100
<b>Table 4.3</b> Engine mode for the steady state test.....	100
<b>Table 4.4</b> Experimental results and the simulation errors.....	116
<b>Table 4.5</b> Experimental results and the simulation errors.....	117
<b>Table 5.1</b> Engine test modes (a) basic mode; (b) injection parameter tests with varied main SOI (green filling), varied EGR (orange filling), varied injection pressure (blue filling) .....	124
<b>Table 5.2</b> Engine test modes for single injections and multiple injections comparison.....	132
<b>Table 5.3</b> Engine test modes for single injection combustion.....	137

<b>Table 6.1</b> Engine test modes: (a) base engine mode calibrated to Euro 4 standard; (b) variations (CA=crank angle).....	148
<b>Table 7.1</b> Engine test modes.....	168
<b>Table A1</b> Throttle actuator specification.....	198
<b>Table A2</b> In-cylinder pressure sensor amplifier specification (5011B10Y50) .....	199
<b>Table A3</b> RS K type thermocouples.....	199
<b>Table A4</b> TCK-4 thermocouple amplifier specification.....	199
<b>Table A5</b> EuroSensor EPT 3100 pressure sensor specification.....	200
<b>Table C1</b> Injection parameter of Mode 1 (1800 rpm, 52 Nm) variations (BTDC = before top dead centre).....	205
<b>Table C2</b> Injection parameter of Mode 2 (1800 rpm, 91 Nm) variations.....	205
<b>Table C3</b> Injection parameter of Mode 3 (2500 rpm, 84 Nm) variations.....	206

## LIST OF PUBLICATIONS

1. Jun Zhang, Hongming Xu, Guohong Tian, Fan Zhang, M. L. Wyszynski, The Univ. of Birmingham; Phil Price, Ford Motor Co. (2010). The Particle Emissions Characteristics of a Light Duty Diesel Engine with 10% Alternative Fuel Blends. **SAE International Journal of Fuels and Lubricant.** 2011 3:438-452. **SAE 2010 Powertrains, Fuels and Lubricants Meeting, Rio de Janeiro, Brazil.**
2. Jun Zhang, Guohong Tian, Hongming Xu, Fan Zhang, Ritchie Daniel, University of Birmingham (2010). The Application of Two Closely Coupled DPFs as the After-treatment System. **SAE 2010 Commercial Vehicle Engineering Congress, Illinois, USA.** **SAE 2010-01-1939**
3. Jun Zhang, Fan Zhang, Guohong Tian, Hongming Xu, Yanfei Li, Ritchie Daniel, University of Birmingham; Haiwen Song, Phil Price, Ford Motor Company, James Gaade, Jaguar Cars Ltd (2010). The Particle Emission Characteristics of a Light Duty Diesel Engine by Using Different Pilot Injections. **SAE 2010 Commercial Vehicle Engineering Congress, Illinois, USA.** **SAE 2010-01-1959**
4. Jun Zhang, Hongming Xu, Guohong Tian, University of Birmingham (2010). The Particle Emission Characteristics of a Light Duty Diesel Engine by Using Different Pilot Injections. **UnICEG, Engine Modelling and Diagnostics, University of Brighton, UK**
5. Jun Zhang (2007), After-treatment for Combustion Engines. **Research Poster Presentation 2007, University of Birmingham, UK.**

6. Shaohua Zhong, Ritchie Daniel, Hongming Xu, Jun Zhang, Dale Turner, Miroslaw L. Wyszynski, University of Birmingham and Paul Richards, Innospec, Incorporated (2010). Combustion and Emissions of 2,5-Dimethylfuran in a Direct-Injection in a Spark-Ignition Engine. **Energy Fuels** **2010**, **24**, 2891–2899, DOI:10.1021/ef901575a
7. Hongming Xu, Jun Zhang, University of Birmingham, Philipp PriceFord Motor Company (2010). Investigation on PM Emissions of a Light Duty Diesel Engine with 10% RME and GTL Blends. **International Particle Meeting, Cambridge University, UK.**
8. Yanfei Li, Guohong Tian, Jun Zhang, Hongming Xu, University of Birmingham (2010). Comparative Experimental Study on Microscopic Spray Atomization Characteristics of RME, GTL and Diesel. **SAE 2010 Powertrains Fuels & Lubricants Meeting, San Diego, USA. SAE 2010-01-2284**
9. Fan Zhang, Hongming Xu, Jun Zhang, Birmingham Univ; Guohong Tian, Univ of Newcastle; Gautam Kalghatgi, Shell Global Solutions UK (2010). Investigation into Dieseline-Fueled Partial Premixed Compression Ignition (PPCI) Using Two-stage Injection Strategies. **Detroit, USA. SAE 2011 World Congress & Exhibition. SAE 2011-01-1411**
10. Jun Zhang, Hongming Xu, University of Birmingham, Phil Price, Ford Motor Company (2010). Non-volatile Particulate Characteristics Influenced by Pilot Injections with EGR. **Submitted to the Journal of Aerosol Science.**

# CHAPTER 1

## INTRODUCTION

The diesel engine is an attractive power unit used widely in many fields, for its great advantages over petrol engines such as lower fuel consumption, lower carbon monoxide emissions, better torque characteristics and higher reliability (Heywood 1988; Stone 1999). However, they are among the main contributors to air pollutions for the large amount of emissions, especially particulates and nitrogen oxides ( $\text{NO}_x$ ) (Heywood 1988). How to control these emissions is one of the most important aspects of modern air quality management.

### 1.1 Background

The first diesel engine dated back to 1892 when Rudolf Diesel invented it with compression ignition. In a typical diesel engine, only air is inducted into the cylinder and the ignition is initiated by injecting a certain amount of fuel directly into the chamber when the air reaches the right temperature and pressure (Heywood 1988). It not only achieves the control of the engine load through the adjustment of the fuel amount, but also eliminates the loss existing in spark ignition engines, where air and fuel are mixed externally and throttled before entering the cylinder. This difference in the initiation of combustion also leads to the emissions from diesel engines differing from those from petrol engines.

### 1.1.1 Diesel Engine Combustion

Typical diesel engine combustion is shown in Figure 1.1 and it can be categorized into four distinct phases: ignition delay, premixed combustion, mixing controlled combustion and late combustion. The liquid fuel injected into the engine cylinder firstly evaporates and mixes with the combustion air. The mixture is compressed by the piston and its pressure and temperature increase until the fuel's ignition point is reached. After this short ignition delay period, the spontaneous ignition starts and initiates the combustion, which raises the in-cylinder pressure to a much higher level. With the combustion processing, it proceeds to a relatively moderate level until it ceases. The burned products along with those unburned are then discharged into the after-treatment system, before being emitted to the atmosphere.

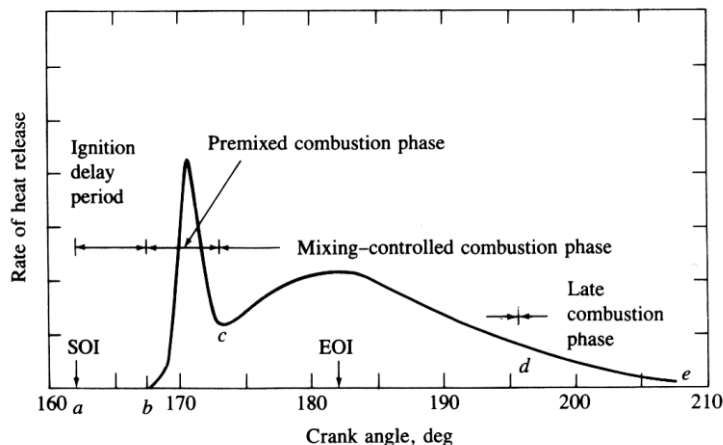


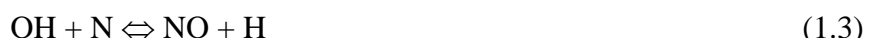
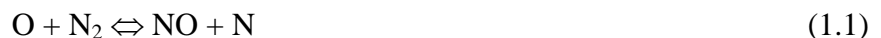
**Figure 1.1** Typical diesel engine combustion heat release (Heywood 1988).

### 1.1.2 Diesel Engine Emissions

The particulates are probably one of the most critical issues of the diesel engine emissions. They are tiny solid or liquid particles and are sometimes referred to as particulate matter (PM) or fine particles (Heywood 1988). Particulates consist of primary particles,

whose diameters are between 20-50 nm and their sizes depend on the numbers of these spherules, which may vary from several to several thousands. Diesel particulates are mainly composed of three parts: soot, soluble organic fraction (SOF) and inorganic fraction. Soot originates from the carbon in the diesel fuels and generates in the combustion environment where the temperature and pressure can reach up to 2800 K and 100 bar. Through the soot's surface growth, agglomeration as well as oxidation at the same time, the particulates form eventually after a final adsorption and condensation of hydrocarbons.

The nitrogen oxides ( $\text{NO}_x$ ) from diesel engines are comparable to those from petrol engines and it is a collection of nitric oxide (NO) and nitrogen dioxide ( $\text{NO}_2$ ). NO is usually produced through the oxidation of atmospheric nitrogen and is the predominant part in  $\text{NO}_x$ . Its formation rate has a great dependence on temperature, which is why high temperature and high oxygen concentrations result in high NO formation. The mechanism is often called the extended Zeldovich mechanism, contributed by Zeldovich and Lavoie (Heywood 1988) as follows,



Generally, the  $\text{NO}_2$  in the diesel engine emissions has a part of 10 %-30 % in the total  $\text{NO}_x$  and it is converted from NO formed in the flame zone as



Unless it is quenched, the  $\text{NO}_2$ 's conversion back to NO is via



Most of the hydrocarbon (HC) results from the incomplete combustion of the fuels and there are several major causes for the diesel engine HC emissions: (1) the fuel-air mixture is too lean to auto-ignite or to support a flame during the primary combustion in the cylinder. They will remain unconsumed if not being oxidized in the expansion process that follows; (2) the fuel is trapped by the nozzle sac which enters the cylinder in the later process or excess fuel is injected, causing over-fueling; (3) quenching and misfiring. The first path is most significant when the engine is running at light load or idling and the third path depends on the temperature of the cylinder wall and the fuel spray impingement.

Carbon monoxide (CO) and carbon dioxide ( $\text{CO}_2$ ) from diesel engines are relatively low. The generation of carbon monoxide (CO) is controlled by the fuel/air ratio and it can also be contributed to by the pyrolysis of the carbon dioxide ( $\text{CO}_2$ ). The CO emissions are more significant in the spark ignition engines as the fuel/air ratio is often close to stoichiometric at part load and more at full load. For operating well on the lean side of stoichiometric, diesel fuel is burned in excess air even at full load, at which point the quantity injected per cycle is still about 50% lean. As for  $\text{CO}_2$ , diesel engines are more efficient than gasoline engines of the same power, resulting in lower fuel consumption (a common margin is 40% more miles per gallon for an efficient turbo-diesel) and thus less carbon dioxide ( $\text{CO}_2$ ).

### 1.1.3 Overview of the Diesel Engine Emission Regulation and Controls

In 2007, Europe finalized its light-duty Euro V emission standards which applied from September 2009 (light commercial vehicles and special needs cars from September 2010) for new models of cars and from January 2011 (light commercial vehicles and special needs cars from January 2012) for all new cars. Compared with Euro IV, it confines the emissions

---

further for carbon monoxide (CO), hydrocarbon (HC), nitrogen oxides ( $\text{NO}_x$ ) and particulate matter (PM) and the latter two had a 28 % and 80 % reduction respectively. While from 2014, Euro VI will be carried into force, and that will put a major restriction on the  $\text{NO}_x$  and particulate numbers. The change of the diesel tailpipe standards listed in Table 1.1 just reflects how diesel engine technology has to be developed accordingly.

**Table 1.1** European emission standards for diesel light commercial vehicles  $\leq 1305 \text{ kg}$   
(Category N1 - I), g/km<sup>(a)</sup>

Tier	Date	CO	$\text{NO}_x$	$\text{HC} + \text{NO}_x$	PM	PN
Euro I	October 1994	2.72	-	0.97	0.14	-
Euro II, IDI	January 1998	1.00	-	0.70	0.08	-
Euro II, DI	January 1998	1.00	-	0.90	0.10	-
Euro III	January 2000	0.64	0.50	0.56	0.05	-
Euro IV	January 2005	0.50	0.25	0.30	0.025	-
Euro V	September 2009	0.50	0.18	0.23	0.005	$6.0 \times 10^{11}$
Euro VI	September 2014	0.50	0.08	0.17	0.005	$6.0 \times 10^{11}$

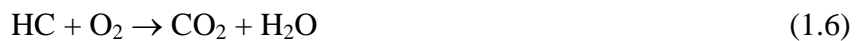
(a) from <http://www.wikipedia.org/>

Driven by these increasingly stringent governmental regulations, manufacturers and lots of researchers have been working on the cleaner engine technologies in the following main directions (Johnson 2006; Johnson 2007; Johnson 2008; Johnson 2009): (1) after-treatment systems such as the diesel oxidation catalyst (DOC) and the diesel particulate filter (DPF); (2) new fuels and additives from renewable resources which also produce less emissions; (3) new combustion strategies through the optimization of the fuel injection pressure and the injection timing; (4) exhaust gas recirculation (EGR).

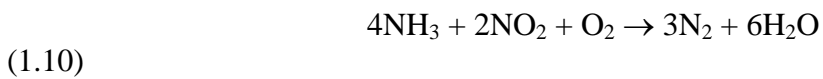
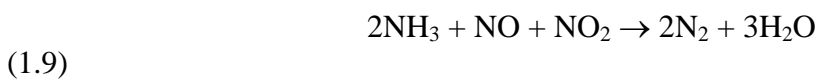
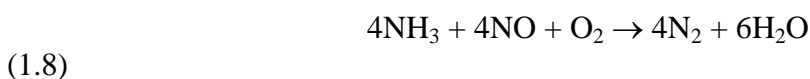
### 1.1.4 The Diesel Engine After-treatment System

The most commonly used after-treatment system for diesel engines can be categorized into the following two groups: (1) catalytic converters which include diesel oxidizing catalysts (DOCs) for HC and CO and reducing catalysts for NO<sub>x</sub>, such as selective catalytic reduction (SCR) and lean NO<sub>x</sub> trap (LNT); (2) diesel particulate filters (DPFs).

A DOC can not only oxidize CO and HC to CO<sub>2</sub> and water in the exhaust stream but also reduce the SOF of particulates. Noble metals such as platinum (Pt) and palladium (Pd) are most suitable as the catalytic material for the high intrinsic activity (Heywood 1988); however, certain temperatures and sufficient oxygen are also required for a thorough oxidation. A standard DOC can have a typical conversion efficiency of 70 %-90 % for HC and 70 %-95 % for CO depending on the catalytic loading and the exhaust heat. The chemical reactions are:



SCR is a way to convert NO<sub>x</sub> into nitrogen and water. A gaseous reductant, typically ammonia or urea, is added to the exhaust gas and is absorbed onto a catalyst, on which the following reactions occur:



If the reductant tank runs dry, the SCR system ceases to function. To avoid this problem, LNT was designed by using the zeolite to trap the  $\text{NO}_x$  molecules. Once the trap is full, the  $\text{NO}_x$  can not be absorbed, and will pass out of the exhaust system until the trap is “purged” or “regenerated” by injecting reactant which reacts with the absorbed  $\text{NO}_2$  to produce  $\text{H}_2\text{O}$  and  $\text{N}_2$ .

A diesel particulate filter (DPF) is the major device to reduce diesel particulate emissions. It traps the particulates when the exhaust flows through and those accumulated particulates will increase back pressure, causing negative effects to the engine performance. Thus, they have to be oxidized by burning off after a certain period of time or through some catalytic means, the process of which is called “regeneration”. The commonly used materials for DPFs are ceramics and metallics. The former includes cordierite, mullite, silicon carbide, etc, while the latter includes sintered metal, wire mesh and metal foam (Konstandopoulos et al. 2000). Besides the most popular structure of honeycomb wall flow monolith, the other geometric configurations of DPFs include cylindrical cartridges, foam monolithic blocks and concentric tubular wall flow elements (Konstandopoulos et al. 2000).

### **1.1.5 New Fuels and Their Blends**

“Energy Crisis” first emerged as early as 1973 when the limitation of the natural resources was highlighted and the importance of using these sources properly was realized. Since then, people have been looking for alternatives for the conventional fuels, which can last no longer than several hundred years at most. Besides, the products of these fuels have posed a serious threat to the public health as well as the environment due to the enormous emissions. So far, the renewable and cleaner alternative fuels include biofuels, hydrogen, oxyhydrogen, alternative fossil fuels etc. For the diesel side, biodiesel and gas to liquid

(GTL) diesel are the two most common alternatives. Belonging to the bio-fuel family, biodiesel consists of long chain esters derived from vegetable oil or animal fat through a process called “transesterification” and it can be used in diesel engines alone or blended with conventional diesel, which is more popular. Gas to liquid (GTL) diesel is converted from natural gas through the “Fischer-Tropsch” process and even the gaseous waste during the production can be recycled for fuel oils. These alternative fuels have shown better emission characteristics than conventional diesel and their application on the diesel engines is becoming more and more popular.

### **1.1.6 New Fuel Injection and Combustion Strategies**

The emissions from diesel engines are believed to be caused by the in-homogeneity of fuel air mixtures during combustion and increasing this homogeneity will bring the local equivalence ratios down, thus for the benefit of fewer emissions. The main methods to achieve this include the use of different fuel injection timings, a reasonable exhaust gas recirculation (EGR) rate, and the adjustment of injection pressure. For current diesel engines, it is very common to have two fuel injections for each engine cycle: the main injection for the engine performance, and the pilot one for the reduction of the noise and NO<sub>x</sub>. This can be increased to three or even five, each functioning for different reasons. EGR is mainly used for the reduction of NO<sub>x</sub> due to its oxygen-replacement and radicals-supply effects. However, it also has a particle producing impact. Therefore how to keep them balanced for an overall lower emission is important.

## 1.2 Objectives and Approaches

The main objective of this research is to focus on the particulate matter control of diesel engines, following the major research directions of the emission control mentioned above and according to them, this study is divided into: after-treatment device, injection strategies and alternative fuels. The approaches include:

- To set up an engine test rig fully equipped with relevant measuring device.
- To set up a one-dimensional engine model.
- To evaluate a set of new after-treatment system for the future emission requirement and the influence the after-treatment system can bring to the engine performance
- To investigate the different fuel injection strategies that can lead to the reduction of particulate and gas emissions
- To investigate the particulate emission characteristics from new fuel blends, along with gaseous emissions.

## 1.3 Thesis Outline

The research work is sparked by the new trend of diesel emission control and it focuses on the most critical problem caused by diesel engines – the particulate matter. Chapter 1 and Chapter 2 of this thesis intend to give a general introduction and review of the research of similar topics carried out around the world, as a base for the author's own research. Chapter 3 is about the commission of the engine test bench, on which the research work was carried out. Besides the Ford diesel engine calibrated to Euro IV emission standard,

there are a data acquisition (DAQ) system for the measurement of the bench's temperatures and pressures, exhaust emission measuring device, an engine cooling system (intercooler, engine cooler, and fuel cooler), and an engine control system. Following this, the possibility of replacing the current DOC with a set of new after-treatment systems is investigated and presented in Chapter 4. In the same chapter, the influence of the exhaust back pressure on the engine performances is further discussed. In Chapter 5, the fuel injection impacts on the engine performance and emissions are looked into using single injection strategies. A proper combination of these injection parameters can lead to advanced combustion with a single injection, when NO<sub>x</sub> and smoke are greatly reduced; however, increased CO and HC are another problem to solve, when compared with those resulting from multiple injections. In Chapter 6, multiple fuel injection strategies are investigated and the influence of the key parameters of the pilot injection to the non-volatile particulates is focused on. Chapter 7 concerns the research of the new fuels. Two typical alternative fuels, namely Rapeseed Methyl Ester (RME) and GTL diesel are blended with conventional diesel at a fairly low rate to meet the 2020 bio-fuel target and the particulate characteristics are carefully studied, along with the other regulated gas emissions. The main conclusions of all the work and the future research directions are presented in Chapter 8.

## CHAPTER 2

### LITERATURE REVIEW

This chapter starts with some background knowledge on the current engine emission regulations and the most critical issue of diesel engines – particulates. It presents the main technologies for the engine emission control, either through the after-treatment or the improvement to the combustion. It also covers new alternative fuels, which might be a solution in the future for fuel shortage and emission problems.

#### 2.1 Engine Emission Toxicity and Regulations

The Los Angeles photochemical smog, which started as early as in the 1940s and the London smog in 1952 are probably two of the most notorious disasters caused by air pollution in the human history, when thousands of people got sick or even died. The first case arose of the high level of ozone through reactions between sunlight and two major vehicle exhausts: oxides of nitrogen and hydrocarbons (Haagen-Smit 1952) and the second was due to a combination of smoke from automobiles and coal burning, a low wind speed and dry weather (Wilson 1996). Since then, people began to realize the importance of environment protection and the price to be paid to the ‘amenity’ for our ‘utility’ (Eastwood 2008).

### 2.1.1 The Toxicity of the Engine Emissions

The four major types of emissions from combustion engines include the particulate matter, oxides of nitrogen, carbon monoxide and hydrocarbons. The former two are especially significant for diesel engines.

Particulate matter (PM) is believed to be a trigger for asthma, lung cancer, cardiovascular issues, and premature death as it can penetrate deep into the lungs and the bronchi, when inhaled by human beings (C. Arden Pope III 2002; Kagawa 2002). Thus, its toxicity is closely related to its size and shape. Generally, the smaller the particles, the more dangerous they are and it is assumed that those in the feathery or geometrically angular shape are more harmful.

The oxides of nitrogen are not all toxic. Nitric oxide (NO) itself is odourless, colourless and relatively non-toxic (Eastwood 2000); however, it can form secondary pollutants such as nitric acid, implicated in acid rain and it also participates in ozone layer depletion. Nitrogen dioxide (NO<sub>2</sub>) is more detrimental to human health. This reddish-brown gas can irritate the lungs and produce pulmonary edema and fatality if inhaled at high concentrations (Peterson et al. 2008). Cough, hemoptysis, dyspnea, and chest pain can also be caused even when exposed to moderate levels of 50 ppm (Battigelli 1971).

Carbon monoxide (CO) is colourless and odourless, just as NO, but it is more dangerous as it can block the delivery of oxygen and cause cellular hypoxia (Shochat et al. 2010), due to haemoglobin's greater affinity for CO than for oxygen. Thus, the human organs with the highest oxygen requirement such as the brain and heart can be affected most significantly. Impairment of judgement, headaches, dizziness and nausea are common

symptoms under the effect of CO and the cardiovascular and nervous systems can also be affected by long term exposure to low levels of CO (Eastwood 2000).

There are a variety of hydrocarbon (HC) compounds and their toxicities are determined by their chemical properties and how they contact with the human body. Pulmonary, neurologic, cardiac, gastrointestinal, hepatic, renal, dermatologic, and hematologic systems can all be susceptible to them and lungs are believed to be the most commonly affected organ (Levine et al. 2009). They can directly cause coughing, sneezing and drowsiness, and they can also form secondary pollutants such as ozone and photochemical smog (Kumar et al. 2002).

Besides the four major tailpipe pollutants, which are subject to law in most countries, there are ‘green house gas’ - carbon dioxide (CO<sub>2</sub>) and other ‘unregulated’ emissions from combustion engines (Schuermann et al. 1990), notably sulphur compounds and ammonia. They all pose a threat to the human being and have drawn great attention.

### **2.1.2 Global Automotive Emission Regulations**

The increasing concerns about these pollutions’ impact to human health and environment became the impetus for governments to take action for their regulation, especially for those derived from the major source - motor vehicles. In 1959, the first emissions legislation was established in California, followed by the first federal standard in 1966. Similar regulations were enacted in Japan in 1966 and in Europe in 1970 (Eastwood 2000). Since then, these regulations, most in the form of statutory limits, have been tightened in a progressive way and that compels industry to develop its emission control technology accordingly. Nowadays, all the industrialised countries around the world have these sorts of limits, which might vary a little in different regions. Before selling their vehicles, the

manufacturers must have them approved for this emissions compliance, when the vehicles are run on dynamometers over different standardised drive cycles based on their type and the emissions are measured.

Concerning the diesel tailpipe emission regulations, they are categorized into three applications: light duty, on-road heavy duty and non-road heavy duty (Johnson 2006). In July 2009, the European Union published its final Euro VI regulation for on-road heavy duty vehicles and set the limits to 400 mg/kW-hr for NO<sub>x</sub> and 10 mg/kW-hr for PM on the European Transient and European Steady State Cycles (Johnson 2010). For light duty passenger cars and commercial vehicles, the limit for PM was set to 5 mg/km, both in Euro V and Euro VI. According to the EC Regulation No 715/2007(amended by Regulation 692/2008 and 595/2009), the particle number was set to  $6.0 \times 10^{11} \text{#/km}$ .

## 2.2 Particulates

Particulates are tiny solid and liquid particles and are sometimes referred to as particulate matter (PM) or fine particles, and their sizes, which are strongly linked to human health issues, vary from several nanometers to several hundred microns (World Resources Institute et al. 1998; C. Arden Pope III 2002; Eastwood 2008).

Generally, particulates from engines can be categorized into three distinct types according to their sizes: nucleation mode (<50 nm), accumulation mode (50-1000 nm) and coarse mode (>1000 nm) (Kittelson 1997) (Figure 2.1). There are also definitions, which are different in the size range, as nucleation mode (<100 nm), accumulation mode (100-900 nm) and coarse mode (>900 nm) (Eastwood 2008).

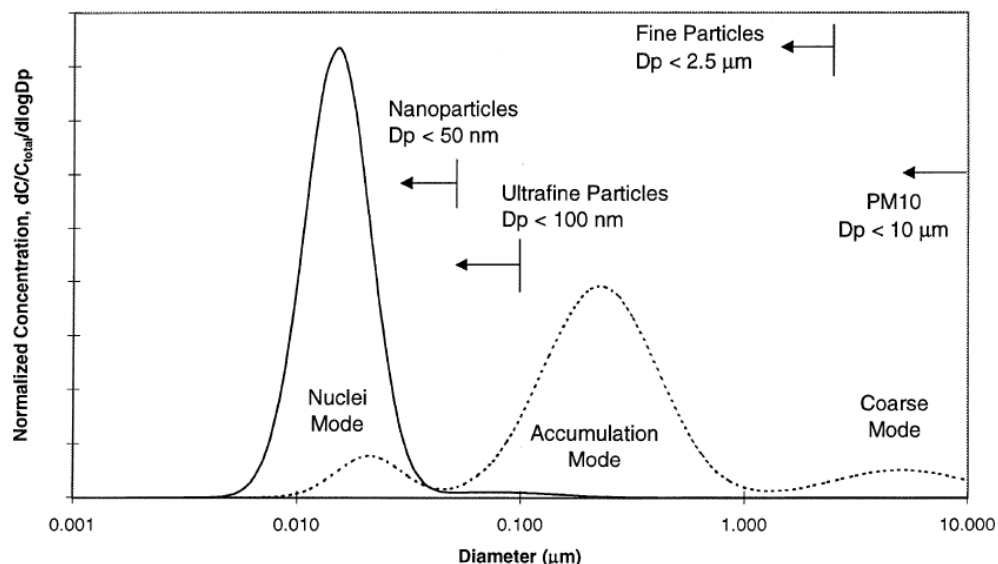


**Figure 2.1** Typical particle size and distribution from combustion engines (Kittelson 1997)

Coarse mode particles are mainly composed of particles forming from the other two modes or atypical rust and scale from the exhaust system. They can easily be stored and released in the exhaust system and this inconsistency makes its manner unpredictable and thus less studied (Eastwood 2008). For the past few years, attention has been mainly drawn on the accumulation mode particles, which have more to do with the particle mass. They consist of some basic blocks called primary particles or spherules (Heywood 1988). The spherules' diameters are around 20-50 nm and their numbers determine the size of the particles. The spherules are composed of solid core parts and some liquid or semi liquid materials attached to the surface of their aggregations, making them "wet" (Eastwood 2008). Nucleation mode particles are more related to the particle number and they are relatively less studied for their obscure and irreproducible nature. Some of them are volatiles and some are solids. Based on the conceptual model recommended by Peter (Eastwood 2008), particulates can be divided into non-volatile/non-soluble, which are mainly generated in the engine, and volatile/soluble, which form later in the exhaust. The former includes the soot and ash fractions while the sulphate, organic and nitrate fractions are categorized in the latter.

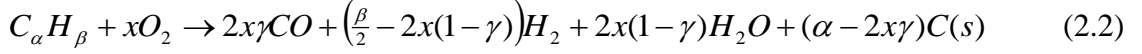
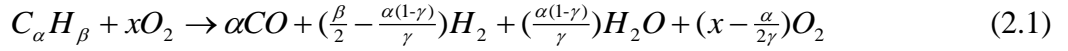
### 2.2.1 The Mechanism of Engine Particulate Formation

Two of the major sources of engine particulates are the fuel and additives, which all go through the combustion process within the engine. The fuel, of course, is to supply the power, while additives are used to improve the engine efficiency, reduce emissions or help to regenerate the diesel particulate filter (DPF) (Burtscher et al. 2000). The extreme characteristics of in-cylinder combustion makes it difficult to carry out some fundamental studies (Heywood 1988), such as the soot formation, and the insights into them have largely resulted from studies of premixed and diffusion flames, ranging from small laboratory scale burners to full scale combustion devices (Santoro 1987; Santoro et al. 1987; Sako et al. 2007).

After being injected into the cylinder, the fuel vaporizes under high temperature and pressure and undergoes two modes of combustion, namely ‘premixed combustion’ and ‘diffusion combustion’. In either of these modes, fast oxidation reactions exist in parallel with pyrolysis. These two reactions compete with each other, and the latter prevails when there is oxygen deficiency, which is the best environment for the formation of soot (Eastwood 2008).

Acetylene (and its higher analogues) and polycyclic aromatic hydrocarbons (PAH) are believed to be the precursors of soot and they grow through surface growth by the attachment of gas phase species or the coagulation and aggregation with other particles until they reach the final maturity. During this process, dehydrogenation and oxidation occur, which keep modifying the particles’ physical structure and chemical characteristics.

The basic equilibria for the classical empirical model for this particle formation include (Li et al. 1995):



Where C/O is easily considered to be the critical ratio, as when this value is larger than unity, some carbon atoms appear as soot. However, in practice, this value is often less than unity, at around 0.5 to 0.8 (Heywood 1988), which means that this method is inapplicable to predict the soot. Other empirical models correlate the soot with different combustion parameters such as the ignition delay (Grigg 1976), and the fuel consumed in the mixing (Han et al. 1997), based on the observations.

For the particle growth mechanism, this empirical equation is suggested (Sunderland et al. 1996):

$$\omega_g = k_g(T)[C_2H_2]^n \quad (2.3)$$

Where  $\omega_g$  is the rate of surface growth ( $\text{kg}/\text{m}^2\text{s}$ ),  $k_g(T)$  is an Arrhenius expression and  $n$  is an index. This equation can be used for simple hydrocarbon flames, based on its association with acetylene. However, it is not applicable in all conditions (Hanisch et al. 1994). ‘Surface sites’ are then defined and the hydrogen atoms are the activator mediating the conversion between two surface states, namely carbon-hydrogen sites and dehydrogenated radical sites (Appel et al. 2000). The reactions include:

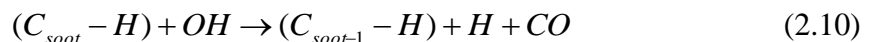
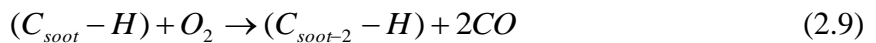




For the particles' agglomeration and oxidation, the Smoluchowski equation (Equation 2.8) and oxidation model (Equation 2.9 and 2.10) (Tao et al. 2004) are used respectively as:

$$\frac{dN}{dt} = -kN^2 \quad (2.8)$$

Where N is the number concentration and k is the agglomeration coefficient.



The two predominant oxidants, O<sub>2</sub> and OH, compete with each other and one may prevail in different conditions of oxidation.

The last stage happens in the exhaust and the atmosphere, where the particulates reach their final maturity and the measurement is usually carried out. Gas to particle conversion dominates in this phase and large quantities of volatiles in the nucleation mode form, which may give measurement falsification.

### **2.2.2 Particulate Measurement**

For the strong correlation between mortality and the particulate size, concerns have been raised recently on which aspect of particles should be emphasized when it comes to health issues: mass or number? Historically, the emissions standards are based on the studies of particle mass concentration, from PM 10 to PM 2.5. However, even PM 2.5 is still very large compared with vehicle particulates (Eastwood 2008) and it is becoming increasingly

clear that regulations on emitted particulate mass from engines, are not a proper measure of the health hazard, as a particle of 10  $\mu\text{m}$  diameter and 1 million particles of 100 nm diameter have similar weight, but the latter is much more dangerous to human health. Although modern engines emit lower particle mass than the older ones, larger numbers are produced (Abdul-Khalek et al. 1998). This pushes forward the transition of the particulate measurement from its mass to number and size distribution.

Currently, most particle-sizing devices report ‘diameter’ of a particle in the measurement and this term is commonly used to present size in aerosol science. It does not necessarily refer to any geometrical dimensions and is actually an ‘equivalent diameter’ of a spherical particle, which has the same response to certain forces. These concepts include the ‘Stoke diameter’, ‘aerodynamic diameter’, ‘electrical mobility diameter’, etc (Eastwood 2008). The scanning mobility particle sizer (SMPS) is one of the most popular pieces of equipment in the automotive industry to measure the particulate size and distribution, and the electrical mobility diameter is measured. An electrical low pressure impactor (ELPI) is used for the aerodynamic diameter. Both of them are suitable for steady state engine tests, but the former is more relevant to the smaller particles (diffusional effects), and the latter to the larger ones (inertial effects) (Gulijk et al. 2003; Eastwood 2008). Other equipment includes a differential mobility spectrometer (DMS) and an engine exhaust particle sizer (EEPS), which also measure the electrical mobility diameter, just as the SMPS. They have a lower detection limit in particle size and a much quicker response than ELPI, thus are more widely used for transient engine tests (Rubino et al. 2005).

Generally, the measurement of particle number distribution emphasizes the nucleation mode particles, which are more vulnerable to measurement falsification due to their volatile

component parts. In practice, before applying these measuring devices, raw engine exhausts are usually diluted in a standard dilution tunnel through constant volume sampling (CVS) and this undoubtedly exaggerates the variability of the measurement results. To solve this problem, a ‘Particulate Measurement Programme’ (PMP) was initiated by the Swiss Environment Protection Agency (EPA), Japan and some European countries, aiming at finding a more sensitive particle metric for the toxicologically relevant particles. It recommended that the non-volatile particle number concentration should be measured and the industry has corresponded with proposals: design of a combination of thermo-diluter and condensation particle counter (CPC) (Kasper 2004) and a solid particle counting system (Montajir et al. 2007).

### **2.2.3 Diesel Engine Particulates**

As early as in 1998, a study of the automotive particulate size, number and mass distribution from European light duty (LD) vehicles was carried out by a group of oil companies such as BP oil, Esso, Shell, etc, when four diesel and three gasoline vehicles were tested using limited fuel matrix and varied driving conditions (Hall et al. 1998). It was noted that the particulates from LD diesel vehicles were much higher than from LD gasoline vehicles and in number terms, it was around 200 for MVEG cycles, more than 2000 at 50 km/h, but down to around 3 at 120 km/h. The largest vehicle technology effect on the particulate emissions was the gasoline/diesel effect and the fuel effects were more significant in the diesel study.

Armas et al. (2008) investigated the exhaust particle size distribution affected by the diesel engine operating conditions. It was found out that the variation of engine speed and torque influenced the exhaust temperature, which consequently changed the oxidation of the

formed soot and particulate nucleation. The increase of the engine speed reduced the accumulation mode particles due to the clear decrease of fuel air ratio and EGR ratio at low torque and the elevated oxidation at higher torques. The increase of torques caused the production of nucleation mode particulates owing to the EGR, which also played an important part in the exhaust particulates formation and its decrease favoured the soot oxidation owing to higher oxygen, and consequently the reduction of soot and accumulation mode particles.

Tanaka et al. (1999) looked into the particulate composition under different engine operating conditions and pointed out that the small aerodynamic diameter particles decreased when the ratio of the soluble organic fraction (SOF) was increased by lowering the engine torque. In addition, the SOF ratio in the large aerodynamic diameter particles was higher than that of the small ones. In the study conducted by Klein et al. (1998), the influence of diesel oxidation catalysts (DOC) on the particulates was investigated. It was demonstrated that the DOC was able to reduce the SOF of PM in the low temperature, thus reducing the particulate sizes. However, in the high temperature, it might oxidize the sulphur into sulphate, which could strongly influence the particulate agglomerations.

Through a high resolution transmission electron microscope (TEM), Lee et al. (2003) investigated the morphology of light duty diesel particulates. It revealed that particulates produced at low engine loads were nebulous with a large amount of SOF, while at high loads, they were in graphitic structures, just as the typical carbon graphite. The primary particle sizes were also influenced by EGR, and in most cases, they increased with the increase of EGR.

More recent research into PM emissions includes the particulate matter characterization from advanced combustions, such as low temperature combustion (LTC)

(Natti et al. 2008) and homogeneous compression charge ignition (HCCI) (Zinola et al. 2009) and the particles from new fuels, such as in Tan et al. (2009), where Jatropha biodiesel fuel was used. Their PM emissions all differed from those from normal diesel combustion.

## 2.3 Diesel Particulate Filter (DPF)

The DPF was first commercially used on passenger cars in Europe more than ten years ago and has now become one of the necessities to meet the future tighter emission regulations. Since invented, it has experienced very rapid development and many related concepts have emerged, incorporating different factors such as the filter materials and geometric configurations, which are the two key characteristics of a DPF (Konstandopoulos et al. 2000).

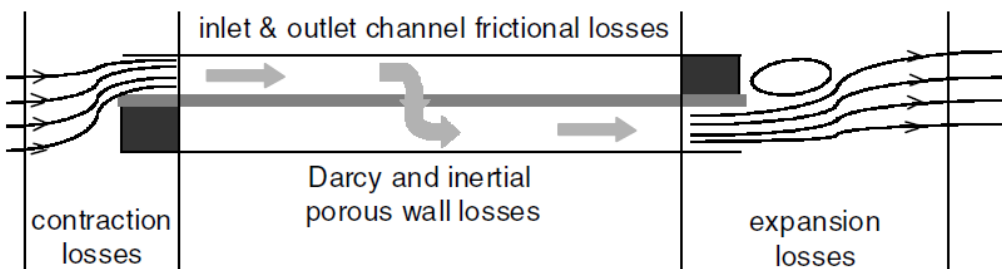


**Figure 2.2** Schematic view of flow pattern through a channel of a wall flow DPF, showing pressure loss components (Konstandopoulos et al. 2001).

Wall-flow is the most commonly used arrangement of DPFs these days, and it is based on a monolithic substrate with alternately plugged inlet and outlet channels (Figure 2.2). The excellent filtration efficiency and minimum backpressure (Ohara et al. 2007) exhibited by this structure determines its popularity in the industry. For a wall-flow DPF, the inertial back pressure is contributed to by the flow through the porous wall, flow contraction at the inlet

channels and flow expansion at the outlet (Konstandopoulos et al. 2001). It keeps increasing with the accumulation of the captured soot, until it is ‘regenerated’. This attribute has been investigated in many papers, and it is common to simplify the whole DPF to a single channel substrate for the research (Dillon et al. 2007; Yoon et al. 2007).

### **2.3.1 DPF Regeneration**

The back pressure caused by the after-treatment system is detrimental to the engine’s performance and its gradual rise with the soot loading in the DPF can cause a concomitant rise in the exhaust temperature. However, it’s inapplicable to use this effect to initiate the DPF’s regeneration for safety reasons (Eastwood 2000).

Generally, the regeneration methods are conveniently categorized as active or passive ones (Konstandopoulos et al. 2000). Active regeneration includes those using external or engine means to thermally burn the soot such as a fuel burner (Kong et al. 2005), electric heating (Turner et al. 1995), injection of hydrocarbons in the exhaust (Bandy et al. 1993; Alano et al. 2010) and the post injection of fuels (Bouchez et al. 2000). The passive regeneration mainly relies on the catalytic means, either through the fuel borne additives (Vincent et al. 1999) or some catalytic filter coating to achieve ‘continuous regeneration’ (Eastwood 2000). The combination of the two is also common in practice.

The regeneration of a DPF has to be carefully controlled. Practically, the back pressure is usually used as an assessing factor for the DPF soot loading, and it is required before an active regeneration is initiated, either to determine the regeneration timing or for safety reasons such as what protection measures should be taken if the DPF is heavily loaded. Uncontrolled regenerations can damage the DPF (Seiler et al. 2008) and deteriorate its

performance, which might also happen due to the thermal aging of DPFs after frequent regenerations (Costa et al. 2007).

Zhan et al. (2006) carried out a project on the identification of DPF related failures and methods to avoid them. The three thermal related DPF failures were the exotherm at the start of the DPF regeneration, traditional runaway regeneration and traditional ‘hot spot’ problems. The proposed strategies to prevent such uncontrolled regeneration included: (1) controlled fuel injection rate for DPF regeneration; (2) high EGR rate when the engine goes to idle during the DPF regeneration; (3) an effective and low-cost flow diffuser at the DPF inlet cone.

Flörchinger et al. (2004) demonstrated an automated DPF regeneration strategy through modification to the ECU control. The inputs included the post injection quantity and timing, and EGR valve position. The open loop strategies were applied on four engine operation points, when additional features were implemented such as undesirable side effects (thermal shock, over heating, etc) prevention and regeneration acceleration. Haralampous et al. (2004) concluded that at low temperature regeneration, the main reaction mechanism involves NO<sub>2</sub> produced on the catalytic sites and partially diffusing back to the soot layer while at high temperature regeneration, the main reaction happened between the oxygen and soot.

### **2.3.2 New DPF Configuration and Materials**

Besides wall-flow type, the other filter configurations include cylindrical cartridges, and foam monolithic blocks (Konstandopoulos et al. 2000). One of the reasons why they are not so widely used is due to the high back pressure these structures can cause.

Silicon carbide and cordierite are still the two dominating materials used for DPF. However, metal, especially metal foam, is becoming more and more attractive for its superior thermal conductivity, more uniform distribution of temperature, and most important, low price (Eastwood 2000). Research of metal foam DPFs (DOCs) has been going on since the 1990s (Yoro et al. 1998; Koltsakis et al. 2006; Koltsakis et al. 2006; Koltsakis et al. 2007), in which, the key points are to optimize the design for less back pressure and two main manufacturing variables: packing density and filtration area. It should also be noted that the major problem with the metal foam is its susceptibility to corrosion.

In the study by Yoro et al. (1998), a radiation heater was combined with a porous metal DPF to solve the low regeneration efficiency problem related with most thick filters for the declination of temperatures. Through computer simulation and experiment on an urban bus, this system has shown promising regeneration performance. Koltsakis et al. (2008) presented the test results of a cross flow foam based catalyzed DPF (CDPF), and they showed that the CDPF had high catalyst-soot reaction rates at low temperatures, due to the depth filtration mechanism and high surface area of the foam. The strong passive regeneration resulted led to a low pressure drop. The metal foam substrate also gave the design more flexibility, and allowed a compact integration of a DOC and a DPF with potential volume and cost savings. Thus, a more effective and less expensive after-treatment system might be achieved.

## 2.4 New Injection Strategies for Diesel Engines

In the early stage of diesel engine emission control, enhancing the fuel metering and ignition systems alone is enough to meet the tailpipe limits (Eastwood 2000). However, with the gradual reduction of the statutory emission limits, the old generation of fuel injection systems on the vehicles could not meet the requirement and that eventually led to the appearance of the new common rail direct injection system, which is now widely adopted.

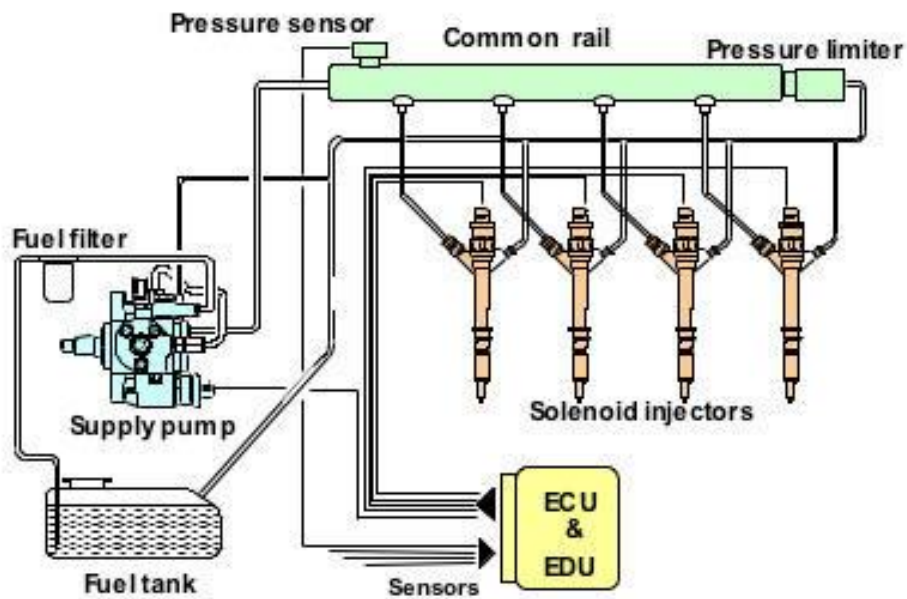


**Figure 2.3** Common rail system (Denso Australia 2010)

Unlike the old fuel injection system, which was cam driven and the injection pressure of which was proportional to the engine speed, the common rail stores the fuel at a high pressure (over 1,000 bar) through a supply pump and feeds it to individual ECU-controlled fuel injectors (Denso Australia 2010). This gives a fairly similar pressure at the start and end of injection as the common rail pressure, and thus a square injection rate. At the same time, the high pressure provides better fuel atomisation when it is injected into the cylinders. The

common rail system also has more precise control of fuel injection timing and quantity through the solenoid or piezoelectric injectors while the old system could only do a limited injection number and timing.

#### **2.4.1 Multiple Injection Strategies**

Multiple injection was first proposed in 1937 and currently the advanced common rail fuel system, which can perform as many as five injections per stroke, gives rise to this injection strategy's application for optimum performance and emission reduction in diesel engines.

According to Vanegas et al. (2008), for two injections (pilot and main injections), pilot injection could reduce NO<sub>x</sub> significantly but also increase smoke emissions. CO and HC could be reduced using a late main start of injection (SOI) and a short duration between the pilot and the main injection; for three injections (pilot, main and post injection), the NO<sub>x</sub> emissions decreased more while CO and HC remained constant. The post injection reduced the smoke.

Roy et al. (2002) studied the impact of injection pressure and split injection on exhaust odour and engine noise and it was found that at idle speed, there was an optimum injection pressure around 60 MPa and the shorter ignition delay the less aldehydes and THC. Besides, split injection at 50/50 could reduce the noise compared to the single injection but produced higher odorous emissions.

The effects of multiple pilot injections on the diesel engine's cold idle stability were investigated by MacMillan et al. (2009) and it was pointed out that a single pilot strategy gave

the best cycle to cycle stability at temperatures down to -10 °C, but at lower temperatures, twin or triple pilot injections were even better.

Liu et al. (2005) showed that widely-separated two-stage combustion: one early-stage pre injection at -50 °ATDC and one late-stage main injection at 13 °ATDC appeared to be a good solution to optimize high speed direct injection (HSDI) diesel engine brake specific fuel consumption (BSFC) and emissions performance at part load, by using computational simulation.

#### **2.4.2 Exhaust Gas Recirculation (EGR)**

Exhaust gas recirculation (EGR) is a nitrogen oxide ( $\text{NO}_x$ ) emissions reduction technique commonly used in diesel engines these days. It works by re-circulating part of the engine's exhaust gas, back to the engine cylinders to replace the oxygen (Kaneko et al. 1975). This can lower the combustion temperature and once the combustion temperature is lowered, the  $\text{NO}_x$  will be reduced consequently based on the Zeldovich mechanism (Heywood 1988). However, using EGR could also lead to lowered power output and increased HC and PM emissions.

EGR can be controlled either by trapping a demanded exhaust gas portion through proper valve timing (internal EGR) (Masahide et al. 2004) or by extracting the exhaust from the exhaust manifold to the inlet manifold (external EGR). In a modern diesel engine, this extraction is usually achieved by using a variable geometry turbocharger (VGT), which creates pressure difference between the exhaust and the inlet manifold, and an EGR valve, which allows the required exhaust flow.

In the early stage of research, EGR's NO<sub>x</sub> reduction characteristics were mainly focused on: Dürnholz et al. (1992) investigated the application of hot EGR and found that it could reduce NO<sub>x</sub> as well as hydrocarbon (HC) and PM emissions, without an adverse affect on the fuel economy. This was particularly significant at low and medium loads. Uchida et al. (1993) combined EGR and supercharging, and achieved improved engine combustion and a reduced NO<sub>x</sub> emission. They also noted that the reduction of NO<sub>x</sub> was almost in proportion to the EGR ratio increase, and with a proper intake boost and fuel injection setting, 50% NO<sub>x</sub> reduction at a 20% EGR ratio could be achieved without deteriorating smoke and HC. Other research includes EGR's effects on diesel knock (Oetting et al. 1979) and fuel consumption (Nakajima et al. 1981).

Recently, its ignition delay characteristic has attracted more and more researchers, and especially in the field of Low Temperature Combustion (LTC), including Homogeneous Charge Compression Ignition (HCCI) or Partially Charge Compression Ignition (PCCI), the application of high level of EGR was preferred.

#### **2.4.3 LTC, HCCI and PCCI Combustion**

Low Temperature Combustion (LTC) is a new combustion concept and has attracted many researchers for its high efficiency and low NO<sub>x</sub> and smoke emissions from diesel engines. It includes Homogeneous Charge Compression Ignition (HCCI) (Najt et al. 1983) and Partially Charge Compression Ignition (PCCI or PCI).

In HCCI, a mixture of fuel, air and residual gases is homogeneous as in the case of the Spark Ignition (SI) engine and it is auto-ignited by compression as in the Compression Ignition (CI) engine (Juttu et al. 2007). The mixture can be either prepared externally through

port injection/evaporation or internally through different single or multiple injections (Weiskirch et al. 2007).

The fuel charge in PCCI combustion is less homogeneous than in HCCI and it was proposed by Okude et al. (2004) to solve the problem of fuel impingement in early injection HCCI, through increasing ignition retardation while injecting fuel in the vicinity of the top dead centre. These two kinds of combustion have proven to be able to break up the NO<sub>x</sub>-PM trade-off (Figure 2.4), which is common in all diffusion controlled combustion systems, and are believed to be the potential solutions to the future diesel engine emissions problems.

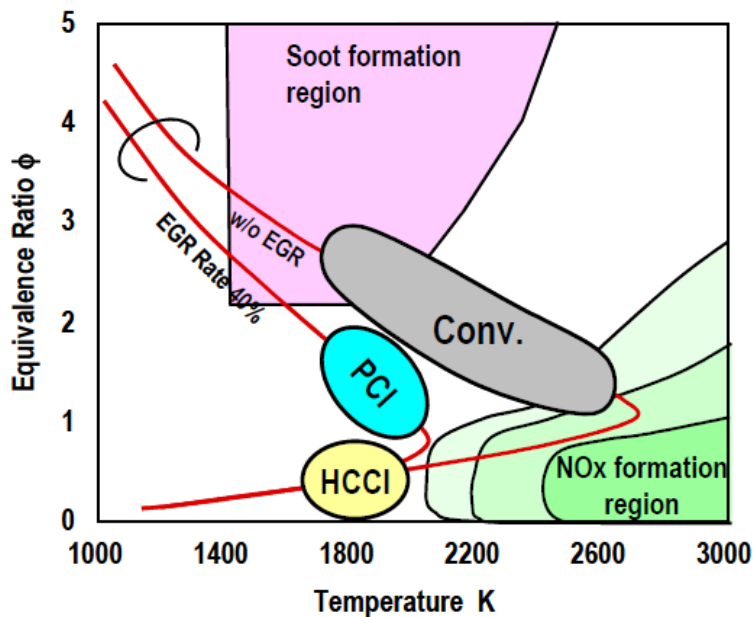


**Figure 2.4** Concepts of PCCI (PCI) and HCCI combustion (Okude et al. 2004)

However, the challenges they are facing include the control of the combustion (timing and rate) and high HC and CO emissions (Neely et al. 2004). It is common in such engines to have misfiring under low engine loads and knock-like intense combustion under high loads (Mohammadi et al. 2005). At the moment, research is still continuing on the improvement to

these new combustion concepts. Different methods such as optimization of the engine design, and the combination of a variety of fuel properties have been investigated extensively in a large number of studies (Akagawa et al. 1999; Kawamoto et al. 2004).

## 2.5 Alternative Fuels for Diesel Engines

Alternative fuels are known as ‘non-conventional’ or advanced fuels. According to the Energy Policy Act of 1992 (US Public Law 102-486 1992), they include biodiesel, ethanol, hydrogen, natural gas etc, which are commercially available for vehicles. Others include biogas, ultra-low sulfur diesel (ULSD), biomass to liquid (BTL), gas to liquid (GTL) etc, which are under development. These alternative fuels can not only secure the world’s energy reserves, considering the limited conventional fuels, but also add benefit for their reduced emissions.

### 2.5.1 Biodiesel

Biodiesel is one of the most popular alternative fuels nowadays and it mainly refers to diesel fuel made from vegetable oils and animal fats. They can be either used alone or blended with fossil diesel in diesel engines, and the latter is more commonly adopted and distributed for use in the fuel market. The ‘B’ factor is used to state the amount of biodiesel in the fuel mix as 100% biodiesel being referred to as B100, while 20% biodiesel is labelled as B20 (Alternative Fuels & Advanced Vehicle Data Center 2010). This marking system has been accepted in most countries around the world.

The production of biodiesel is through a process called ‘transesterification’ (Alternative Fuels & Advanced Vehicle Data Center 2010). During the process (Figure 2.5),

the raw vegetable oil or animal fat has to be first pre-treated or filtered to remove water and contaminants and then mixed with an alcohol and a catalyst. The oil molecules, namely ‘triglyceride’, react with the mix (usually methanol and sodium hydroxide), and are reformed into methyl esters (referred to as Fatty Acid Methyl Ester- FAME) and glycerine, which are then separated and purified. If ethanol is used instead of methanol, the methyl esters produced are called Fatty Acid Ethyl Ester (FAEE). Generally, 100 kilograms of oil or fat and 10 kilograms of methanol can produce 100 kilograms of biodiesel and 10 kilograms of glycerine (Alternative Fuels & Advanced Vehicle Data Center 2010).

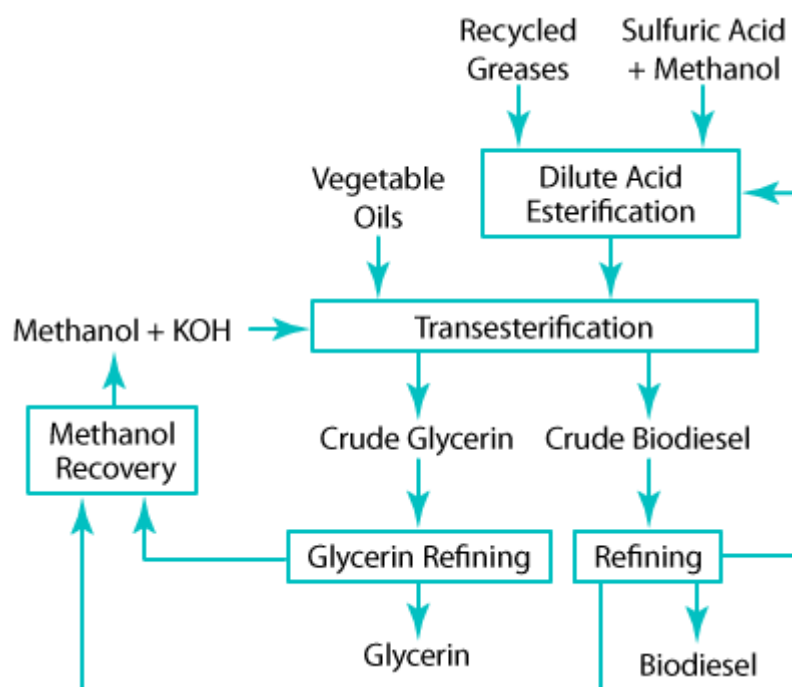


**Figure 2.5** Schematic of biodiesel production path (Alternative Fuels & Advanced Vehicle Data Center 2010)

According to the US Energy Information Administration (Figure 2.6), biodiesel production and consumption has increased significantly since 2005. In 2008, the US produced 682,530 thousand gallons (equalling around 2583 million litres) of biodiesel and the consumption was 320,220 thousand gallons (equalling around 1212 million litres). In Europe,

biodiesel production in 2008 was increased by 35.7% compared to 2007, reaching 7,755 thousand tonnes (equalling around 8783 million litres) and the production capacity is still growing rapidly.

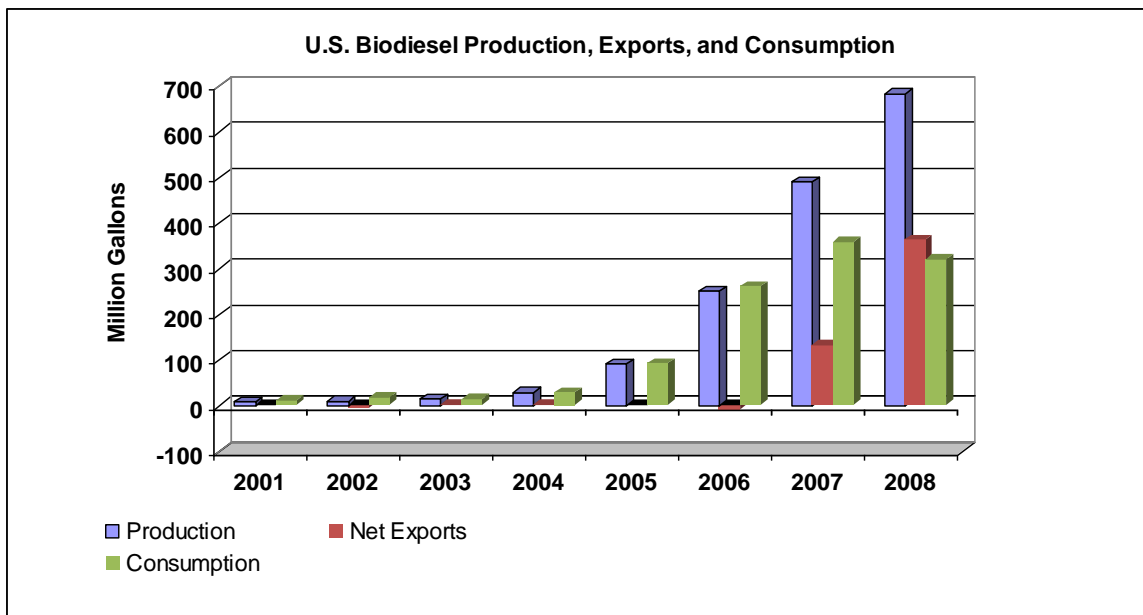


**Figure 2.6** Biodiesel Supply and Consumption (US Energy Information Administration 2009)

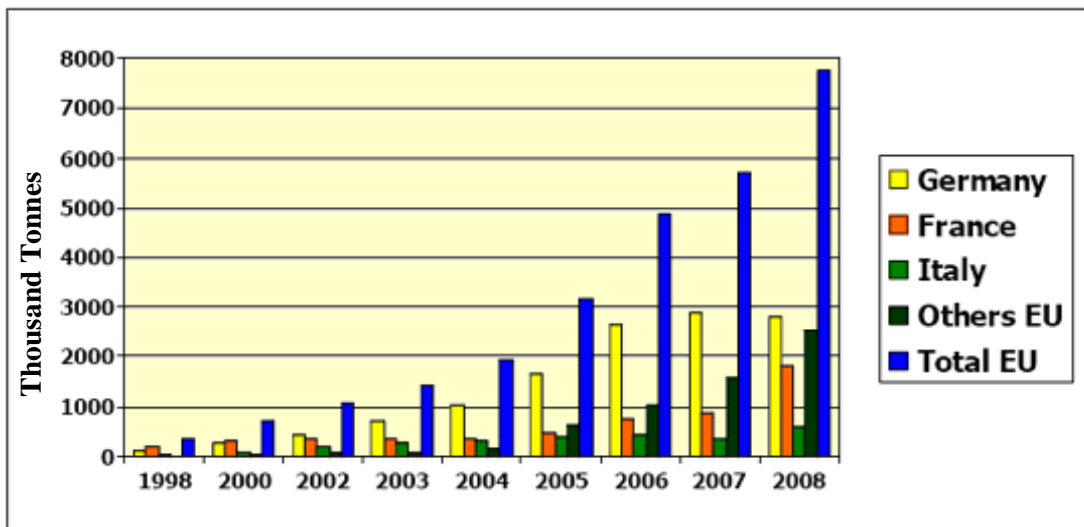


**Figure 2.7** The EU biodiesel industry (European Biodiesel Board 2010)

Currently, rapeseed and soybean oils are most commonly used as the biodiesel feedstock. Other crops such as jatropha, and sunflowers can also be applied. Animal fat feedstock includes tallow, lard, chicken fat, etc, which are usually by-products of meat production.

The performance and emissions of biodiesel, mainly rapeseed methyl ester (RME), and its blend with conventional diesel have been investigated in many studies. They show that biodiesel (RME) leads to a general reduction of engine emissions: CO, THC and smoke (Yoshida et al. 2008; Arr\afgle et al. 2009; Kousoulidou et al. 2009). However, its influence to NO<sub>x</sub> is not clear and under certain cases, NO<sub>x</sub> can even be increased (Kawano et al. 2008). Higher fuel consumption with higher blend concentration of biodiesel is also indicated in these studies (Nwafor 2004; Mayer et al. 2005; Zhang et al. 2008).

### **2.5.2 Gas to Liquid (GTL) Diesel**

In relatively advanced production and commercial fields, GTL diesel is expected to become the second U.S. Energy Policy Act ("EPAct") diesel fuel, for its much cheaper price than biodiesel. However, its blend treatment from the government has not been qualified, as the 'B' factor for biodiesel (Peckham 2002).

As shown in Figure 2.8, GTL diesel is commonly converted from natural gas (or other gas hydrocarbons) through a method called Fischer-Tropsch Process, which was introduced by Franz Fischer and Hans Tropsch in 1923 and first used to convert coal-derived synthesis gas into useful compounds. During the process, the main components in the natural gas - methane is oxidized to carbon dioxide, carbon monoxide, hydrogen and water, then treated into synthesis gas, and finally reacted over the catalyst into the liquid hydrocarbons.

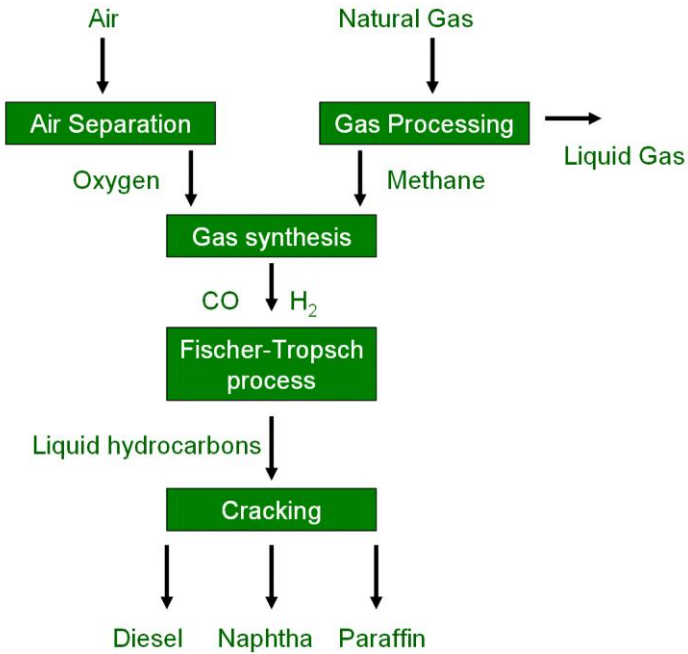


**Figure 2.8** GTL process using the Fischer Tropsch method (Dexcel 2008)

GTL diesel's compatibility with the current diesel vehicles and fuel distributing system is one of its major benefits. This means that it can be transported through the existing pipelines and dispensed at existing fuel stations (Alternative Fuels & Advanced Vehicle Data Center 2009). Other benefits include its near zero sulphur content, similar or better vehicle performance and cleaner emissions than the conventional diesel.

According to the studies, the use of GTL diesel fuel and its blends in unmodified engines enables significant reductions on HC, CO and PM emissions without compromising NO<sub>x</sub> emissions (Schaberg et al. 2005) and it is recommended that the calibration strategies should be carried out for better full load performances and catalyst efficiency (Kitano et al. 2007). Also, concerning GTL's lubricity, appropriate additives are needed (Oguma et al. 2004).

### 2.5.3 Combined Alternative Fuels with New Injection Strategies

It is not surprising for the development of combined research where the new technologies are merged for the aim of engine emission reduction. Zheng et al. (2008) investigated low temperature combustion (LTC) using neat biodiesel on a common rail engine and found that the biodiesel was better sustaining in the combustion than the diesel fuel in LTC, achieved through the retarded start of injection (SOI) and EGR. Stringer et al. (2008) looked into dual injection strategies using both conventional diesel and biodiesel and it indicated that biodiesel emissions were preferable to diesel emissions and out of all the cases, the lowest NO<sub>x</sub> from biodiesel was achieved with a pilot injection at 30 ° BTDC and a main injection at 10 ° TDC.

Biodiesel could be also used in LTC, when NO<sub>x</sub> and soot were both reduced. Weall et al. (2007) investigated a DI diesel engine HCCI fuelled with diesel and biodiesel, and it showed that biodiesel HCCI (B90 RME) reduced CO and THC by up to 35% at low loads than diesel fuel, and at higher loads, it reduced smoke by a factor 3. The application of dual fuel mixture (gasoline and diesel) in PCCI was also discussed by them and the results showed that with an increased proportion of gasoline, smoke was reduced at high operating loads, benefiting from higher volatility and increased ignition delay. At low loads, the NO<sub>x</sub> and smoke were still comparable to diesel operation. This indicated the possibility of widening the low emission operating regime though the combination of fuel properties.

## 2.6 Summary

In this chapter, the impact of diesel engine emissions, mainly particulates, on the environment and human health and the evolution of their control legislations and methods have been reviewed. It started with some background knowledge on the toxicity of the emissions, and proceeded with a deeper understanding of the PM formation inside and outside the engine. Current measurement methods of the PM were also discussed and they focused on the number concentration and the size and distribution of the particulates, which were more related with human health issues. It is recommended that the non-volatile particle number concentration should be measured for a more accurate and reliable PM number measurement.

New PM control methods include the use of a diesel engine after-treatment system, which has become necessary to satisfy current and future legislation. New materials and structures of the DOC and DPF have supplied more options for effective PM reduction applications. The application of alternative fuels to cope with fuel shortage and to lower emissions has also been discussed. For fuel injection, the optimization of multiple injections as well as single injections has shown a great potential to further reduce PM. Properly adjusting the injection settings can even lead to different combustion modes such as PCCI and HCCI, which break the trade-off of PM and NO<sub>x</sub> in normal diesel combustion, and have much lower emissions at the same time.

## CHAPTER 3

### RESEARCH METHODOLOGY

The whole test rig for the research is described in this section. It also covers all the equipment used for the experiment, such as the Horiba gas emission analyzer, the scanning mobility particle sizer (SMPS), the AVL smoke meter, and the engine control system. The Ricardo WAVE model is also introduced. Figure 3.1 gives the overview of the test cell.

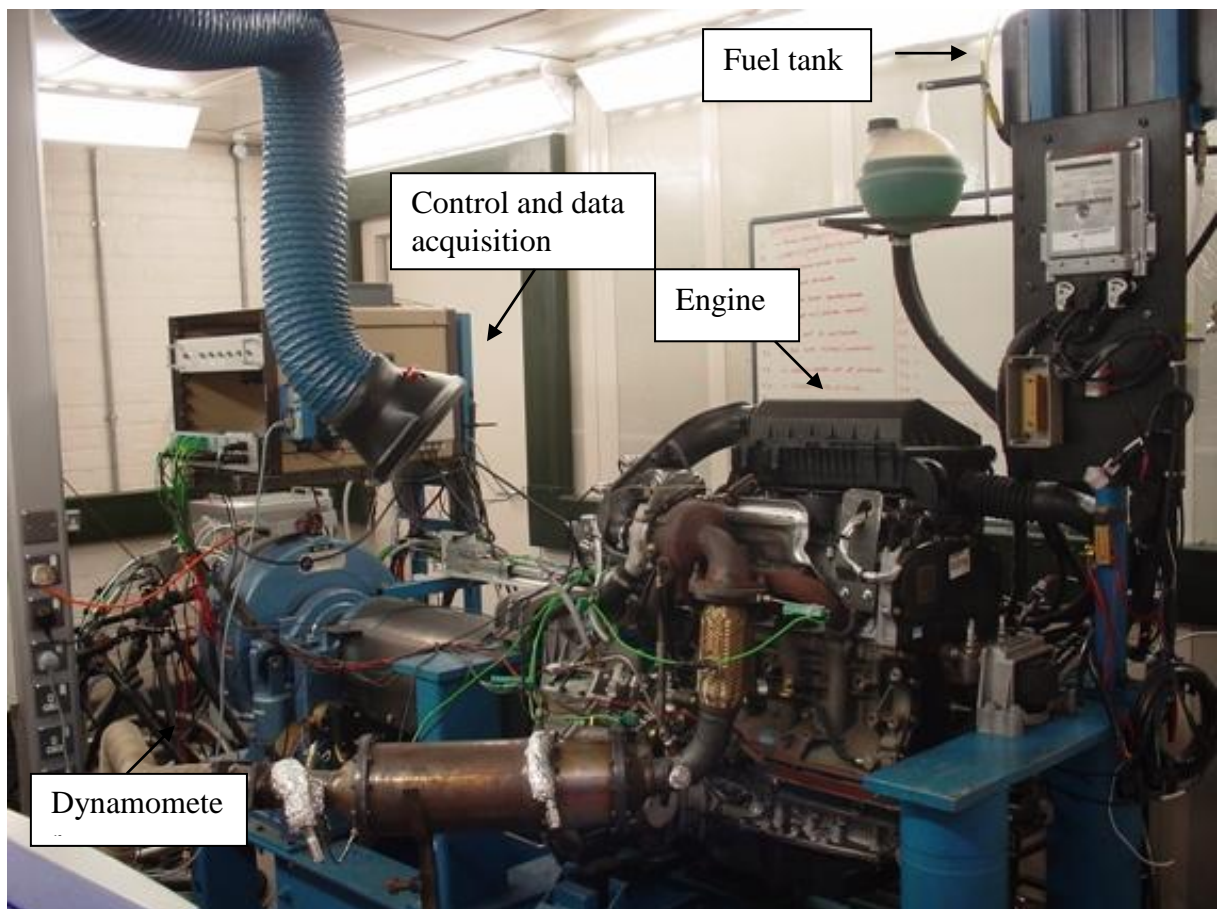


**Figure 3.1** The Ford Puma diesel engine test cell

### 3.1 Engine and Instrumentation

#### 3.1.1 Engine

The engine used in the research was an I4 Ford Duratorq diesel engine, codenamed ‘Puma’ (Table 3.1). Its commercial application includes the Ford Transit Van, the Ford Mondeo and Jaguar X type cars and the specification is shown in Table 3.1.

**Table 3.1** Engine specifications

Engine Type	Ford 130 PS Puma upgrade TDCI
Bore	86 mm
Stroke	94.6 mm
Connecting Rod Length	160 mm
Compression Ratio	16.6
Engine Capacity	2198.05 cc
Max Power	96 kW ( $\pm 5\%$ )@3500 rpm
Max Torque	310.0 Nm( $\pm 5\%$ )@1600-2500 rpm
Max No-load Speed	4900 rpm $\pm 50$ rpm
Max Cylinder Pressure	150 bar

The engine is equipped with a Variable Geometry Turbocharger (VGT), cooled EGR, a common rail direct injection system, a standard DOC and DPF. It was calibrated to EURO IV emission standard. Figure 3.2 shows its characteristics.

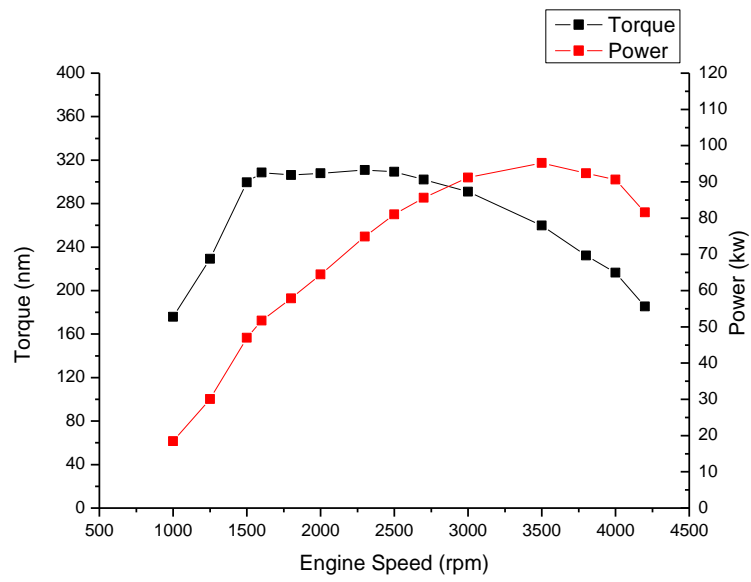


**Figure 3.2** Engine characteristics graph

### 3.1.2 Engine Start and Control System

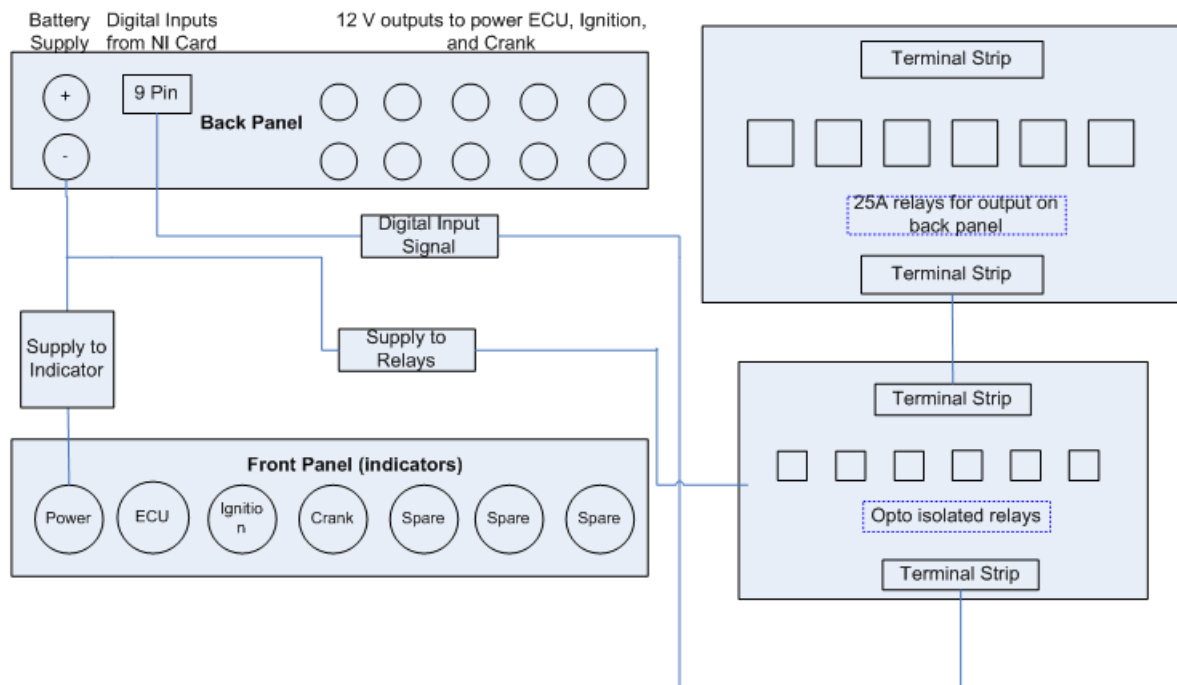


**Figure 3.3** Engine's starting system

The engine's starting system (Figure 3.3) is powered by a Ford 12V battery (NO.160103), which also powers the engine motor starter. Through a Labview interface, the switches for the ECU power, fuel injection ('Ignition') and motor starter ('Crank') are manually controlled. When they are turned on, digital signals are created by an USB 6218 National Instrument (NI) card (details in 3.1.6), and sent to the relays. At the same time, the indicators on the front panel are on. Once the engine is started, the 'Crank' signal has to be switched off to avoid damages to the motor starter.

The engine control system was purchased from ATI Accurate Technologies. It includes a VISION Network Hub/ VN12, a standard calibration package, a USB A-B over-molded cable, a DC/CAN 180/180 5 pin Lemos (1B size) cable and an ECU CAN interface cable. The basic idea, through its communication to the engine ECU (Figure 3.4), is to achieve real time data acquisition and calibration/control over the engine.

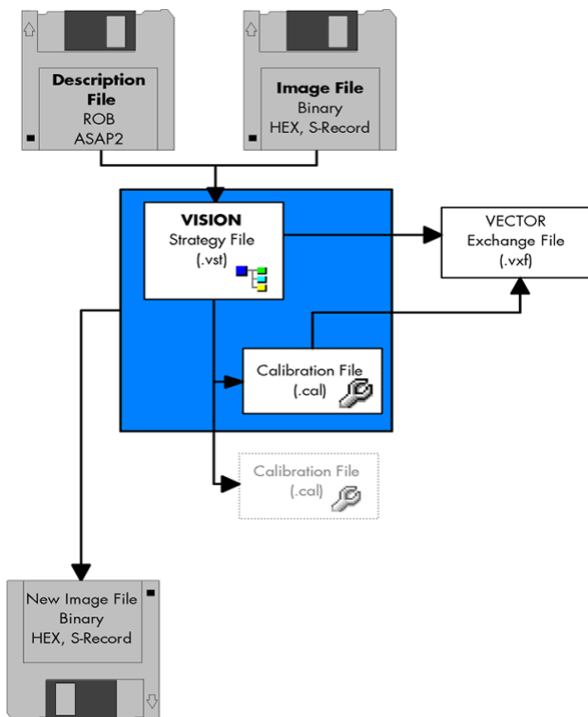


**Figure 3.4** How the control system works with ECU files

Before the control system starts to work, a specialized calibration is required and during its application, a project file and a strategy file are needed. The former contains information on the test set-up and tells the control system what test hard-wares are being used, along with any unique properties of these devices. The latter stores the device description information, memory images and system settings, which are usually the control module under development. Both of them are supplied by the engine suppliers. For different test purposes, such as for different emissions standards, different calibration files can be used.

The interface of the ATI engine control system is shown as Figure 3.5. A full list of all the engine parameters can be displayed in the screen and recorded real time. Most of the parameters are self-adjusted based on the engine map for different calibration files, and some can be manually adjusted during the test.

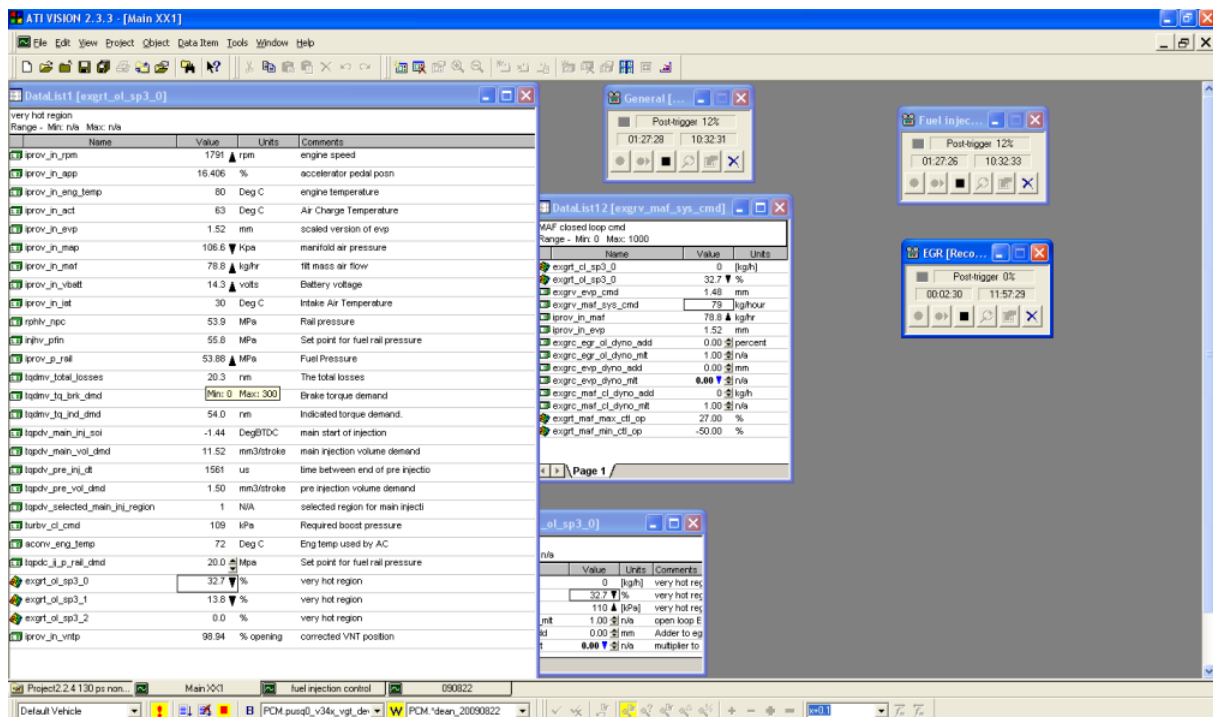


**Figure 3.5** The interface of the ATI engine control system

### 3.1.3 Dynamometer

The dynamometer used in the test was an inherently reversible EC38TA Eddy current dynamometer produced by Froude Consine Limited (Figure 3.6). It is cooled by water running in a closed flow circuit while the rotor operates in a dry gap. Its speed and load were measured through a sixty tooth wheel and magnetic pulse pick-up and a strain gauge load cell respectively.

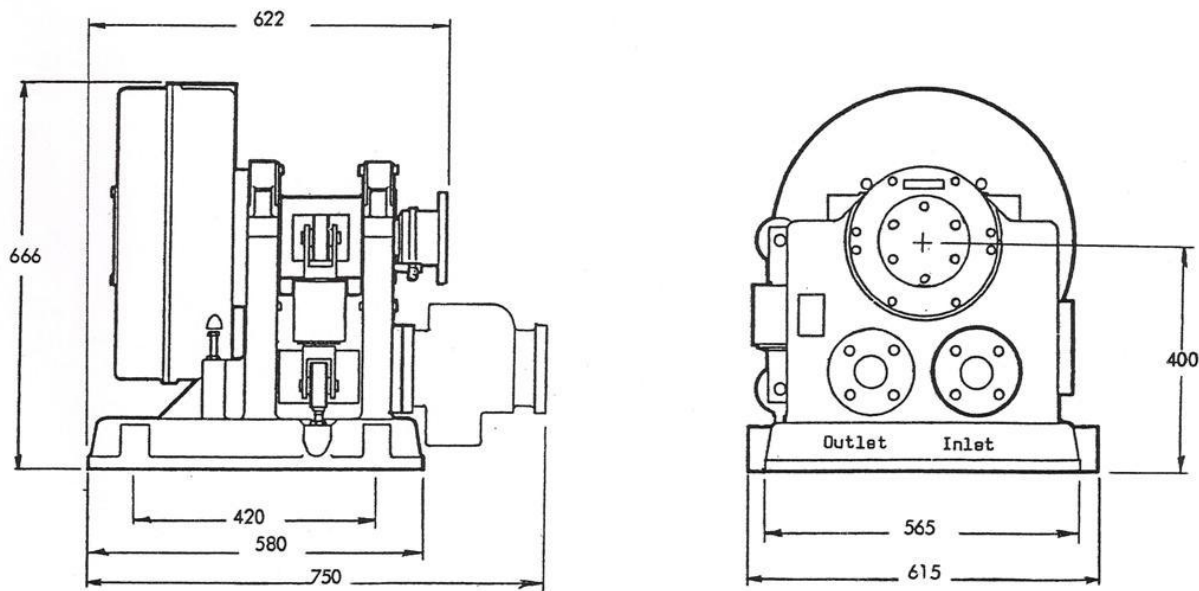


**Figure 3.6** Overall dynamometer dimensions (mm)

The dynamometer has a maximum torque of 477.5 Nm and the power curve is shown in Figure 3.7. The requirement for the cooling water is a minimum flow rate of 6,350 litre/hr and a minimum pressure of 0.75 kg/cm<sup>2</sup> under all operating conditions. For safety reasons, the water outlet orifice plate was connected with a differential pressure switch, which could trip a plant shutdown once the differential pressure was below 0.35 kg/cm<sup>2</sup>.

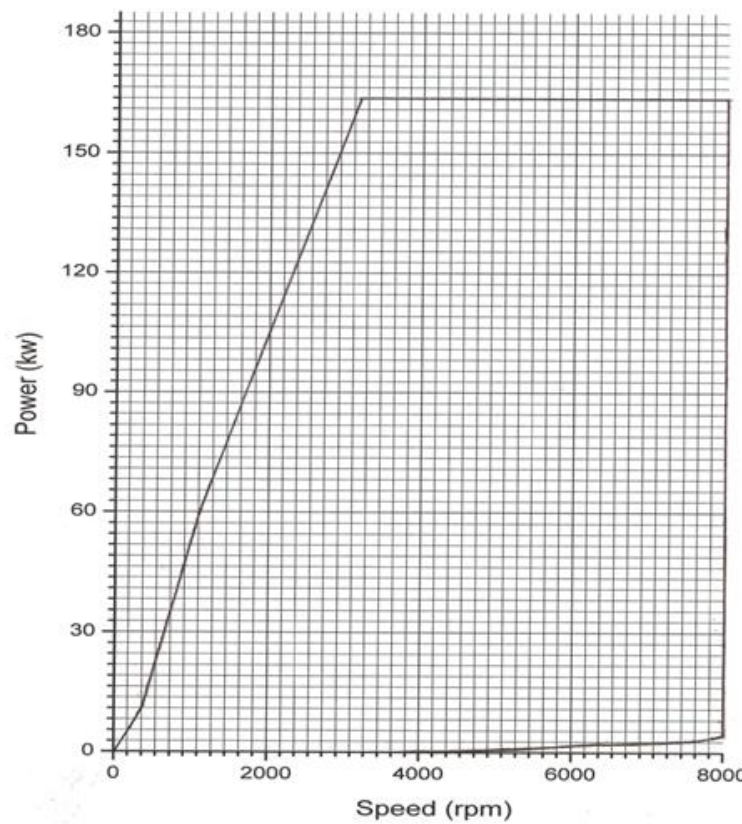


**Figure 3.7** Dynamometer power curve (mm)

Referring to Figure 3.6, the half coupling on the dynamometer was used to connect the engine through a driveshaft and for the test rig, the NDE Clarke A Type (Figure 3.8) with  $L_z = 490$  mm and  $L_a = 60$  mm. For the safety reasons, a shaft guard was installed.

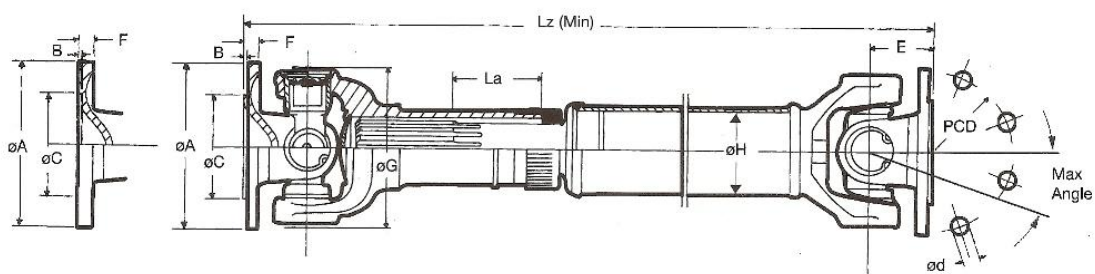


**Figure 3.8** NDE Clarke drive shaft

Two adaptors (Figure 3.9) were also adopted for the connections from the driveshaft both to the dynamometer and the engine respectively. Each is 30 mm thick and that gives a total install length of 550 mm.

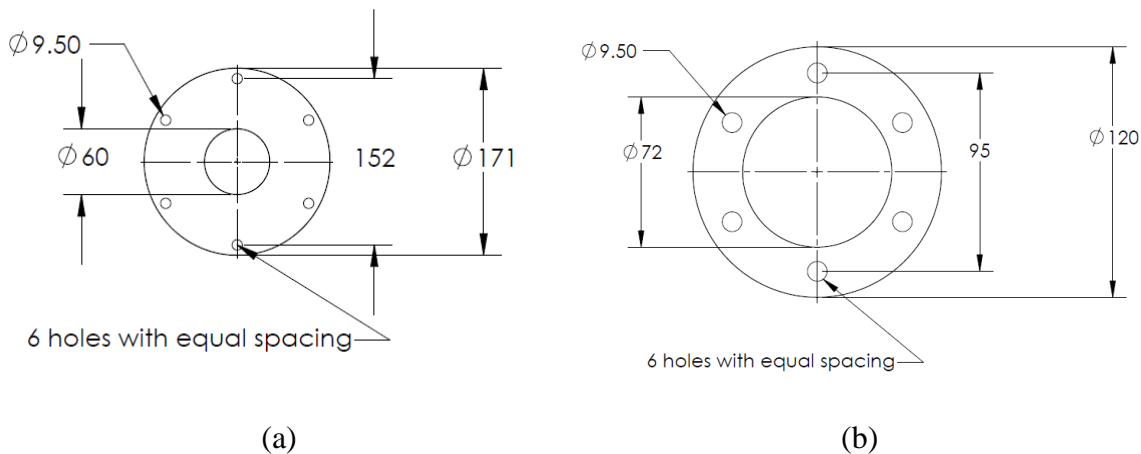


**Figure 3.9** (a) The dimension of the adaptor for the dynamometer end; (b) the dimension of the adaptor for the dynamometer end

### 3.1.4 Dynamometer Control System

#### (a) CP CADET System

The control system used for the dynamometer was the CADET system from CP Engineering (from May 2007 till October 2008). It is computer based and it can achieve manual or automatic control over the engine, when a pre-defined test is run. The system comprises the following main parts: (1) a PC running the CADET software, with a user interface such as a winged keyboard, a mouse and a monitor; (2) a control cabinet; (3) a transducer box; (4) a throttle actuator; (5) others including the connection looms, a electric box, an emergency stop loom, a interface enclosure etc.

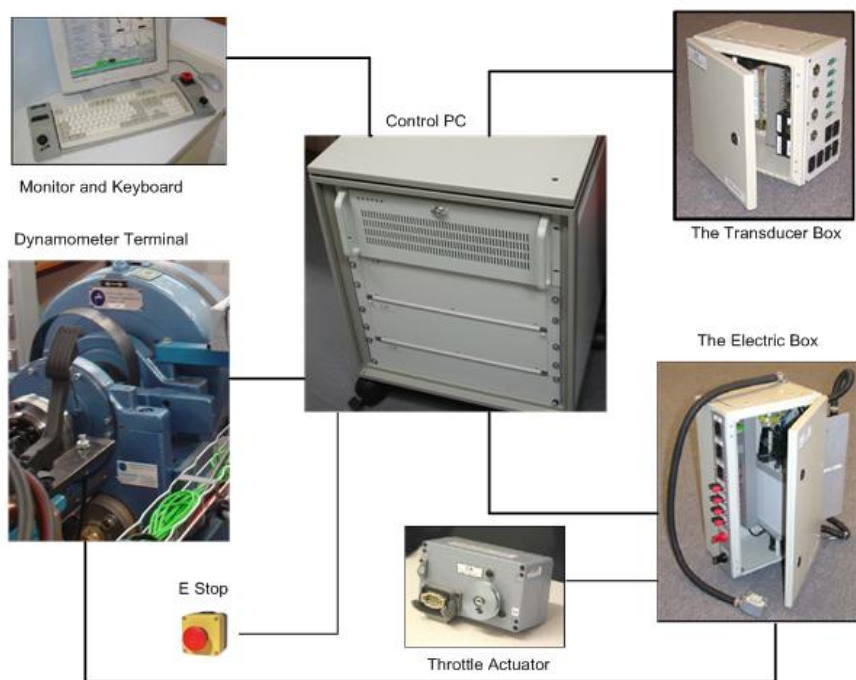


**Figure 3.10** The CADET system

As Figure 3.10 shows, the control cabinet is connected with the dynamometer terminal box with a 15 meter 37 way D-type to 37 way D-type loom for the signals such as load cell and speed pick up while another loom of the same type supplies connections between the cabinet and the engine electric box. The transducer box is mounted in the cell and it contains several modules to support a variety of transducers such as the pressure transducer, the platinum resistance thermometer (PRT), and the thermocouple inputs. The electric box is connected with a 220 V power supply as well as a cell battery, which also supplies power to the engine starter motor. The oil pressure switch and any hall-effect type speed sensors are powered by a 24 V supply.

The throttle actuator consists of a permanent magnet DC motor, a servo-potentiometer a single reduction gearbox, a cable drum and an output shaft, which connects the engine throttle with an industrial tension cable. Its structure is as follows:

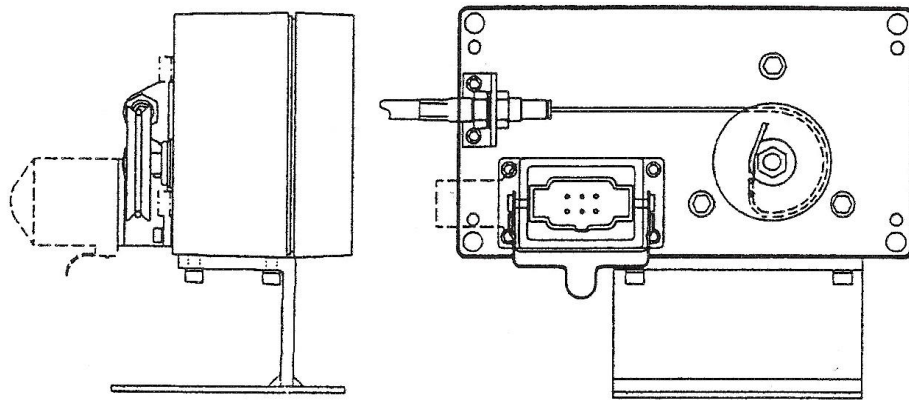


**Figure 3.11** The sketch of the throttle actuator (supplied by CP Engineering)

#### (b) Schenck System

From October 2008, another control system - Series 2000 D/W from Schenck was used to control the dynamometer. It consists of one power supply and one control unit LSG 2000 (Figure 3.12).

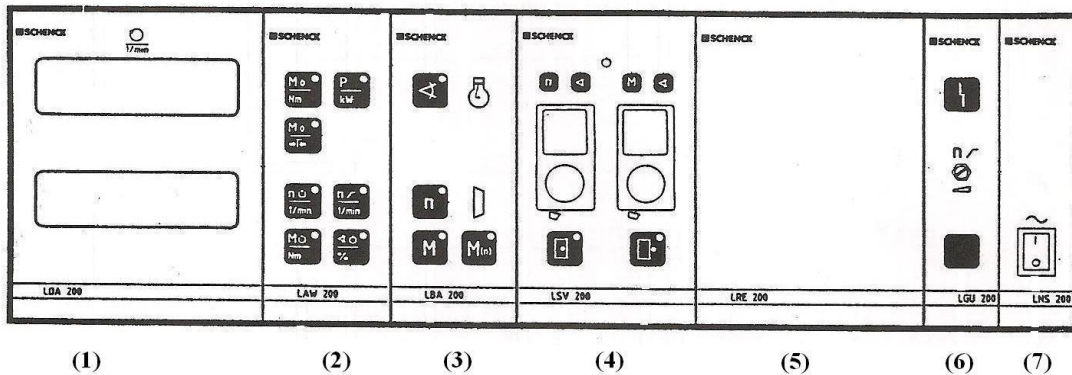


**Figure 3.12** Control unit LSG 2000

The control unit includes: (1) digital indicator; (2) selection of indication; (3) selection of mode of operation; (4) pre-selection of command value; (5) control unit; (6) pre-setting of limiting values and monitoring; (7) mains switch. It can perform several types of

controls over the dynamometer such as speed control, torque control and linear or squared curve control. The engine can also be position controlled by it, when it operates at a constant throttle angle.

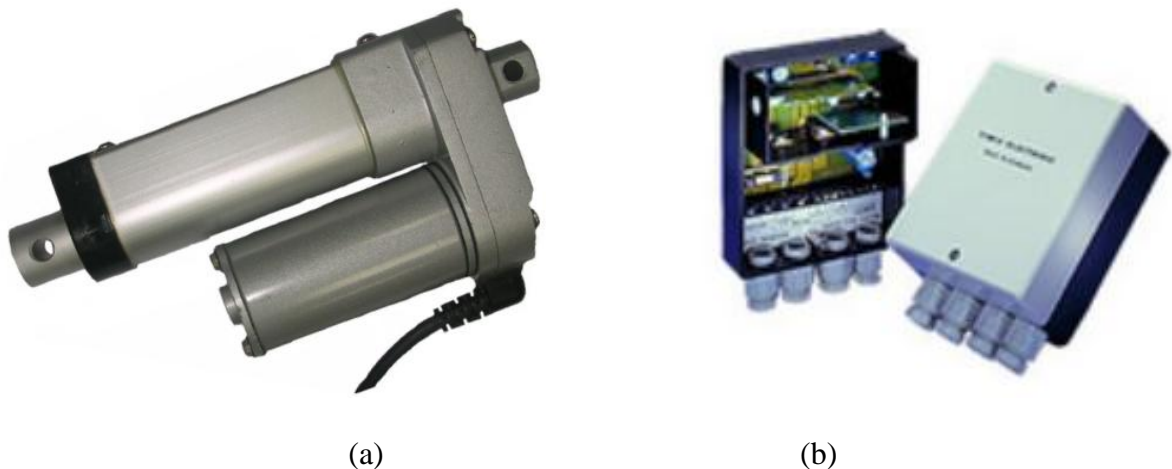


**Figure 3.13** (a) actuator (b) actuator control

The new throttle control system consists of an IDM3 actuator and an actuator control IDSV01 (Figure 3.13), which operates from 0-5 V signals. The actuator was bought from Industrial Devices Limited, and its specification is shown in Table 3.2 (Appendix Table A1, Figure A1). The actuator control corresponds to a voltage signal, which is created by an USB 6218 National Instrument card (details in 3.1.6), and drives the actuator to the position represented by the signal.

**Table 3.2** Actuator specification

Stroke	150 mm
Speed	45-57 mm/s
Capacity	120 N
Power Supply	24V DC
Protection	IP65

### 3.1.5 In-cylinder Pressure Data Acquisition

For the in-cylinder pressure measurement, a Kistler quartz pressure sensor (Type: 6056A42) was used. The sensor is installed in Cylinder 1 (Figure 3.16) with a glow plug adaptor (Type 6542Q18X2) and its specification is shown as in Table 3.3:

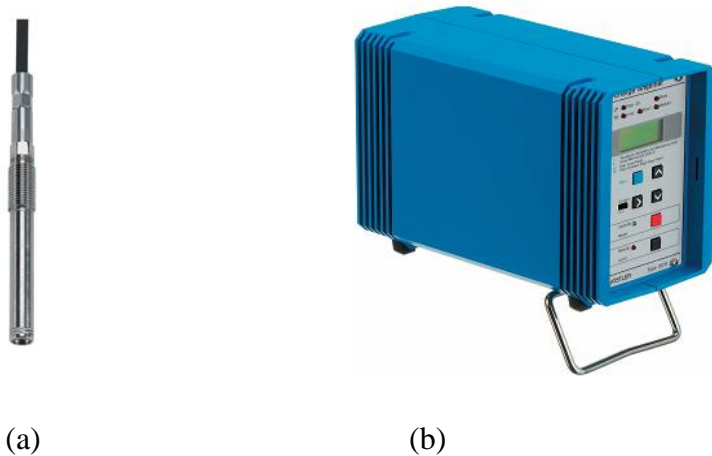


**Figure 3.14** (a) Kistler pressure sensor (b) Charge amplifier

**Table 3.3** Kistler pressure sensor specification

Measuring range	bar	0...250
Overload	bar	300.0
Sensitivity	pC/bar	≈-20
Natural Frequency	kHz	≈160 (sensor)
Non linearity	% FSO	<±0.3
Operating temperature range	°C	-20...350
Thread		M5 × 0,5
Front diameter	mm	4.4
Thermal shock dp (short time)	bar	<±0.5

A mains-operated, microprocessor controlled single-channel charge amplifier (Type: 5011B10Y50) (Figure 3.14b) was used to convert the electrical charge produced by the sensor into a proportional voltage signal, which was then recorded through a National Instrument PCI6251 card. The specification of the amplifier is shown in Appendix Table A2. It has a

drift compensation function (Figure 3.15), which is common in engine measuring technology for un-cooled sensors. The drift is detected as a slowly changing signal and is compensated either positively or negatively by using a closed-loop control. The reference line is always kept on zero.

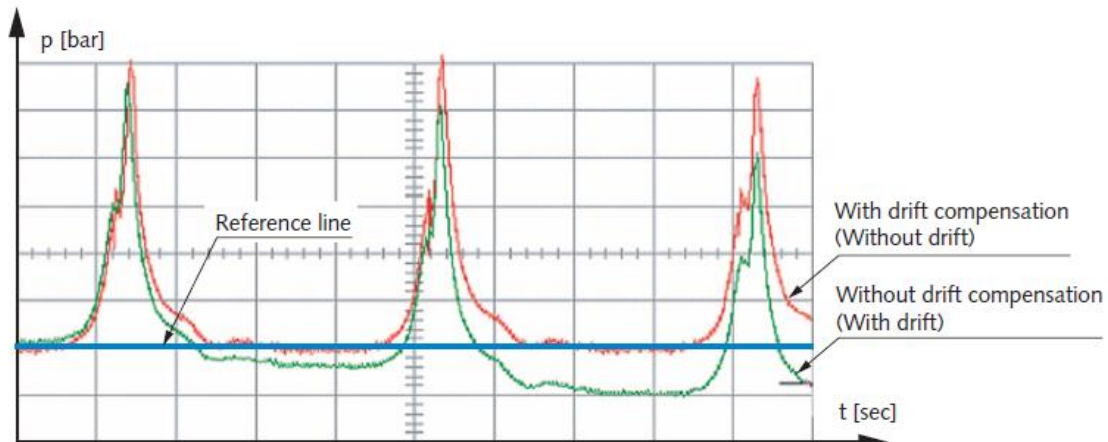


**Figure 3.15** Pressure measurement of the charge amplifier with/without drift compensation

**Table 3.4** Shaft encoder specification

Signals	square wave
Operating voltage	5 V $\pm$ 5 %
Scan frequency	300 kHz
Output	5 V Line-Driver
Output signals	2 channels A and B: phase-shifted 90° electrically, 360 pulses per revolution; zero-pulse: 1 pulse per revolution 90° electrically; all signals with inversion possible
Permissible shaft loads	axial 10 N, radial 20 N
Rotating speed	Max. 6000 rpm.
Vibration	10 g (20 Hz up to 2000 Hz)

An A500/016(41500043) type shaft encoder from AMI Elektronik is installed in alignment with the engine crank shaft through a flexible coupling. As the specification in

Table 3.4 shows, two  $90^{\circ}$  phase-shifted signals A and B, along with their inversions are generated for each crankshaft revolution, which can be used to identify the crankshaft position. For the same revolution, a zero pulse is also generated for the use of triggering the in-cylinder pressure measurement. However, there are two zero pulses for one whole engine cycle (two crankshaft revolutions), and the camshaft signal (one per engine cycle) is then used to select and keep one of them by using an octal D-type flip-flop.

The in-cylinder pressure sensor signals after the amplifier are acquired by a high speed M series National Instrument card, Model PCI-6251. Its specification is shown in Table 3.5.

**Table 3.5** PCI-6251 National Instrument card specification

Product Name	PCI-6251
Analogue Input Channels	16 (Single-Ended) 8 (Differential)
Analogue Output Channels	2
Analogue Sample Rate	1.25 MS/s
Resolution	16 bits
Maximum Voltage Range	-10 V , 10 V
Digital I/O	24 (Bidirectional)
Max Clock Rate	10 MHz
Logic Levels	TTL
Counters	2 (32 bits)

The in-cylinder pressure signal is sent to Analogue Input (AI) channel 0 of the NI card (Appendix Figure A3), and signal A from the shaft encoder, which gives 360 pulses per revolution, is fed into the PFI 1.0 as the clock. The manipulated signal from the monitoring of the zero pulses and the camshaft signal is fed into PFI 1.1 to trigger the in-cylinder pressure data acquisition in AI channel 0. In the tests, the in-cylinder pressures in 50 engine cycles were recorded each time, and the results were averaged before the combustion analysis.

The heat release rate  $dQ/d\theta$  is calculated using the following equation (Heywood 1988):

$$\frac{dQ}{d\theta} = \frac{\gamma}{\gamma-1} p \frac{dV}{d\theta} + \frac{1}{\gamma-1} V \frac{dp}{d\theta} \quad (3.1)$$

where  $\gamma$  is the ratio of specific heats ( $c_p/c_v$ ),  $\theta$  is the crank angle,  $V$  and  $p$  are the instantaneous volume of the engine cylinder and the instantaneous cylinder pressure respectively.

### 3.1.6. Temperature and Pressure Measurement

The measurement points of the test system are shown in Figure 3.16. They include the temperatures for the compressed air before the intercooler (T1), the exhaust before the DOC (T2), the filter inlet air (T3), the engine coolant after the heat exchanger (T4), the engine oil (T5), the fuel cooling water (T6), the turbocharger (T7), the dynamometer cooling water (T8), the engine coolant before the heat exchanger (T9), the fuel (T10), the exhaust after the DPF (T11) and the exhaust before the DPF (T12) and the pressures for the filter inlet air (P1), the exhaust before the DOC (P2), the exhaust before the DPF (P3), the exhaust after the DPF (P4), the engine coolant before the heat exchanger (P5), the compressed air after the intercooler (P6), fuel (P7), and the compressed air before the intercooler (P8). The 12 thermocouples are K type stainless steel sheath ones, 3mm × 0.15m (Appendix Table A3), bought from RS and their output are sent to three 4 channel TCK-4 thermocouple amplifier units (Appendix Table A4, Figure A2), which were purchased from Audon Electronics for a high level voltage output to reduce the noise and to compensate for the cold junction, before being read by the data acquisition card. The pressure sensors are EPT 3100 media isolated pressure transmitters (Appendix Table A5), from EuroSensor, the maximum range of which are 2 bar. The sensors were all calibrated.

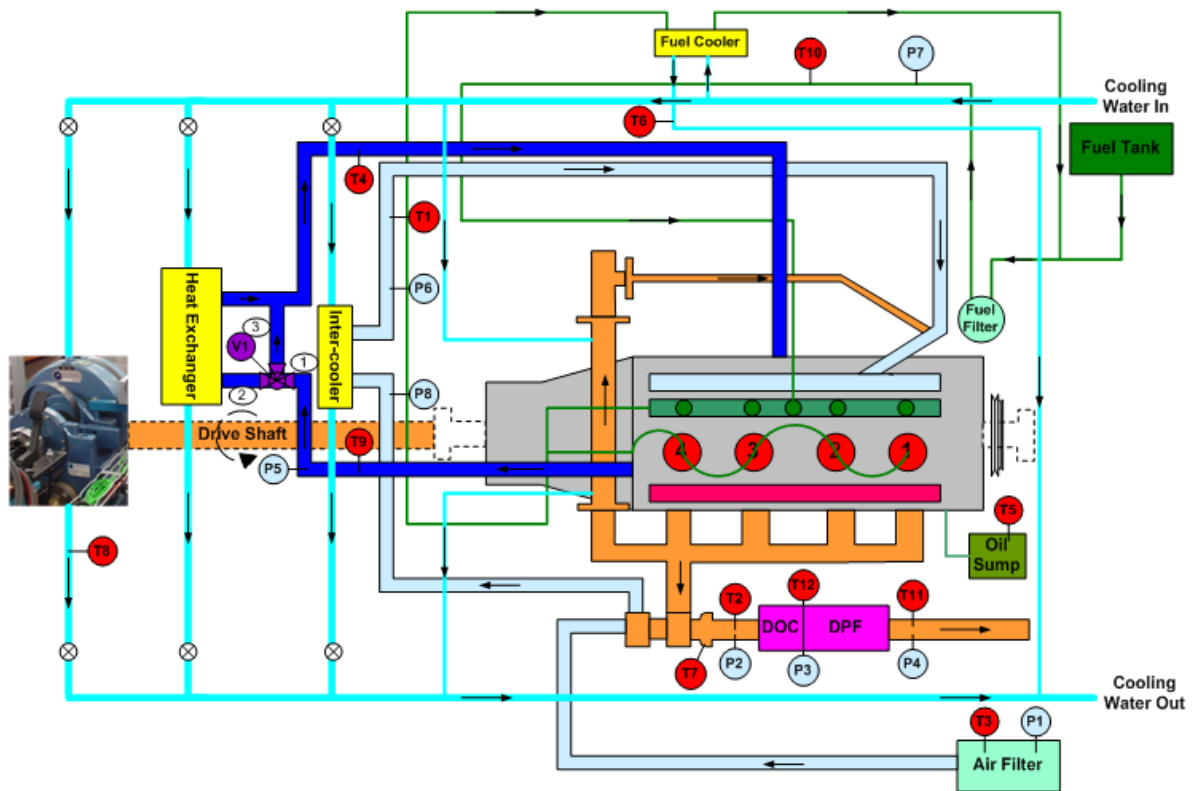


**Figure 3.16** Layout of the engine test system

A National Instrument card USB-6218 (Appendix Figure A4) was used for the data acquisition of all these temperatures and pressures. Its specification is shown as follows (Table 3.6). The Analogue Input (AI) channels 0-7 are used for the 8 pressure sensors P1 - P8, and AI channels 8 -19 for the 12 thermocouples T1 - T12; AI 20 for the engine torque signal, read directly from the dynamometer. Another 5 channel AI 21-25 are for the signal outputs from Horiba MEXA 7000, namely THC, CO (high range), CO<sub>2</sub>, CO (low range), NO<sub>x</sub>.

**Table 3.6** USB-6218 National Instrument card specification

Product Name	USB-6218
Analogue Input Channels	32 (Single-ended) 16 (Differential)
Analogue Output Channels	2
Analogue Sample Rate	250 ks/s
Resolution	16 bits
Maximum Voltage Range	-10 V , 10 V
Digital I/O	8 (Input only), 8 (Output only),
Max Input/Output Range	0 V, 5.25 V / 0 V, 3.8 V
Logic Levels	TTL
Counters	2 (32bits)

### 3.1.7 The Fuel and the Fuelling System

The fuels used in the study were all supplied by Shell and their properties are listed below (Table 3.7). Standard European diesel fuels conforming to the EN590 specifications were used in most tests and only in the alternative fuel tests, rapeseed methyl ester (RME) and gas to liquid (GTL) diesel, blended with standard diesel by a volume of 10 % were applied.

**Table 3.7** Test fuel properties

PROPERTY	UNIT	Diesel	RME	GTL Diesel
Ester content	% (m/m)	/	99.44	/
Density @ 15°C	kg/m <sup>3</sup>	834.9	883.3	781
Viscosity @ 40°C	mm <sup>2</sup> /s	2.87	4.441	3.1
Flash point	°C	68.5	171.5	91
Sulphur content	mg/kg	8.6	<3.0	<3.0
Carbon residue	% (m/m)	0.13	<0.1	<0.3
Cetane number		51.1	51	77
Total contamination (particulate)	mg/kg	6.0	1.6	1.6
Lubricity	µm	402	/	612
Distillation (Initial Boiling Point)	°C	181.3	/	204
Aromatics	%,m	/	/	<0.1

The diesel fuel is transported from the fuel store through a centrally controlled pump (Figure 3.16) and is kept in a 30 litre fuel tank in the test cell, about 2m above the floor. The fuel is filtered by a Ford YC15-9176-AB filter before going into the high pressure pump of the common rail. For the alternative fuel tests, the 10 % RME and GTL diesel were blended before being put into the fuel tank.

### **3.1.8 Cooling System**

As Figure 3.16 shows, three major coolers were used for the engine test system. A GL320-1428-5 heat exchanger from E J Bowman was used for the engine coolant. It is a standard three-pass shell and tube type, intended for closed circuit cooling (heating) of electrical equipment using demineralised water supplied by the central cooling tower. It has cupro-nickel tubes, cast aluminium shell and cast iron end covers, and the three pass flow on the tube side will give the best performance when the two flow rates are similar.

A thermal valve (Appendix Figure A5) was also set up at the same time for the coolant temperature control as V1 shown in Figure 3.16. The valve works in the diverting/by-pass operation, when a single temperature fluid - the coolant from the engine passes over the sensing elements in Port 1 and is split leaving the valve in either Port 2 or Port 3, thus achieving smooth control. The temperature is kept between 77 °C to 85 °C and the maximum pressure is 12 bar.

The intercooler used was also from E J Bowman, and it is a FC100-4074-2 model, which is suitable for engines up to 110 KW (147 HP). The temperature of the cooled compressed air was measured as T1 in Figure 3.16 and it can be adjusted by regulating the cooling water valve. The returning fuel was cooled by an EC-80-3145-1 model cooler, from

the same company, before being led back to the fuel tank. An extra cooler EC12A was used to cool the engine oil.

## 3.2 Exhaust Measurement

### 3.2.1 Engine Exhaust Gas Emissions

The emission gas of the engine was directly sampled and sent through a temperature controlled (190°C) heated line to the Horiba MEXA 7100 DEGR, where the gas concentration was measured. The operation gases include burner air (O<sub>2</sub> and THC component), fuel (H<sub>2</sub> 40 % ± 1 % /He), O<sub>2</sub>, N<sub>2</sub> and shop air (THC under 10 ppmC) and the calibration gases include zero N<sub>2</sub>, CO, CO<sub>2</sub>, NO<sub>x</sub>, O<sub>2</sub>/N<sub>2</sub>, THC/air or N<sub>2</sub>. Its measurement components and accuracy are listed in Table 3.8 (%FS is the percent of range full scale):

**Table 3.8** Horiba MEXA-7100 DEGR component specifications

Model	Comp.	Method	Range	T90	Noise
AIA-260	CO-L	NDIR (250 mm cell)	100-3K ppm	3.5 s	±1.0 % FS
	CO-H	NDIR (10 mm cell)	1-10 % vol	2.0 s	±1.0 % FS
	CO <sub>2</sub>	NDIR (10 mm cell)	1-16 % vol	2.0 s	±1.0 % FS
FCA-266	THC	Hot-FID	100-20K ppmC	2.0 s	±1.0 % FS
	NO <sub>x</sub>	CLD (atmospheric)	100-5K ppm	3.5 s	±1.0 % FS
IMA-262	O <sub>2</sub>	MPD	10-25 % vol	2.5 s	±1.0 % FS
	EGR-CO <sub>2</sub>	NDIR (10 mm cell)	1-10 % vol	2.0 s	±1.0 % FS

The methods used for the measurements are:

Non-dispersive Infrared (NDIR) for CO - The principle of NDIR is based on the fact that a molecule, consisting of different atoms absorbs infrared energy at specific wavelengths and that the degree of absorption is proportional to the concentration at a constant pressure.

Flame Ionization Detection (FID) for HC - FID uses the phenomenon in which ions, generated by the heat energy when hydrocarbons are introduced into a hydrogen flame, are proportional to the number of carbon atoms in the sample.

Chemiluminescence (CLD) for NO<sub>x</sub> - Samples with NO and O<sub>3</sub> are mixed in a reactor, where NO is oxidized to NO<sub>2</sub>. Part of the NO<sub>2</sub> generated is in an excited state and when it returns to the ground state, it releases the energy as light, whose degree is directly proportional to the quantity of NO molecules before reaction. Thus NO concentration can be acquired by measuring the amount of light.

Magneto-pneumatic Detection (MPD) for O<sub>2</sub> - MPD relies on the fact that oxygen has a much greater response to a magnetic field than other gases. So when the sample gas flows through a magnetic field, a pressure change is caused according to the concentration of oxygen.

### **3.2.2 Engine Smoke Emissions**

AVL Smoke Meter 415SG002 is a filter-type meter used to measure the soot content in the exhaust of the engine and its specification is given in Table 3.9. It works by taking a subset of the exhaust gas from the exhaust gas line with a probe and sucking through a filter paper. The blackening of the filter paper is then measured with a reflectometer, and described as a factor of Paper Blackening (PB), whose values vary from 0 (clean) to 10 (absolutely

black). PB primarily depends on the soot concentration in the exhaust gas as well as the "effective filter length" (exhaust gas volume related to the filter area.). It is presented as:

$$PB = \frac{100 - R_R}{10} \quad (3.2)$$

$$R_R = \frac{R_P}{R_F} \cdot 100\% \quad (3.3)$$

where  $R_P$  is the reflectometer value of sample,  $R_F$  is the reflectometer value of the unblackened paper and  $R_R$  is the relative brightness of the sample (relative radiance factor).

The result of the smoke measurement is usually displayed as filter smoke number (FSN). FSN is the value of PB when the corresponding effective sampling length is 405 mm and the sampled volume is related to 298 K and 1 bar.:

**Table 3.9** AVL smoke meter specifications

Measurement Range	Smoke Value: 0-10 FSN Soot Concentration: 0-32000 mg/m <sup>3</sup> Pollution Level: 0-100 %
Resolution	0.001 FSN, 0.01 mg/m <sup>3</sup> , 0.01 %
Repeatability	$\sigma \leq \pm(0.005 \text{ FSN} + 3 \% \text{ of measurement value})$
Exhaust Gas Back Pressure	-100—400 mbar
Permissible exhaust temperature at sampling point	600 °C max

### 3.2.3 Engine Emission Particulate Number Size Distribution

A scanning mobility particle sizer (SMPS) (Model 3936) from TSI was used in the test to measure the particulate size distributions and concentrations. It consists of a Model 3080

electrostatic classifier (EC) (Figure 3.17), a Model 3775 condensation particle counter (CPC) and two differential mobility analysers (DMAs), one Model 3081 DMA and one Model 3085 nano DMA, which have a measuring range of 10-1000 nm and 2-150 nm respectively.

The main parts of the EC include an impactor, a sheath-air flow controller, a neutralizer, a high-voltage controller and a DMA, which work together to process a polydisperse aerosol and provide a mono-disperse output: the impactor removes particles above a known particle size by inertial impaction; the sheath flow controller maintains a constant flow through the sheath flow loop; the neutralizer supplies a known charge distribution on the aerosols entering the DMA and the charge on the centre rod of the DMA is supplied by the high voltage controller.

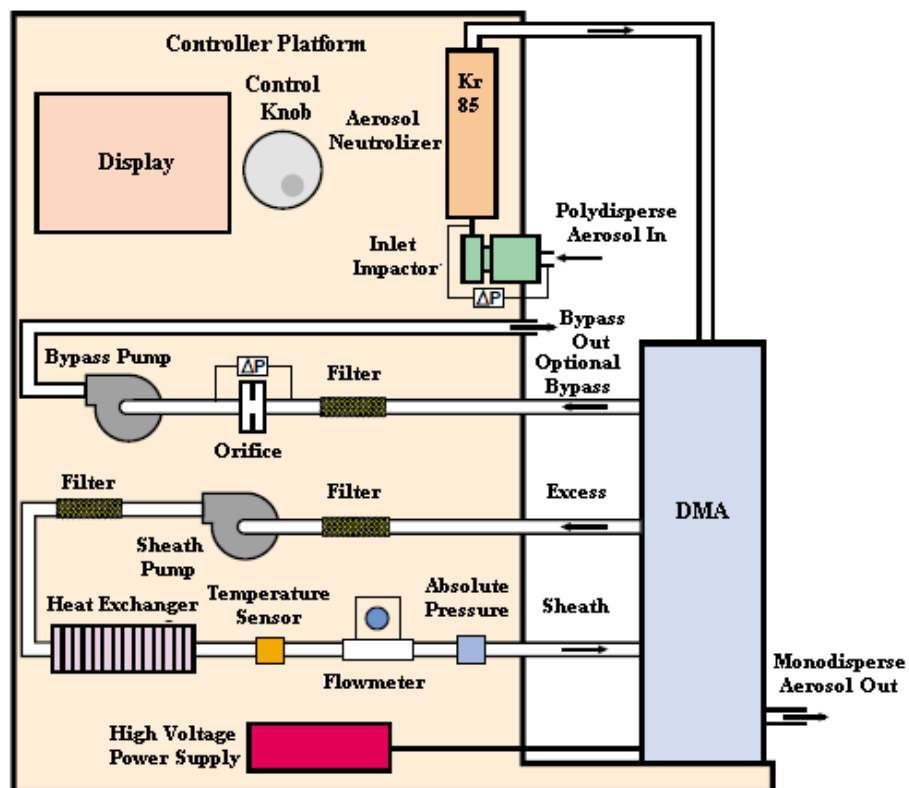


**Figure 3.17** Schematic Diagram of the EC

The rod is maintained at a controlled negative voltage, and due to the electric field, it attracts positively charged particles, which are carried axially downward with the sheath airflow and those with a narrow range of electrical mobility can exit the DMA as the mono-disperse flow through a twelve-hole slit in the rod. Particles with negative charge stick to the outer electrode which is grounded and the neutral ones are removed unaffected with the excess flow.

In a CPC, heterogeneous condensation is used to grow particles, their concentration number can then be counted. Thus, the smallest particle size which can be detected is determined by the saturation ratio of the condensing vapor ( $p$ ), which is mostly butyl alcohol. The relationship between the saturation ratio and the minimal particle size is controlled by the Kelvin equation:

$$p / p_s = \exp[4\sigma M / \rho R T d^*] \quad (3.4)$$

where  $p_s$  = the saturation vapor pressure at a given temperature,  $\sigma$  = the surface tension,  $M$  = molecular weight,  $\rho$  = the density of the liquid,  $R$  = universal gas constant,  $T$  = absolute temperature,  $d^*$  = the Kelvin diameter (the droplet diameter that will neither grow nor evaporate at the saturation ratio).

Once the particles have grown to an optically detectable size, they pass through a light beam and scatter light onto a photo-detector and then the number is counted.

### 3.2.4 Diluter

For any particulate number measurement instrument, there is always a specific measuring range, wherein the measurement is possible or the best accuracy of the determined

values can be reached. Particulates emitted by diesel engines are usually in high concentrations, and that requires the exhaust gas to be properly diluted to a certain level before the measurement is carried out.

A rotating disk diluter works through a disk with hemispheric cavities, which rotates on a steel block equipped with two aerosol channels. The amount of raw gas is well defined in every disk cavity and it is transported from the raw gas to the dilution air channel. The dilution air is usually heated to evaporate liquid particles, and an extra thermal block can be used to further reduce the volatiles. The dilution ratio (DR) is adjusted through the potentiometer on the control unit and it is expressed as:

$$DR = \frac{CF}{pot[\%]} \quad (3.5)$$

where CF is the calibration factor, pot is the potentiometer position.

In the tests, two thermo-diluters were used. One was a 379020A PMP model from TSI and the other was an ASET15-1 model from Matt Engineering. They supplied thermo-dilution by heating the dilution air to 300 °C (from A-B-D-C-D in Figure 3.18) (Kasper 2004) and removed the volatiles which had a great influence on the particle number measurement.

Two different dilution ratios were used in the tests for the thermal dilution. One was 90:1, and the other 542:1. For non-thermo dilution, a 379020A model diluter from TSI was used and the dilution ratio was set to 60:1.

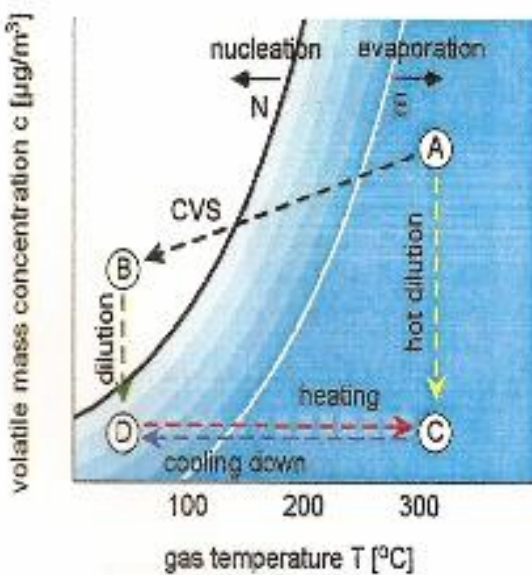


**Figure 3.18** Thermo Dilution (Kasper 2004)

### 3.2.5 Scanning Electron Microscope (SEM)

A Jeol JSM-7000F FE Scanning Electron Microscope (SEM) with Schottky emitter was used to analyze the particle morphology in the tests. It scans the sample's surface with a high energy beam of electrons, which produce signals of the surface topography information when interacting with the sample atoms. For conventional imaging, specimens must be electrically conductive, at least at the surface and electrically grounded. As the samples in the tests were captured on glass fibre filters, before placing them in the SEM specimen chamber, they were coated with metals (gold in the tests).

**Table 3.10** Jeol JSM-7000F FE SEM specification

Resolution	1.2 nm at 15 kV, 3.0 nm at 1 kV
Magnification	10 – 500,000
Sample size	150 mm max. 200 mm option
Gas used	dry nitrogen

### 3.3 DPF Regeneration

Two thermal methods were used in the tests to regenerate the DPF. One was by keeping the DPF in the furnace at a constant high temperature after a proper ramping. The other was by injecting extra fuel upstream of the DOC to raise the exhaust temperature.

#### 3.3.1 Furnace

For the off-board regeneration, the DPF was placed in the wire wound ceramic muffle chamber of a muffle furnace and ramped to a target temperature at a rate of 2 °C/minute (to ensure no substrate damage regardless of soot load), and then held at 600 °C for 5 hours. This ensured that the soot accumulated inside all burned off.

#### 3.3.2 Arvin Meritor Vaporizer

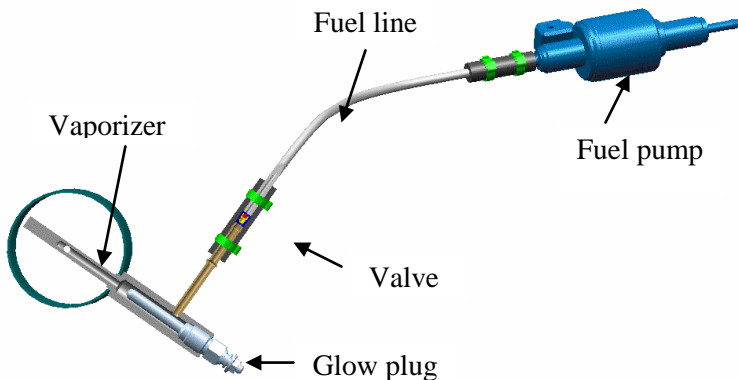


**Figure 3.19** The ZS-ArM vaporizer system

For the on-board DPF regeneration, a ZS-ArM vaporizer developed by Arvin Meritor was employed to inject a certain amount of fuels in the exhaust, which increased the exhaust temperature up to 600-650 °C (Figure 3.19). It consists of a vaporizer, a glow plug, a fuel

pump and connector, a fuel line and an ECU, which work together to initiate a complete and homogeneous regeneration with high efficiency.

A controlled quantity of fuel is delivered via the pump and is then vaporized by the heated glow plug. It reacts on the DOC with the oxygen components within the exhaust and generates the required heat. To ensure a fast light off time of the DOC, with the additional fuels, the vaporizer should be positioned as far as possible upstream of the catalyst and in such a way that there is a good mixing of vapour and the exhaust.

The ECU (Figure 3.20) was used to monitor a number of parameters such as the engine speed, the temperatures along the exhaust system, the back pressure and the fuel injection frequencies to maintain a proper DPF regeneration. The system can be initiated either manually or automatically by monitoring the back pressure. Once the correct dosage of fuel to achieve the required temperature is found, it can be saved in a table for future reference.

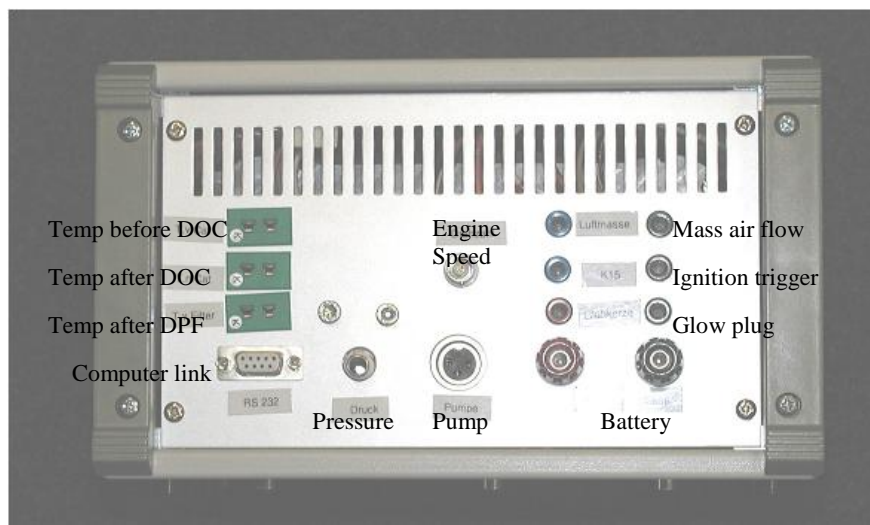


**Figure 3.20** The ECU

### 3.4 One Dimensional Engine Model

Ricardo WAVE is a computer aided engineering software for the one dimensional analysis of pressure, mass flow, and energy dynamics in various manifolds, ducts and plenums, presented as building blocks. A WAVE model can be regarded as networks of these building blocks, along with some special machinery components included in its library, such as the engine cylinders, turbochargers etc, which makes it a perfect tool for simulating the internal combustion engine. It has been widely used in the car industry for engine performance and dynamic system control development, thermal and acoustics analysis and even hybrid, combustion and emission simulation. Generally, for any simulation, the processes include: (1) Pre-processors; (2) Solvers; (3) Post-processors. Pre-processors are the first step to start the simulation and analysis. They require the users to input all the necessary information for the model to perform. WaveBuild is the primary pre-processor and in its interface, the users have to arrange and network a series of building blocks and special components for a specific target. Once the WaveBuild is successfully set up, solvers can be used to analyze the data provided by the pre-processors. The calculated results can then be viewed in the post-processors.

#### 3.4.1 Woschini Model

Two major sub-models in the WaveBuild include the Woschini model and the Diesel Wiebe model. The former uses Woschni (1967) correlation and the convective heat transfer coefficient ( $h_g$ ) is expressed as:

$$h_g = 0.0128D^{-0.20}P^{0.80}T^{-0.53}v_c^{0.8}C_{enht} \quad (3.6)$$

where D is the cylinder bore, P is the cylinder pressure, T is the cylinder temperature,  $v_c$  is a characteristic velocity and  $C_{enht}$  is an additional scaling multiplier.  $v_c$  is the sum of the mean piston speed and an additional combustion-related velocity that depends on the difference between the cylinder pressure and the pressure that would exist under motoring conditions. It is either expressed as:

$$v_c = C_1 v_m + C_2 \frac{V_D T_r}{P_r V_r} (P - P_{mot}) \quad (3.7)$$

in Woschni's original (1967) correlation or as:

$$v_c = \max \left[ \left( C_1 v_m + C_2 \frac{V_D T_r}{P_r V_r} (P - P_{mot}) \right), \left( C_1 v_m \left( 1 + 2 \left( \frac{V_c}{V} \right)^2 IMEP^{-0.2} \right) \right) \right] \quad (3.8)$$

in Woschni's modified version (1990), when a load compensation term is used.

$V_m$  is the mean piston speed;  $V_s$  is the swirl velocity;  $V_r$ ,  $P_r$ ,  $T_r$  are reference volume, pressure and temperature respectively;  $V_c$  is the clearance volume;  $V_d$  is the displacement and  $C_1$  is a dimensionless quantity, which can be expressed as

$$C_1 = 6.18 + 0.417 \left( \frac{V_s}{V_m} \right) \quad (3.9)$$

during scavenging or

$$C_1 = 2.28 + 0.308 \left( \frac{V_s}{V_m} \right) \quad (3.10)$$

when the valves are closed.

### 3.4.2 Diesel Wiebe Model

The Diesel Wiebe model incorporates: (a) an ignition delay model; (b) a Wiebe combustion model; (c) a pilot injection model.

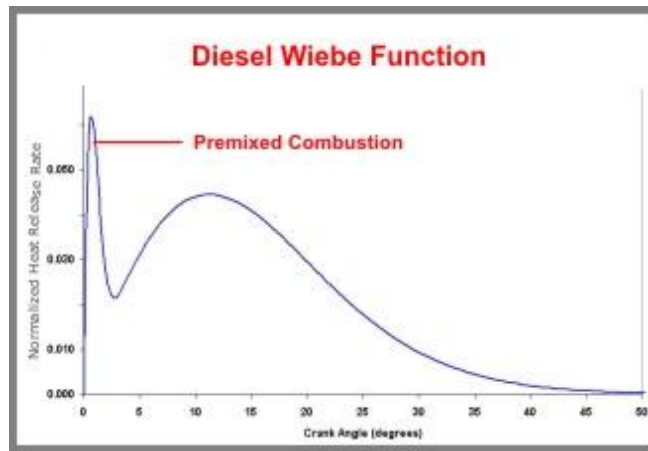


**Figure 3.21** Diesel Wiebe function in WaveBuild

- (a) The ignition delay is calculated using the in-cylinder temperature and pressure plus and the cetane number correlation. It is expressed as

$$\Delta\theta_{delay} = 323 \exp^{\min(2100C/T_{sum}, 800)/P_{sum}} \quad (3.11)$$

$$\text{where } C = \frac{67}{25 + ce \tan e} \quad (3.12)$$

$$T_{sum} = \sum_n \frac{T_c^n + T_c^0}{2} \frac{\Delta\theta_n}{\theta_{n+1} - \theta_0} \quad (3.13)$$

$$P_{sum} = \sum_n \frac{P_c^n + P_c^0}{2} \frac{\Delta\theta_n}{\theta_{n+1} - \theta_0} \quad (3.14)$$

Where  $T_c^n$  ( $T_c^0$ ) and  $P_c^n$  ( $P_c^0$ ) are the current (initial) cylinder temperature and pressure respectively;  $\Delta\theta_n$  is the time step size in degrees and  $\theta_0$  is the beginning of the ignition delay interval in degrees.

- (b) The Wiebe combustion model correlates the premixed burn, diffusion burn and late burn of the combustion, which are expressed as three different parts in the following equation:

$$W = p_f \{1 - [1 - (0.75\tau)^2]^{5000}\} + d_f \{1 - [1 - (cd_3\tau)^{1.75}]^{5000}\} + t_f \{1 - [1 - (ct_3\tau)^{2.5}]^{5000}\} \quad (3.15)$$

Where  $W$  is the accumulative mass fraction burned,  $p_f$  is the premixed fuel fraction,

$$d_f = (1 - p_f)(1 - \alpha), \quad (\alpha = 0.60[\min \Phi, 0.85])^2 \quad (3.16)$$

$$t_f = (1 - p_f)\alpha, \quad (3.17)$$

$$\tau = \frac{\theta - \theta_b}{125 \left( \frac{RPM}{BRPM} \right)^{0.3}} \quad (3.18)$$

$$cd_3 = \frac{0.055}{1 + 0.5 \min(\Phi, 0.85)} \quad (3.19)$$

$$ct_3 = \frac{3.7cd_3}{1.12 \min(\Phi, 0.85) + 1} \quad (3.20)$$

Where  $\Phi$  is the equivalence ratio and  $\theta_b$  is the start of combustion.

- (c) The pilot injection model deals with the split injection. In this model, all the pilot fuel is assumed to be burned as a premixed flame, and all the

main fuel as a diffusion flame with a late burn, for which different Wiebe functions are used. Ignition delay model is only used for the pilot fuel combustion.

### 3.5 Experimental Data Uncertainties Analysis

This part is a summary of experimental data uncertainties based on the manufacturers' product specifications. It includes accuracy and error information for: the dynamometer, the temperature and pressure transducers and the gaseous emission measuring device.

For the control of the EC38TA eddy current dynamometer, the Schenck system was used. Its torque indicator should indicate actual value  $0 \pm 1$  for the torque at zero speed. If the deviation is higher, a preload smaller than  $\pm 1\%$  of the full range can be eliminated by actuating the calibration key under the condition when the speed is zero. The effect of mains voltage changes is negligible. For the speed measurement, the gap between the actuator and the digital magnetic pickup pole piece has been adjusted so that the operating point is established above the sensitivity curves supplied.

The in-cylinder pressure measurements was carried out with the Kistler 6056A pressure sensor coupled with a Kistler 5011B charge amplifier. The pressure sensor sensitivity is approximately 20 pC/bar. The linearity was measured by the manufacturer to below  $\pm 0.3\%$  FSO (Full Scale Output). The typical amplifier's range error is  $\leq \pm 0.5\%$  when the range is  $\geq 100$  pC and  $\leq 2\%$  when the range is  $< 100$  pC. Its drift at 25 °C is  $< \pm 0.07$  pC/s. Concerning its drift compensation effect, it is comparable with high pass filter. At operating frequencies of 5 Hz, the amplitude error is  $< 1\%$ . The measured values are averaged over a time of 50

engine cycles before doing heat release analysis and this might bring the random errors to an acceptable level.

For the temperature measurement, the thermocouples were RS thermocouples and the amplifiers were from Audon Electronics. The calibration error for the amplifiers is  $\pm 1$  °C at 25°C and the gain error is  $\pm 0.75$  %. For the pressure measurement, the EPR3100 pressure sensors have a total error band of  $\pm 1\%$  FS from -10 °C to 60 °C and  $\pm 2\%$  FS from -40 °C to -10 °C & 60 °C to 85 °C.

The gaseous emissions were measured with Horiba MEXA 7100 DEGR. The errors are all  $\leq \pm 1\%$  FS based on the manufacturer's specification. For the smoke measurement with AVL Smoke Meter 415SG002, the error  $\sigma$  is  $\leq \pm (0.005 \text{ FSN} + 3\% \text{ of measurement value})$ . A scanning mobility particle sizer (SMPS) (Model 3936) was used for the PM emission measurement and the error varies under different settings.

### 3.6 Summary

This chapter describes the experiment set-up system in the tests. It includes the engine instrument, where all the tests were carried out, the data acquisition system, exhaust measuring and analyzing device and the one dimension engine model tool. The specifications of the engine and dynamometer were given in detail, along with their control systems. The mechanisms involved in the emission measurement were discussed. Major models in Ricardo Wave were also presented, which included the Woschini model and the Diesel Wiebe model.

## CHAPTER 4

### APPLICATION OF TWO CLOSELY COUPLED DPFs AS THE DIESEL ENGINE AFTER-TREATMENT SYSTEM

In this chapter, the application of two closely coupled Diesel Particle Filters (DPFs), composed of an assistant DPF and a main standard honeycomb DPF is examined. Besides the gaseous emissions, the impact to the particle size and distributions by using the new system is investigated. To achieve that, a series of tests were carried out on a light duty common-rail Euro 4 diesel engine and the emissions were measured and compared with those when a standard DOC + DPF system was used for the after-treatment. The back pressure problem existing in most after-treatment system is also studied in this chapter, through a one dimension WAVE model.

#### 4.1 Problems and Possible Solution to the Current After-treatment System

Since the first emissions regulation came into force in 1959 in California (Eastwood 2000), the car companies around the world are compelled to reduce their engine emissions accordingly. In the early days, the emissions limits could be easily met by improving the primary combustion through the enhancement to the fuel injection system. However nowadays, the gradual reduction in these limits has made this method impossible or more difficult to achieve the target, at least by working alone. This problem stimulated the

improvement of the after-treatment system, which first appeared as early as the 1890s. For diesel engines, unburned hydrocarbons and carbon monoxide are not as severe as particles and oxides of nitrogen. A DOC can oxidize most CO and HC to CO<sub>2</sub> and water in the exhaust stream but also reduces the SOF of particles. To reduce diesel particulate emissions, a DPF is thought to be necessary to meet the future regulations and it is common to have a DOC closely coupled with a ceramic monolith DPF as the main diesel engine after-treatment system, when the engine is calibrated to be more ‘smoky’ for the reduction of NO<sub>x</sub>, based on the trade-off between these two major emissions. This system has proved its success and has been adopted in most cars nowadays (Eastwood 2008). However, the current problems with it include the activation of the DOC, DPF’s high cost, regeneration control, back pressure etc. Solutions are being sought to keep its cost and back pressure low, the regeneration less frequent and more flexible, and its packaging in the car optimized.

#### **4.1.1 Cost and Installation**

Currently, the silicon carbide wall flow DPFs are the most popular used in the car industry. Their advantages such as the high melting point, high trapping efficiency have made them virtually un-replaceable. However, their high cost for the complex production and the packaging issue in a car are big problems for the manufacturers. For a passive regeneration DPF, it is preferable to install it as closely as possible to the engine exhaust tailpipe. This helps to enhance the regeneration by the use of NO<sub>x</sub> and makes it easier to raise the temperature to 600 °C, when the soot will burn. However, the SiC based DPFs are not thermally stable, and the restricted installation space makes its integration into the whole after-treatment system and the optimization of the exhaust flow difficult. One of the options is to reduce the size of the DPF; however, this is closely linked with its soot storage capacity

and the back pressure, which means that more frequent thermal regeneration is needed and higher back pressure will be caused for the same work load.

#### **4.1.2 Concept of Solutions to the Problems**

Nowadays, metallics including sintered metal, wire mesh and metal foam are used more and more for DPFs, for their good filtration properties, low thermo capacity, high specific area, and most importantly, cheap cost (Yoro et al. 1998; Koltsakis et al. 2006; Koltsakis et al. 2007). A well catalyzed DPF can also perform a good catalytic regeneration using NO<sub>x</sub> as well as showing good conversions for HC and CO (Eastwood 2000). These all lead to the idea of replacing a DOC with a low-cost, easily-regenerated DPF, which can work as a DOC and trap the particulates at the same time.

#### **4.1.3 Research Objective**

This study aims to investigate the application of two closely coupled Diesel Particle Filters (DPFs), composed of a small catalyzed metal-foam assistant DPF and a main honeycomb standard DPF, to cope with future legislation. The emissions were measured and compared with those when a standard DOC + DPF system was used for the after-treatment.

## **4.2 Engine Test Modes and Procedures**

Test fuels — Standard European diesel fuels conforming to the EN590 specifications were used for the tests (Table 3.7).

Exhaust measurement — The Horiba MEXA 7100 DEGR, AVL smoke meter (415SG002) and a scanning mobility particle sizer (SMPS) (Model 3936) were used in the

test to measure the gaseous emissions, smoke and particulate size distribution and concentration respectively. The long DMA was used, with a measuring range of 10-1000 nm. The diluter is from TSI model 379020 and the dilution ratio was set to 60:1.

Engine test modes — Transient Test A: In this test, two modes of engine operation were selected composing of one small test fractions (Table 4.1) whereby the engine was ramped between these two points. After the engine warm-up, 432 fractions are repeatedly and continuously run for 6 hours for each test section. Three sections are then run over three consecutive days for one whole test. Large amounts of soot were created for the transient acceleration and deceleration events.

**Table 4.1** Engine mode for transient test A

Mode	Engine Speed (rpm)	Torque (Nm)	Duration (s)	Ramp (s)	Settling Time (s)
1	1150	20	10	15	5
2	2600	40	10	5	5

By weighing the increase of the DPF after the tests, the comparison of the soot reduction efficiencies between the DOC and ADPF was achieved. Before each test, the DPF was regenerated in an electric oven to make sure it was clean of soot. The weighing of the DPF was carried out using an electric scale with a 0.1 g resolution. However, before this, the DPF was heated in the preheated oven (150 °C) for one hour in order to remove any water. The first test was run for 15.5 hours and the other two for 18 hours.

Transient Test B: In this test, six modes were combined as one test fraction (Table 4.2), and the engine was run at the same speed, but with different torques in each of the six

modes. One whole test was composed of seventy repeats and continuous fractions and for a duration of 6 hours after the engine warmed up.

**Table 4.2** Engine mode for transient test B

Mode	Engine Speed (rpm)	Torque (Nm)	Duration (s)
1	2000	5	90
2	2000	15	120
3	2000	60	60
4	2000	90	30
5	2000	150	60
6	2000	200	15

This testing cycle was a simplification and extension of the previous test A and the weighing of the DPF was completed using the same method.

Steady state test: Table 4.3 shows each mode in the steady-state test. These were recommended by the supplier of the engine for the study and covered different engine speeds and loads.

**Table 4.3** Engine mode for the steady state test

Mode	Engine Speed (rpm)	Torque (Nm)	BMEP (bar)	Load (%)
1	2500	83.92	4.8	27.07
2	1800	90.91	5.2	29.33
3	1800	51.58	2.95	16.64
4	3100	234.27	13.4	75.57
5	2500	248.26	14.2	80.08
6	3100	114.51	6.55	36.94
7	2500	120.63	6.9	38.91
8	1800	137.24	7.85	44.27

## 4.3 Pressure Drop along the Two Different After-treatment Systems

### 4.3.1 Transient Test A

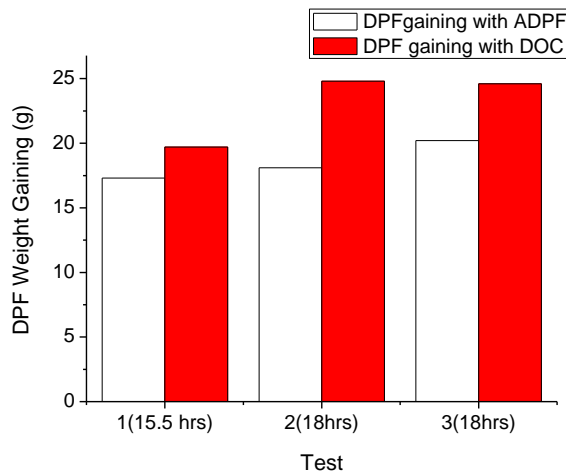


**Figure 4.1** DPF weight gaining with ADPF and DOC

Figure 4.1 presents the results of Transient Test A. Generally, a DPF has a filtration efficiency of up to 99 %. It is assumed that after the coupled DOC/ADPF and DPF, there are no or negligible particle masses emitted as the smoke number after the DPF was around 0.04 for both conditions. Thus, by weighing the increase of the DPF after the tests, the comparison of particle trapping efficiencies between the DOC and ADPF can be achieved. This shows that the averaged soot loading rate of the DPF for each test was similar, whether coupled with the DOC or the ADPF. For the latter, after the three tests, the main DPF's weight increase was lowered to 17.3 g, 18.1 g and 20.2 g from 19.7 g, 24.8 g and 24.9 g respectively, when the DOC was replaced by the ADPF. In other words, the ADPF showed a much better soot-reduction effect over the DOC and the reduction rate was as high as 27 %.

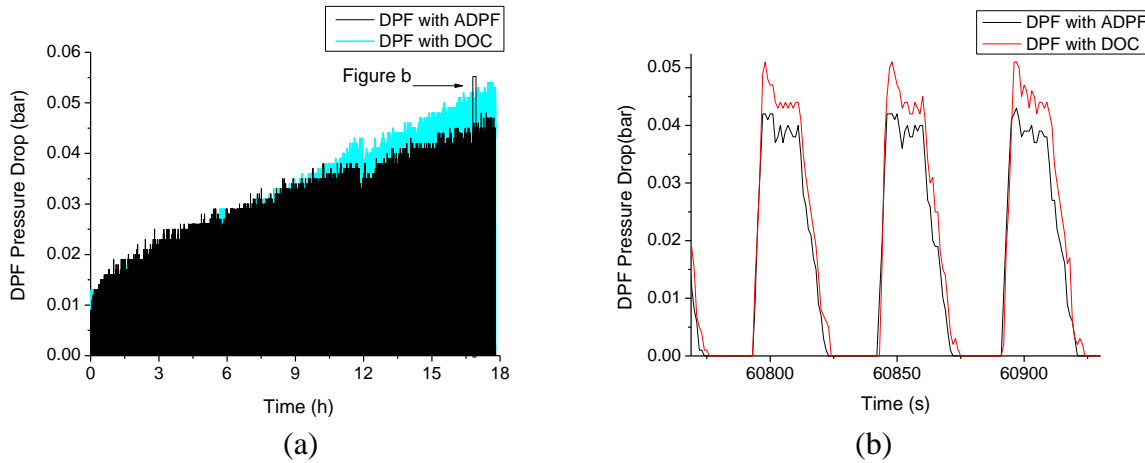


**Figure 4.2** DPF pressure drop (a) for one test (18 hours), (b) details under three engine cycles

Figure 4.2 (a) shows that during the first 9 hours, the DPF pressure slope was higher when coupled with DOC than with ADPF. As for practical application, trap loading is usually assessed by the pressure drop across it (Eastwood 2000). The exhaust flow rates can be assumed to be the same because the engine modes were the same. Therefore, when coupled with the ADPF, less soot was trapped in the main DPF, due to the ADPF's trapping and oxidizing function, than when it was coupled with the DOC.

Figure 4.2 (b) shows a more detailed DPF pressure drop. This underwent a cycle of changes along with the engine modes: when the engine was running in Mode 2 (high speed, relatively higher torque), the pressure drop was high. However, in Mode 1 (low speed, low torque), the pressure loss decreased to zero (the frequency of the fluctuation is 0.02 Hz, the same as the test cycle). This was due to the different exhaust flow rates under the two engine conditions. When coupled with the DOC, the DPF's pressure drop was 5 mbar higher than with the ADPF.

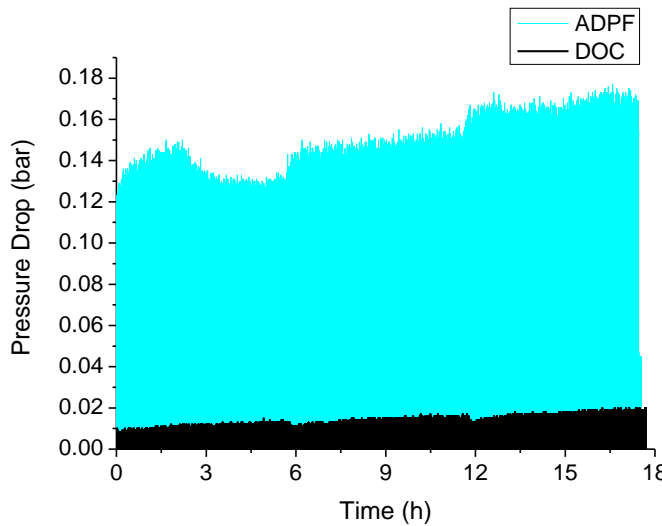


**Figure 4.3** ADPF/DOC pressure drop

Figure 4.3 shows the pressure drops across the ADPF and DOC during testing. According to the figure, the ADPF suffered higher pressure drops than the DOC in this test, about 0.13 bar more. This was firstly due to the material (metal foam) characteristics and secondly, the engine mode, when the exhaust flow fluctuation was severe. However, this problem was much improved in steady flow tests, referring to Figure 4.6 (a) and Figure 4.8, as the exhaust flow fluctuation was smoothed. It is interesting here that there was a reduced pressure drop across the ADPF in the first 6 hours, possibly due to the oxidation of the soot accumulated inside.

#### 4.3.2 Transient Test B

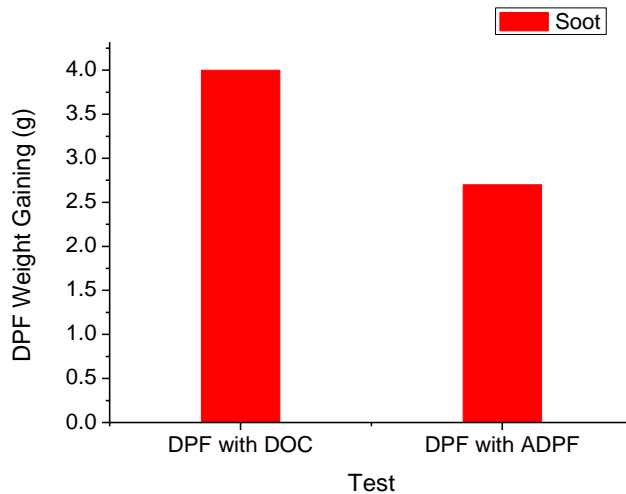


**Figure 4.4** Transient Test B test result

The results of the Transient Test B are shown in Figure 4.4. After 6 hours of engine running, the DPF with the DOC gained 4 g of soot and 2.7 g with the ADPF. This indicates that the ADPF had a 32.5 % better particle trapping efficiency compared to the DOC.

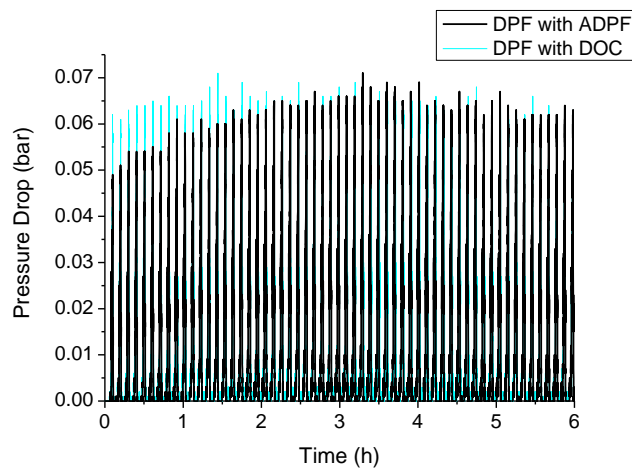


**Figure 4.5** DPF pressure drop when coupled with APDF and DOC

The pressure drops across the DPF and the coupled DOC/APDF were also studied in this test and the results are presented in Figure 4.5. When coupled with an ADPF, the main

DPF showed lower pressure loss characteristics at the beginning. However, after 2 hours, the results became very similar to those when it was coupled with a DOC and reached a very stable state. Transient Test B was conducted following Transient Test A, as the pressure drop of the ADPF at the finishing point in Figure 4.3 was the same as the one at the starting point in Figure 4.6 (a) around 0.16 bar. In Transient Test A, the ADPF's pressure drop increased to 0.16 bar as the particles accumulated, which was also the reason for the high pressure drop at the beginning of this test. However, it decreased with time until a fairly stable condition of 0.04 bar was reached, caused by its own passive regeneration. The pressure drop across the DOC remained at an extremely low level due to its wall flow characteristics and the change of the engine modes. This is reflected in Figure 4.6 (b).

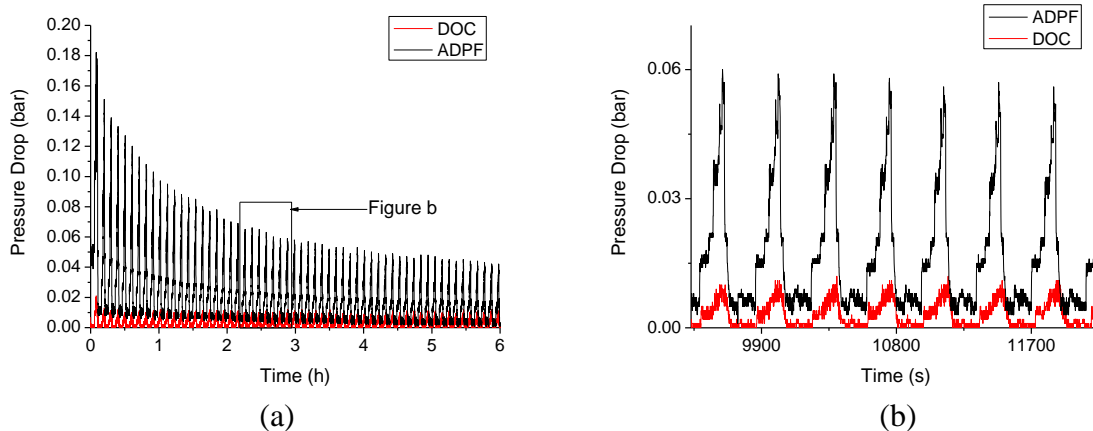


**Figure 4.6** ADPF/DOC pressure drops (a) for one test (6 hours), (b) details under eight mode cycles

In the test cycle, the engine was run at a given fixed speed, but with different torque conditions. The pressure loss of the ADPF followed this torque variation but that of the DOC was only slightly influenced (Figure 4.7). It indicates that the exhaust flow rate can have a very large influence on the pressure drop of a trapping filter. When it comes to assessing the trap loading for regeneration from the pressure drop, a careful consideration of the flow

condition is necessary. This is actually the problem during thermal regeneration in a real driving event.

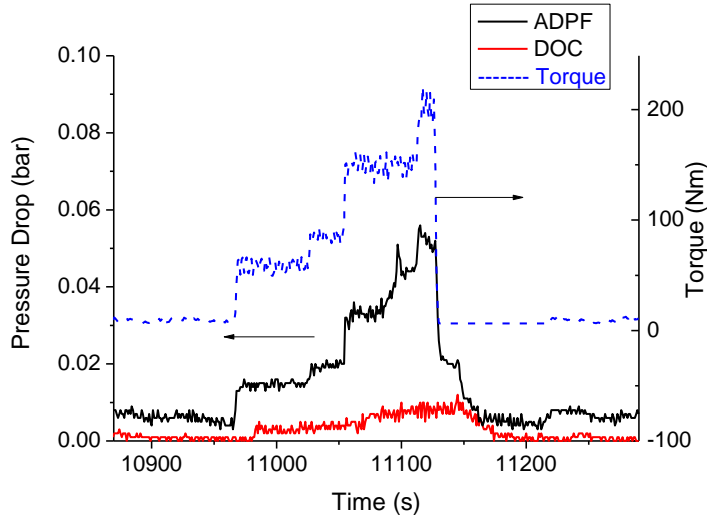


**Figure 4.7** Pressure drop of ADPF and DOC over a constant speed (2000 rpm) and varied engine torque cycle (5 Nm/15 Nm/60 Nm/90 Nm/150 Nm/200 Nm)

#### 4.3.3 Steady State Test

Figure 4.8 presents the pressure drops of the ADPF, the DOC and the main DPF. The ADPF produced a generally acceptable back pressure under these steady-state engine modes. This might be caused by the oxidation of the accumulated soot, as these modes had higher loads and thus higher exhaust temperature. At the same time, this may be affected by the reduced exhaust flow fluctuation. The pressure drop across the DOC results from the friction between the exhaust gas and the walls. The DPF had a generally smaller pressure drop and the differences were mainly caused by the different exhaust flows in the eight modes. In Mode 4, when the engine speed and load were the highest, the DPF had the highest pressure drop up to 130 mbar for the large exhaust flow.

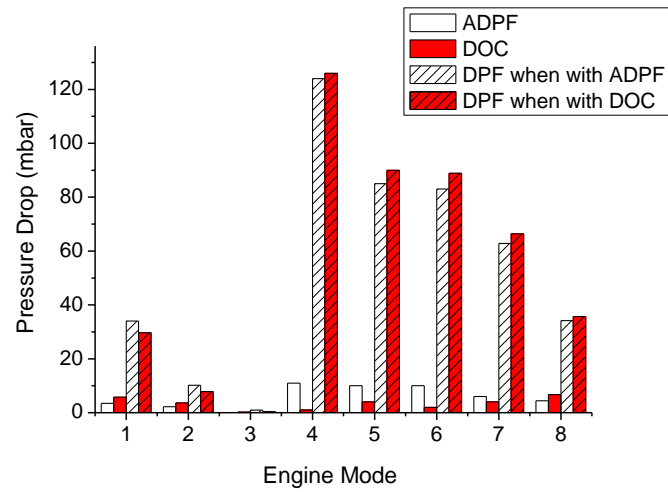


**Figure 4.8** Pressure drops of DOC, SC and DPF for each engine mode

## 4.4 Emissions along the Two Different After-treatment Systems

### 4.4.1 Gaseous Emissions

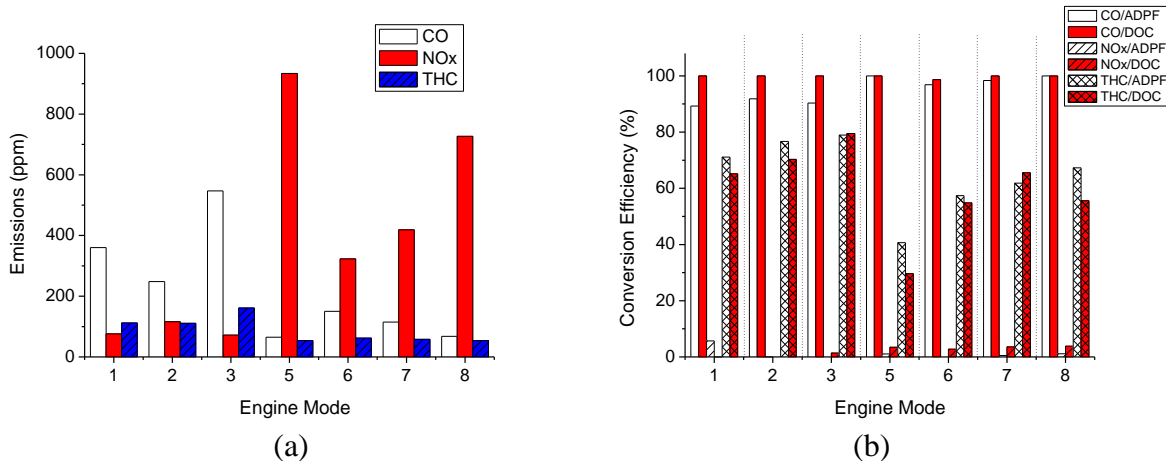


**Figure 4.9** (a) Engine gas emissions of CO, NO<sub>x</sub> and THC (b) gaseous emission reduction efficiencies of ADPF and DOC for each engine mode (ppm = part per million)

The tests were all carried out under the steady-state test. Figure 4.9 (a) shows the emissions of CO, NO<sub>x</sub> and THC at the different engine modes. The conversion efficiency for the DOC was very good for CO (up to 100 %) and similarly for the ADPF in the medium load range. However, they worked more efficiently in the higher load modes because the exhaust

temperature was higher. The THC conversion efficiency for both was similar, around 40-60%.

#### 4.4.2 Smoke Emissions

Figure 4.10 is the 3-D engine-out smoke map under the eight selected modes. It shows that at engine speeds between 1500-2500 rpm and loads between 10-40 %, the engine emits large amounts of smoke; the peak occurred at 2500 rpm. This smoke production is a result of the compromise in the calibrated injection strategy for the NO<sub>x</sub>-smoke trade-off, largely due to the use of EGR. Outside this speed and torque area, the smoke emitted will be reduced. However, when the load was increased to more than 75 %, there was another smoke peak. The lowest smoke concentrations are observed at around 70 % load.

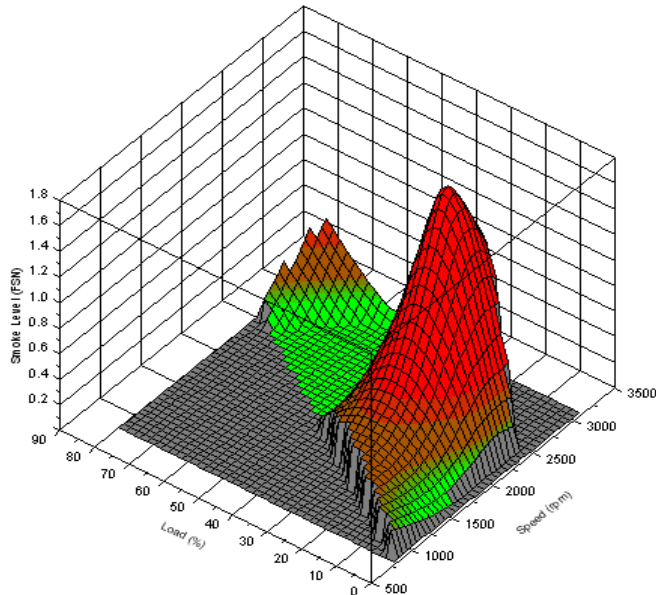


**Figure 4.10** 3-D map for engine speed, load and smoke level for each mode

The tests were all carried out under the steady-state test. For coupled ADPF/DOC, the smoke numbers before and after the device were measured and are presented as the smoke reduction efficiencies in Figure 4.11 (b). After three repeats the advantage of the ADPF over

DOC was confirmed. It is very clear that in Modes 1, 4 and 5 when the engine was running at high speeds and relatively higher loads, the superiority is much higher at 28.5 %, even during Mode 1 operation, which generated the most smoke. The ADPF also works very well in Mode 8 (at 13 % efficiency) when the engine emitted the lowest amount of smoke. In other modes, the superiority of ADPF's smoke reduction efficiency over the DOC is slightly less evident (2.5-10 % better).

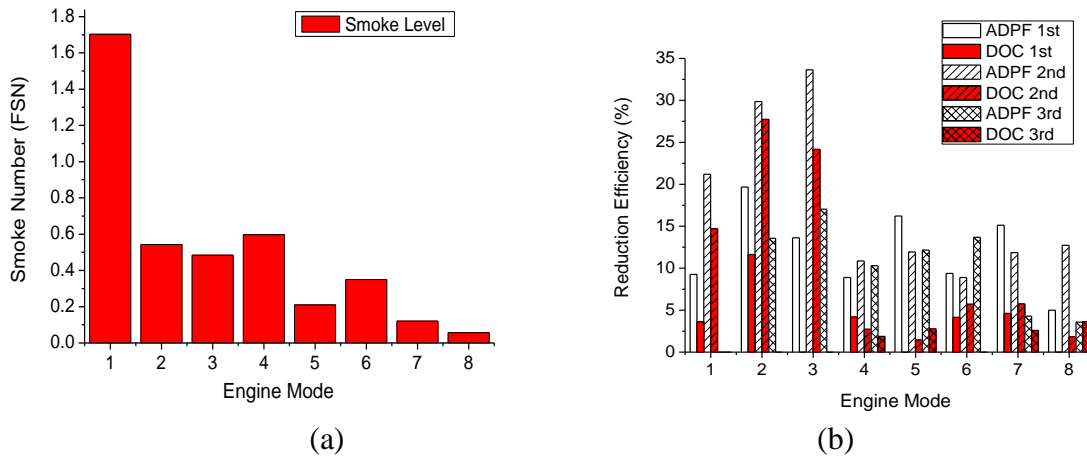


**Figure 4.11** (a) Smoke level of the engine modes; (b) smoke reduction efficiencies of ADPF and DOC for each engine mode

#### 4.4.3 PM Characteristics

Particulates along the after-treatment system were measured using the SMPS when the engine was running in two different modes (1200 rpm, 30 Nm and 1200 rpm, 60 Nm) and the results are shown as Figure 4.12. It indicates that the ADPF and the DOC had similar particle reduction effects as the particle number was reduced by 15.9 % and 11.3 % respectively in the low load engine mode and 25.3 % and 16.9 % in the relatively higher load mode. This was due to the DOC's oxidation and the ADPF's oxidation as well as trapping effects. The main DPF showed significant performance in particle trapping as the filtration efficiencies were up

to 99 %. However, it was also noticed that a large variation of particle numbers existed after the DPF, which might have been caused by the re-entrainment of the particles from the DPF wall deposits.

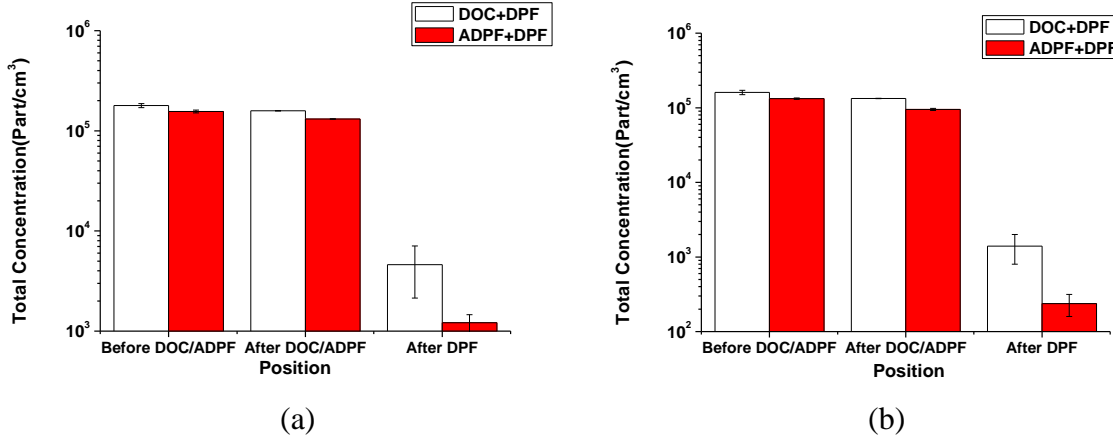


**Figure 4.12** (a) Particle total concentration along the after-treatment system (1200 rpm, 30 Nm); (b) particle total concentration along the after-treatment system (1200 rpm, 60 Nm)

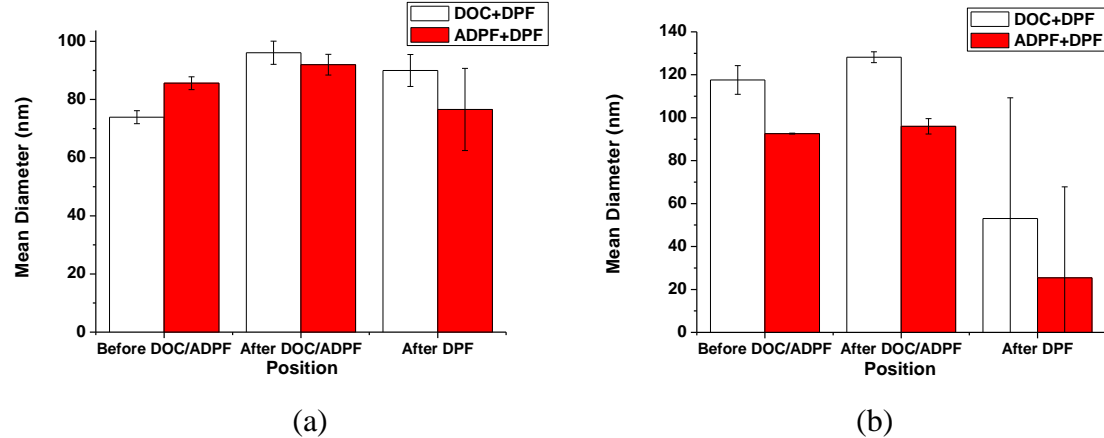


**Figure 4.13** (a) Particle mean diameter along the after-treatment system (1200 rpm, 30 Nm); (b) particle mean diameter along the after-treatment system (1200 rpm, 60 Nm)

According to Figure 4.13, the particulate mean diameters were increased after DOC/ADPF and this was believed to be caused by the two device's oxidation effect on some of the nucleation mode particles, which were mainly hydrocarbon volatiles. This was particularly notable in the low load mode, when these volatiles were more prone to be produced (Figure 4.13 (a)). While at higher load mode, fewer volatiles were present and this

influence to the mean diameter was less significant. The mean diameters of particles after DPF were case sensitive due to the small number of particles that were able to survive the trapping.

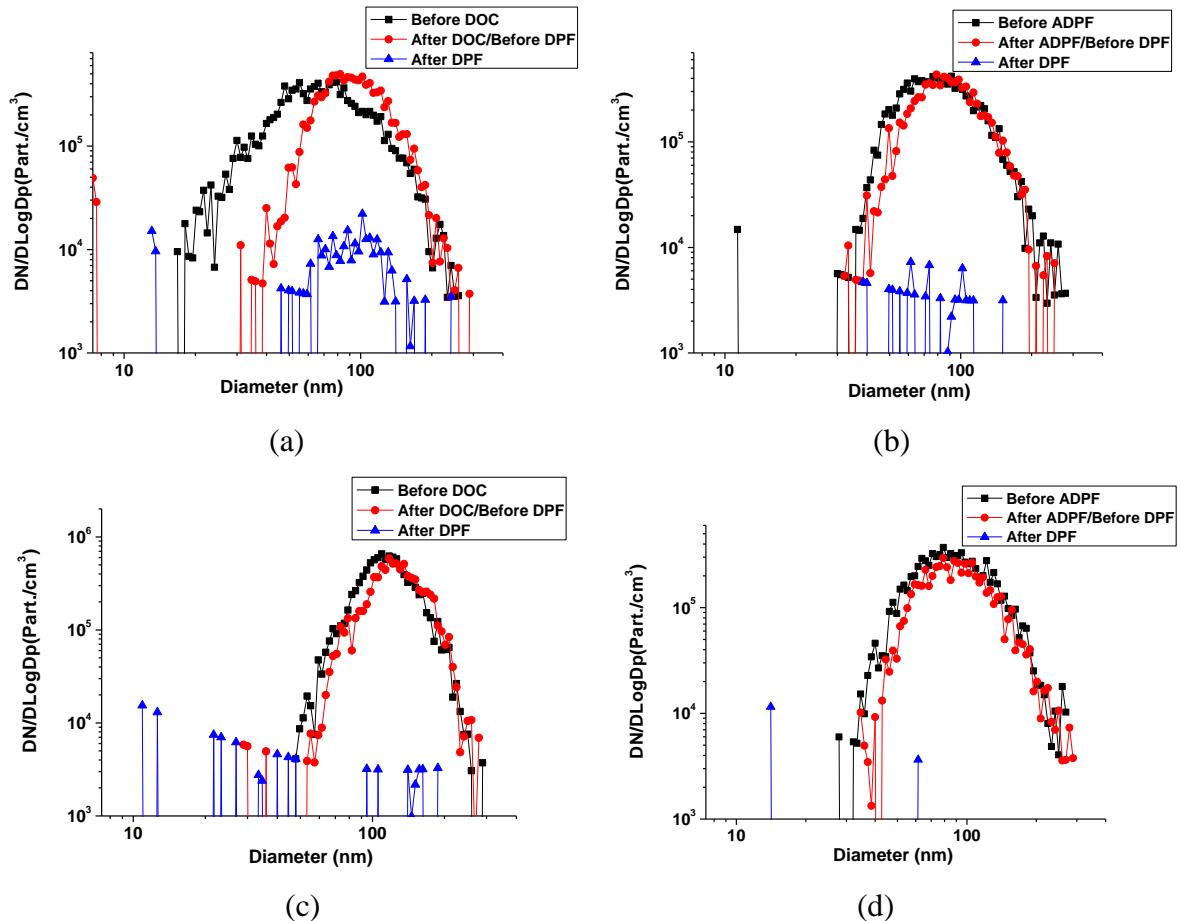


**Figure 4.14** Particle size and distribution (a) along the DOC+DPF system (1200 rpm, 30 Nm); (b) along the ADPF+DPF system (1200 rpm, 30 Nm); (c) along the DOC+DPF system (1200 rpm, 60 Nm); (d) along the ADPF+DPF system (1200 rpm, 60 Nm)

Figure 4.14 shows the details of how these particles changed after each after-treatment device. Based on (a) and (b), when the engine was running at 1200 rpm, 30 Nm, the DOC oxidized those sized below 60 nm, which were mainly hydrocarbons, however, accumulation particles were increased, and this was probably due to the oxidation of larger particles such as those in the coarse mode. The main DPF trapped most of the particles, even those in the smallest size range, but there were still some escaping whose diameter was around 100 nm.

The ADPF eliminated those hydrocarbon volatiles just as the DOC, but didn't influence much the total particle distribution. When the engine was running at 1200 rpm, 60 Nm, the influence of DOC/ADPF to the particle distribution was less significant for reduced volatiles. The DPF still performed well in this case and only those sized around 100 nm escaped the trap. This indicated that the monolith DPF actually had a good trapping efficiency for nucleation mode particles and this is even more remarkable with the increase of the engine load. In certain situations, such as the fluctuation of the exhaust stream which could result in the release of a large amount of small particles deposited on the DPF walls.

## **4.5 Impact of the Exhaust Back Pressure on the Engine Performance**

Considering the detrimental effects it may bring, the impact of the exhaust device back pressure on the engine performance was investigated. This extended research started with the one dimensional modelling of the I4 diesel engine through Ricardo WAVE 7.2. After the model was successfully set up, the influence of the exhaust system back pressure to the engine performance, mentioned in the previous chapter, was investigated through simulation.

### **4.5.1 One Dimensional Diesel Engine Model Set up**

The diesel engine model includes: the air intake system, the fuel injection system, the engine cylinders, the exhaust system, Exhaust Gas Recirculation (EGR) and the compressor and turbocharger system (Figure 4.15).

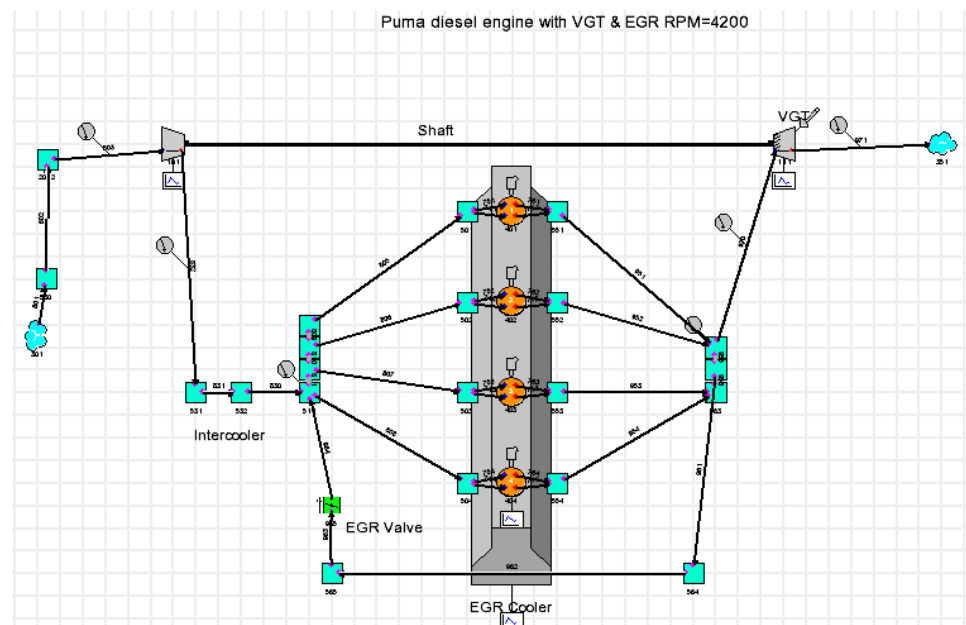


**Figure 4.15** WaveBuild of the I4 diesel engine

The air filter is represented by two complex Y junctions (square blue blocks), as shown on the left side of the canvas, and ambient air flows into them through a set of ducts. The inputs for the Y junctions and ducts include temperature, pressure, volume, fluid composition, structure and other general dimensions. In most cases, default values are used and major modifications are only applied in the settings of the volume and the initial temperature and pressures. After being compressed by the compressor, the air is cooled by an intercooler, also in the form of two complex Y junctions.

The most critical unit in the EGR control is a butterfly valve, to represent the EGR valve. Its plate angle is set as a variable, whose opening is adjusted for different engine conditions, corresponding to different EGR rates. The exhaust gas re-circulated is first cooled by an EGR cooler, and then joins the compressed air before entering the engine cylinders.

The four cylinders are the yellow circles shown in the canvas (Figure 4.15). The most important inputs to them are the engine valve diameters and lift profiles. Others include the

flow coefficient profiles and valve swirl coefficient profiles. For each cylinder, four valves are used, two for the intake and two for the exhaust.

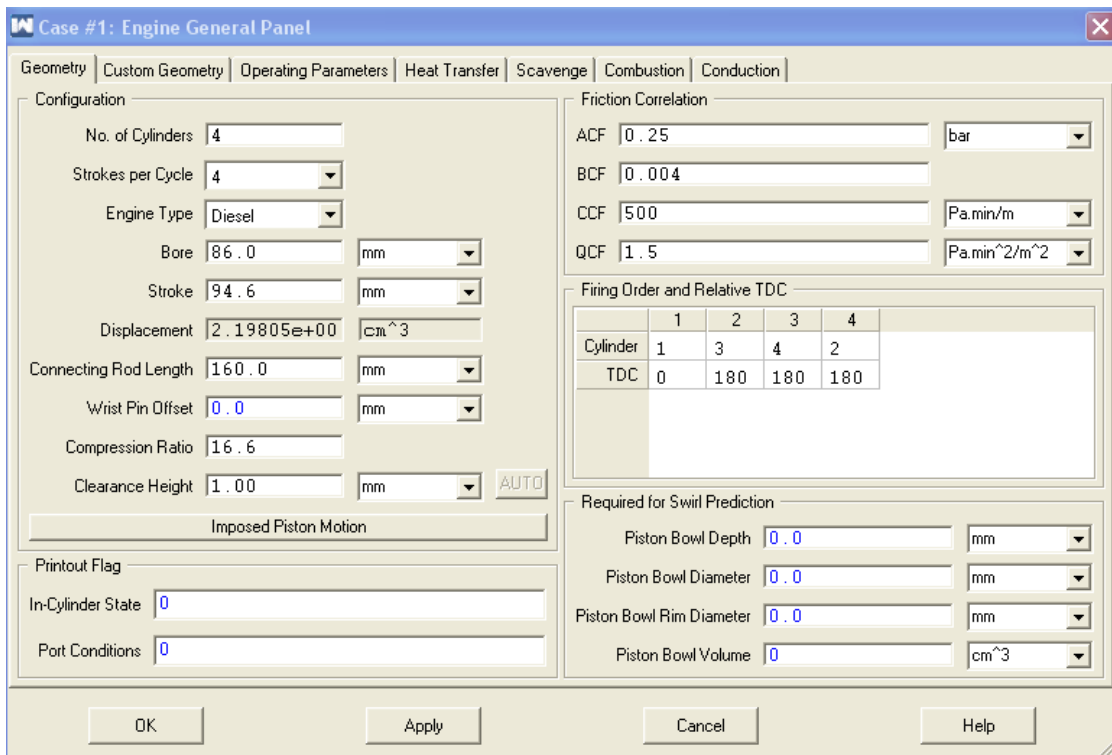


**Figure 4.16** Engine general panel in WaveBuild

The engine general panel (Figure 4.16) contains all the core information of the engine to be modelled, such as the geometry, operating parameters, a heat transfer sub-model (Woschni model), a combustion sub-model (Diesel Wiebe model) and an extra diesel jet model for emission predictions, which was not used in this application. The engine configurations are described in Table 3.1.

The exhaust system has the same structure as the air inlet system. Before being compelled to the ambient, the exhaust gas is used to drive the turbocharger and the compressor, which are connected with one shaft (Figure 4.15). The compressor and VGT (Variable Geometry Turbocharger) maps were obtained from the supplier and set as inputs.

Other settings in the two units include the initial rack position of the VGT and the speed of the compressor, which are important to locate the engine mode in the two maps (Appendix Figure B1, B2).

#### 4.5.2 Model Validation

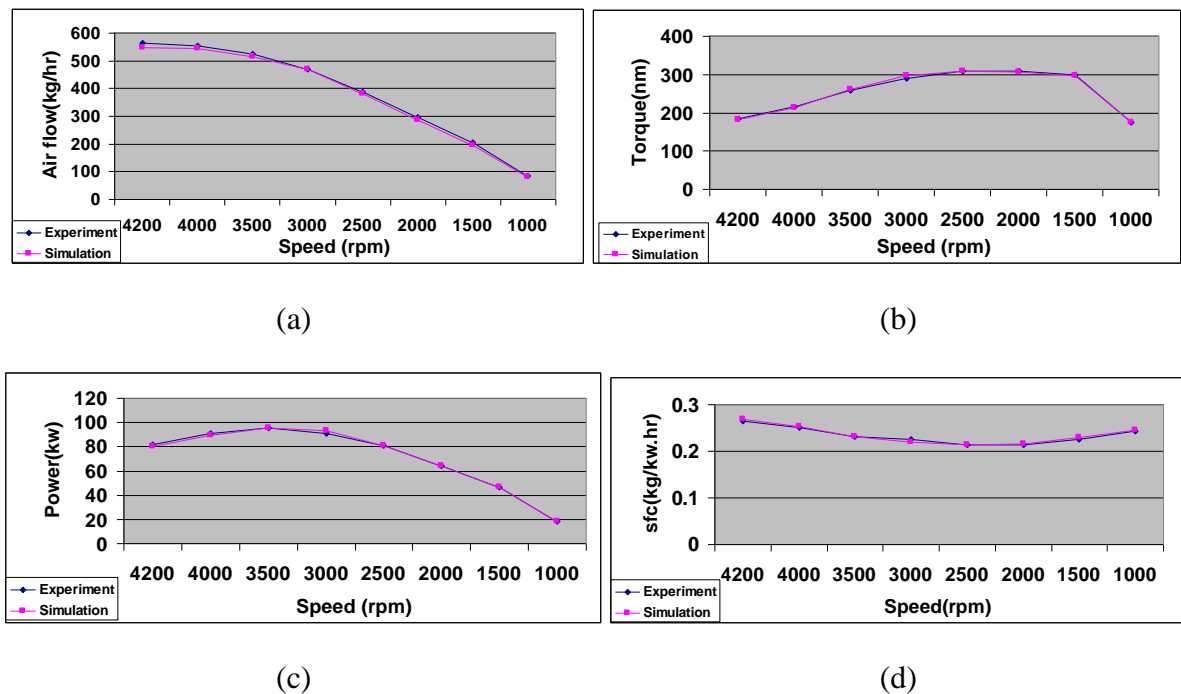


**Figure 4.17** Experimental and simulated (a) air flow, (b) torque, (c) power, (d) sfc. (blue curve=experiment, red curve=simulation)

The engine full load characteristics shown in Figure 3.2 were first used to validate the WAVE model after it was set up. The air flow, engine torque, power and specific fuel consumption results from the experiments were used as basic references. By continuously adjusting and optimizing the model, final simulation results were achieved, and the errors were below 5 %, compared with the experiment results.

**Table 4.4** Experimental results and the simulation errors

Speed (rpm)	Air flow (kg/hr)	Error (%)	Torque (NM)	Error (%)	Power (kw)	Error (%)	Sfc (g/kw.hr)	Error (%)
4200	565.665	3.4	185.44	1.5	81.6	1.6	264.4	1.5
4000	554.829	1.9	216.54	1.2	90.64	1.1	250.4	1.2
3500	524.127	1.7	259.87	0.01	95.21	0.05	230.9	0.01
3000	468.012	0.2	290.87	2.4	91.2	2.6	225.8	2.4
2500	387.387	1.2	309.38	0.1	81	0.1	213.3	0.06
2000	296.442	2.9	307.96	0.2	64.42	0.1	214.4	0.2
1500	204.981	4.1	299.5	1.1	47	1.0	226	1.1
1000	86.043	5.1	175.76	0.7	18.46	1.0	243.5	0.7

#### 4.5.3 Model Application

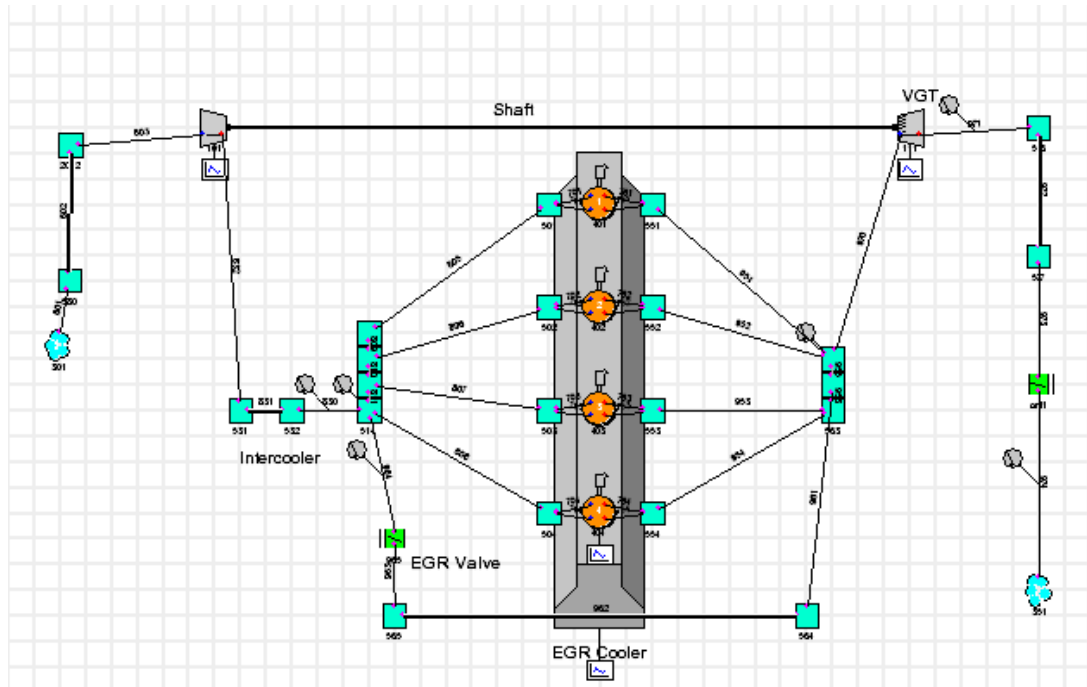


**Figure 4.18** WaveBuild of the I4 diesel engine with back pressure simulation

Exhaust back pressure has been one of the most critical problems of the diesel engine after-treatment system. In this application, the problem has been simplified to a butterfly

valve, whose valve opening determined the simulated DPF back pressure as Figure 4.18 shows.

The three engine modes in Table 4.5 were selected and the engine performance with 0 % DPF clog (butterfly valve fully open) was first simulated and compared with the experiment results (Figure 4.19). Then the valve openings were set to 62.8 ° and 41.1 °, representing typical 45 % DPF clog of soot and 75 % clog respectively.

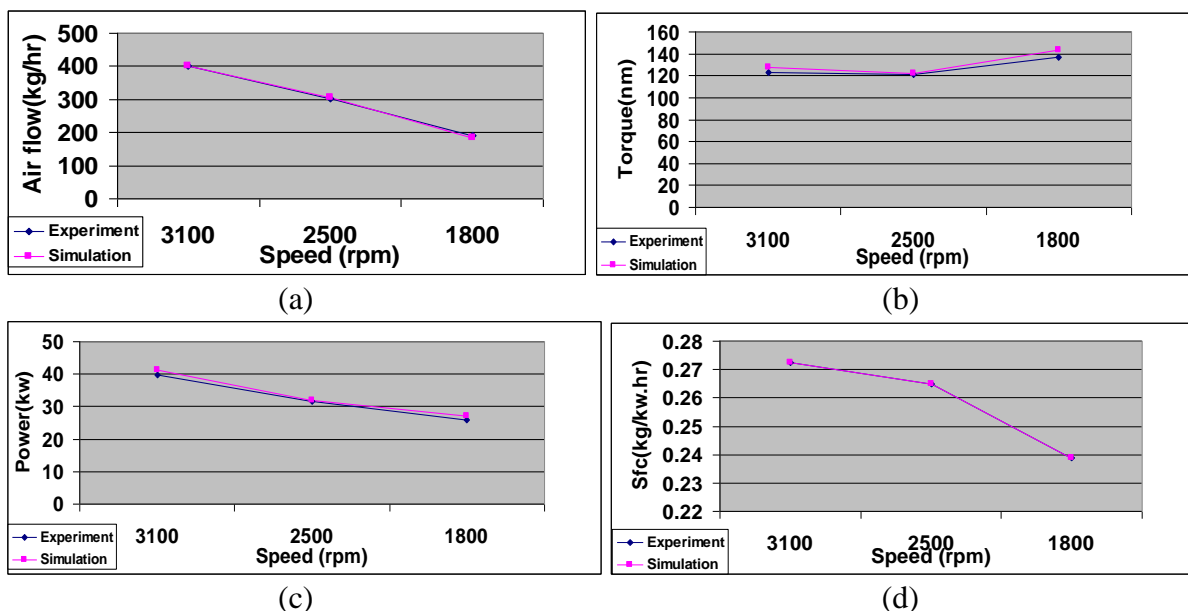


**Figure 4.19** Experimental and simulated (a) air flow, (b) torque, (c) power, (d) sfc. ( blue curve=experiment, red curve=simulation)

**Table 4.5** Experimental results and the simulation errors

Speed (rpm)	Air flow (kg/hr)	Error (%)	Torque (Nm)	Error (%)	Power (kw)	Error (%)	Sfc (kg/kw.hr)	Error (%)
3100	401.8	0.03	123	3.7	39.9	3.7	0.27	0.01
2500	303.2	0.7	121	1.8	31.7	1.3	0.26	0.01
1800	189.6	5.2	137	4.3	25.8	6.5	0.24	1.6

The inlet air flow, boost pressure, exhaust pressure, exhaust temperature, brake torque and power, and BSFC resulting from increased DPF clog (thus raised back pressure) were all investigated (Figure 4.20).

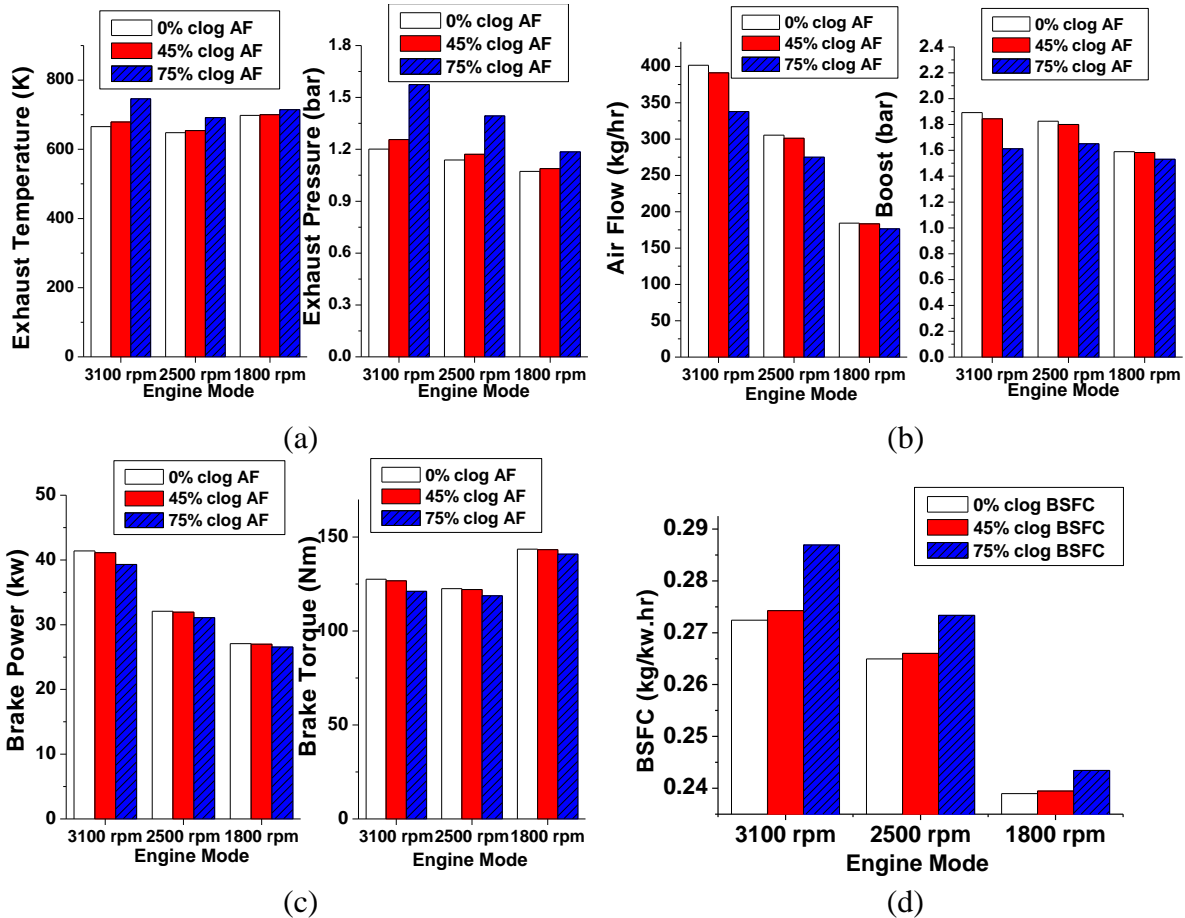


**Figure 4.20** Simulation of engine performance with increased DPF clog (c) exhaust pressure and temperature, (b) air flow and boost, (c) brake torque and power, (d) bsfc

According to Figure 4.20, the exhaust pressure deteriorates with the increase of the clog of the DPF. This is particularly significant in high speed mode (3100 rpm) as it increases from 1.2 bar to 1.57 bar when the DPF clog is increased from 0 % to 75 %. The engine inlet air flow is remarkably affected by the increased back pressure in this mode too; it was reduced by 16 %. The brake power, torque and BSFC were less influenced. In the 3100 rpm engine mode, if 75 % of the DPF is blocked, power and torque will be reduced by 5 % with an increase of BSFC by 5 %. The block of the DPF could also increase the exhaust temperature.

In these three modes, the highest increase also happens in the 3100 rpm mode by 80 K, when 75 % of the DPF is blocked.

To summarize, it can be noted that, increased exhaust back pressure could deteriorate the engine performance, and this is particularly significant in high speed mode and when the soot loading of the DPF exceeds 75 %. Therefore if the DPF loading could be kept below 75 % during the engine running, severe engine performance penalty could be avoided. Thus an accurate measuring of the soot loading is important.

## 4.6 Summary

Experimental studies have been carried out on a light duty common-rail diesel engine calibrated to Euro 4 standard in order to assess the performance of a catalyzed metal-foam assistant DPF coupling with a monolith DPF for the replacement of the traditional DOC + DPF after-treatment system. Some of the advantages of the former over the latter have been found while certain limitations were also revealed. Extended investigations into the impact of the exhaust back pressure caused by the after-treatment system on the engine performance were carried out through simulation methods. The conclusions drawn from the research up to date are as follows:

1. Using an ADPF to replace the DOC shows significant smoke reduction before the main DPF. For the soot trapping advantages of the ADPF over the DOC by up to 30 %, the main monolith DPF can be made smaller, lighter and thus less expensive and the regeneration can be made less frequently as a result.

2. Under most test conditions experienced, the catalyzed ADPF shows a comparable performance to DOC in the conversion of gaseous emissions, mainly for CO and THC, and this conversion effect was especially significant under high load engine conditions.

3. The ADPF can cause some unavoidable back pressure and this might be significant under some transient engine conditions. The back pressure has a close correlation to the engine modes, to be more specific, the exhaust flow rate. Under steady engine conditions, the ADPF's back pressure could be reduced to 10 mbar from 160 mbar when it was under the transient engine modes.

4. In this test, DOC and the ADPF were able to reduce the number of particulates in the nucleation mode, mainly due to their catalytic effects. Most of the particulates reduced were volatiles, whose diameters are below 60 nm and their reduction could lead to the increase of the particulate mean diameter. Particles in the accumulation mode could be increased by DOC for larger particles oxidized, such as those in the coarse mode, into smaller ones.

5. The monolith DPF had a good trapping efficiency for PM number, up to 99 %. However, particulates with a diameter of 100 nm were still able to escape. The trapping efficiency of DPF was dependent on the engine modes, and it improved with the increase of the engine load. In certain cases, the exhaust stream could re-entrain particulates from the wall deposits in the DPF, leading to varied number concentrations.

6. Typical DPF loadings of 45 % and 75 % were simulated through a one dimensional model and it was found out that the exhaust pressure deteriorates with the increase of the clog of the DPF. This is particularly significant in high speed mode. In this mode, the engine inlet air flow and exhaust temperature were also affected while the brake power, torque and BSFC

were less significantly influenced. If the DPF loading could be kept below 75 % during the engine running, severe engine performance penalty could be avoided. Thus an accurate measuring of the soot loading is important.

## CHAPTER 5

### PM CHARACTERISTICS WITH SINGLE INJECTIONS

In a common rail system, the fuel is first supplied to the common header from the fuel tank and then to the injectors, by which it is injected into the combustion chamber. For the engine combustion, the ultimate goal is to have the efficiency maximized and emissions minimized and nowadays, this is usually through a modern electronic control unit (ECU), which receives the operating parameter signals such as the engine speed and intake manifold pressure through different sensors and controls the fuel to be injected. This chapter firstly investigated the engine performance and emissions influenced by the single injection parameters, including the main injection time, the injection pressure and EGR. Then they were compared with those from typical multiple injections. Advanced combustion mode such as PCCI induced by single injections for low emissions of PM and NO<sub>x</sub>, was lastly discussed.

#### 5.1 Fuel Injection Impact on the Engine Performance and Emissions

With the modern engine injection system, a desired engine fuel air ratio can be precisely controlled under all the operating conditions. Thus good engine performance, emissions and fuel economy can be achieved.

### 5.1.1 Fuel Injection Parameters

Generally, the fuel injection timing into the cylinder is a key to good combustion. It is measured in degrees of crank angle of the piston before top dead centre (TDC) and an optimal timing depends on different engine design, as well as engine modes. The injection timing affects the ignition delay for the significantly changed air temperature and pressure that results, and under normal engine conditions, the minimum delay occurs with the start of injection at about 10 to 15 °BTDC (Heywood 1988). It has been commonly accepted that higher combustion efficiency, in-cylinder pressure and temperature and lower PM emissions can be achieved through a proper calibration of the start of injection (SOI) for a more complete combustion. However, NO<sub>x</sub> emissions can be increased due to the increased temperature.

Injection pressure is closely related to the fuel spray behavior. Large pressure differences across the injector nozzle are required to atomize the fuel and enable its rapid evaporation. Better combustion efficiency can be achieved through the increase of the injection pressure, which optimizes the fuel spray and the fuel mixing with the combustion air. However, if not properly controlled, this can also lead to the impingement of fuel on the cool cylinder surface and that can increase the emissions of unburned hydrocarbons. Higher NO<sub>x</sub> emissions are still problems when the injection pressure is increased.

In a diesel engine, NO<sub>x</sub> emissions are usually controlled through EGR, which replaces the oxygen in the combustion air. By doing this, the amount of power and fuel burned are also reduced. This leads to reduced combustion efficiency and increased PM emissions.

### 5.1.2 Engine Test Modes

The basic engine test mode (single injection) is shown in Table 5.1 (a) and there were 3 variations for each injection parameter (see Tables 5.1 (b)) when the other two were fixed.

**Table 5.1** Engine test modes (a) basic mode; (b) injection parameter tests with varied main SOI (green filling), varied EGR (orange filling), varied injection pressure (blue filling)

(a)

Mode	Engine Speed (rpm)	Torque (Nm)	BMEP (bar)	Load (%)	EGR (%)
1	1600	40	2.28	12.90	30

(b)

	Main SOI (°BTDC)	EGR (%)	Injection Pressure (MPa)
SOI test	5	55	50
	15	55	50
	17	55	50
EGR test	5	44	50
	5	50	50
	5	55	50
Injection pressure test	5	30	50
	5	30	80
	5	30	120

### 5.1.3 Main Injection Timing

The in-cylinder pressure, heat release and ignition delay caused by different main injection SOIs are shown in Figure 5.1. The tests were carried out at 1600 rpm, 40 Nm, when the EGR was 55% and the injection pressure was 500 MPa. The 17 °BTDC was the maximum value the ATI system could set for a single main injection under such an engine

mode. It shows clearly that with the advance of the main injection timing, the heat release was advanced. The rates of heat release were also magnified.

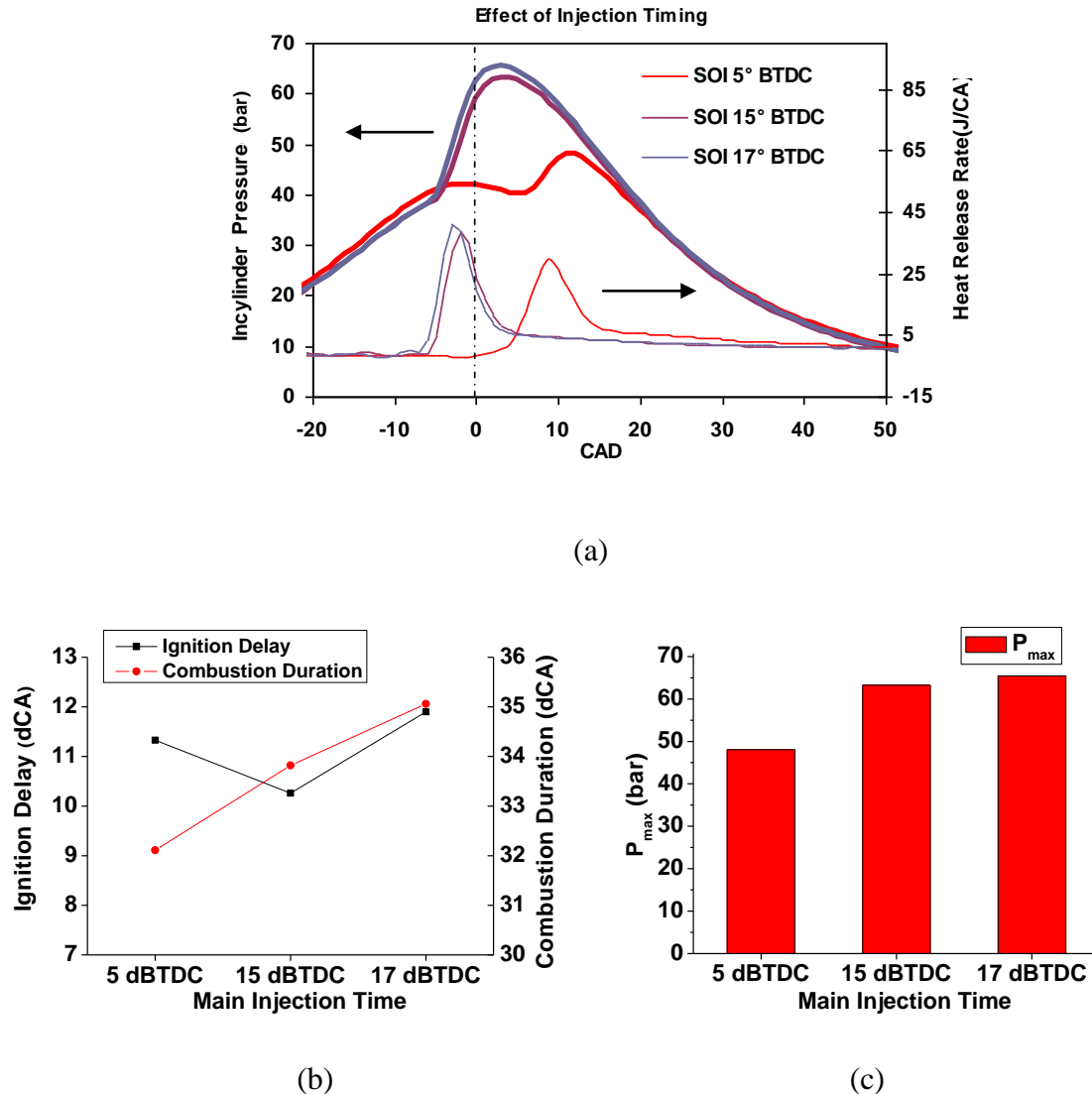


**Figure 5.1** (a) In-cylinder pressure and heat release (CAD= crank angle degree) (b) ignition delay (c)  $P_{max}$  with different main SOIs

The ignition delay is defined as the duration between the fuel injection and the start of combustion (0% mass fraction burned (mfb)) based on the heat release. According to Figure 5.1 (b), the ignition delay was the smallest when the fuel was injected at 15 °BTDC. When the injection was further advanced or injected closer to TDC, the delay increased, by 2 °CA in

this case. The combustion duration was defined as the time between 10% mfb and 90% mfb. It was also noted from Figure 5.1 (b) that the combustion duration was actually extended by the advance of the injection timing. Figure 5.1 (c) shows that the maximum in-cylinder pressure  $P_{max}$  was raised from 48 Bar to 65 Bar when the injection timing was advanced from 5 °BTDC to 7 °BTDC.

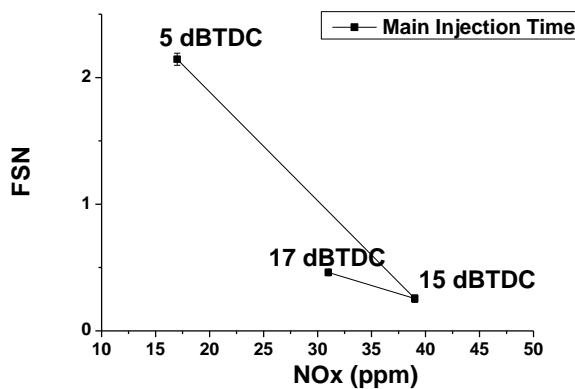


**Figure 5.2** Smoke and  $\text{NO}_x$  trade-off using different main SOI

The smoke and  $\text{NO}_x$  trade-off is shown in Figure 5.2. For a single injection, when the main injection SOI was advanced from 5 °BTDC to 15 °BTDC, the  $\text{NO}_x$  emission increased and the smoke decreased as expected, due to the improved combustion. However, when the SOI was further advanced to 17 °BTDC,  $\text{NO}_x$  slightly reduced and smoke increased. This corresponded to the best combustion efficiency when the fuel was injected at 15 °BTDC. At this point, the ignition delay was the smallest.

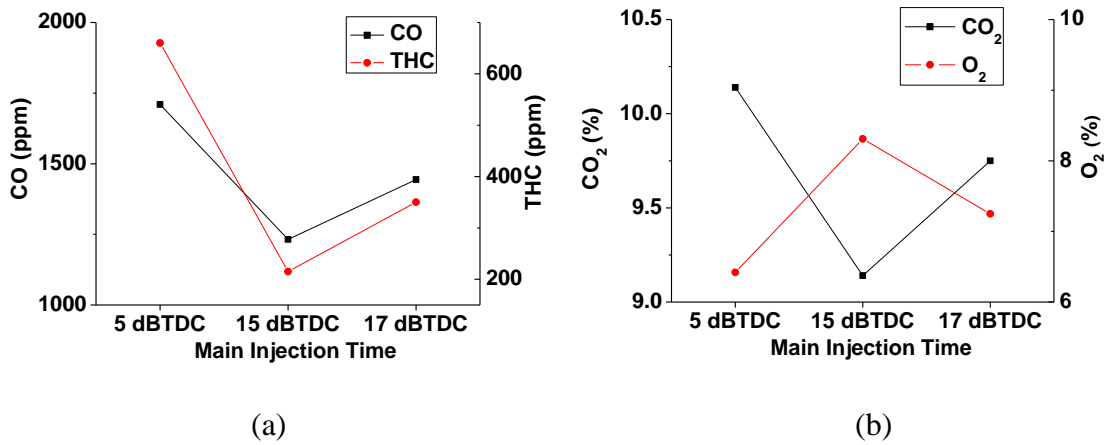


**Figure 5.3** (a) CO and THC emissions (b) CO<sub>2</sub>/O<sub>2</sub> trade-off using different main SOI

According to Figure 5.3 (a) and (b), CO, THC and CO<sub>2</sub> all reduced when the main SOI was advanced from 5 °BTDC to 15 °BTDC as the above reason indicated. Just as the smoke increased, they then slightly increased when the main SOI further increased to 17 °BTDC.

#### 5.1.4 EGR

EGR's effect on the in-cylinder pressure, heat release, ignition delay and P<sub>max</sub> is shown in Figure 5.4. The tests were carried out at 1600 rpm, 40 Nm, when the main injection SOI was 5 °BTDC and the injection pressure was 500 MPa.

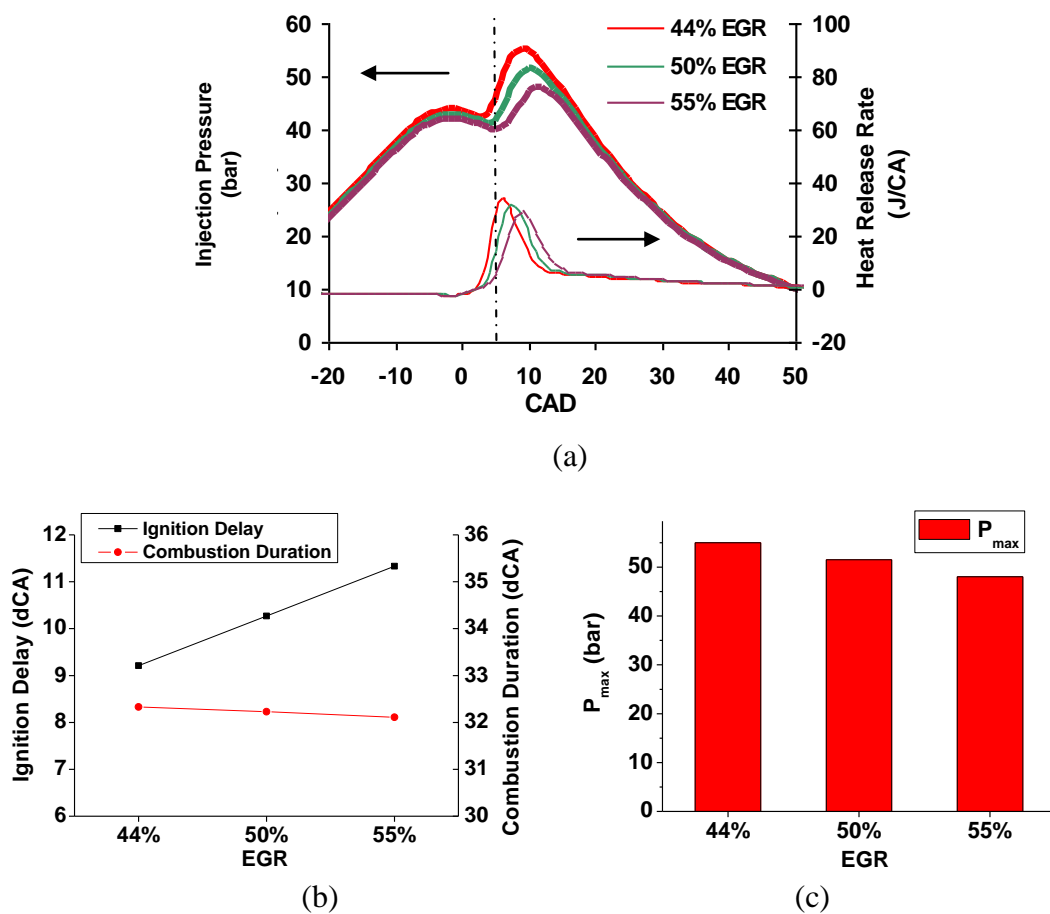


**Figure 5.4** (a) In-cylinder pressure and heat release (b) ignition delay (c)  $P_{max}$  with different EGR

For its oxygen replacement effect, more EGR led to a smoothed and delayed combustion as when the EGR increased from 44 % to 55 %, the ignition delay was increased and the peak value of the heat release was reduced. This led to reduced NO<sub>x</sub> emissions. It should also be noted here that the impact of EGR on the combustion duration was not significant as Figure 5.4 (b) shows. Although the mixing time for the fuel and combustion air was prolonged, smoke was actually increased in this case, as EGR replacing the combustion air meant less oxygen was present during the combustion. For the same reason, HC and CO were also increased (Figure 5.6). This reduction of combustion efficiency meant an increase of fuel consumption to maintain the same speed and torque. Correspondingly, the CO<sub>2</sub> emissions were increased.

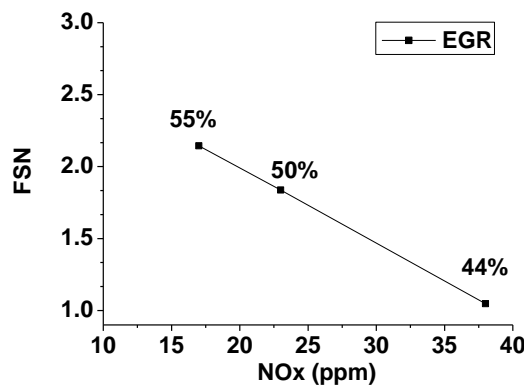


**Figure 5.5** Smoke and NO<sub>x</sub> trade-off using different EGR

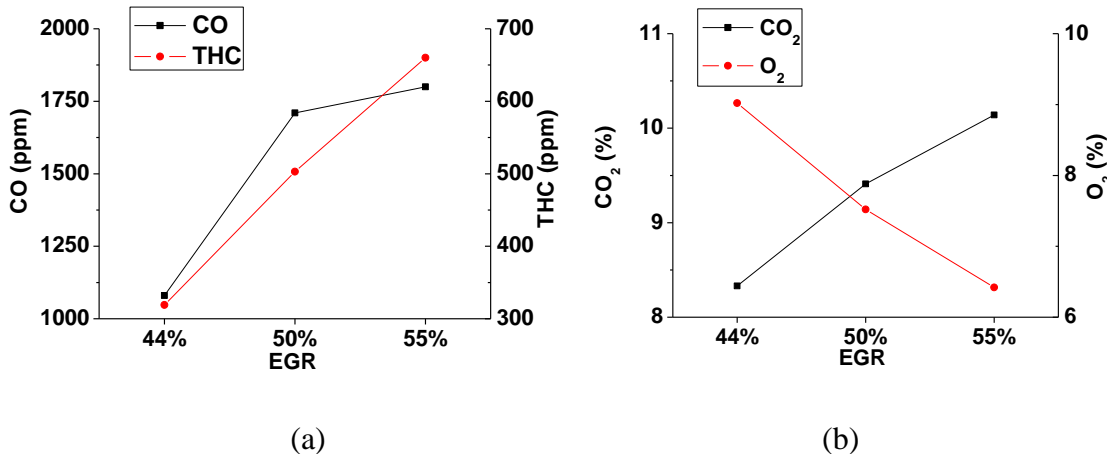


**Figure 5.6** (a) CO and THC emissions (b) CO<sub>2</sub>/O<sub>2</sub> trade-off using different EGR

### 5.1.5 Injection Pressure

Figure 5.7 is the in-cylinder pressure, heat release, ignition delay and P<sub>max</sub> when different injection pressures were used. The tests were carried out at 1600 rpm, 40 Nm. The main injection SOI remained 5 °BTDC and the EGR was 30 %. When the injection pressure was increased from 50 MPa to 120 MPa, the heat release was advanced and magnified. The ignition delay was shortened by about 1 °CA. This was due to improved fuel spray and correspondingly reduced the smoke while increasing the NO<sub>x</sub> as shown in Figure 5.8.

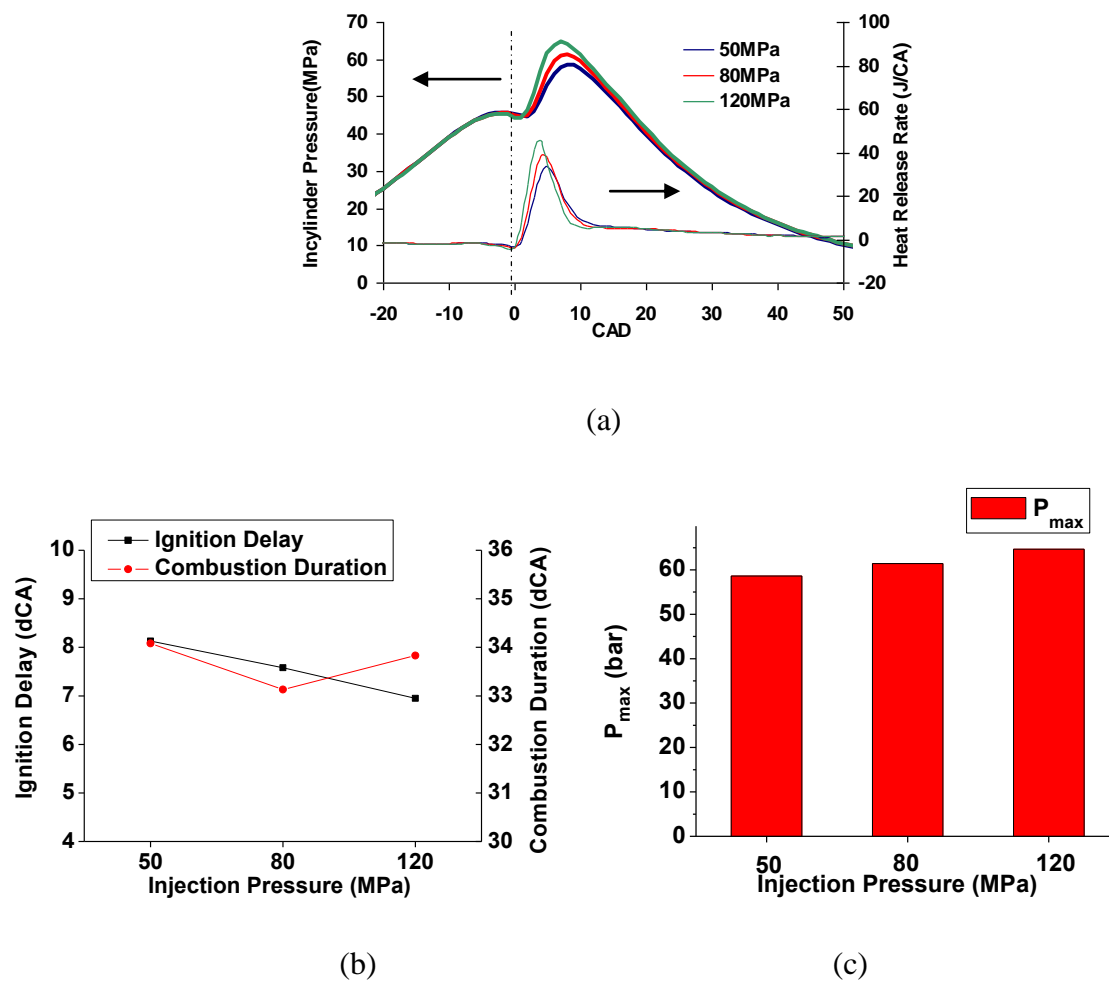


**Figure 5.7** (a) In-cylinder pressure and heat release (b) ignition delay (c)  $P_{max}$  with different injection pressures

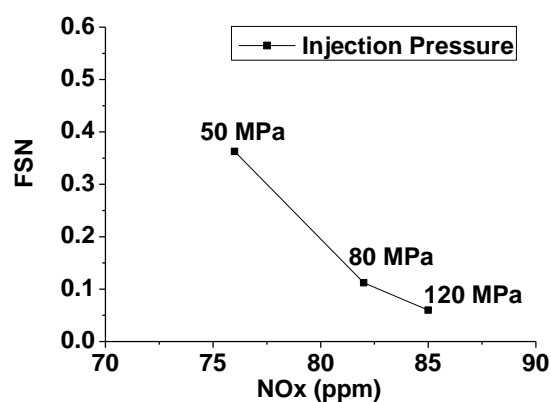


**Figure 5.8** Smoke and NO<sub>x</sub> trade-off using different injection pressure

However, it was also noticed that increasing the injection pressure had a CO and THC penalty, as Figure 5.9 (a) shows, both of the emissions increased. This might have been contributed to either by the fast combustion, when there was not enough time for the fuel and air to be well premixed or the increased impingement with the increased injection pressure. This also led to the increase of the CO<sub>2</sub> emissions, indicating higher fuel consumption.

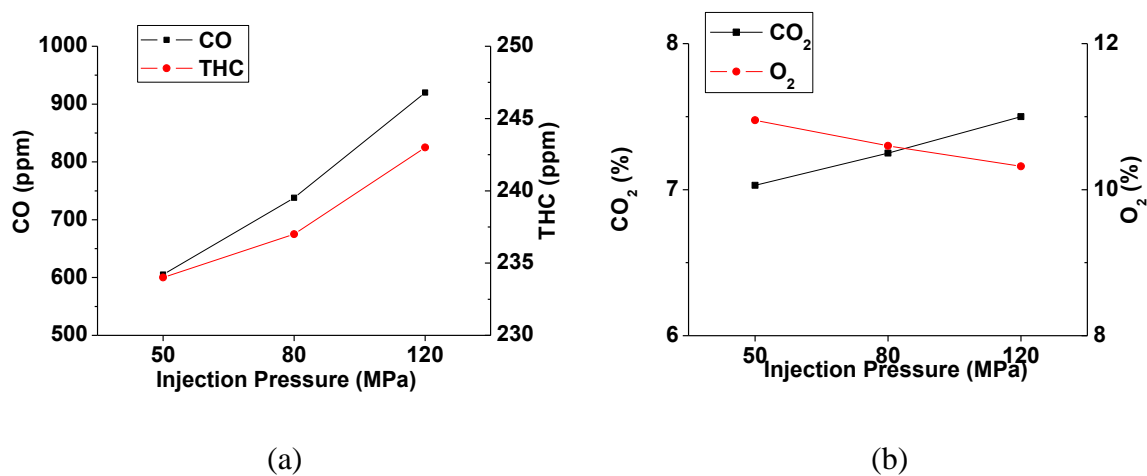


**Figure 5.9** (a) CO and THC emissions (b) CO<sub>2</sub>/O<sub>2</sub> trade-off using different injection pressure

## 5.2 Single Injections VS Multiple Injections

For modern diesel engines, it is common to use multiple injections instead of single injections. A small amount of fuel, namely ‘pilot injection’, is usually injected just before the main injection to reduce the engine noise, as well as optimizing injection timing and quantity for variations in fuel quality, cold starting, etc. These multiple injections can even be increased to five injections per stroke in some cases.

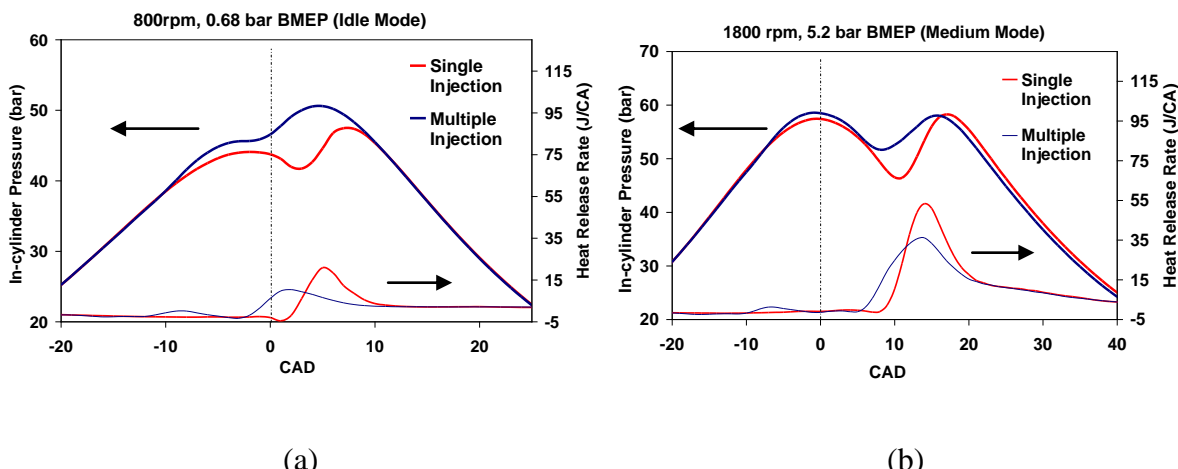
Table 5.2 shows the 3 engine modes (shown as Idle, Medium and High engine modes in the figures) selected in this test, which all used multiple injections (one pilot injection before the main injection) and were calibrated to Euro 4 emission standard. For each

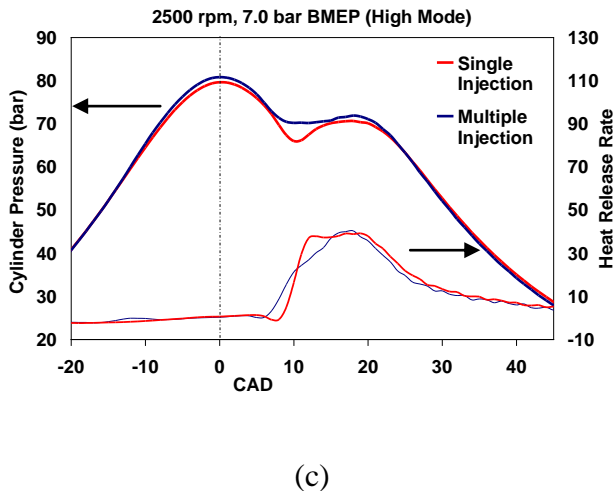
corresponding single injection strategy, the speed, torque and SOI of the main injections were fixed.

**Table 5.2** Engine test modes for single injections and multiple injections comparison

Mode	Engine Speed (rpm)	Main SOI (BTDC)	BMEP (bar)	Injection Pressure (MPa)	EGR	Pilot Fuel (mm <sup>3</sup> /stroke)
Idle	800	-1	0.68	23	0	1.5
Medium Speed/Load	1800	-2.69	5.2	84	21.5%	1.5
High Speed/Load	2500	-2.69	7.0	129	0	1.5

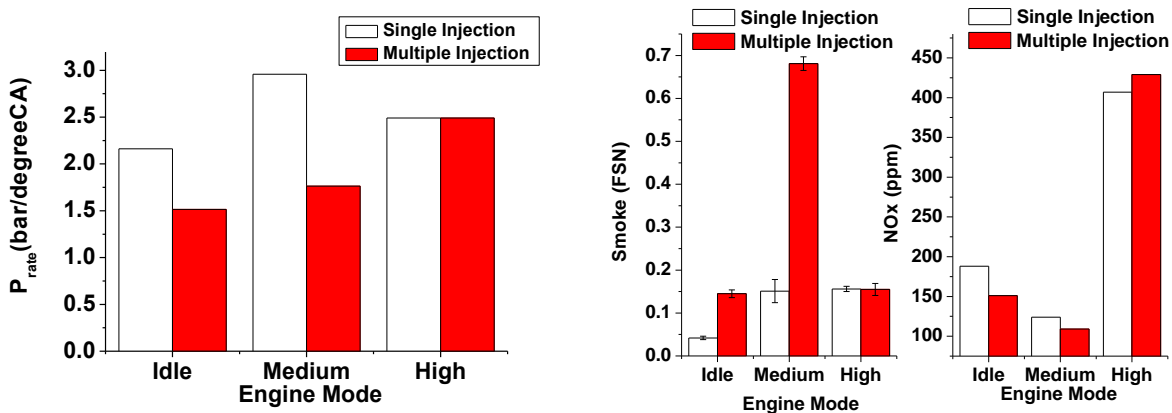
Figure 5.10 shows the in-cylinder pressure and heat release of the three engine modes when single and multiple injections were used. It shows clearly that by using pilot injection, the main combustion was advanced and the heat release peak was reduced. This was due to the pilot fuel, which raised the in-cylinder temperature and shortened the ignition delay of the main combustion. These effects were particularly significant at idle and medium speed/load modes.





(c)

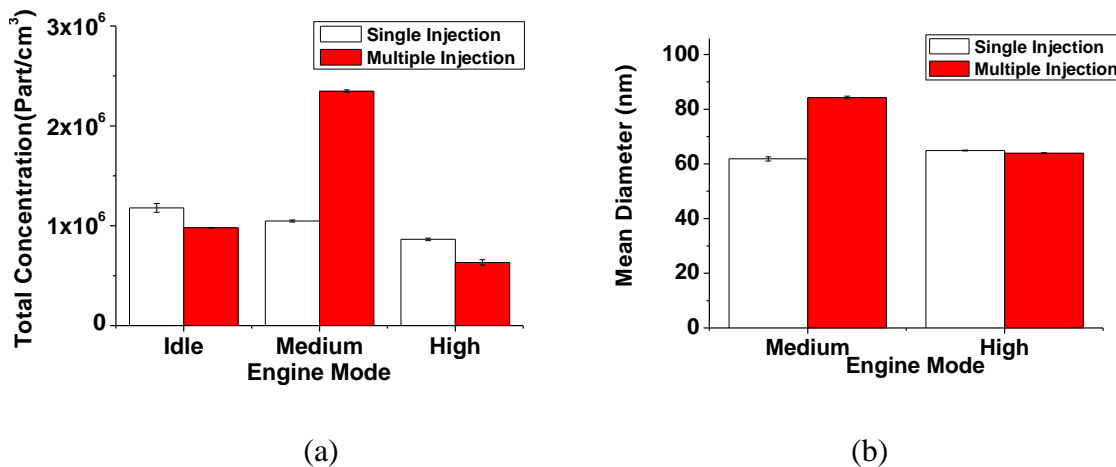
**Figure 5.10** In-cylinder pressure and heat release with single and multiple injections (a) idle mode (b) medium mode (c) high mode



**Figure 5.11** (a)  $P_{rate}$ ; (b) smoke and NO<sub>x</sub> emissions with single and multiple injection

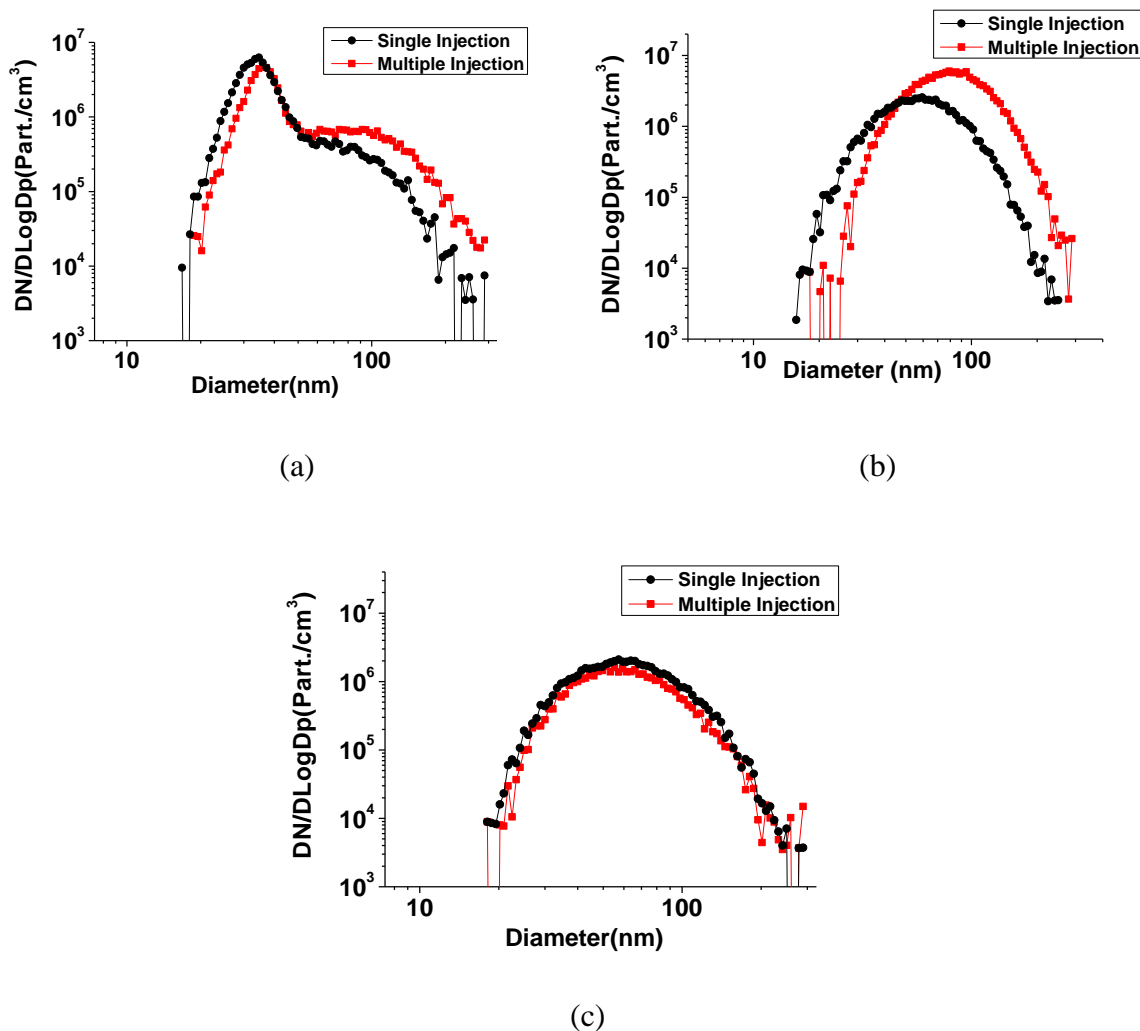
During the tests, the engine noises were much higher when single injections were adopted. According to Figure 5.11 (a), by using multiple injections, the  $P_{rate}$ , which is closely related to engine noise, was reduced from around 2.2 Bar/ $^{\circ}$ CA to around 1.5 Bar/ $^{\circ}$ CA in the idle mode, and from around 3 Bar/ $^{\circ}$ CA to around 1.7 Bar/ $^{\circ}$ CA in the medium speed/load mode. In the high speed/load mode, it was not much affected. Figure 5.11 (b) shows the smoke and NO<sub>x</sub> emissions emitted with single injections and multiple injections under the

three different engine modes. The pilot injection quantity used was  $1.5 \text{ mm}^3/\text{stroke}$ . With multiple injections, the smoke emissions were increased while  $\text{NO}_x$  was reduced more than when single injections were used. This impact was very clear under idle and medium engine speed/load. The results also show that at the medium engine speed/load mode, the engine suffered much higher smoke than in the other two modes. This was due to the use of EGR in this mode.



**Figure 5.12** The total particle number and mean diameter with single and multiple injection:  
 (a) total particle concentration; (b) particle mean diameter

The total particle number and the derived particle mean diameter are shown in Figure 5.12 (at idle, the particles presented a bimodal distribution, so the mean diameter is not shown). Compared with Figure 5.18, the use of the pilot injection increased the smoke in the idle mode but actually reduced the total particle numbers by 17 %. This indicates that more large particles were produced while the small ones were reduced. It also presented a good particle number reduction at high speed/load, shown by Figure 5.12 (a). Here, the total particle number was reduced by 27 %. However, the mean particle diameter wasn't affected in this mode.



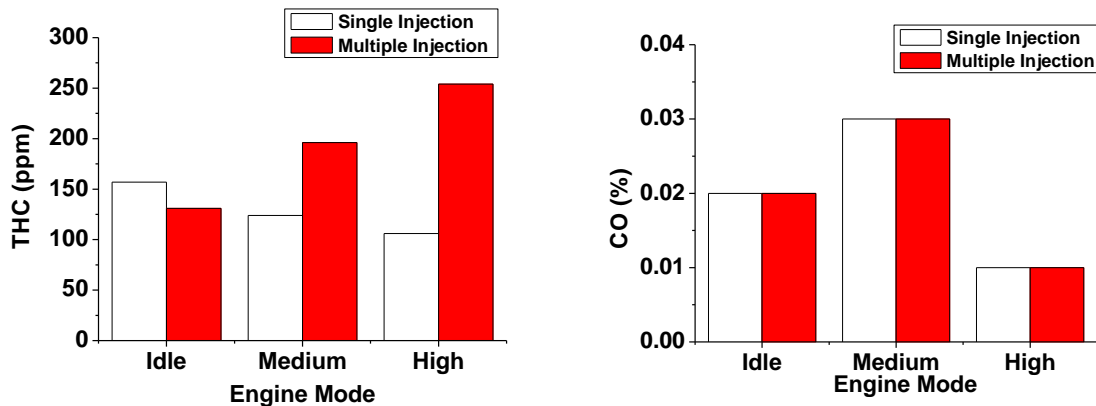
**Figure 5.13** Particle size and distribution with single and multiple injection (a) idle mode (800 rpm, 0.68 bar BMEP); (b) medium speed/load mode (1800 rpm, 5.2 bar BMEP); (c) high speed/load mode (2500 rpm, 7.0 bar BMEP)

Figure 5.13 shows the influence of the injection strategies on the particle size distribution under the three engine modes. Generally, the use of pilot injection tends to produce larger particles. At idle the distribution was bimodal and the peak in the nucleation mode shifts around 30 nm to 35 nm. The number in the accumulation mode was increased. In the medium speed/load mode, the mono-modal peak was shifted from 60 nm to more than 80 nm, as was reflected in the increase of the particle mean diameter in Figure 5.12 (b). At the same time, the number of particles in the accumulation mode was significantly increased

along with the reduction of the nucleation mode with diameters below 45 nm. According to Figure 5.13 (c), the particle size and distribution was little affected by the pilot injection at high speed/load.

To summarize, it has been found that impacts of multiple injections on the PM emissions have a close relationship with the engine speed and load. The use of small quantities of pilot injection could lead to the increase of particle number under medium engine speed and load modes and the use of EGR could exacerbate this effect. However, under idle or high speed/load mode, particle numbers were reduced. Using multiple injections tends to produce larger particles, and this effect was not distinctive under high engine speed/load mode.

Figure 5.14 is the THC and CO emissions when the two injection strategies were used. It has been noted that, with multiple injection, hydrocarbon was increased and this was particularly significant under high speed/load mode. CO was little affected.



**Figure 5.14** Gaseous emissions with single and multiple injections: (a) THC, (b) CO

### 5.3 PCCI Combustion with Single Injections

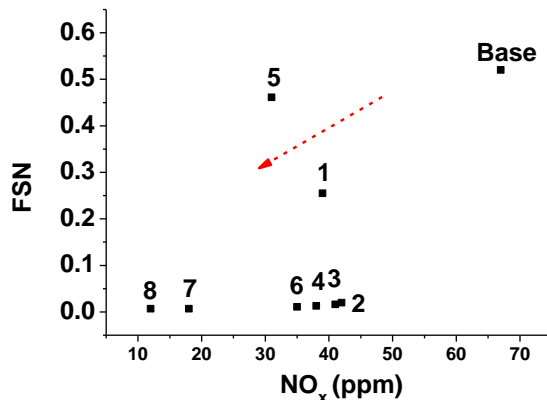
To meet the future emissions requirement, especially for the PM and NO<sub>x</sub>, one plausible way to apply the single injections on diesel engines is to lead the combustion into the PCCI or HCCI region. The objective is to combine the advantages of high injection pressure and advanced injection time, which are both effective in reducing PM. At the same time, to avoid suffering a high level of NO<sub>x</sub>, large amounts of EGR are used. The tests were carried out at 1600 rpm, 40 Nm (Table 5.3) and the base mode was from the engine map, which was composed of a pilot injection and a main injection, calibrated to Euro 4 emissions standard. From Mode 1 to Mode 8, different injection pressures, injection time and EGR were tried for low emissions of smoke and NO<sub>x</sub>.

**Table 5.3** Engine test modes for single injection combustion

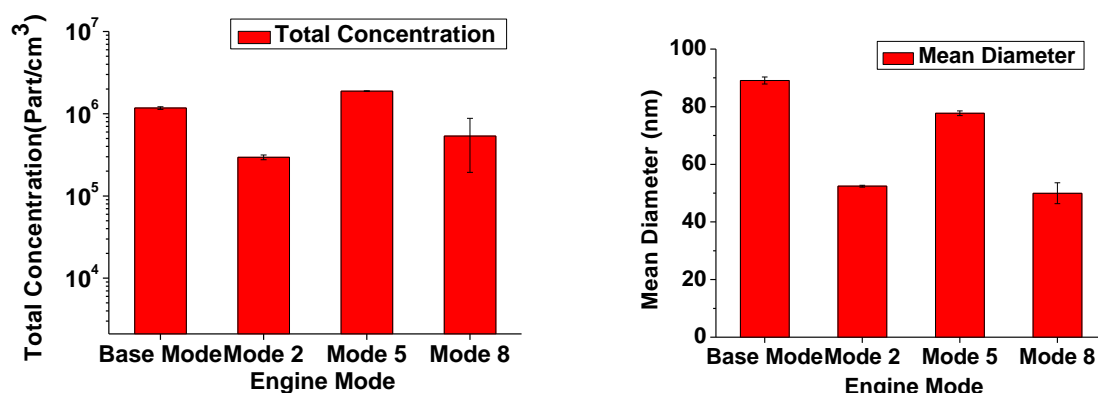
Mode	Main SOI (°BTDC)	EGR (%)	Injection Pressure (MPa)
Base	-1	30	50
1	15	55	50
2	15	55	80
3	15	55	100
4	15	55	120
5	17	55	50
6	17	55	120
7	17	57	120
8	17	60	120

Figure 5.15 is the smoke, NO<sub>x</sub> and particulate emissions under all the engine modes. The base mode is the typical diesel combustion with pilot injection. For all the single injection modes, Mode 1 and 5 had the lowest injection pressure of 50 MPa, just as the base mode. These modes had the worst smoke emissions. Modes 2, 3, 4 and 6 had the same EGR

(55%), slightly increased main SOI (from 15 °BTDC to 17 °BTDC) and injection pressures (from 80 Mpa to 120 Mpa). It is noted that, under this engine mode, when it was above 80 Mpa, the injection pressure had little influence on the smoke emissions. However, its increase could reduce the NO<sub>x</sub> slightly, from 42 ppm to 35 ppm. Modes 7 and 8 had the highest EGR, injection pressure and a most advanced main SOI. They also had the lowest emissions of smoke and NO<sub>x</sub>, reduced by up to 98.7 % and 82 % respectively compared to the base mode. It is noted that if carefully calibrated, single injections could lead to a relatively lower level of smoke and NO<sub>x</sub> than with the multiple injections.



(a)



**Figure 5.15** (a) Smoke and NO<sub>x</sub> emissions (b) particulate concentration (c) particle mean diameter of the engine modes

The particle concentrations and mean diameters of the base mode, Mode2, Mode 5 and Mode 8 are also shown in Figure 5.15. Compared with the base mode, particles in Mode 5 were increased by 61% while in Mode 2 and Mode 8, they were reduced by 75 % and 54 % respectively. Particles in the base mode had the largest mean diameter of 89 nm, and the smallest was in Mode 8, equalling 50 nm.

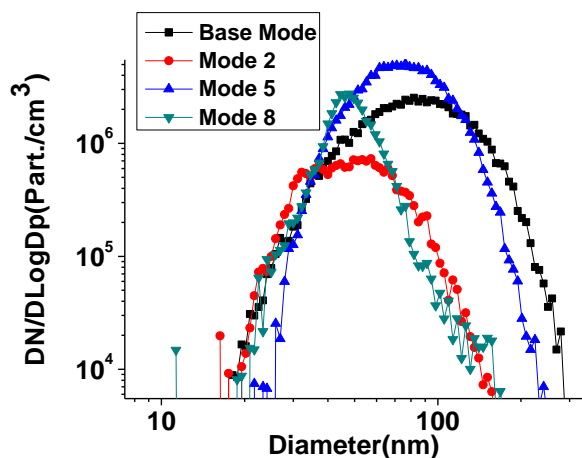


**Figure 5.16** Particle size distribution of the base mode, Mode 2, Mode 5 and Mode 8

According to the particle size distribution in Figure 5.16, the particles all showed a mono-modal distribution. Although the EGR was increased from 30 % in the base mode to 55 % in Mode 2, which was favorable for the particle production, the effect of the advanced injection pressure and high injection pressure led to a net reduction of PM, especially those with a diameter larger than 35 nm. In Mode 5, the main SOI was advanced by 2 °CA than in Mode 2; however, due to the reduced injection pressure, particles still increased. This was improved in Mode 8, when the highest injection pressure was used.

Referring to Figure 5.17, heat release of the base mode had two sources: one was its pilot combustion starting at 12 °BTDC and the other was the main combustion starting at -8 °BTDC. The pilot fuel was injected as early as at 18 °BTDC and finished at 15 °BTDC. The

main injection started at -1 °BTDC and finished at -7 °BTDC. Mode 2 and Mode 8 had advanced and magnified heat releases compared with the main release of the base mode, and their combustion duration was longer. Most importantly, after the injection finished, there were still 4 °CA and 8 °CA's time (Figure 5.18 (a)) for the fuel to mix with the combustion air, which gave a more homogeneous mixture. This explains the reduction of PM emissions.

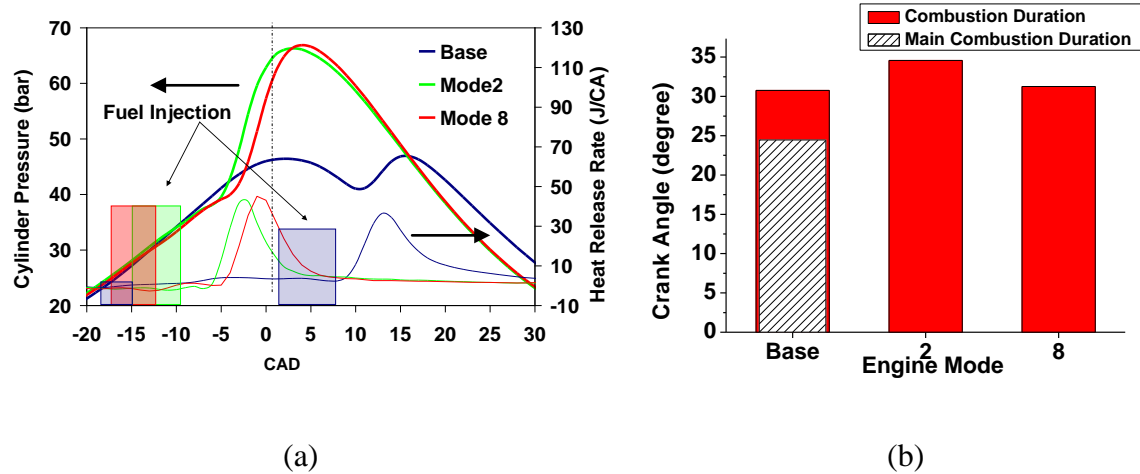


**Figure 5.17** (a) In-cylinder pressure, heat release and fuel injection time (b) combustion duration of the base mode, Mode 2 and Mode 8

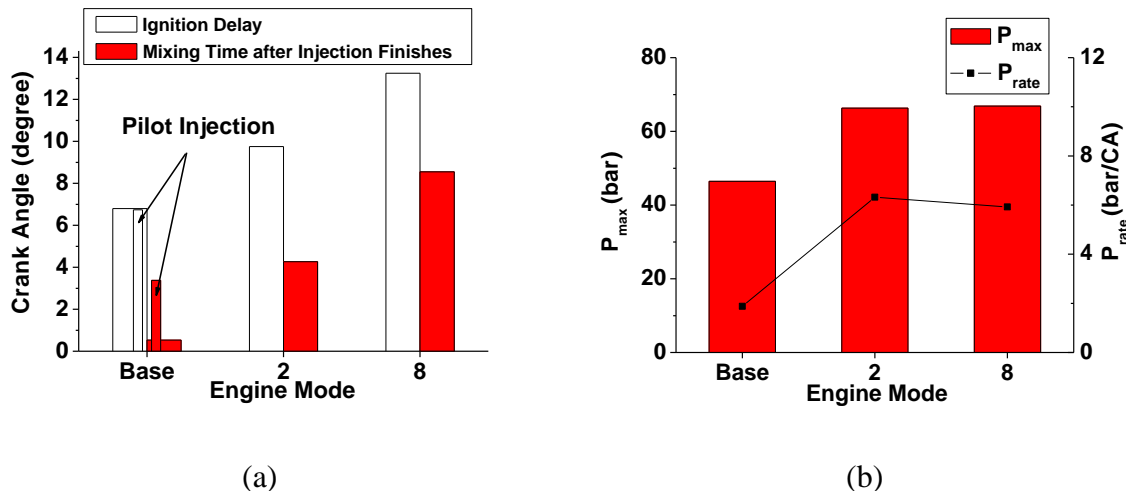


**Figure 5.18** (a) Ignition delay and fuel mixing time after the injection finished (b) P<sub>max</sub> and P<sub>rate</sub> of the base mode, Mode 2 and Mode 8

However, it should be noted that single injection combustion could result in higher pressure rising rate  $P_{rate}$  (Figure 5.19 (b)) and high  $P_{rate}$  leads to high engine noise. Besides, the engine usually suffered high CO and THC as well, due to the large amount of EGR used.

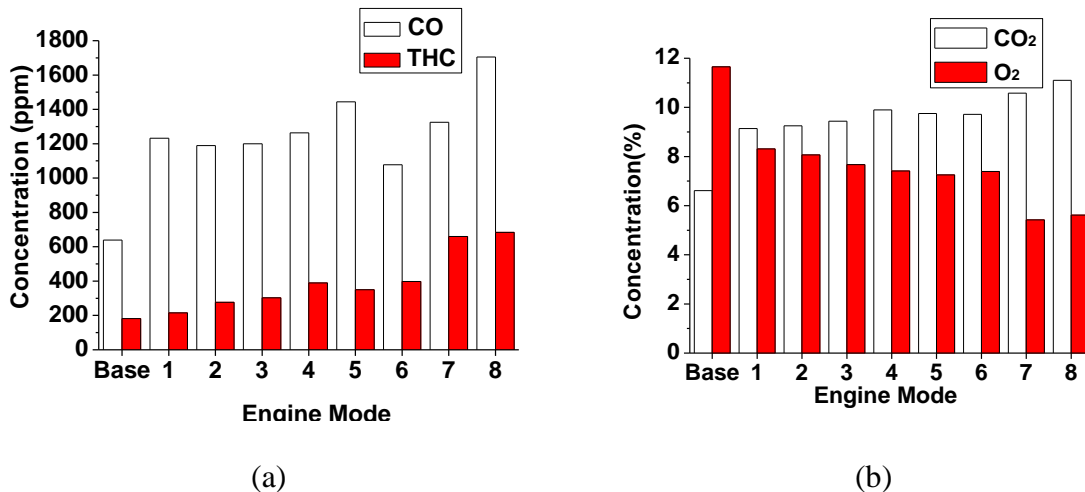


**Figure 5.19** (a) CO and THC emissions (b) CO<sub>2</sub>/O<sub>2</sub> trade-off of the single injection PCCI test

Similar research was conducted such as in (Kawano et al. 2005), the diesel HCCI was controlled by various EGR and late intake valve closing (LIVC). Up to 60 % EGR was used in the tests. It was noted that the suitable injection pressure and injection timing were 160 MPa and 25 °BTDC. In those tests, THC and CO emissions did not drastically increase without high fuel consumption, except for the case of long additional intake valve opening. Also through single injection, in (Ojeda et al. 2008), besides the early premixed injection strategy, when the fuel was injected at 60 °BTDC, a late premixed injection strategy was also tested, in which the fuel was injected close to TDC with heavy EGR (55%). It seemed that second method was even better for having improved the fuel vaporization and limited the THC emissions down to 1800 ppm. The NO<sub>x</sub> was kept below 15 ppm while the soot was below 0.5 FSN.

## 5.4 Summary

How engine injection parameters influencing the engine's performance and emissions is discussed in this chapter. They include single and multiple injections of normal diesel combustion as well as single injection-induced PCCI combustion. It is concluded that

1. The fuel injection parameters on the engine performance and emissions were also investigated. The advance of the main injection timing could advance the heat release and magnify the rates of heat release, thus reducing the smoke, THC and CO. However, NO<sub>x</sub> could be increased. EGR led to a smoothed and delayed combustion and reduced NO<sub>x</sub> emissions. At the same time, the smoke, THC and CO could be increased. Increasing the injection pressure could advance and magnify the heat release, due to improved fuel spray and correspondingly reduce the smoke and increase the NO<sub>x</sub> emissions. THC and CO could also be increased.
2. Impacts of different injection strategies on the engine emissions have a close relationship with the engine speed and load. The use of small quantities of pilot injection could lead to the increase of particle numbers under medium engine speed and load modes and the use of EGR could exacerbate this affect. However, under idle or high speed/load mode, particle numbers were reduced. Using a pilot injection before the main tended to produce more THC and larger particles, and this latter effect was not distinctive under high engine speed/load mode.
3. By combining the influence of these injection parameters on particulate and NO<sub>x</sub> emissions, calibrated single injection strategies for PCCI combustion could reduce the two emissions by more than 80 % compared to the normal multiple injections. However, P<sub>max</sub> and

THC and CO emissions were extremely high and this could be dealt with using a normal DOC.

## CHAPTER 6

### PM CHARACTERISTICS WITH PILOT INJECTIONS

Pilot injection has been used widely in diesel engines for its NO<sub>x</sub> and noise reducing effects. However, little data on particulate characteristics due to pilot injection controls are available. In this chapter, the non-volatile particulate emissions under the pilot injection's impacts is studied using a light duty common-rail Euro 4 diesel engine, to comply with the particle metrics of the European Emission Regulations (Regulation NO 715/2007, amended by 692/2008 and 595/2009). The key parameters of the pilot control: fuel quantity and injection timing, and the particulate number concentrations and size distributions, are investigated using different combinations.

#### 6.1 Multiple Injections

The emissions of diesel engines are believed to be caused by the in-homogeneity of fuels during combustion and increasing this homogeneity will bring the local equivalence ratios down, thus giving the benefit of less emissions. A methodology to achieve this is the multiple fuel injections strategy, which, as it suggests, includes multiple injections at various timings and quantities of fuel, combined with high injection pressure and the use of calibrated Exhaust Gas Recirculation (EGR). An accurate calibration of these control parameters has proved to achieve better performance of diesel combustion (Stringer et al. 2008; Vanegas et al.

2008), thanks to the common rail fuel injection system (Nagata et al. 2004; Denso Australia 2010), and this has been widely adopted in modern diesel engines nowadays.

### 6.1.1 Pilot Injection

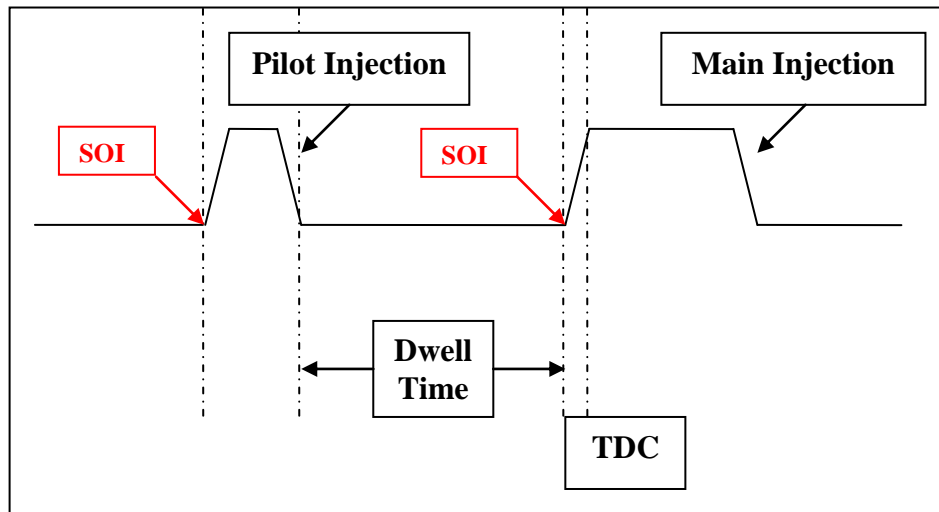


**Figure 6.1** Sketch of a typical injection

In current production engines, the most commonly used multiple fuel injection strategy includes one pilot injection before a main injection. Sometimes this can include a post injection, to further promote improved combustion and emissions reduction. The pilot injection can reduce engine noise and oxides of nitrogen ( $\text{NO}_x$ ), but it can also increase the smoke emissions (Zhang 1999; Roy et al. 2002). An early post injection is used to reduce this smoke and might lead to a slight decrease in  $\text{NO}_x$ . Finally, a late Start of Injection (SOI) of the main injection helps to reduce the carbon monoxide (CO) and hydrocarbon (HC) emissions under certain engine conditions (Vanegas et al. 2008). A typical profile of the multiple injection strategy is shown (Figure 6.1).

The quantity of pilot fuel is usually small compared to the quantity of the main fuel, so the emissions from the pilot combustion can be ignored in most cases and the total emissions

are solely dependant on the main combustion. The widely accepted mechanism of using the pilot injection technique is to raise the in-cylinder temperature and shorten the ignition delay of the main combustion (Carlucci et al. 2004). This brings about a low rate of initial combustion and avoids raising the gas temperature too quickly. Thus, the NO<sub>x</sub> emissions, which have a close relationship with temperature, can be reduced. At the same time, for a shortened ignition delay, the premix phase of the main combustion decreases. In other words, more diffusion combustion occurs, which might produce more smoke. However, under certain modes, especially with the increase of the pilot fuel portion and the engine load (Carlucci et al. 2003) the pilot combustion can be strengthened, and this may influence the total emissions in an opposite way (Okude et al. 2007).

### **6.1.2 Research Objective**

Based on the UNECE GRPE Particulate Measurement Programme (PMP), this study aims to investigate the non-volatile particle characteristics under different pilot injections through a thermo-diluter, when most of the volatiles were removed. By varying the injection conditions, the particle numbers and size distributions were examined and compared.

## **6.2 Engine Test Modes and Procedures**

Test fuels — Standard European diesel fuels conforming to the EN590 specifications were used for the tests (Table 3.7).

Exhaust measurement — The Horiba MEXA 7100 DEGR, AVL smoke meter (415SG002) and scanning mobility particle sizer (SMPS) (Model 3936) were used in the test to measure the gaseous emissions, smoke and particulate size distribution and concentration

respectively. The long DMA with a measuring range of 10-1000nm was used. The diluter is from TSI model 379020A and the dilution ratio was set to 90:1.

Heat release — Because of the difficulty of accurately determining the premixed combustion from the heat release profile, the following index was used (Figure 6.2).

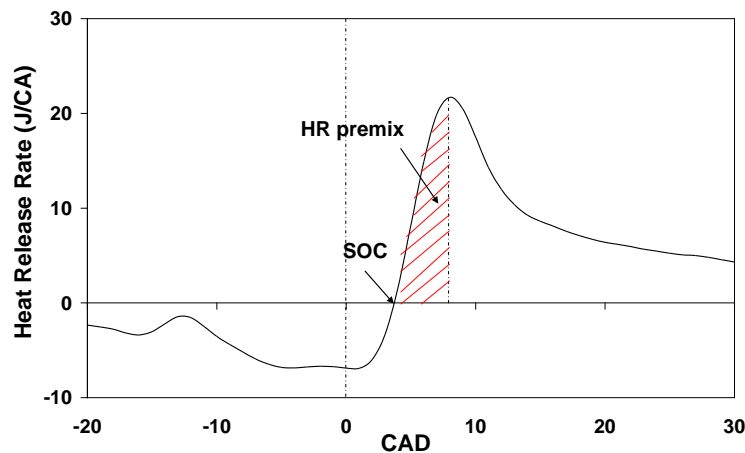


**Figure 6.2** HRR premix: index of the heat release during the premixed combustion

Engine test modes — Table 6.1 shows the 3 engine test modes (shown as Mode 1, Mode 2 and Mode 3) selected in this study. For each engine mode, the injection pressure, EGR and the SOI of the main injections were fixed. There were 12 variations of pilot injection timing and fuel quantity (see Appendix Tables C1, C2, and C3). The base mode is the mode calibrated to the Euro 4 emissions standard on the engine map. The samples and measurements were performed at the same location, upstream of the DOC and 10 minutes after the engine temperature reached 80 °C. For each test, measurements were repeated three times consecutively to provide an average, and are shown with error bars.

**Table 6.1** Engine test modes: (a) base engine mode calibrated to Euro 4 standard; (b) variations (CA=crank angle)

(a)					
Mode	Engine Speed (rpm)	Main SOI (BTDC)	Torque (nm)	Injection Pressure (MPa)	EGR (%)
1	1800	-1.69	52	23	28
2	1800	-2.69	91	84	22
3	2500	-2.06	84	129	30

Pilot Injection	1.5 (mm <sup>3</sup> /stroke)	3 (mm <sup>3</sup> /stroke)	4.5 (mm <sup>3</sup> /stroke)
Base-5° CA	(a)	(e)	(i)
Base Mode	(b)	(f)	(j)
Base+5° CA	(c)	(g)	(k)
Base+10° CA	(d)	(h)	(l)

## 6.3 Effects of Pilot Injections on PM Emissions

### 6.3.1 Effect of Pilot Fuel Quantity

#### a. In-cylinder pressure and heat release

The impact of the pilot fuel quantity on the engine combustion is shown in Figure 6.3. According to the graphs, the increase of the pilot fuel tended to: 1. advance the main combustion; 2. reduce the HRR peak of the main combustion; 3. increase the HRR peak of the pilot combustion. This was caused by the strengthened pilot combustion, which more significantly raised the in-cylinder gas temperature, and shortened the main ignition delay. To maintain the same engine speed and torque, the increase of the pilot fuels meant the reduction

of the main injection fuel, and that was the main reason why the HRR peak of the main combustion was reduced. It can be also noted that the increase of the pilot fuel had little influence on the start of the pilot combustion and for the same quantity of the pilot fuel, the pilot combustion was more evident when the engine load increased, referring to (a) and (b). This was also noticed in (Carlucci et al. 2003).

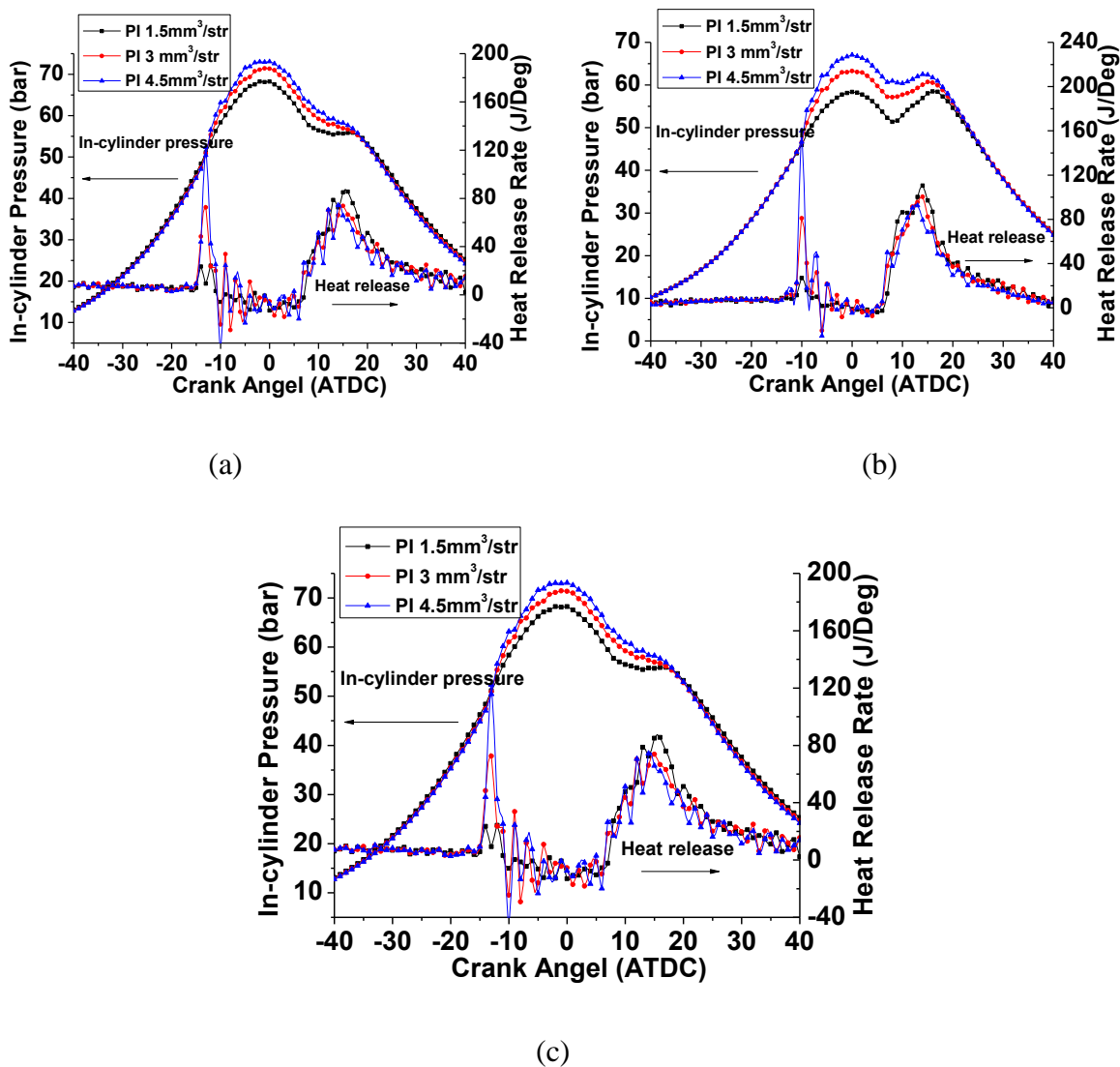


**Figure 6.3** In-cylinder pressure and heat release with different pilot fuel quantity (a) Mode 1  
 (b) Mode 2 (c) Mode 3

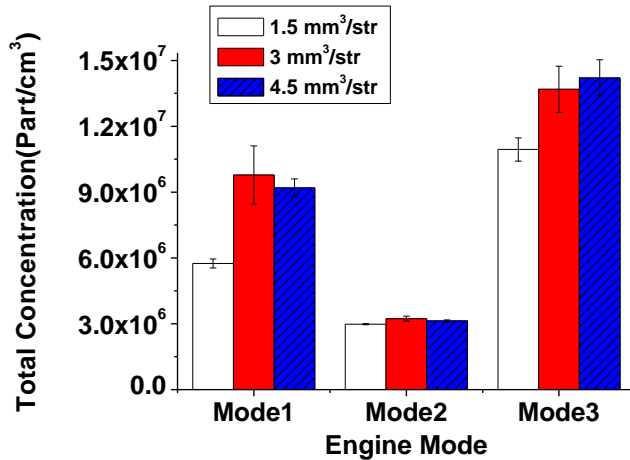
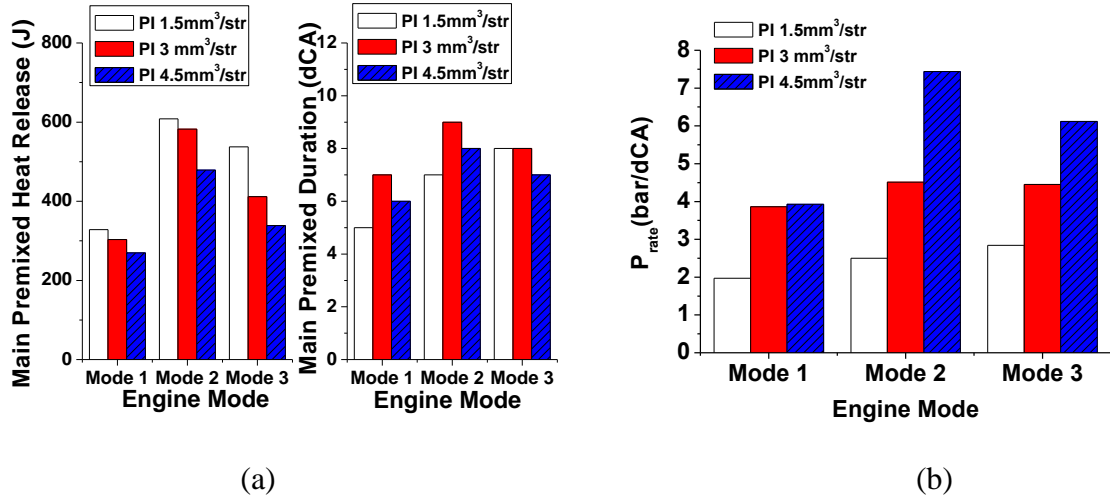
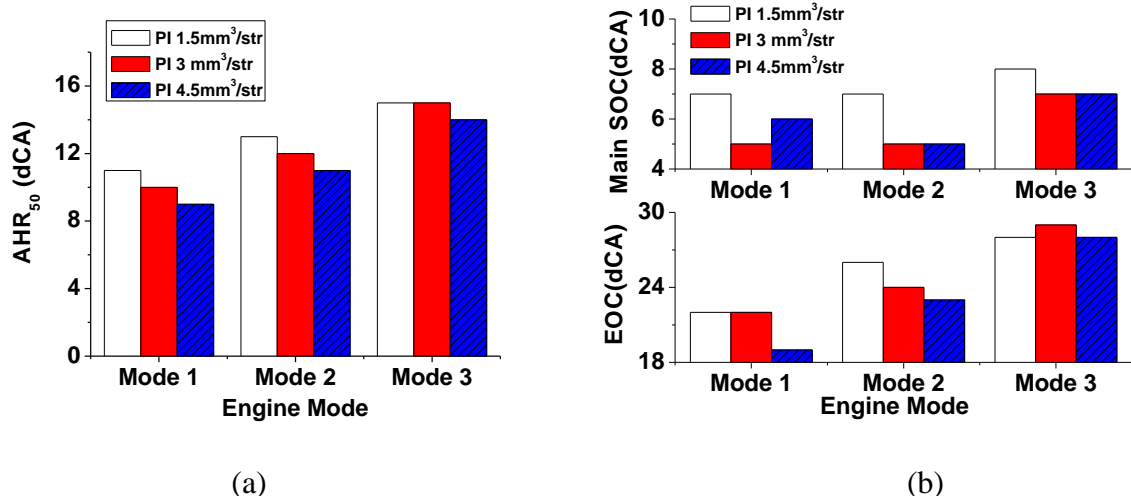
**b. Total particulate number and mean diameter****Figure 6.4** Total particulate numbers with different pilot fuel quantities (base mode)

Figure 6.4 presents the influence of the pilot fuel quantity on the total particulate number concentrations. It shows that the increase of the pilot fuel generally led to the increase of the particulate concentrations. In these three modes, when the pilot fuel was gradually increased from  $1.5 \text{ mm}^3/\text{stroke}$  to  $3 \text{ mm}^3/\text{stroke}$  and finally  $4.5 \text{ mm}^3/\text{stroke}$ , the total particulate number was increased by 70% and 60% in Mode 1, 8% and 5% in Mode 2 and 25% and 30% in Mode 3 respectively. This is believed to be caused by the reduction of the main HRR peak, corresponding to the reduction of released energy in the premixed phase of the main combustion (Badami et al. 2001) (Figure 6.5 (a)). Figure 6.5 shows that  $P_{\text{rate}}$  also increased with the increase of the pilot fuel quantity.



**Figure 6.5** (a) Premixed-controlled main combustion duration and heat release (base mode);  
 (b)  $P_{rate}$  under different pilot fuel quantities

$AHR_{50}$  was the crank angle at which 50% of the heat was released. Figure 6.6 (a) indicates that it decreased with the increase of the pilot fuel. The influence of the pilot fuel quantity to the combustion timing shown in Figure 6.6 (b) and according to it, the main combustion was advanced by 1 – 2 degree crank angle with the increase of the pilot fuel quantity.



**Figure 6.6** (a)  $AHR_{50}$  (b) EOC and main SOC under different pilot fuel quantities

In Mode 1, the impact of the pilot injection on the particulates was the most significant. This was due to its: 1. high pilot fuel's percentage of the total fuel; 2. high EGR ratio (Figure 6.7) as EGR was able to exaggerate the pilot's effects on emissions, combustion noise and in-cylinder pressure, which was illustrated in (Tanaka et al. 2002).

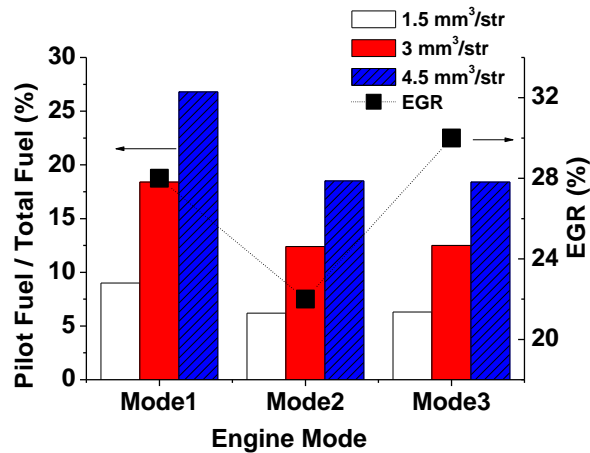


**Figure 6.7** Total particulate numbers with different pilot fuel quantities (base mode)

The increase of the fuel quantity also led to more large particulates. This is due to the increased total particulate number which strengthened the agglomeration of the spherules after they formed during combustion. They collided with each other and merged into larger congregations.

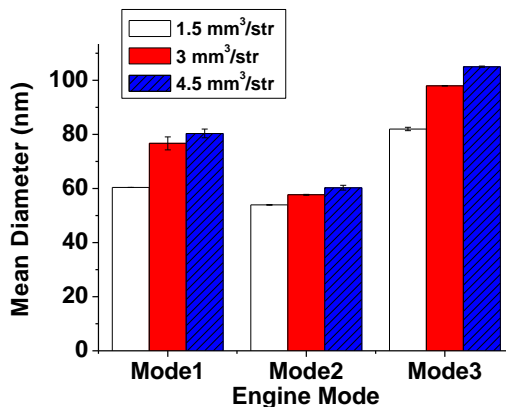


**Figure 6.8** Mean particulate diameters with different pilot fuel quantities (base mode)

### c. Particulate size distribution

The impact of the pilot fuel quantity on the particulate size and distribution is shown in Figure 6.9. In the three graphs presented, the particulates all showed a mono-modal structure with the accumulation mode particulates peaking at 60-90 nm. It indicates that with the increase of the pilot fuel quantity, the number of the accumulation mode particulates increased, while the nucleation mode particulate number decreased. Accumulation mode particulates were more remarkably influenced by the pilot fuel than the nucleation mode particulates. In Mode 2, when the torque was the highest, the pilot fuel impact was the least significant.

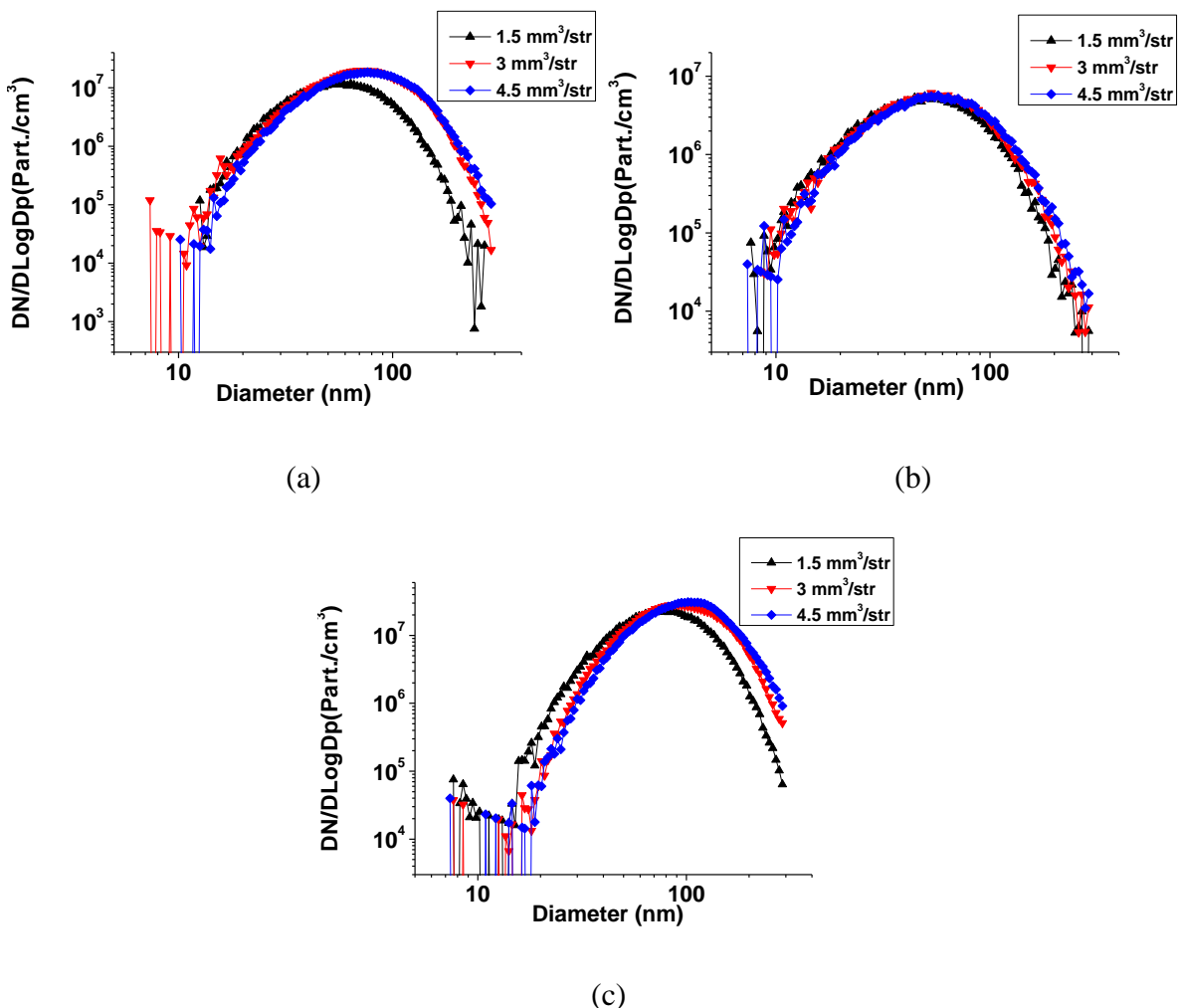
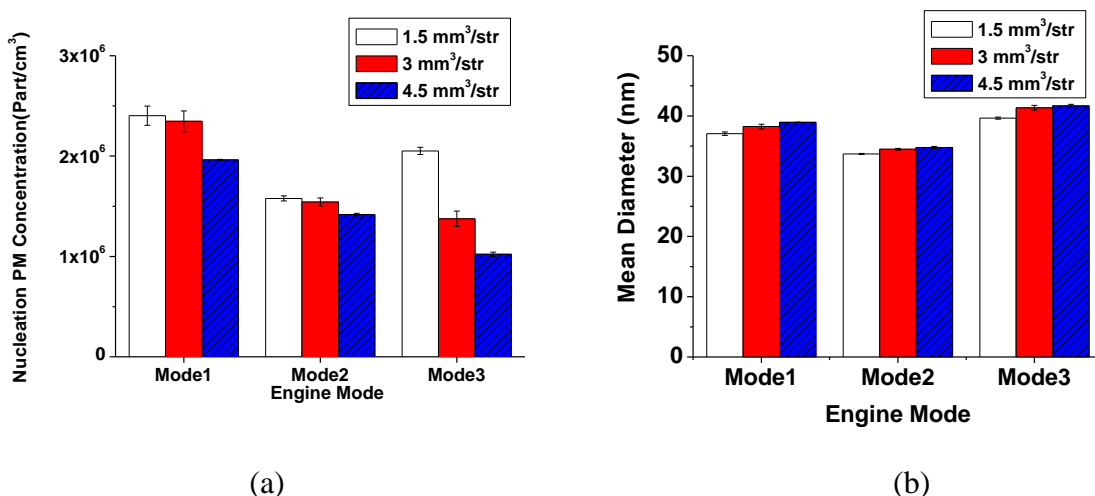


**Figure 6.9** Particulate size distributions with different pilot fuel quantities (base mode)

#### d. Nucleation and accumulation mode particulates

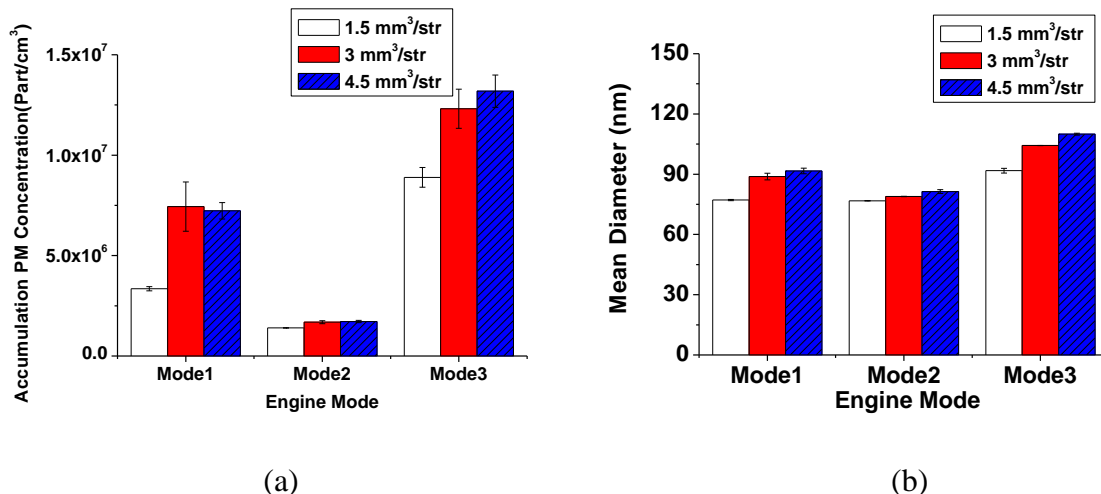
With the help of the thermo-condition, the volatile components in the nucleation mode were minimized. At the same time, the nucleation of sulfuric acid was also avoided as the measurement was taken before the DOC. Nucleation mode particles, whose diameters are below 50 nm, can be treated as a gathering of the solid carbonaceous spherules formed from the combustion and ash fractions contained in the fuel or lubricant.

Figure 6.10 shows the nucleation mode particle concentrations and mean diameters when different pilot fuel quantities were used. It indicates that at the same engine speed and torque, the total particulate number in the nucleation mode decreased with the increase of the pilot fuel. As the pilot fuel was gradually increased from  $1.5 \text{ mm}^3/\text{stroke}$  to  $3 \text{ mm}^3/\text{stroke}$  and finally  $4.5 \text{ mm}^3/\text{stroke}$ , the total particulate number was slightly reduced by 2.4% and 18.3% in Mode 1, 2.2% and 10.2% in Mode 2 and 33% and 50% in Mode 3 respectively. The mean diameters were little impacted upon, and the maximum increase was 2 nm in Mode 3.



**Figure 6.10** Nucleation mode particles (a) concentration, (b) mean diameter with different pilot fuel quantities (base mode)

The accumulation mode particle concentrations and mean diameters with different pilot fuel quantities are presented in Figure 6.11. Opposite to the nucleation mode one, the total accumulation particulate number significantly increased with the increase of the pilot fuel by 122% and 116% in Mode 1, 20% and 22% in Mode 2 and 38% and 48% in Mode 3 respectively. This was the reason for a net increase of the total particulates shown in Figure 6.4. The mean diameters were also increased, and the variation ranged from 2 to 18 nm.



**Figure 6.11** Accumulation mode particle (a) concentration, (b) mean diameter with different pilot fuel quantities (base mode)

### 6.3.2 Effect of Pilot Injection Timing

#### a. In-cylinder pressure and heat release

Figure 6.12 shows the impact of the pilot fuel injection timing on the engine combustion when 1.5 mm<sup>3</sup>/stroke pilot fuel was used. It indicates that the advance of the pilot fuel injection tended to: 1. advance the pilot combustion; 2. increase the pilot ignition delay.

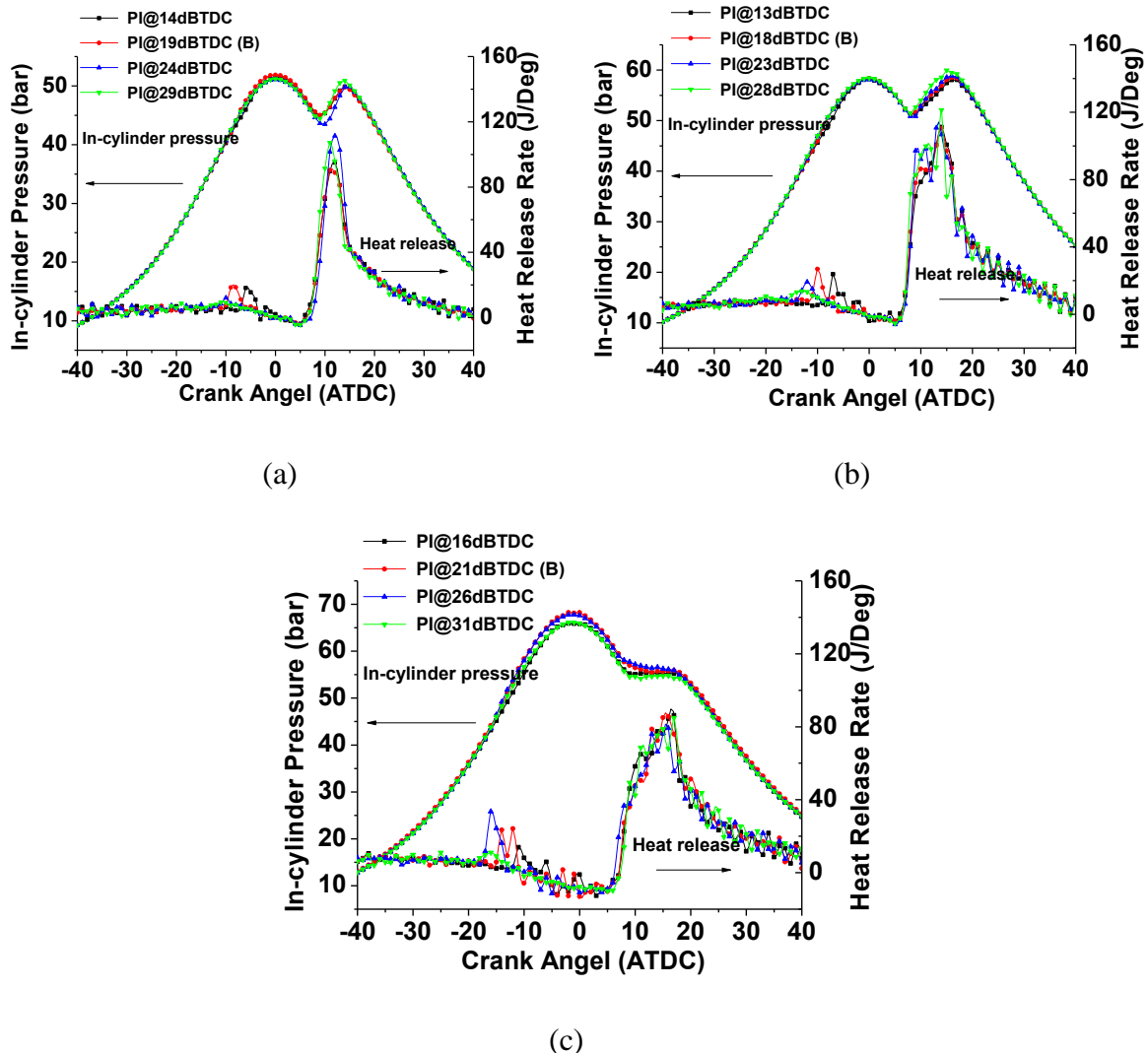


**Figure 6.12** In-cylinder pressure and heat release with different pilot injection timing (1.5 mm<sup>3</sup>/stroke) (a) Mode 1 (b) Mode 2 (c) Mode 3

It also tended to influence the main premixed combustion as Figure 6.13 (a) shows, in either of the three modes. Similar researches in Okude et al. (2007) noted that the earlier the pilot injection timing, the lower the peak rate of the main heat release. This corresponds to Mode 3. While in Carlucci et al. (2003) the HRR peak of the main combustion actually increased with the advance of the pilot injection timing, which corresponds to Mode 1 and 2 in this test. However, in either of these modes, the premix combustion durations were both shortened. Badami et al. (2001) pointed out that main combustion reached minimum intensity

when the pilot dwell time was around 500 us and further advance or delay of the pilot injection could lead to the increase of the main HRR peak. Similarly, it can be also noted from Figure 6.12 that there was a pilot injection timing ‘limit’. If the pilot fuel was injected towards this limit, the pilot combustion was more signified, and correspondingly, the main combustion HRR peak was reduced. In most cases,  $P_{rate}$  increased with the advance of the pilot injection in this test.

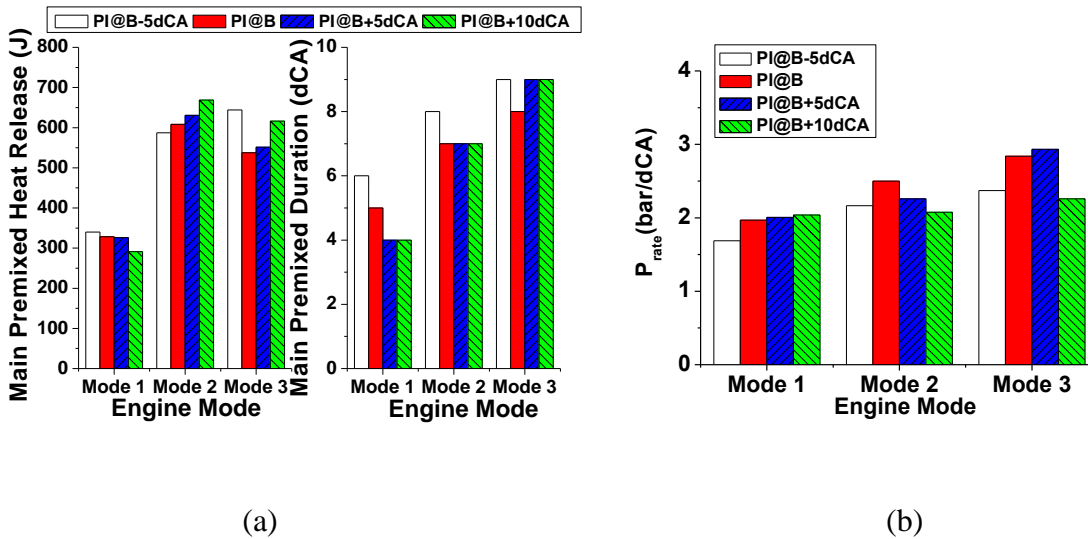


**Figure 6.13** (a) Premixed-controlled main combustion duration and heat release (base mode);  
 (b)  $P_{rate}$  under different pilot fuel injection timing

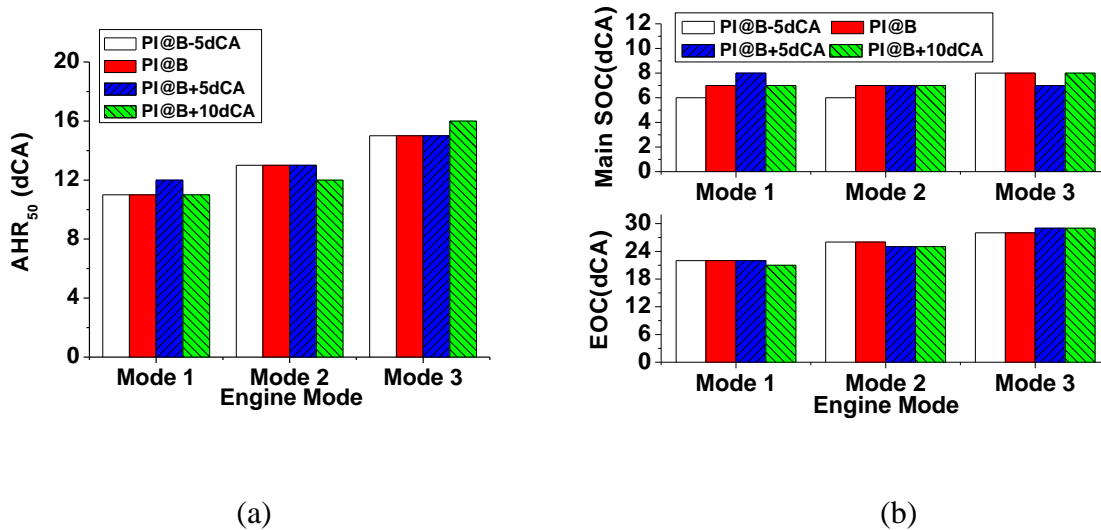


**Figure 6.14** (a) AHR<sub>50</sub> (b) EOC and main SOC under different pilot fuel injection timing

According to Figure 6.14, the influence of the pilot injection timing on AHR<sub>50</sub> or the start of the main combustion was not significant, although in Mode 1, it may seem to delay the main combustion.

**b. Total particulate number and mean diameter**

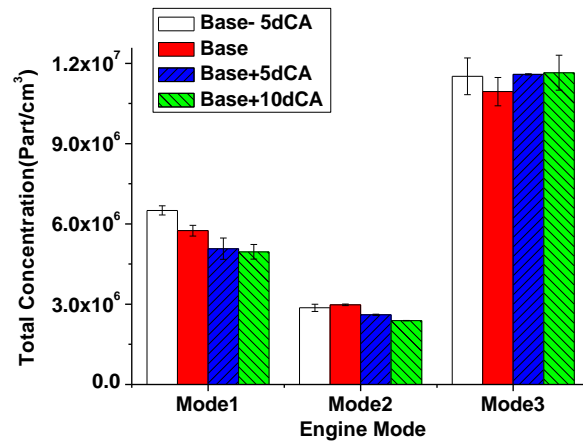


**Figure 6.15** Total particulate numbers with different pilot fuel injection timings (1.5 mm<sup>3</sup>/stroke)

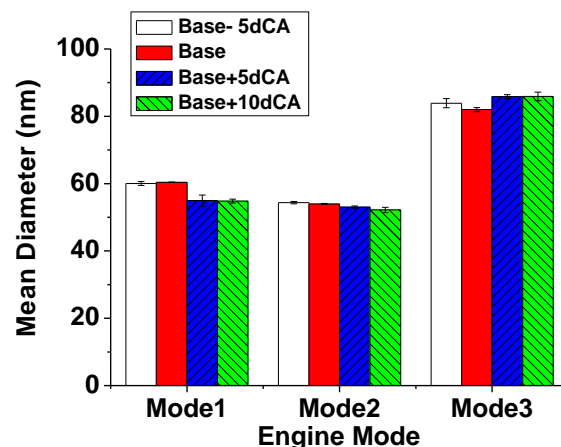


**Figure 6.16** Particulate mean diameter with different pilot fuel injection timings (1.5 mm<sup>3</sup>/stroke)

The total particulate concentrations and mean diameters with different pilot fuel injection timings ( $1.5 \text{ mm}^3/\text{stroke}$  quantity) are shown in Figure 6.15 and Figure 6.16 respectively. Due to the signified main premixed combustion, advancing the pilot injection showed a good particulate number reduction effect and when this advance reached  $15^\circ\text{CA}$ , particulate numbers decreased by 23.8 % in Mode 1 and 16.7 % in Mode 2. However, in Mode 3, this effect was less noticeable, as the total number was only slightly increased by 1% when the injection timing was advanced from  $16^\circ\text{BTDC}$  to  $31^\circ\text{BTDC}$ . The mean diameters were little affected by the pilot injection timing and the variation was below 5 nm.

### c. Particulate size distribution

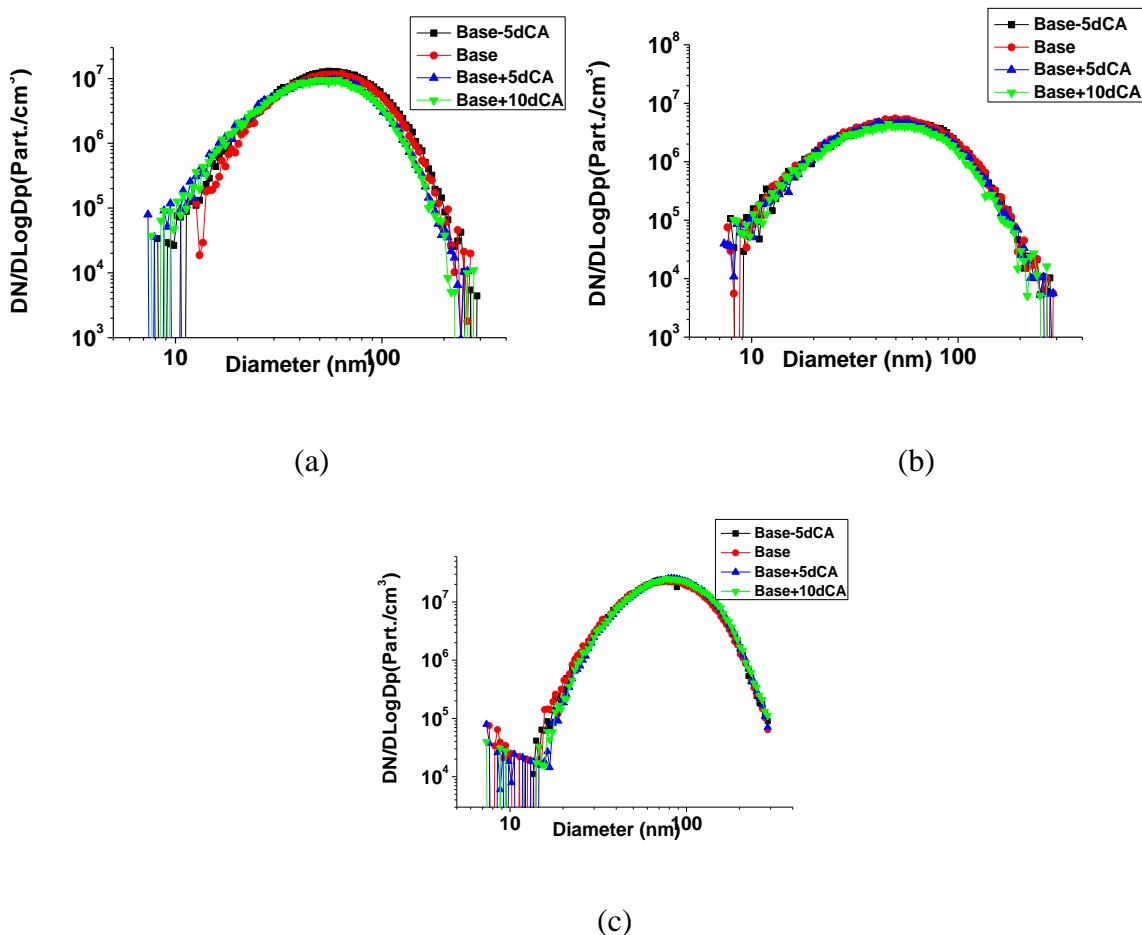


**Figure 6.17** Particulate size distributions with different pilot fuel injection timings ( $1.5 \text{ mm}^3/\text{stroke}$ )

The particulates size and distributions in Figure 6.17 still have the mono-modal structure and the peaks of the accumulation mode particulates are almost identical in each mode.

#### d. Nucleation and accumulation mode particulate

Figure 6.18 presents the nucleation mode particulate concentrations and mean diameters with different injection timings. According to the figure, the advance of the pilot injection reduced the particulate number but showed no significant influence to the mean diameters. Compared with the initial injection (Base-5 °CA), advancing the injection time by 15 °CA slightly reduced the nucleation mode particulate number by around 10%.

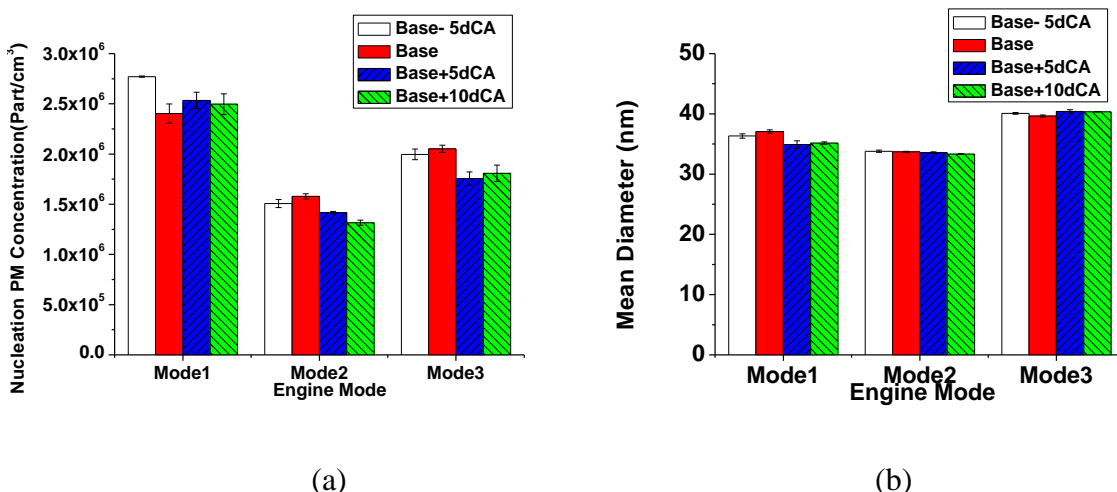


**Figure 6.18** Nucleation mode particles (a) concentration, (b) mean diameter with different pilot fuel injection timings (1.5 mm<sup>3</sup>/stroke)

With the advance of the pilot injection, the change of the accumulation mode particulate number is the same as the nucleation mode. This was especially remarkable in Mode 1 (Figure 6.19 (a)). When the pilot injection was advanced from 14 °BTDC to 29 °BTDC, the number was reduced by more than 30%. In Mode 2, the reduction was less but

still reached 21% when the injection timing was advanced by 15 °CA. In Mode 3, the particulate concentration was increased by 3%. The mean diameters varied between 1- 3 nm.

Referring to Figure 6.15, it can be noted that the reduction of particulates with the advance of the pilot injection was the result of the decrease of nucleation and accumulation mode particulates in both Modes 1 and 2, while in Mode 3, this effect was less significant, due to the increase of the accumulation particulate, which compensated the reduction of the nucleation mode particulates.

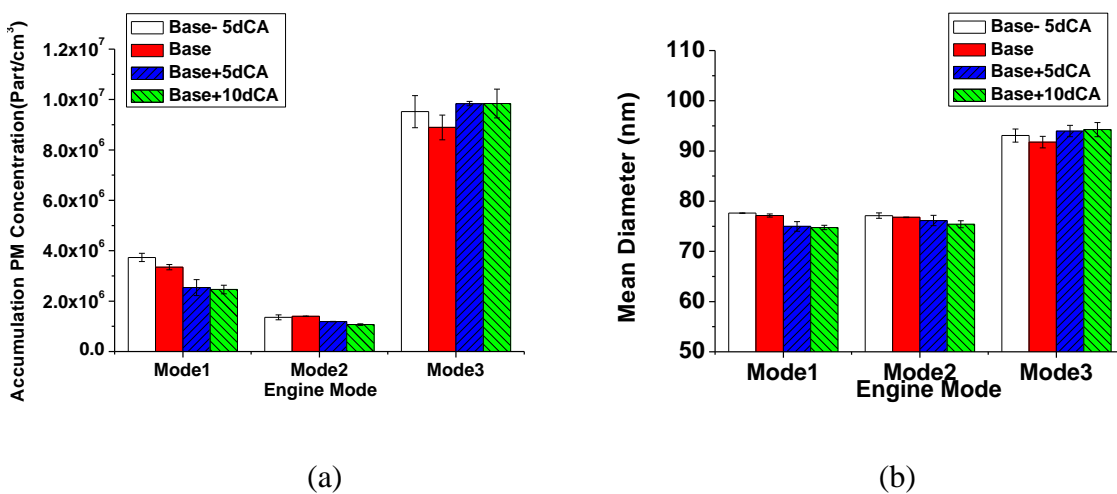


**Figure 6.19** Accumulation mode particles (a) concentration, (b) mean diameter with different pilot fuel injection timings ( $1.5 \text{ mm}^3/\text{stroke}$ )

### 6.3.3 Restrictions of the Pilot Injection Parameters

Further extending the tests, it can be noted that the impact of pilot injection timing and fuel quantity on particulate numbers are dependent on the engine conditions (Figure 6.20). Although the advance of the pilot quantity generally reduced particulates, under certain conditions, such as in Mode 1 (Figure 6.20(a)), when a higher quantity of pilot fuel used, it actually increased the total particulate concentration with the advance of the injection time.

The same is true for the pilot fuel quantity as in Figure 6.20(c): the increase of the fuel quantity reduced the particulate number in Mode 3, when the pilot fuel was injected at 30 °BTDC.

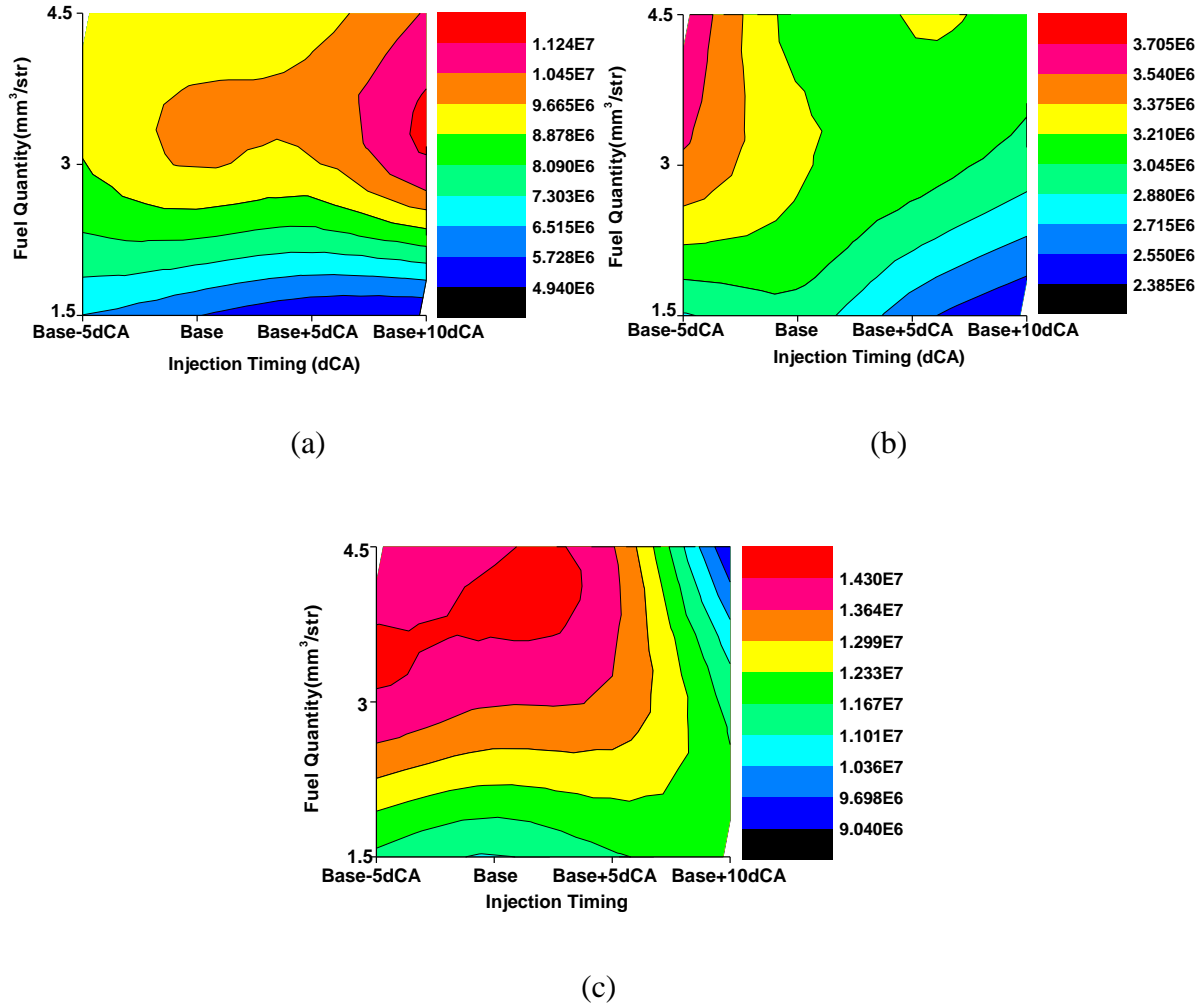


**Figure 6.20** Total particulate numbers with different pilot fuel quantity and injection timings  
 (a) Mode 1 (b) Mode 2 (c) Mode 3

Pilot combustion was more significant when its fuel quantity was increased and generally the advance of the injection timing led to better combustion. However, if it was too advanced, the pilot combustion might deteriorate, which might influence the total PM emissions greatly (Figure 6.21).

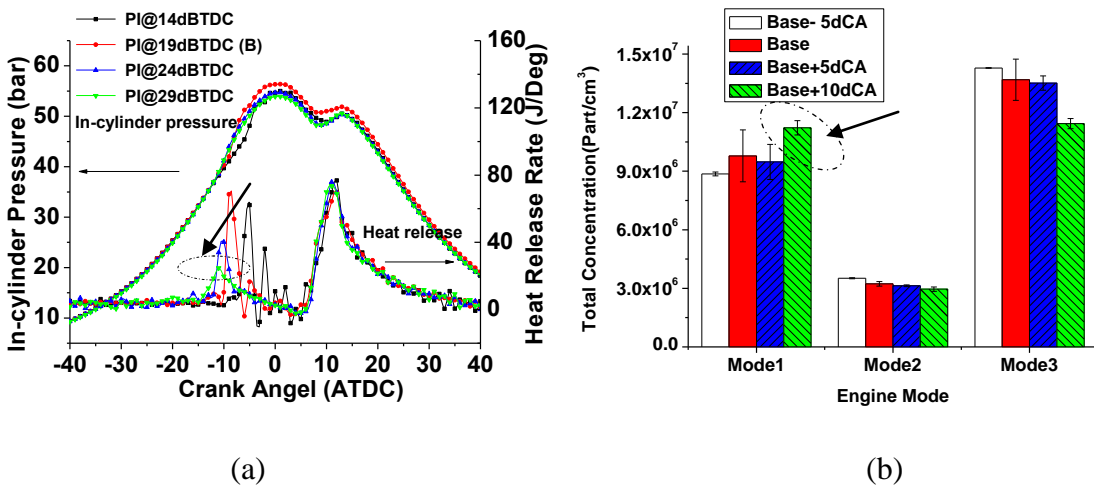


**Figure 6.21** (a) Heat release and (b) total concentration of Mode 1 with  $3 \text{ mm}^3/\text{stroke}$  pilot injection at  $29^\circ\text{BTDC}$

## 6.4 Summary

The pilot injection's impact on the particle emissions were studied using a light duty common-rail Euro 4 diesel engine with EGR. The results illustrated how a pilot injection alongside a main injection could influence the in-cylinder combustion and emissions by varying its key factors: injection quantity and injection timing.

1. It has been noticed that the pilot injection impact has a close relationship with the engine speed and load and EGR.
2. The increase of pilot fuel quantities reduced the main premixed combustion and increased both the particle number and the mean diameter. This was due to its significant impact on the accumulation mode particulates, whose increase shadowed the decrease of nucleation mode particulates.
3. The advance of the pilot injection timing generally signifies main premixed combustion and showed a good particle number reduction effect, contributed to the reduction

of particulates in both nucleation and accumulation mode. It also leads to a smaller particle mean diameter for all the engine modes.

4. Pilot fuel quantity and injection timing influence both the ignition delay and HRR peak of the pilot and main combustions. In most cases, the impact on the latter determined the total particulate emissions, because the main injection occupies the larger fraction of the total fuel. In certain cases, such as with high fuel quantity, the pilot fuel can be signified or when the injection was too much advanced, the pilot combustion may deteriorate. This may alter the expected trend of the particulate emission change, solely based on its influence on the main combustion.

## CHAPTER 7

# PM CHARACTERISTICS WITH ALTERNATIVE FUEL BLENDSS

In this chapter, the particle emission characteristics of 10% alternative diesel fuel blends (Rapeseed Methyl Ester and Gas-to-Liquid) are investigated through the tests carried out on a light duty common-rail Euro 4 diesel engine. Under steady engine conditions, the study has been focused on particle number concentration and size distribution where the non-volatile parts were also measured through the use of extra thermo-dilution, to comply with the particle metrics of the European Emission Regulations (Regulation NO 715/2007, amended by 692/2008 and 595/2009). The particle characteristics during the engine warming up are also investigated.

## 7.1 Biodiesel and GTL Diesel Blends

### 7.1.1 Benefits and Blending Ratio

Biodesel is one of the new alternative fuels, whose use is driven by the fossil fuel shortage and promoted by the increasing nationally defined fiscal means. It is commonly produced from a variety of raw materials through reaction called ‘transesterification’ (Gerpen et al. 2004). The transesterified biodesel mainly contains mono-methyl ester of long chain fatty acids and compared with the conventional diesel, it has the following advantages:

1. higher cetane ratings; 2. virtually containing no sulphur content or aromatic hydrocarbons, with better lubricating properties; 3. more complete combustion in engines for containing more oxygen, although with lower calorific values; 4. higher flash point for safer storage and delivery. 5. can help to reduce emissions such as particulates. These have been proved in many studies (Nwafor 2004; Kawano et al. 2008).

However, its physical and chemical characteristics make it facing challenges when used in commercial engines. A major disadvantage of biodiesel is the reduced oxidation stability, compared with mineral diesel. There is a potential impact on fuel injection equipment components, as described by FIE manufacturers (FIE Manufacturers 2007). One of the workable ways is to blend it with the commercial diesel at a relatively low percentage (Mayer et al. 2005; Kawano et al. 2008; Yoshida et al. 2008; Kousoulidou et al. 2009). According to the ACEA agreement on biofuels made in 2008 (ACEA 2008), it was agreed that 7% was the maximum permissible blend level for commercial diesel engines without making any modifications. Nowadays, the new diesel supplies from fuel companies have bio-components up to 7%.

Unlike biodiesel, Gas to Liquid (GTL) diesel is not yet widely available for the public use. However, for its abundant resources, there is a growing demand and the developing conversion technologies are making it another option to be the future alternative of the conventional diesel (US Energy Information Administration 2010). Similar to biodiesel, GTL produces fewer emissions than fossil diesel, and having it blended with fossil diesel is a possible way in the near future. GTL is produced by converting natural gas or other gaseous hydrocarbons into longer-chain hydrocarbon diesel, through methods such as Fischer-Tropsch. Compared with conventional diesel, GTL has the following advantages: 1. higher cetane

ratings; 2. virtually containing no sulphur content or aromatic hydrocarbons; 3. can help to reduce emissions such as carbon monoxides, particulates and etc. The density of GTL is normally lower than a typical EN590 compliant mineral diesel, and this limits the amount that can be blended without stepping outside the density / viscosity limits prescribed in the EN590 standard. These were presented in (Schaberg et al. 2005; Kitano et al. 2007).

### **7.1.2 Research Objective**

The present study aims to investigate the particles characteristics from the combustion of 10% blend of RME and GTL (comparable to the 2020 fuel blends target) on a Euro 4 engine without any modification. The measurement has been taken using 2 methods: one is based on the UNECE GRPE Particulate Measurement Programme, where thermo-dilution is used, and the other without using thermal dilution.

## **7.2 Engine Test Modes and Procedures**

Test fuels — In the test, Standard European diesel fuels conforming to the EN590 specifications, 10% RME and 10% GTL diesel were used (labeled as RME 10, GTL 10 respectively). The properties of the fuels used are listed in Table 3.7.

Exhaust measurement — The Horiba MEXA 7100 DEGR, AVL smoke meter and Scanning Mobility Particle Sizer (SMPS) (Model 3936) were used in the test to measure the gaseous emissions, smoke and particulate size distribution and concentration respectively. The long DMA with a measuring range of 10-1000nm was used. The dilution ratio of the diluter was set to 60:1 for non thermo-dilution (Diluter from TSI, Model 379020A) and for thermo-dilution this was increased to 181:1 for the primary dilution and 3 for the secondary

one, which gave a total dilution ratio of 542:1 (the diluter was from Matter Engineering AG, Model ASET15-1). A Jeol JSM-7000F FE Scanning Election Microscope was used to analyze the particulate morphology.

Engine test modes — Table 7.1 shows the 8 engine test modes selected and recommended by the supplier of the engine for this study, which covered different speeds and loads. EGR was used in Mode 2, 3 and 6, and the EGR valve opening for the diesel fuel was also listed. For all the three types of fuels, the engine was running at the same speed and torque. The injection strategies were adjusted automatically by the ECU calibrated for diesel fuel without any modification. The sampling and measurement were achieved at the same test point upstream the DOC after 10 minutes engine stabilization. For each mode, measurements were carried out three times in a row and the results were averaged.

**Table 7.1** Engine test modes

Mode	Engine Speed (rpm)	Torque (Nm)	Load (%)	EGR Valve Opening (%)
1	800	2.1	0.68	0
2	1800	30	9.68	30.91
3	1800	30	9.68	15.45
4	1800	30	9.68	0
5	1800	134	43.23	0
6	3100	35	11.29	18.18
7	3100	138	44.52	0
8	3100	230	74.19	0

## 7.3 PM Number and Size Distribution from Diesel, RME10 and GTL10

### 7.3.1 PM Number Concentration

Figure 7.1 shows the total exhaust particulate number concentration of the eight engine modes when fuelled with diesel, RME 10 and GTL 10 respectively.

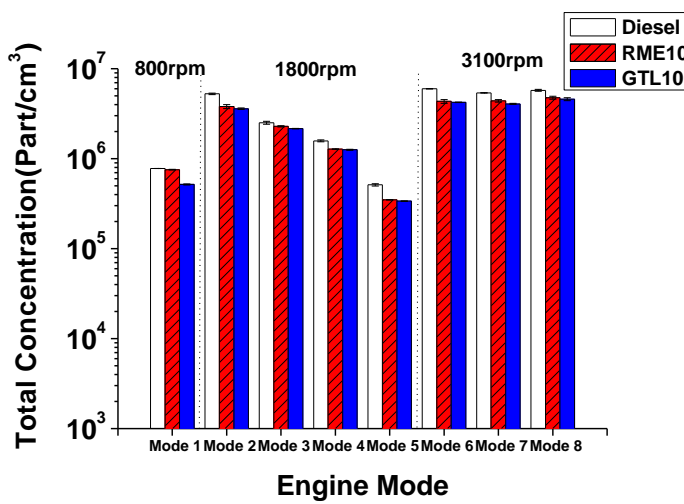


**Figure 7.1** Exhaust particulate number concentrations (total)

Effect of alternative fuel blends — It is very clear that adding either of the two alternative fuels, even at a percentage as low as 10%, could reduce the particle numbers in a similar way and this effect was even more significant when the engine was running in the middle speed range and high speed range with low loads. As shown in mode 2, mode 5 and mode 6, RME 10 reduced the particle number by 28%, 32% and 28% and GTL 10 by 32%, 34% and 29%, respectively, compared with diesel. In the idle mode, GTL 10 emitted the least particles, 33% less than diesel, while RME 10 showed little improvement. This effect has been illustrated in many papers and it is believed that for the high cetane number and aromatics and sulphur -free characteristics, the 10% GTL diesel blend could improve the PM

emission, while the oxygen contents contained and also the aromatics-free characteristics of the 10% RME could achieve similar PM reduction.

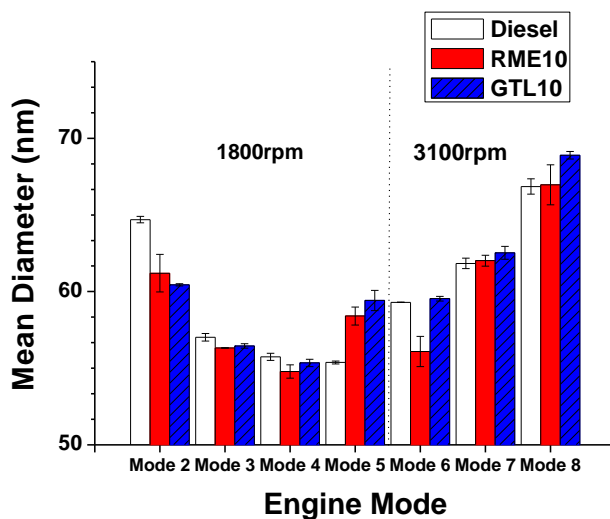
**Effect of engine speed and torque** — For the eight engine modes, the particle numbers varied from  $5 \times 10^5/\text{cm}^3$  to around  $6 \times 10^6/\text{cm}^3$ . The engine emitted the least concentration of particles in Mode 5 for all the three types of fuels when it was running at 1800 rpm, 134 Nm and no EGR was used. Mode 4 and Mode 5 had the same speed of 1800 rpm, with no EGR and when the torque was increased from 30 Nm to 134 Nm, the particle numbers were reduced by 68% for diesel, 73% for RME 10 and 73% for GTL 10 respectively. Under high speed engine conditions, the total particle numbers were increased with the load for RME 10, while for diesel and GTL 10, they were slightly reduced. The increase of speed could result in more particles, as in Mode 7 the particle number was 10 times more than that in Mode 5.

**Effect of EGR** — EGR is mainly used for the reduction of NO<sub>x</sub> and its impact on the particulates has been discussed by many people such as (Natti et al. 2008). EGR's particle producing effects were caused by its oxygen-replacement, radicals-supply effects and higher heat capacity. From Mode 2 to Mode 4, the EGR valve opening was reduced from around 31% to 0% (no EGR), and the particle numbers were reduced by 70% for diesel, 66% for RME 10 and 65% for GTL 10 respectively. In Mode 3, when the EGR valve was 15% opened, the effect of the alternative fuel blends to the particle numbers was least significant.

### 7.3.2 PM Mean Diameter

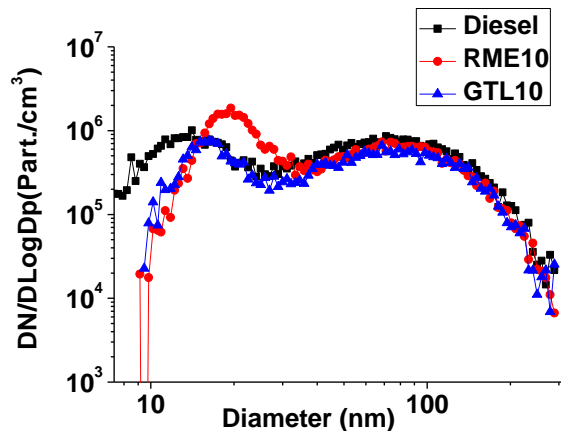
Figure 7.2 is the counted mean particle diameters of the eight engine test modes, derived from the SMPS results. The influences of the fuel properties to the diameters are not clear, although RME 10 seems to show the smallest mean diameter for most of the engine modes. However, for all the three fuels, the increase of engine torque led to an increase of the

particle mean diameter, either in middle speed or high speed range. EGR not only increased the particle numbers, it also tended to create larger particles as the figure shows for Mode 2, 3 and 4.



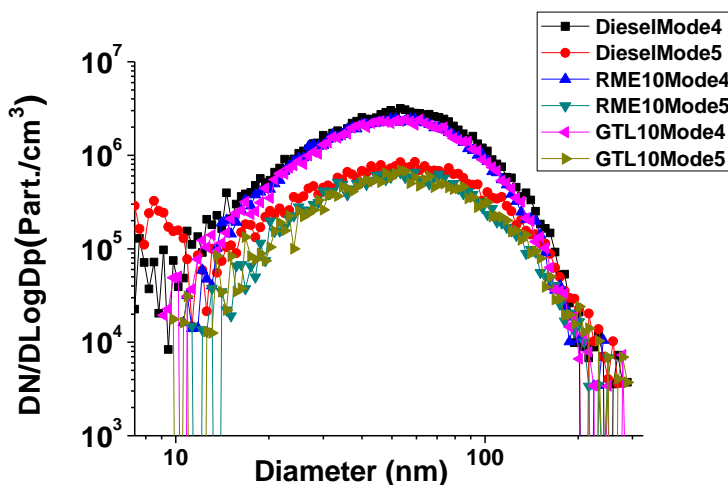
**Figure 7.2** Particle mean diameter

### 7.3.3 PM Size and Distribution



**Figure 7.3** Number weighted particle size distributions at 800 rpm (total)

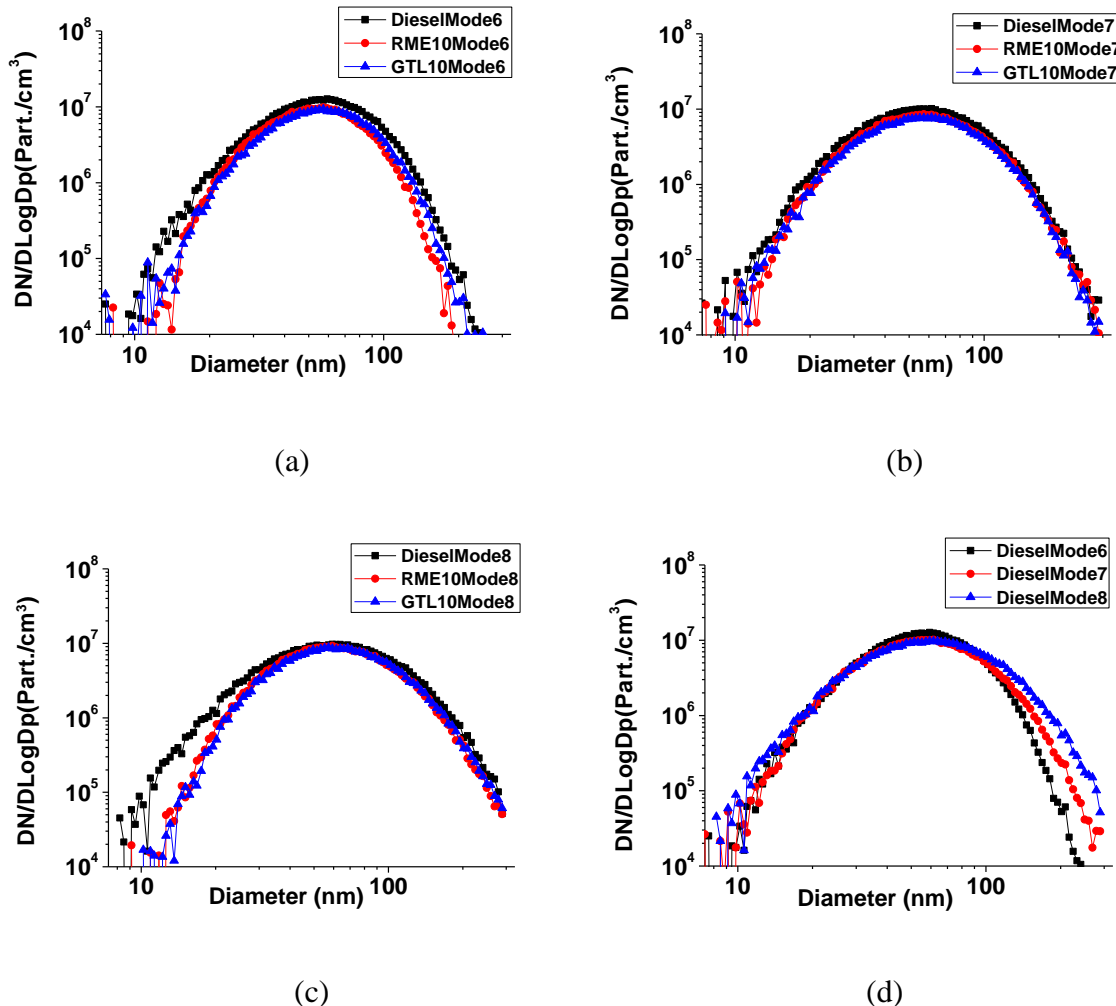
Figure 7.3 is the number weighted particle size distributions for the engine idle mode when fuelled with diesel, RME 10 and GTL 10 respectively. They are very similar and all show a bimodal size distribution. For the three types of fuels, the particles had two peaks, one at around 80 nm while the other varied. It is very clear that, adding either RME or GTL to diesel could reduce the particle numbers; however, there was an increase in the number of particles at diameter of around 20nm with the addition of 10% RME. This corresponds to the small difference in total particle numbers between diesel and RME 10 in Figure 7.1 and the reduction of particle number for GTL10 was contributed by the reduction of nucleation mode particles with a diameter of 10nm.



**Figure 7.4** Number weighted size distributions at 1800 rpm (total)

Figure 7.4 shows the number weighted particle size distribution with two different loads at 1800 rpm. Unlike the idle mode just presented, the particle numbers at this speed all peaked at around 55 nm and showed a mono-modal feature for all the three fuels. The engine load had a great impact on the particle numbers and increased the peak by half an order of

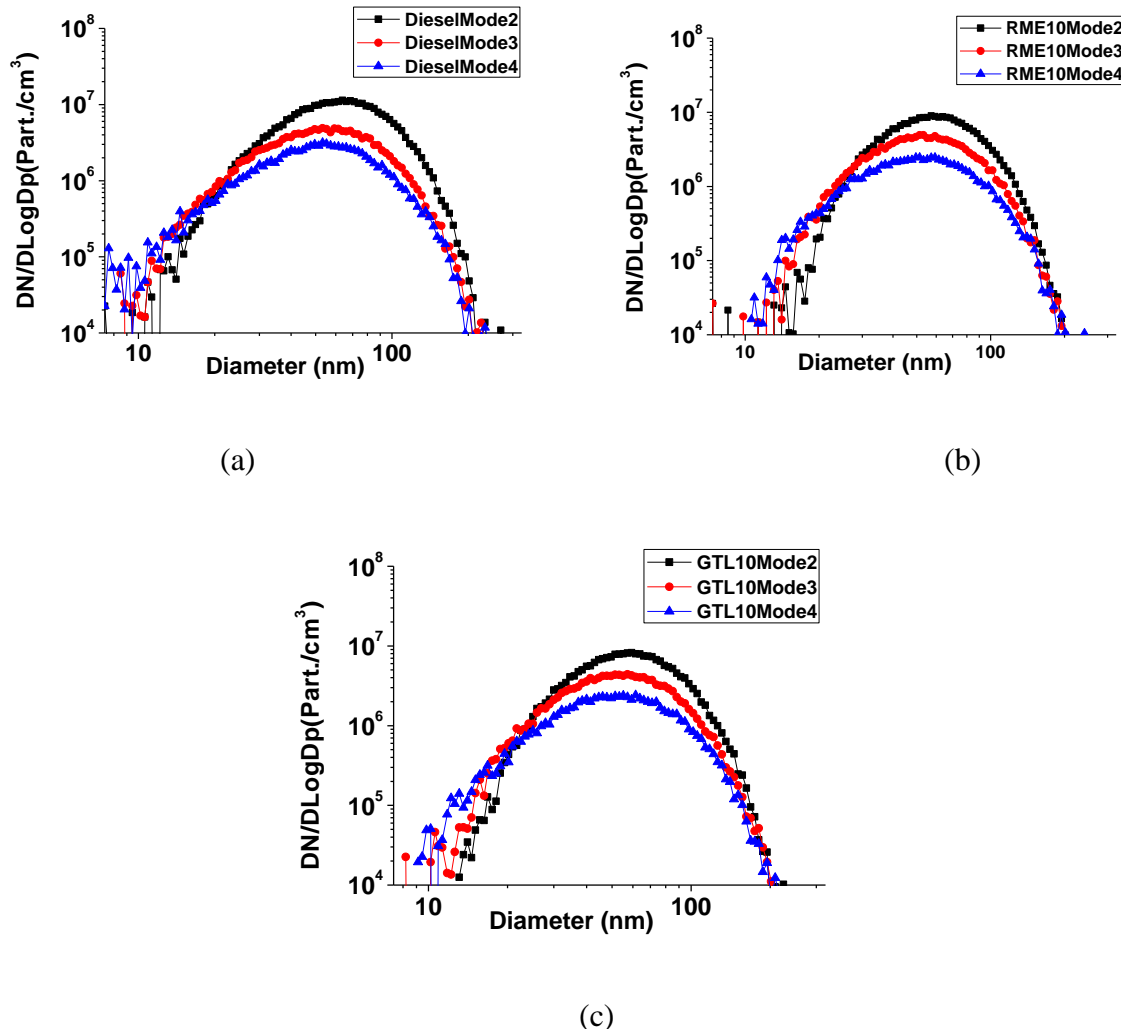
magnitude when it was increased from 10% to 43%. This might have been caused by more solid surface areas being produced for the volatiles to be attached.



**Figure 7.5** Number weighted size distributions at 3100 rpm: (a) Mode 6 (b) Mode 7 (c) Mode 8 (d) load increased from Mode 6 to Mode 8

Figure 7.5 shows the number weighted particle size distribution at 3100 rpm. The addition of RME or GTL reduced particles in the whole size range for all the three different loads, especially at high load as (c). In the three modes, the particles all peaked around 55-60 nm and the increase of the torque tended to produce more large particles, which led to the increase of the particle diameters shown in Figure 7.2.

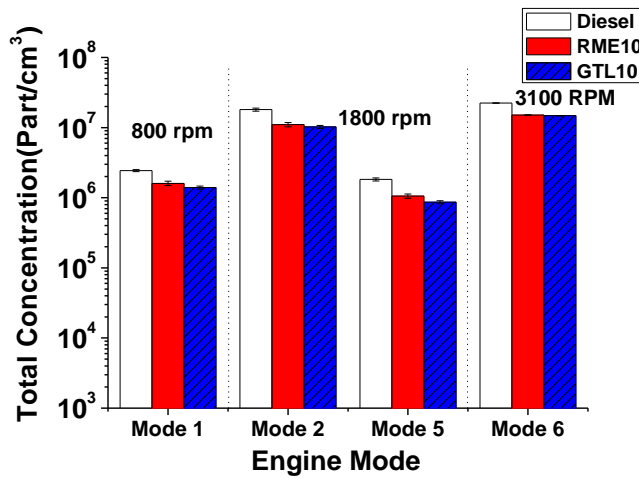
EGR — As mentioned earlier, for all the three tested fuels, reduced EGR corresponded to a decrease in both the total particle numbers and the mean diameter, shown in Figure 7.1 and Figure 7.2. It also increased the particles in the smallest size range with a diameter of around 10 nm. This was particularly apparent with diesel.



**Figure 7.6** Number weighted size distributions at 1800 rpm with different EGR: (a) EGR valve opening 31% (b) EGR valve opening 15% (c) No EGR (total)

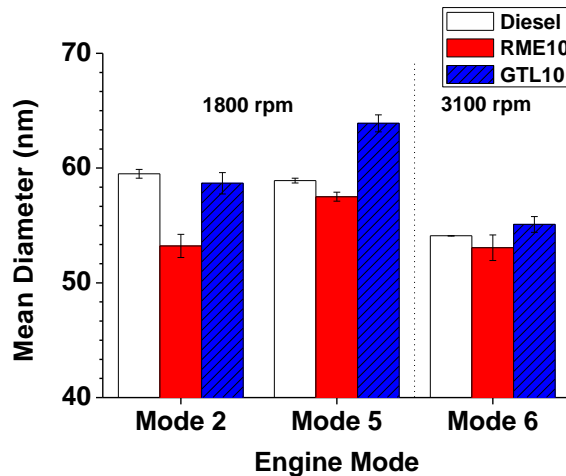
### 7.3.4 Non-volatile Particulates

Generally, the proportions of nonvolatile are important for total particles as they adsorb volatiles when they are strongly present. Otherwise insufficient non-volatiles mean insufficient solid surface area and that will promote the nucleation. Figure 7.7 shows some selected modes of non-volatile particles emitted after the thermo dilution.



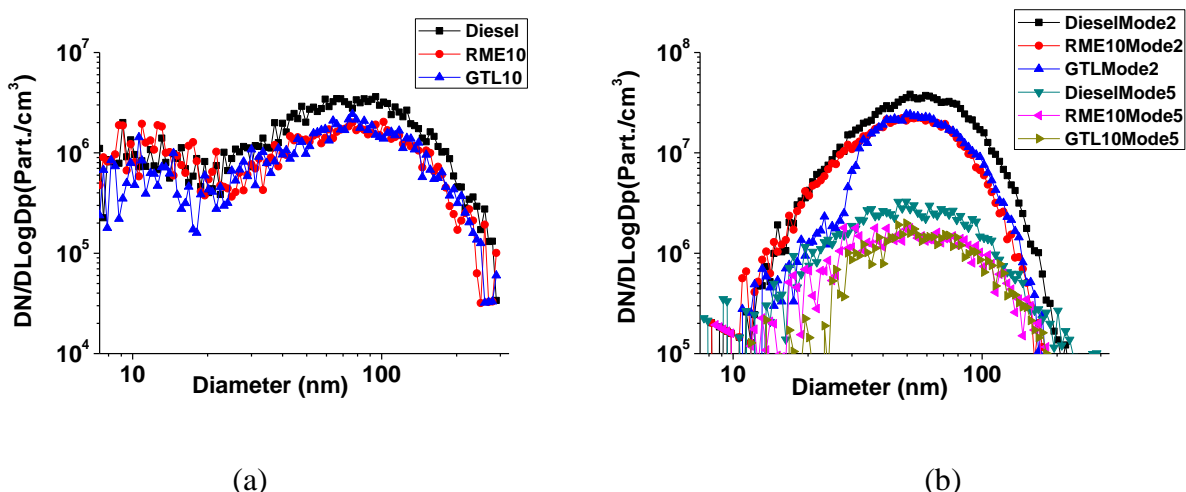
**Figure 7.7** Exhaust particulate number concentrations (non-volatiles)

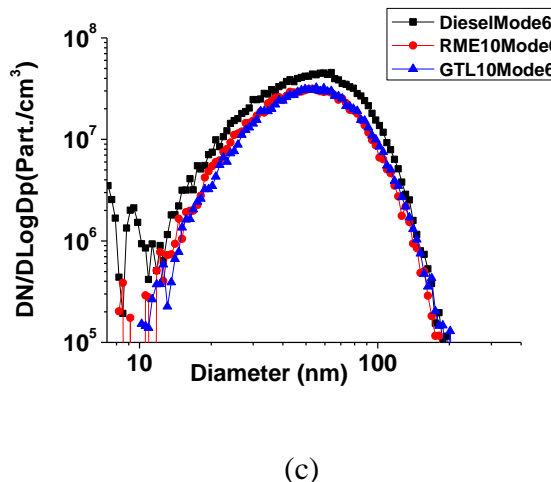
For the same engine modes 2, 5 and 6, RME 10 reduced the particle numbers by 39%, 42% and 33% respectively compared with diesel, while GTL10 by 43%, 53% and 34%. These were all higher than the particle number reduction rates when thermo-dilution was not used (Figure 7.1). It indicated that RME10 and GTL10 did improve the in-cylinder combustion as fewer non-volatiles were produced; however, the particles created due to the existence of volatiles in the exhaust and dilution in the later process diminished this improvement.



**Figure 7.8** Non-volatile particle mean diameter

Figure 7.8 is the mean diameters of the selected modes for the non-volatile particles when the thermo-dilution was used. From Mode 2 to Mode 5, it shows that the increase of engine load tended to produce larger non-volatile particles; while the same modes in Figure 7.2 showed an opposite trend in the total particles. Taking account of the engine conditions, it can be assumed that high engine load favors carbonaceous particulates while, the low engine load favors organic particles and the increase of engine load favors larger particles, most in accumulation mode: this corresponds to Figure 7.9 (c); at the same time, the use of EGR could result in more volatiles, most in nucleation mode.





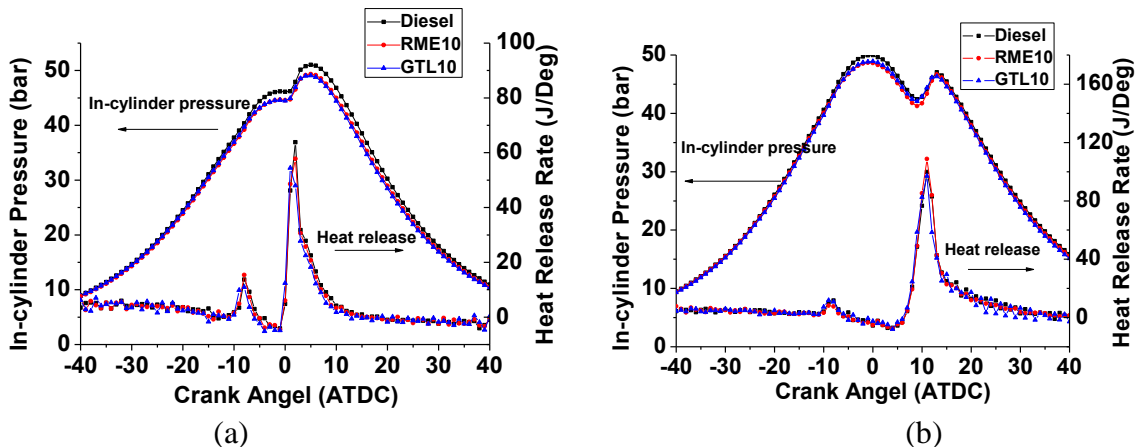
(c)

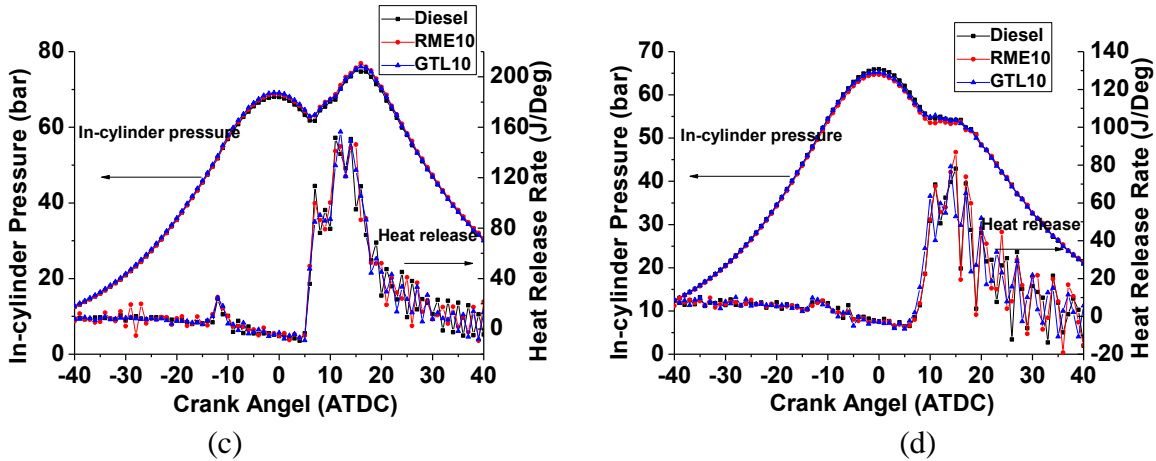
**Figure 7.9** Non-volatiles' number weighted particle size distributions at (a) 800 rpm; (b) 1800 rpm; (a) 3100 rpm

In Figure 7.9 (a), (b) and (c), the non-volatiles emitted by diesel fuels were more than those produced by RME 10 or GTL 10 and their sizes tended to be bigger.

### 7.3.5 In-cylinder Pressure and Heat Release

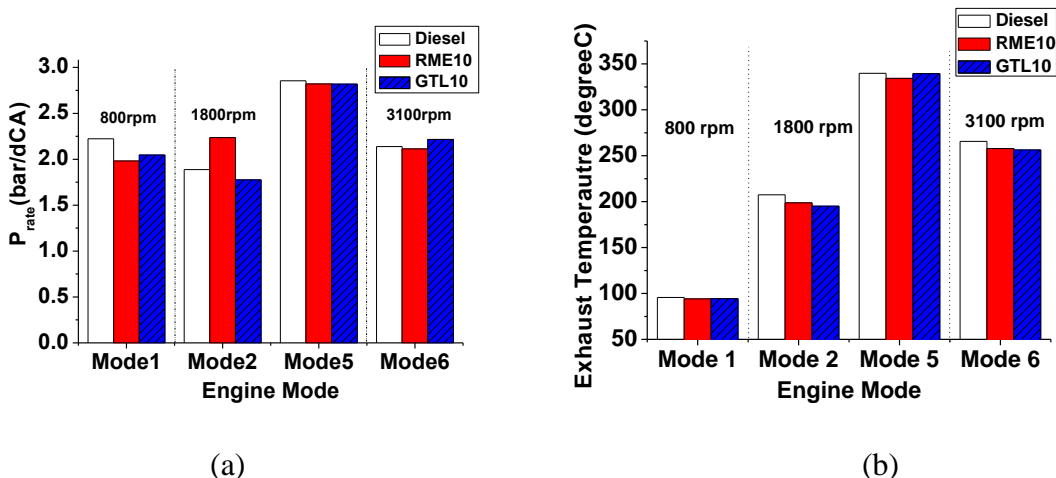
The in-cylinder pressure and heat release of Mode1, 2, 5 and 6 with the three types of fuels were also analyzed as follows (Figure 7.10):





**Figure 7.10** In-cylinder pressure and heat release for (a) Mode 1 (800 rpm, 2.1 Nm); (b) Mode 2 (1800 rpm, 30 Nm); (c) Mode 5 (1800 rpm, 134 Nm); (d) Mode 6 (3100 rpm, 35 Nm)

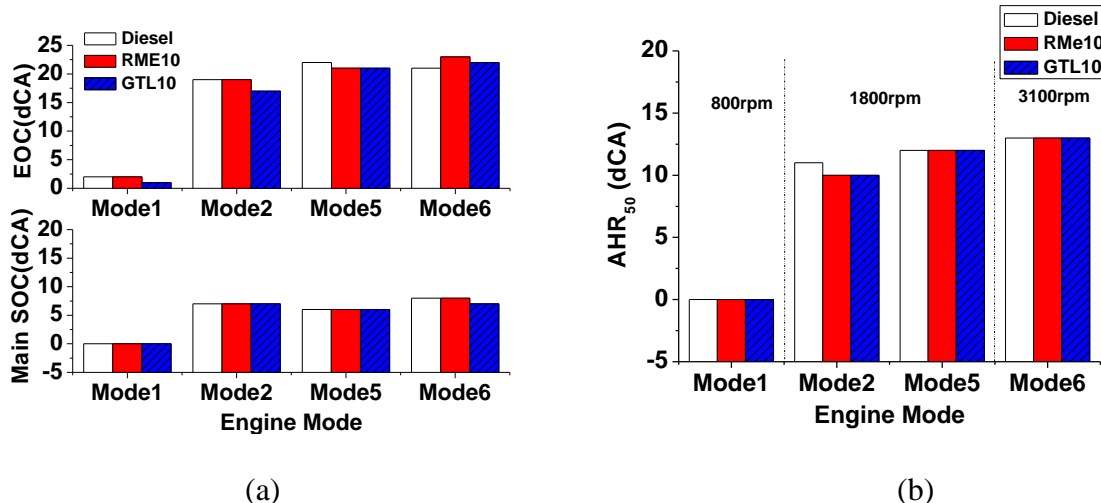
For the 4 cases listed, the heat release of GTL10 shows a general minimum peak value of all the three fuels; however, the difference is quite small. It indicated that for a blend ratio as low as 10%, GTL or RME didn't show much impact to the total heat release and the particle reduction they induced might have been contributed to their chemical influence to the spherules' formation (such as the accumulation and oxidation), possibly sulphur content related.



**Figure 7.11** (a)  $P_{rate}$  (b) exhaust temperature

Figure 7.11 shows the  $P_{rate}$  and exhaust temperature of the four engine modes when the three fuels were used. According to (a), the  $P_{rate}$  for RME 10 and GTL10 was slightly lower except in Mode 2. In this mode, the  $P_{rate}$  was higher than the other two when RME10 was used, and correspondingly, the heat release peak value from RME10 combustion was higher than those when diesel and GTL10 were used. Concerning the exhaust temperature in (b), it seemed that those due to the combustion of RME10 and GTL10 were lower than that of diesel. This might have been contributed by the lower energy density of RME and GTL.

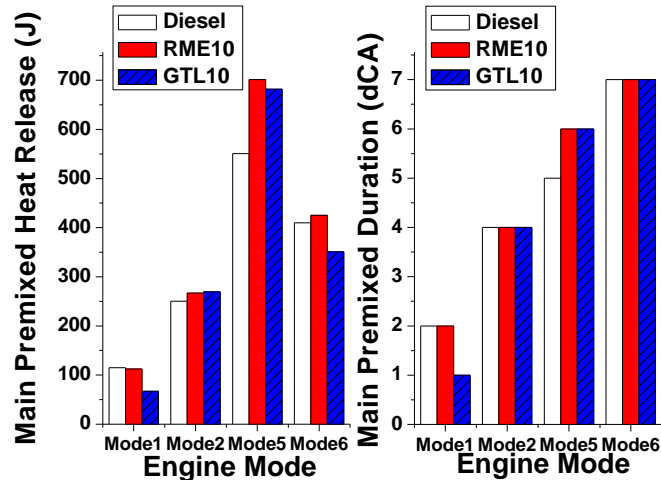
The  $AHR_{50}$  and the end of combustion (EOC) were defined as point 50% and 90% of the total heat release. According to the two graphs (Figure 7.12), they were not much affected by the fuel qualities used. Neither was the start of the main combustion. Thus, it can be noted that adding 10% alternative fuels to diesel had little influence to the combustion timing.



**Figure 7.12** (a) Main start of combustion (SOC) and the end of combustion; (b)  $AHR_{50}$

Referring to Figure 6.2, the premixed combustion was defined. It was also used here, and the heat release and duration of the premix phase combustion were calculated as presented in Figure 7.13. It shows clearly that more heat was released during the main

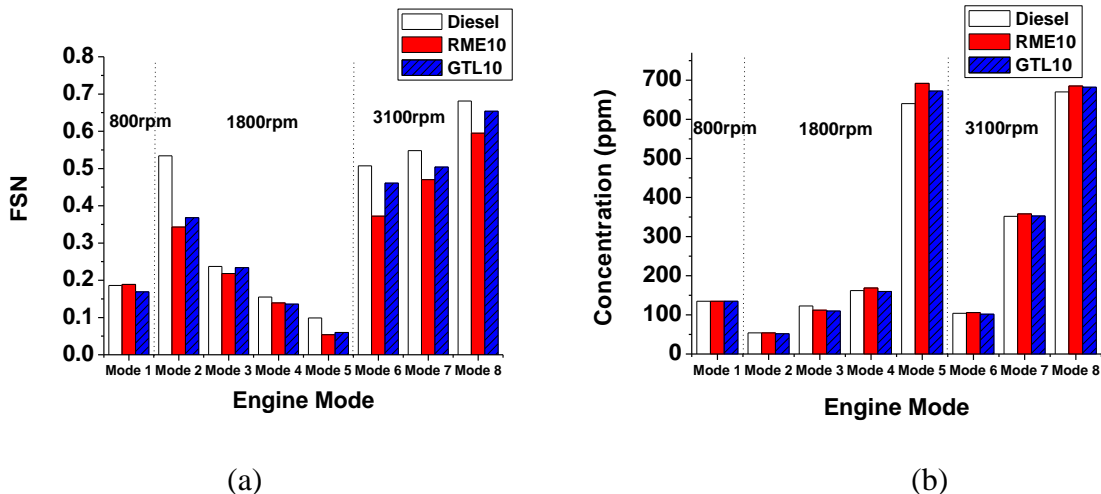
premixed phase when RME10 and GTL10 were used but the combustion duration was not significantly affected. This might be one of the reasons why PM was reduced.

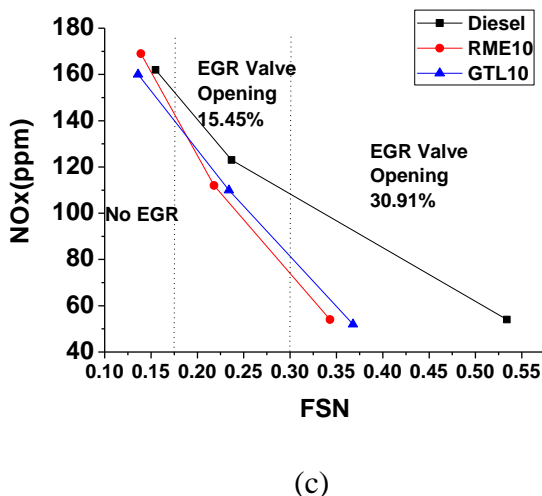


**Figure 7.13** Premixed-controlled main combustion duration and heat release

## 7.4 PM Mass and Morphology from Diesel, RME10 and GTL10

### 7.4.1 PM Mass





(c)

**Figure 7.14** (a) FSN (b) NO<sub>x</sub> concentration (c) smoke and NO<sub>x</sub> trade off for different EGR

Figure 7.14 (a) is the filter smoke number (FSN) of all the engine modes. Its trend of variation is not quite the same as the particle numbers shown in Figure 7.1. It indicates that when a smoke meter used the particle opacity for the calculation of mass, it not necessarily correlates to the particle numbers. This is particularly clear in high speed mode (Mode 6 to Mode 8); although in certain conditions (Mode 2 to Mode 5), they might seem relevant. The trade off between smoke and NO<sub>x</sub> for different EGR is also indicated in Figure 7.14 (c) for all the three fuels.

#### 7.4.2 PM Morphology

The SEM images of captured particles of for the three tested fuels are shown in Figure 7.15. All the samples were captured using 47 mm circle glass microfiber filters from Whatman for a period of 10 min under engine Mode 4 (1800 rpm, 30 Nm) condition.

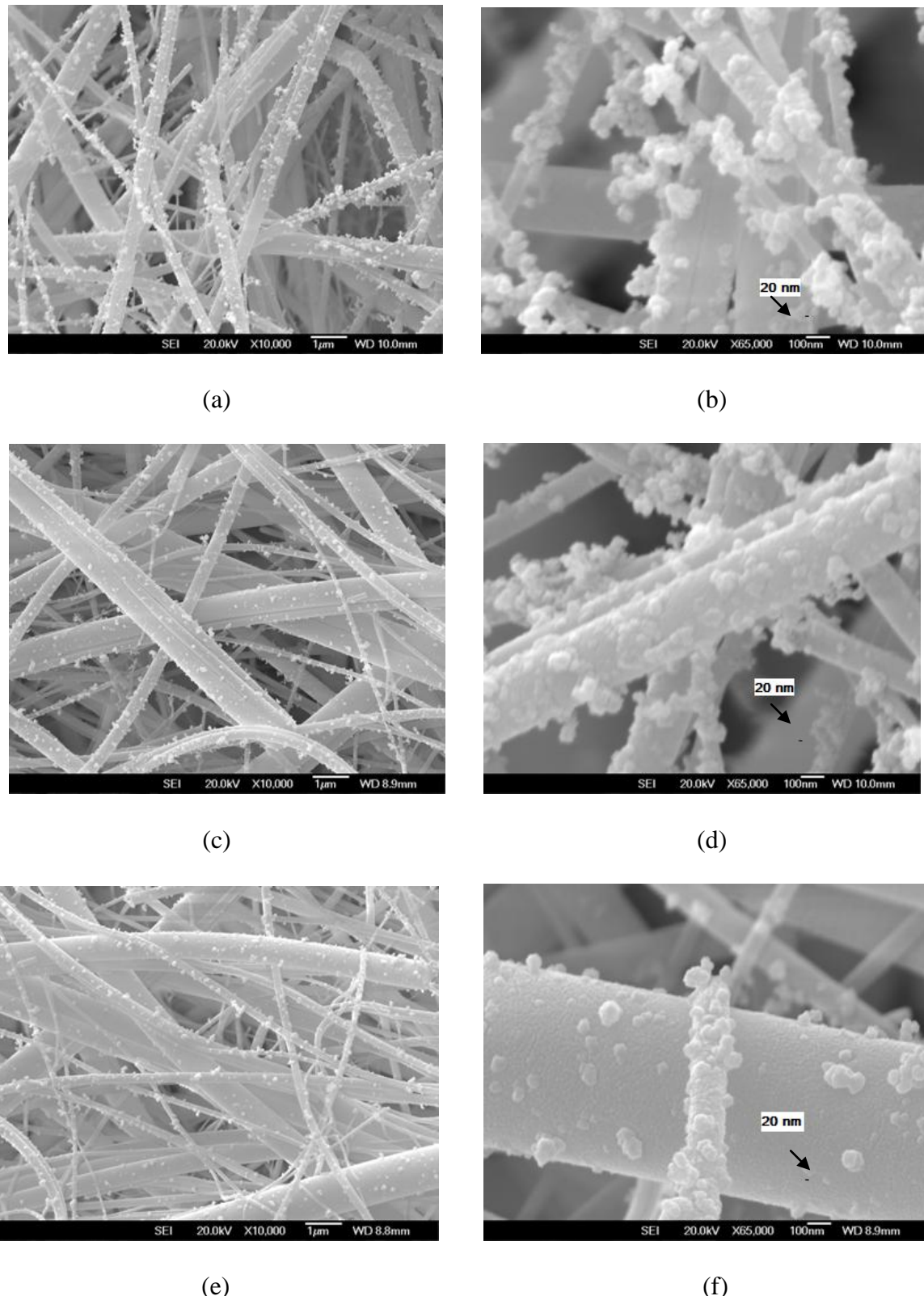


**Figure 7.15** Particle morphology (captured under engine mode of 1800 rpm, 30 Nm): (a) Diesel magnification of 10000; (b) Diesel magnification of 65000; (c) RME 10 magnification of 10000; (d) RME magnification of 65000; (e) GTL10 magnification of 10000; (f) GTL10 magnification of 65000

Comparing the images of Figure 7.15 (a), (c) and (e), under the same magnification of 10000, it is clear that particles from diesel combustion had more clusters than those from the RME10 or GTL10 and Figure 7.15 (b), (d) and (f) give an indication that the primary particle size from the combustion of all the three fuels is around 20 nm.

## 7.5 Non-volatile PM Characteristics during Warm-up from a Cold Start

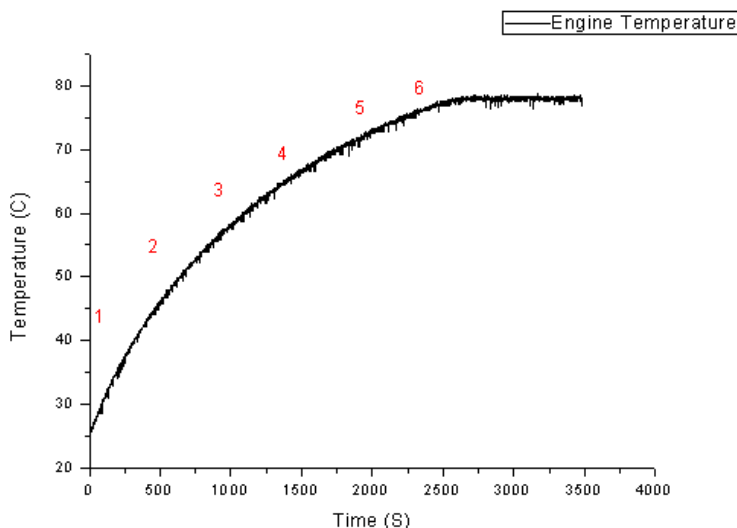


**Figure 7.16** Engine temperatures during the idling warming up

The non-volatile particulate size distribution was investigated during the warming up and RME10 was used in this test. Here SMPS was only employed to show the trend of changes of the particles for a period of time as the condition was not constant. After the engine was started it was kept idling (800 rpm, 2.1 Nm), and the data were recorded with an 8 minutes interval (labeled as Point 1- 6 in Figure 7.16) until the engine coolant temperature reached a constant of 80 °C.

### 7.5.1 Number Weighted Size Distribution

As shown in Figure 7.17, at the beginning, the number of particulates was much higher, and most of the particulates were in nucleation mode while the accumulation mode particulates were relatively constant during the period. It can be assumed that this was contributed by the following reasons: (1) large amount of soot from incomplete combustion; (2) the temperature was low at low load; during the pyrolysis or oxidation process of the combustion, the fuels were mostly likely to quench on the engine cylinder walls and the mutated hydrocarbons contributed to a large part of the emitted particulates.

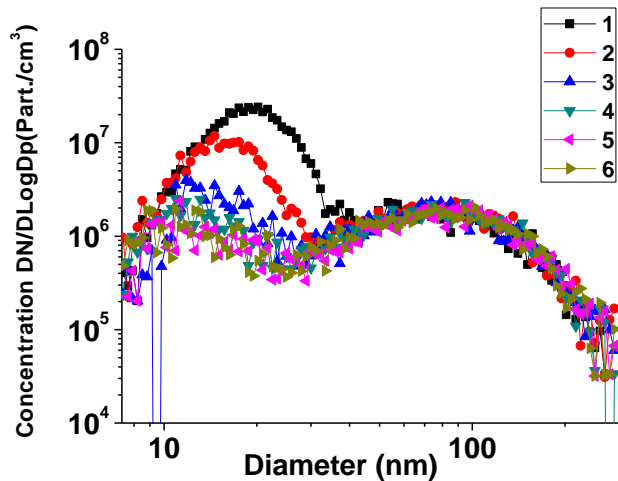


**Figure 7.17** Number weighted size distribution during the warming up (non-volatiles)

As the engine warmed up, the number of the particulates decreased sharply. That was mainly because of the increase of the engine temperature which led to improved fuel mixing and more complete combustion, and thus fewer particles. The particle to particle conversion for the high concentration described by Smoluchowski's coagulation equation (Eastwood 2008) and Hinds' coagulation model might have also contributed to the reduction of the particle concentration (Eastwood 2008).

### 7.5.2 Surface Area Weighted Size Distribution

The surface area of particulates is a very important parameter in the particle study as it determines one mode of particle growth, ‘adsorption’. The adsorption involves attaching gas molecules to the particle surfaces by some bonds (e.g. van-der-waals) and it can even happen in unsaturated conditions. This parameter influences both the particle mass and the particle number significantly (Eastwood 2008).

Referring to Figure 7.18, the surface area of the particles in nucleation mode changed a lot with their numbers during the warming up. However, those in accumulation mode, which are the main participants in the process of adsorption, remained pretty much the same.

It is clear that the engine temperature is probably the most significant factor for the formation of the particulates during the warming up. The oxidation is promoted with the increased temperature and this has a great influence to the particles in nucleation mode, while those in accumulation mode are not much affected.

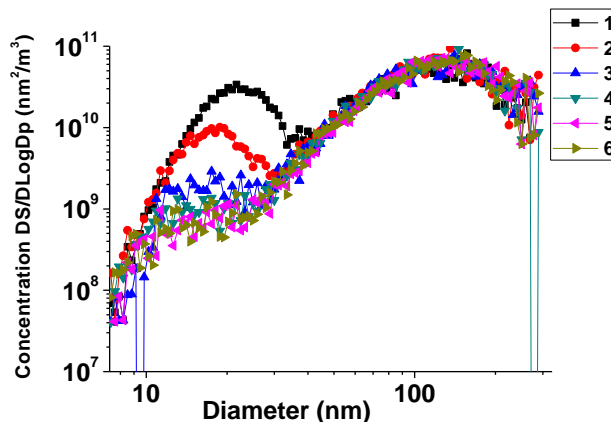


**Figure 7.18** Surface area weighted size distribution during the idling warming up  
(non-volatiles)

### 7.5.3 Mass Weighted Size Distribution

The mass-size distribution map, Figure 7.19, shows that the particulates in accumulation mode dominated the mass. However, at the very beginning of warming up, the very high number of particles displayed a small peak in nucleation mode and this peak was smoothed quickly as time went by.

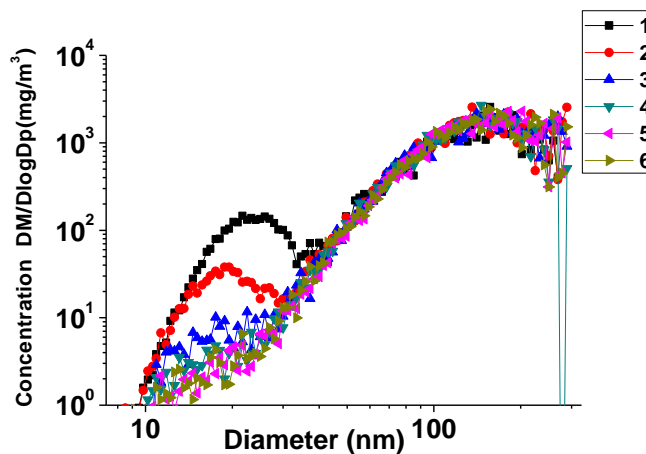


**Figure 7.19** Mass weighted size distribution during the idling warming up (non-volatiles)

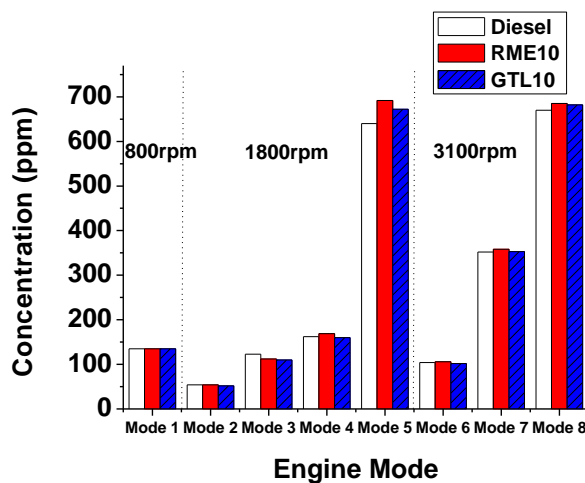
## 7.6 Gaseous Emissions from Diesel, RME10 and GTL10

### 7.6.1 Emissions of NO<sub>x</sub>

Although the nitrate fraction in the particulates is reported by many laboratories, it doesn't contribute much to the particulates, less than 1% percent, which means to meet the emissions legislation, it is unnecessary to eliminate it. It mainly comes from the NO<sub>2</sub> and the reactions are:

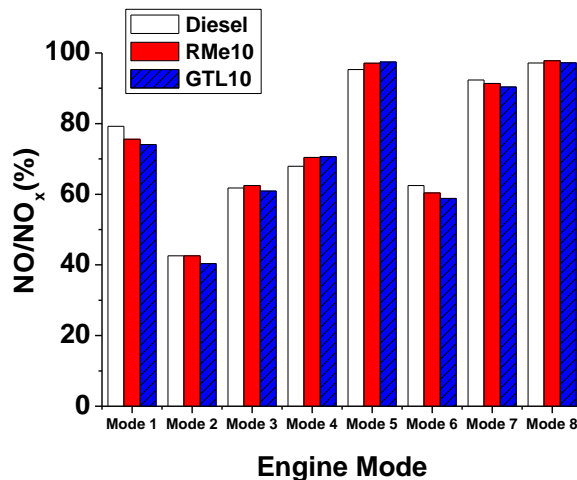


The reason why it worth the attention is that its actions compete with those generating the sulphate fraction, and it might be used to suppress the latter, which has a share of around 5% of the particulate composition. Besides, as the sulphates in the diesel are decreasing, the sulphate fraction in the particulates might be replaced by the nitrate one in the future. According to Figure 7.20, the differences of NO<sub>x</sub> caused by the fuel properties were not clear. In certain modes such as mode 4 or mode 5, which were middle or high load modes, the oxygenates' effects might have been promoted for RME 10, resulting in a more complete combustion. In these two modes, NO<sub>x</sub> was increased by 2% and 6% respectively. In the low load modes such as Mode 2 and Mode 3, for the use of EGR, NO<sub>x</sub> was greatly reduced. In mode 5 and mode 8, heavy NO<sub>x</sub> was produced for the high loads, thus high temperatures.



**Figure 7.20** NO<sub>x</sub> emissions

NO fractions of the total NO<sub>x</sub> were shown in Figure 7.21. It indicated that NO was relatively low in the low engine load modes. This was because of the low temperature and in the expansion stroke, NO was prone to be converted to NO<sub>2</sub>. In middle or high load modes, more than 90% of NO<sub>x</sub> were NO.


 Figure 7.21 NO/NO<sub>x</sub> emissions

### 7.6.2 Emissions of THC and CO

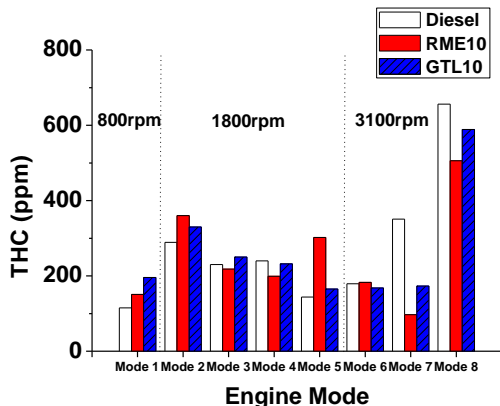


Figure 7.22 THC emissions

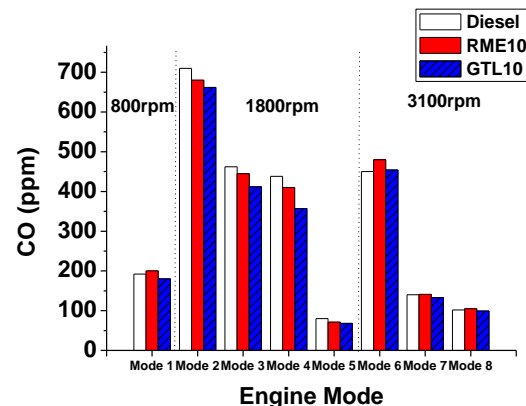


Figure 7.23 CO emissions

Biodiesel and GTL diesel's effectiveness in reducing the THC and CO has been proved in lots of experiments for their high cetane number and aromatics-free characteristics (Figure 7.22 and 7.23). Besides, the oxygenates contained in the biodiesel also help. In the six test modes, the adding of 10% RME or GTL diesel showed a general reduction of HC and this effect was most significant in the high speed high load mode as the emission was reduced by 35% for RME 10 and 20% for GTL 10 respectively. This might have been caused by the

non-aromatic characteristics of the two fuels which became more remarkable in high temperature. Besides, the oxygenates contained in RME10 contributed to a further reduction.

The CO emissions from the fuels are shown in Figure 7.23. Just like HC, RME 10 and GTL 10 also reduced the emission. In mode 2, when the impact was most prominent, the reduction ratio was as high as 12% for RME 10, and 17% for GTL 10. In mode 5, mode 7 and mode 8, the fuel properties' influence was not significant as in these three modes, the loads were high, and the CO produced was very low.

### 7.6.3 Emissions of CO<sub>2</sub>

The differences of CO<sub>2</sub> for the three types of fuels were neglectable, although in some modes, biodiesel and GTL diesel blends did increase the emission slightly for a more complete combustion (Figure 7.24). The CO<sub>2</sub> emitted by the biodiesel will go back the ecosphere for a closed-loop carbon recycle and the net increase is zero. O<sub>2</sub> (Figure 7.25) is another index for CO<sub>2</sub>, which has an opposite trend of change. Its percentage in the exhaust will have some influence to the downstream DOC oxidation as well as the particulates variation in the exhaust system.

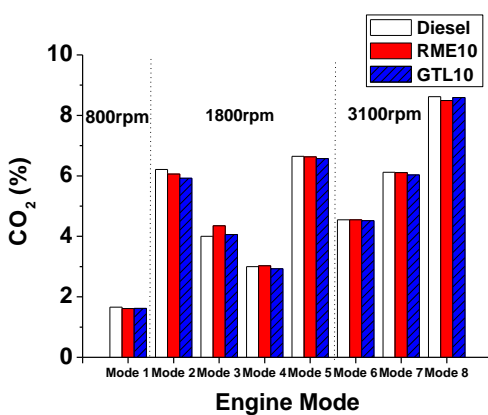


**Figure 7.24** CO<sub>2</sub> emissions

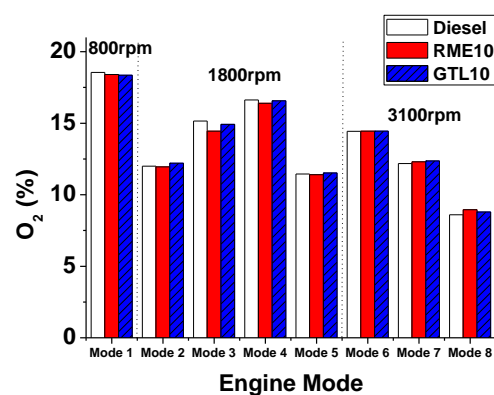


**Figure 7.25** O<sub>2</sub> emissions

## 7.7 Discussion and Summary

### 7.7.1 The Reliability of Thermo Dilution

The Particle Number (PN) metric has now been formally transposed into European emissions regulations (Regulation NO.715/2007, amended by 692/2008 and 595/2009), which, from the other side, also puts forward the requirement that the measurement be reasonably reproducible. However, particles are highly dynamic and if not properly controlled, the measuring methods may give rise to their variation and even has a significant influence to the results. After coming out of the engine, the exhaust plume goes through the transfer line and the dilution tunnel before the measurement, where lots of changes can happen. To minimize the bogus results caused, the transfer line has to be made as short as possible and the dilution tunnel has to be well conditioned. The biggest problem now is the irreproducibility of particulates in the nucleation mode. The particles of this mode have been researched since mid-1990s and are still not so well understood, as they are beyond the detection range of most measuring devices. It is argued that the dilution ratio is probably the most important parameter influencing the measurement results. It is now a consensus that this parameter has no significant effect on the formation of accumulation mode particles and with a high dilution, the re-nucleation of particles is not noticeable. To minimize artifacts in measurement, the dilution ratio should be at least above 40. In fact, if the laboratory condition is to be made more close to the real world where the dilution ratio is infinity, the dilution ratio should be as high as possible. It is believed that the dilution ratio only influences the gas-particle conversion in the exhaust plume for the saturation of the volatiles, which are vulnerable to many factors especially in the real world. The thermo dilution used in the tests

did get rid of these influences, and gave more stable results (Kasper 2004; Montajir et al. 2005).

However, even this methodology still needs much experimental fine tuning to get more reliable measurements, and other related issues such as a proper dilution ratio also need to be raised. In the whole tests of this research, for the non-thermo dilution, a dilution ratio of 60 was used while for the thermo-dilution, the ratio was raised to 543. How these influence the test results still need further investigation.

### **7.7.2 Summary**

The particles characteristics from the combustion of 10% blend of RME and GTL (comparable to the 2020 fuel blends target) were investigated in this study. The tests were carried out on a Euro 4 diesel engine and two methods were applied for the measurement: one was based on the UNECE GRPE Particulate Measurement Programme, where thermo-dilution was used for the non-volatile particles; and the other without using thermal dilution for the total particles.

1. Compared with conventional diesel, 10% RME and 10% GTL additions lead to a similar reduction in both total particle numbers and non-volatile part numbers (through influence to the combustion), under various engine conditions.
2. The influences of the fuel properties to the particle mean diameters are not clear, although emissions from RME 10 appear to have the smallest mean particle diameters under most of the engine test modes.
3. For all the three fuels, the increase of engine load results in a reduction of particle numbers and increase of particle mean diameters. It is also shown that low engine load favors

organic particles formation and high engine load favors larger carbonaceous particles formation, most in accumulation mode. The increase of either engine speed or EGR increases the particle numbers as well as the mean diameters and the particles increased by EGR is mainly in nucleation mode.

4. The particles with all the three fuels under engine idling conditions demonstrate clear bimodal size distributions. In other cases, the distributions are mono-modal. Mixing either RME or GTL with diesel reduces the accumulation mode particles and some nucleation particles in the larger size range ( $>30\text{nm}$ ); however, RME 10 could also increase those in the small size range under certain cases ( $<20\text{nm}$ ).

5. SEM images show that the particles from diesel combustion have more clusters than those from the RME10 or GTL10 and the primary particle size of all the three fuels is around 20 nm.

6. Cold starts could result in much higher nucleation particles due to incomplete combustion and these particles are reduced when the engine is warmed up. During this process, engine temperature is the most significant factor determining the particle size distribution through its effect on combustion as well as particle oxidation.

7. RME 10 and GTL10 showed a general reduction of THC and CO. For THC, the effect was most significant in high load modes while for CO, in low modes. The influence of the 10% RME and GTL diesel to the  $\text{NO}_x$  and  $\text{CO}_2$  emissions were less remarkable.  $\text{NO}_2$  mainly existed in the low engine load modes.

## CHAPTER 8

### CONCLUSIONS AND FUTURE WORK

The research work in this thesis has focused on the particulate emission control and related issues for diesel engines. It consists of three major parts with respect to the after-treatment device, the injection strategies and the new fuels. This chapter summarizes the conclusions drawn in this studies and makes some recommendation for future work in the relevant areas

#### 8.1 Conclusion Remarks

##### 8.1.1 The After-treatment System

Replacing the DOC with a catalyzed DPF showed significant smoke reduction before the main DPF for the soot trapping advantages of the DPF over the DOC by up to 30%. Its catalyst also showed a comparable performance to the DOC in the conversion of gaseous emissions, including CO and THC, and particulates in the nucleation mode. The main DPF is still the major device for particulates trapping with a trapping efficiency up to 99%, although those with diameters smaller than 100 nm were still able to escape. If the assistant DPF can be properly optimized, the main monolith DPF can be made smaller, lighter and thus less expensive and the regeneration can be made less frequently as a result. In real driving, the

accurate real time measurement of the after-treatment system is important as high loadings could deteriorate the engine performance.

### **8.1.2 Single Injections**

Compared with the multiple injection strategy, a carefully calibrated single injection was able to allow the engine to operate in the PCCI combustion region and reduce the particulates and NO<sub>x</sub> at the same time by combining an advanced main injection timing and high injection pressure with high EGR. In this PCCI region, the two emissions could be reduced by more than 80% compared with using the normal multiple injections. However, high P<sub>max</sub> and THC and CO emissions were the problems resulted, which require the after-treatment system to be altered accordingly if this combustion is to be adopted in production engines.

### **8.1.3 Multiple Injections**

The pilot injection's impact on the particle emissions has a close relationship with the engine speed and load and EGR. Generally, a smaller quantity of the pilot fuel and advance of the pilot injection timing could reduce the particulate numbers by influencing the main combustion. In certain cases, such as with high fuel quantity, an increase of pilot fuel or very advanced timing could signify and alter the expected trend of the particulate emission change.

### **8.1.4 Alternative Fuels**

Compared with conventional diesel, 10% RME and 10% GTL additions lead to a similar reduction in both total particle numbers and non-volatile part numbers, under various engine conditions. The particulate distribution only showed a bi-modal distribution in idle mode while in other modes, it was mono-modal. Engine load, speed and EGR influenced the

particulate distribution in the same way for all the three types of fuels and generally the increase of engine load results in a reduction of particle numbers and increase of particle mean diameters, and the increase of either engine speed or EGR increases the particle numbers as well as the mean diameters. Cold starts could result in much higher nucleation particles due to incomplete combustion. RME 10 and GTL10 also showed a general reduction of THC and CO.

## 8.2 Future Work

The present study can lead to the recommendation as follows for the future work:

### 8.2.1 DPF on Particulate Trapping under Transient Mode

The present work has shown that the DPF had a good particulate trapping efficiency under steady-state conditions. However, this performance may be different in transient mode. The fluctuation of the exhaust flow as well as the temperature may influence the trapped soot distribution, and thus change the particulate emissions after the DPF. Thus CFD modelling and experimental research into these conditions is recommended.

### 8.2.2 One Dimensional Emission Model

The more advanced model -- diesel jet combustion model in the WaveBuild could be further explored as it has the ability to predict combustion heat release rate from user-specified fuel injection rate and injector geometry and predict NO<sub>x</sub> and soot emissions. Although the model can be only activated for one cylinder of an engine, the burn rate of the jet combustion model can be directly used for the other cylinders in the same run after it is

activated and stored. This is particularly useful in the studies of emissions influenced by the test rig set-up.

### **8.2.3 PCCI and HCCI**

Low temperature combustion (LTC) has proven to be an ideal way to minimize the particulates and NO<sub>x</sub> at the same time, and certainly, its THC and CO emissions are worth investigating. This can be an extension of the present work which was accomplished only to a preliminary extent with single injections. The expanding of the test modes, such as different injection pressure, timing, number of injections and EGR are recommended.

### **8.2.4 Higher Portion of Alternative and Engine Map Optimisation for Biodiesel Blends**

The present study focused on the emissions of low blends of alternative fuels to 10% to meet the 2020 fuel blends target. However, this portion of new fuels can be increased considering the increased future requirement. Thus an optimization of the engine map covering full speed-load engine conditions is recommended. This can lead to a further reduction of emissions and an increase of fuel economy.

### **8.2.5 Particulate Measurement**

Most diesel engine particulate measurements are conducted in labs which differ from the actual situation in the ambient atmosphere when the exhaust is diluted to almost infinity. How to avoid or minimize these artefacts of measurement protocols is important and a proper legislation of the measurement is necessary. This includes the settings of the exhaust tunnel and dilution conditions such as the temperature and dilution ratio. Thus the measurement could reflect the true effect of particulates on public health.

### **8.2.6 Particulate Chemical Composition**

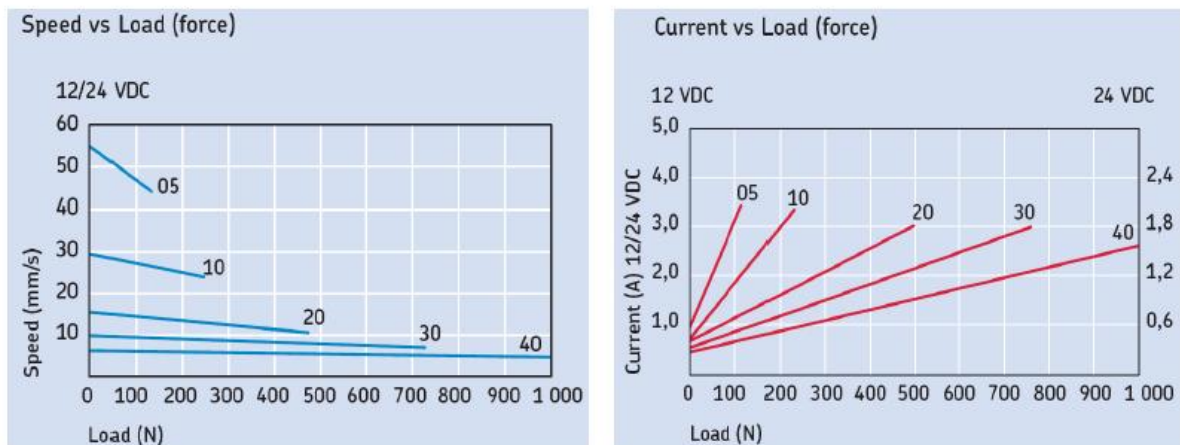
With the reduction of sulphur content in the diesel fuel, sulphates will not be often seen as important parts of particulates. However, other components such as the nitrites, and ashes, especially with the use of alternative fuels, may rise as new problems. Studies into the chemical composition of particulates are thus recommended.

## APPENDIX

### A. RESEARCH METHODOLOGY

**Table A1** Throttle actuator specification

Gear Ratio	5:1	10:1	20:1	30:1	40:1
Input Voltage	12v / 24v DC				
Load Capacity	120N	240N	500N	750N	1000N
Static Load	2300N				
Stroke Length	50, 100, 150, 200, 250, 300mm				
Speed at Full Load	45mm/s	24mm/s	13mm/s	8mm/s	6mm/s
Speed at NO Load	57mm/s	30mm/s	17mm/s	10mm/s	8mm/s
Duty Cycle	25%				
Operating Temperature Range	-40 to +85°C				
Limit Switch	Built in Factory Set				
Protection	IP66				



Potentiometer***						
Stroke	50	100	150	200	250	300
Ohm/mm	94,4	94,4	47,2	47,2	15,72	15,72

**Figure A1** Throttle actuator performance graph

**Table A2** In-cylinder pressure sensor amplifier specification (5011B10Y50)

Specification	Range	Tolerance	
Range Error	pC < 100	Max < $\pm 3\%$	Typ < $\pm 2\%$
	pC $\geq 100$	Max < $\pm 1\%$	Typ < $\pm 0.5\%$
Low-pass Filter	kHz 0.01...30	< $\pm 10\%$	
Output Noise	pC 99.9	mVrms < 0.5	mVpp < 4
	pC 10	mVrms < 1.5	mVpp < 8
Drift at 25 °C	< $\pm 0.07$ pC/s		

**Table A3** RS K type thermocouples

## Type K Industrial Mineral Insulated Probe

- St. steel 310 or Inconel 600 sheath versions. MgO insulation  
0.15 to 2m probes  
Stainless steel is more flexible  
Inconel has excellent oxidation resistant properties  
100 mm of 7//0.2 PTFE cable  
M8 x 1.0 thread  
Gland available 1//8 BSP

**Temperature range:**

- Probe 0° to +1100°C
- Pot seal 0° to +180°C

**Table A4** TCK-4 thermocouple amplifier specification

Power Supply +5V @ 30mA, 9-28V @ 40mA
Operating Temperature 0-70°C
CJC Temperature Range 0-70°C
Calibration Error @ 25°C $\pm 1^\circ\text{C}$
Gain error $\pm 0.75\%$
Nominal Thermocouple Output 10mV/°C
Bandwidth 15kHz
Usable Output current 5mA
Dimensions 90mm x 53mm x 57mm

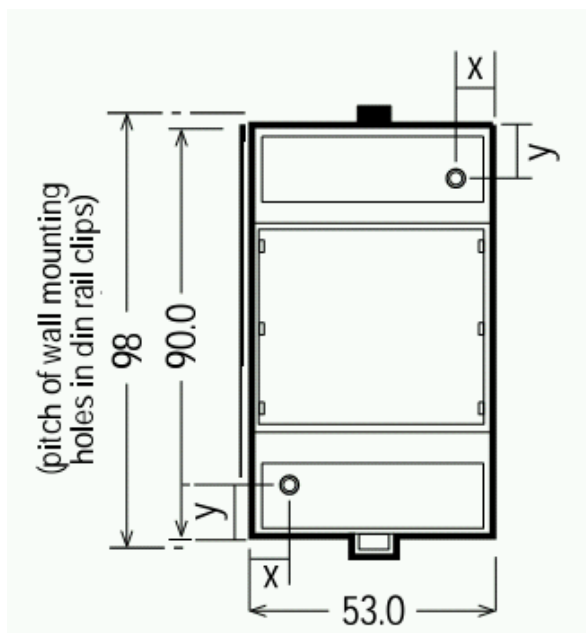
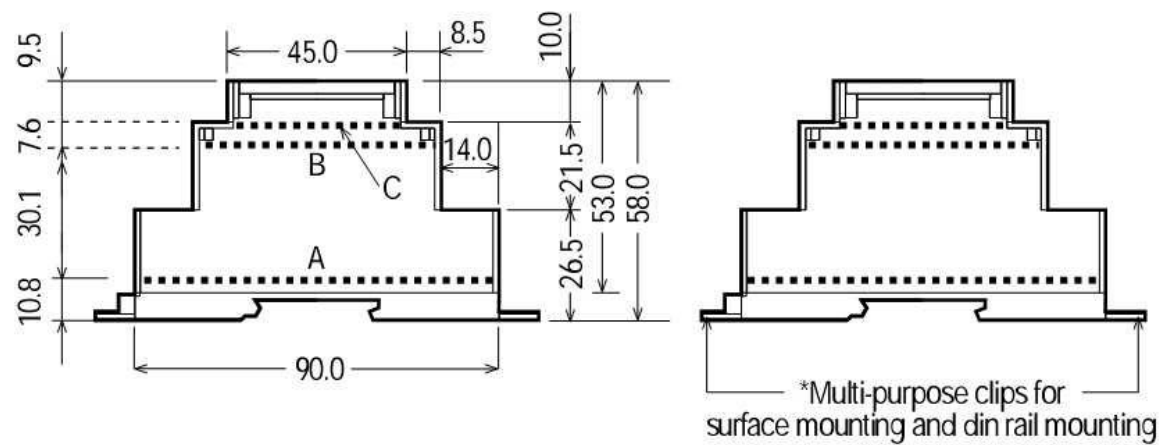


**Figure A2** TCK-4 thermocouple amplifier dimension

**Table A5** EuroSensor EPT 3100 pressure sensor specification

Accuracy	< $\pm 0.5\%$ BFSL
Stability (1 year)	< $\pm 0.1\%$
Overrange pressure	2 $\times$ rated pressure
Burst pressure	$\pm 1\%$ FS, from -10 °C to 60 °C
	$\pm 2\%$ FS, from -40 °C to 85 °C
Pressure cycles	> 10 million

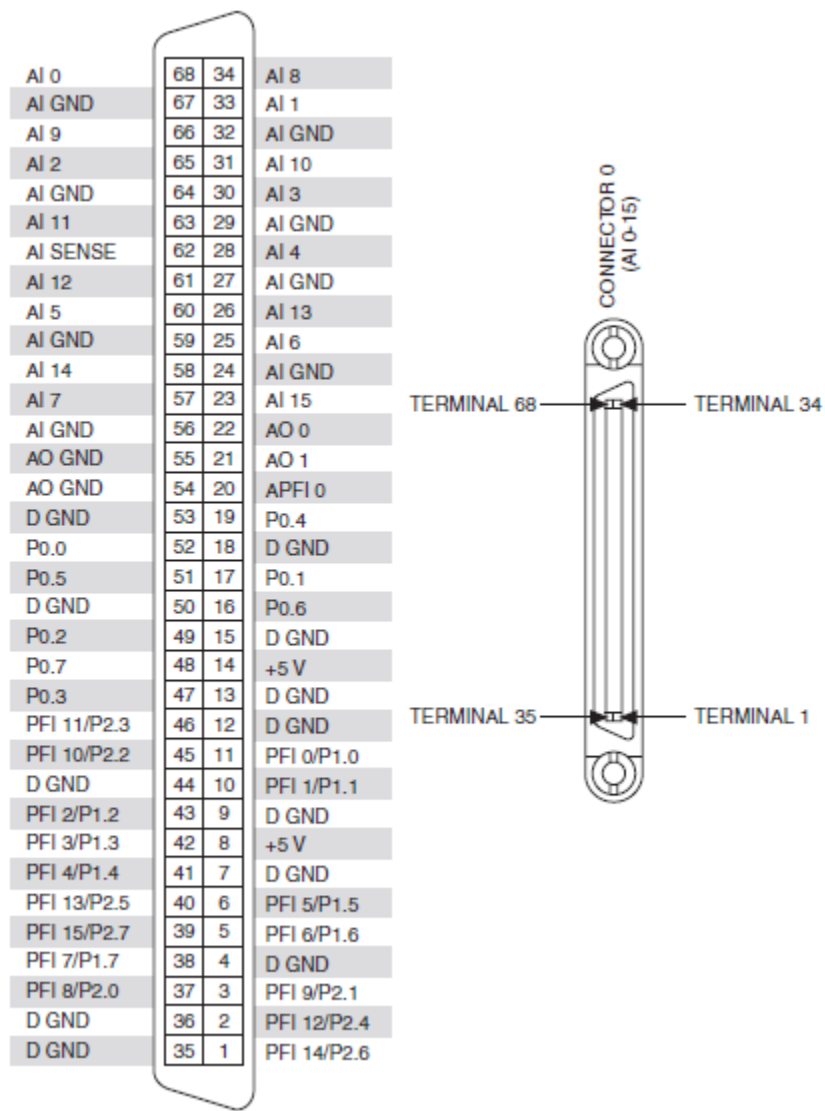
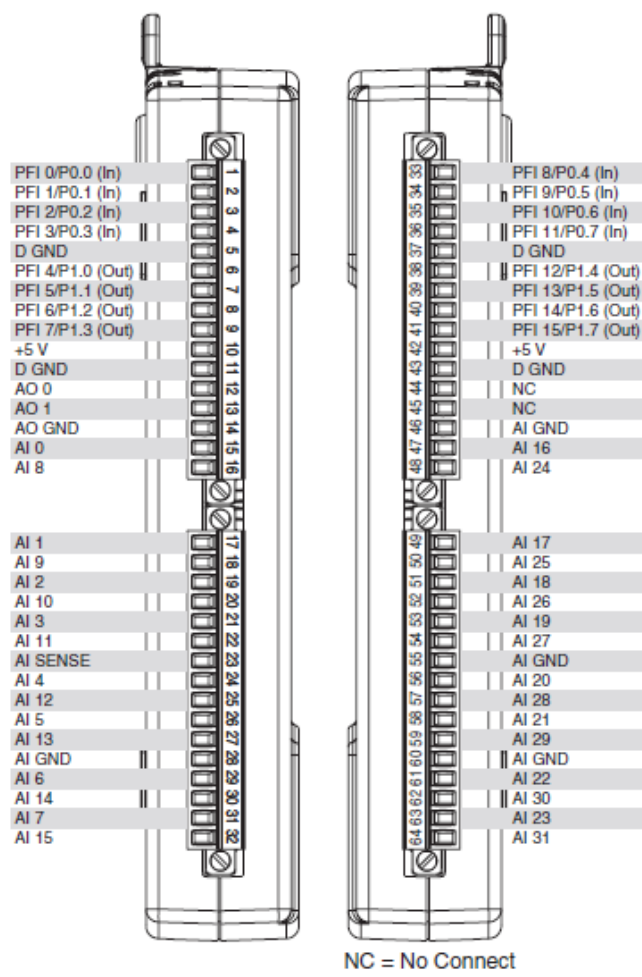
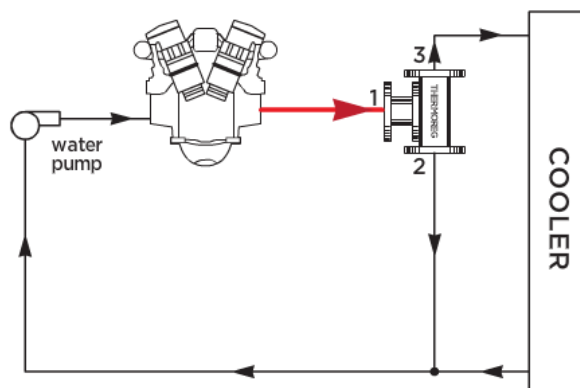


Figure A3 PCI 6251 pin out



**Figure A4** USB 6218 pin out



Cooling water control.  
Cooling by radiator or heat exchanger.

**Figure A5** Thermo-valve piping diagram

## **B. APPLICATION OF TWO CLOSELY COUPLED DPFS AS THE DIESEL ENGINE AFTERTREATMENT SYSTEM**

[Not available in the digital version of this thesis]

## C. PM CHARACTERISTICS WITH PILOT INJECTIONS

**Table C1** Injection parameter of Mode 1 (1800 rpm, 52 Nm) variations (BTDC=before top dead centre)

	Pilot SOI (BTDC)	Pilot Quantity (mm <sup>3</sup> /stroke)	Dwell Time (us)	Main SOI (BTDC)	Total Quantity (mm <sup>3</sup> /stroke)
(a)	14	1.5	1089	-1.69	16.3
(b)	19	1.5	1561	-1.69	16.6
(c)	24	1.5	2024	-1.69	16.3
(d)	29	1.5	2487	-1.69	16.6
(e)	14	3	1067	-1.69	16.5
(f)	19	3	1530	-1.69	16.3
(g)	24	3	1993	-1.69	16.2
(h)	29	3	2456	-1.69	17.2
(i)	14	4.5	1017	-1.69	16.2
(j)	19	4.5	1480	-1.69	16.8
(k)	24	4.5	1943	-1.69	16.7
(l)	29	4.5	2406	-1.69	17.3

**Table C2** Injection parameter of Mode 2 (1800 rpm, 91 Nm) variations

	Pilot SOI (BTDC)	Pilot Quantity (mm <sup>3</sup> /stroke)	Dwell Time (us)	Main SOI (BTDC)	Total Quantity (mm <sup>3</sup> /stroke)
(a)	13	1.5	1096	-2.69	24.6
(b)	18	1.5	1559	-2.69	24.1
(c)	23	1.5	2022	-2.69	24
(d)	28	1.5	2485	-2.69	24.4
(e)	13	3	1077	-2.69	24
(f)	18	3	1540	-2.69	24.2
(g)	23	3	2003	-2.69	24
(h)	28	3	2466	-2.69	24.5
(i)	13	4.5	1037	-2.69	24
(j)	18	4.5	1500	-2.69	24.3
(k)	23	4.5	1963	-2.69	24.2
(l)	28	4.5	2426	-2.69	24.7

**Table C3** Injection parameter of Mode 3 (2500 rpm, 84 Nm) variations

	Pilot SOI (BTDC)	Pilot Quantity (mm <sup>3</sup> /stroke)	Dwell Time (us)	Main SOI (BTDC)	Total Quantity (mm <sup>3</sup> /stroke)
(a)	16	1.5	922	-2.06	23.7
(b)	21	1.5	1256	-2.06	23.6
(c)	26	1.5	1589	-2.06	23.7
(d)	31	1.5	1922	-2.06	23.7
(e)	16	3	897	-2.06	24
(f)	21	3	1230	-2.06	24
(g)	26	3	1563	-2.06	24
(h)	31	3	1896	-2.06	24
(i)	16	4.5	867	-2.06	23.2
(j)	21	4.5	1200	-2.06	24.5
(k)	26	4.5	1533	-2.06	25
(l)	31	4.5	1866	-2.06	25

## **LIST OF REFERENCES**

- Abdul-Khalek, I. S., Kittelson, D. B., Graskow, B. R., et al. (1998). "Diesel exhaust particle size: measurement issues and trends". SAE 980525
- ACEA (2008). "ACEA Statement on biofuels"
- Akagawa, H., Miyamoto, T., Harada, A., et al. (1999). "Approaches to Solve Problems of the Premixed Lean Diesel Combustion". SAE 1999-01-0183
- Alano, E., Amon, B. and Jean, E. (2010). "Fuel Vaporizer: Alternative Solution for DPF Regeneration". SAE 2010-01-0561
- Alternative Fuels & Advanced Vehicle Data Center. (2009). "Gas to Liquids Benefits."
- Alternative Fuels & Advanced Vehicle Data Center. (2010). "B20 and B100: Alternative Fuels." from [http://www.afdc.energy.gov/afdc/fuels/biodiesel\\_alternative.html](http://www.afdc.energy.gov/afdc/fuels/biodiesel_alternative.html).
- Alternative Fuels & Advanced Vehicle Data Center. (2010). "Biodiesel Production." from [http://www.afdc.energy.gov/afdc/fuels/biodiesel\\_production.html](http://www.afdc.energy.gov/afdc/fuels/biodiesel_production.html).
- Appel, J., Bockhorn, H. and Rrenklech, M. (2000). "Kinetic modeling of soot formation with detailed chemistry and physics : Laminar premixed flames of C<sub>2</sub> hydrocarbons." Combustion and flame 121.
- Armas, O., Ballesteros, R. and Gomez, A. (2008). "The Effect of Diesel Engine Operating Conditions on Exhaust Particle Size Distributions." Journal Automobile Engineering. Vol 222, NO. D8.

- Arr\afgle, J., Tormos, B., L\aopez, J. J., et al. (2009). "Analysis of the Potential of Biodiesel as an Alternative Fuel for Current and Future HSDI Engines". SAE 2009-01-0480
- Badami, M., Millo, F. and D'Amato, D. D. (2001). "Experimental investigation on soot and NOx formation in a DI common-rail diesel engine with pilot injection". SAE 2001-01-0657
- Bandy, W. J. and Graboski, M. S. (1993). "Reliable catalytic particulate trap regeneration by exhaust hydrocarbon enrichment". SAE 932661
- Battigelli, M. C. (1971). "Biological significance of nitrogen oxides". SAE 710298
- Bouchez, M. and Dementhon, J. B. (2000). "Strategies for the Control of Particulate Trap Regeneration." SAE 2000-01-0472.
- Burtscher, H. and Matter, U. (2000). "Particle Formation Due to Fuel Additives". SAE 2000-01-1883
- C. Arden Pope III, R. T. B., Michael J. Thun, et al. (2002). "Lung Cancer, Cardiopulmonary Mortality, and Long-term Exposure to Fine Particulate Air Pollution." JAMA 287(9).
- Carlucci, P., Ficarella, A. and Laforgia, D. (2003). "Effects of pilot injection parameters on combustion for common-rail diesel engines". SAE 2003-01-0700
- Carlucci, P., Ficarella, A. and Laforgia, D. (2004). "Effects on combustion and emissions of early and pilot fuel injections in diesel engines." International Journal of Research. Vol 6, NO. 1.

Costa, H. D., Shannon, C. and Silver, R. (2007). "Thermal and Chemical Aging of Diesel Particulate Filters". SAE 2007-01-1266

Denso Australia. (2010). "Diesel Fuel Injection." from <http://www.denso.com.au/Products/Aftermarket-Automotive-Components/Diesel-Fuel-Injection>.

Dexcel. (2008). "GTL process using Fischer-Tropsch process." from [http://en.wikipedia.org/wiki/File:GTL\\_process.GIF](http://en.wikipedia.org/wiki/File:GTL_process.GIF).

Dillon, H., Maupin, G., Carlson, S., et al. (2007). "Visualization Techniques for Single Channel DPF Systems". SAE 2007-01-1126

Dürnholz, M., Eifler, G. and Endres, H. (1992). "Exhaust-gas recirculation~A measure to reduce exhaust emissions of DI diesel engines". SAE 920725

Eastwood, P. (2000). Critical topics in exhaust gas aftertreatment. Research Studies Press Ltd. ISBN 0-86380-242-7

Eastwood, P. (2008). Particulate Emissions from Vehicles. John Wiley & Sons Ltd. ISBN 978-0-7680-2060-1

European Biodiesel Board. (2010). "the EU Biodiesel Industry." from <http://www.ebb-eu.org/stats.php#>.

FIE Manufacturers (2007). "Fatty Acid Methyl Ester Fuels as a Replacement or Extender for Diesel Fuels". Diesel Fuel Injection Equipment Manufacturers Common Position Statement

Flörchinger, P., Zink, U., Cutler, W., et al. (2004). "DPF Regeneration-Concept to Avoid Uncontrolled Regeneration During Idle". SAE 2004-01-2657

Gerpen, J. V., Shanks, B., Pruszko, R., et al. (2004). "Biodiesel Production Technology". National Renewable Energy Laboratory

Grigg, H. C. (1976). "The role of fuel injection equipment in reducing 4-stroke diesel engine emissions". SAE 760126

Gulijk, C. V., Marijnissen, J. C. M., Makkee, M., et al. (2003). "The Choice of Instrument (ELPI and/or SMPS) for Diesel Soot Particulate Measurements". SAE 2003-01-0784

Haagen-Smit, A. J. (1952). "Chemistry and Physiology of Los Angeles Smog." Industrial and Engineering Chemistry. Vol 44 (6) . pp 1342–1346.

Hall, D. E., Goodfellow, C. L., Heinze, P., et al. (1998). "A study of the size, number and mass distribution of the automotive particulate emissions for European light-duty vehicles". SAE 982600

Han, S. B., Hinze, P. C., Kwon, Y. J., et al. (1997). "Experimental investigation of smoke emission dependent upon engine operating conditions". SAE 971658

Hanischa, S., Jandera, H., Papea, T., et al. (1994). "Soot mass growth and coagulation of soot particles in C<sub>2</sub>H<sub>4</sub>/air-flames at 15 bar " Symposium (International) on Combustion 25(1).

Haralampous, O. A., Koltsakis, G. C., Samaras, Z. C., et al. (2004). "Reaction and Diffusion Phenomena in Catalyzed Diesel Particulate Filters". SAE 2004-01-0696

Heywood, J. B. (1988). Internal combustion engine fundamentals. ISBN0-07-100499-8

Johnson, T. V. (2006). "Diesel Emission Control in Review". SAE 2006-01-0030

Johnson, T. V. (2007). "Diesel Emission Control in Review". SAE 2007-01-0233

Johnson, T. V. (2008). "Diesel Emission Control in Review". SAE 2008-01-0069

Johnson, T. V. (2009). "Diesel Emission Control in Review". SAE 2009-01-0121

Johnson, T. V. (2010). "Review of Diesel Emissions and Control". SAE 2010-01-0301

Juttu, S., Thipse, S. S., Marathe, N. V., et al. (2007). "Homogeneous Charge Compression Ignition (HCCI): A New Concept for Near Zero NOx and Particulate Matter (PM) from Diesel Engine Combustion". SAE 2007-26-020

Kagawa, J. (2002). "Health effects of diesel exhaust emissions--a mixture of air pollutants of worldwide concern." Toxicology 181-182: 349-353.

Kaneko, Y., Kobayashi, H. and Komagome, R. (1975). "The effects of exhaust gas recirculation and residual gas on engine emissions and fuel economy". SAE 750414

Kasper, M. (2004). "The number concentration of non-volatile particles~Design study for an instrument according to the PMP recommendations". SAE 2004-01-0960

Kawamoto, K., Araki, T., Shinzawa, M., et al. (2004). "Combination of Combustion Concept and Fuel Property for Ultra-Clean DI Diesel". SAE 2004-01-1868

Kawano, D., Ishii, H. and Goto, Y. (2008). "Effect of Biodiesel Blending on Emission Characteristics of Modern Diesel Engine". SAE 2008-01-2384

Kawano, D., Suzuki, H., Ishii, H., et al. (2005). "Ignition and Combustion Control of Diesel HCCI". SAE 2005-01-2132

Kitano, K., Misawa, S., Mori, M., et al. (2007). "GTL Fuel Impact on DI Diesel Emissions." JSAE 20077188.

Kittelson, D. B. (1997). "Engines and Nanoparticles: A Review." Journal of Aerosol Science 29 (5/6): 575-588.

Klein, H., Lox, E., Kreuzer, T., et al. (1998). "Diesel particulate emissions of passenger cars - New insights into structural changes during the process of exhaust aftertreatment using diesel oxidation catalysts". SAE 980196

Koltsakis, G. C., Katsaounis, D. K., Markomanolakis, I. A., et al. (2007). "Metal Foam Substrate for DOC and DPF Applications". SAE 2007-01-0659

Koltsakis, G. C., Katsaounis, D. K., Markomanolakis, I. A., et al. (2006). "Design and Application of Catalyzed Metal Foam Particulate Filters". SAE 2006-01-3284

Koltsakis, G. C., Katsaounis, D. K., Samaras, Z. C., et al. (2006). "Filtration and Regeneration Performance of a Catalyzed Metal Foam Particulate Filter". SAE 2006-01-1524

Koltsakis, G. C., Katsaounis, D. K., Samaras, Z. C., et al. (2008). "Development of Metal-Foam-Based Aftertreatment System on a Diesel Passenger Car". SAE 2008-01-0619

Kong, Y., Kozakiewicz, T., Johnson, R., et al. (2005). "Active DPF Regeneration for 2007 Diesel Engines". SAE 2005-01-3509

Konstandopoulos, A. G., Kostoglou, M., Skaperdas, E., et al. (2000). "Fundamental Studies of Diesel Particulate Filters: Transient Loading, Regeneration and Aging". SAE 2000-01-1016

Konstandopoulos, A. G., Skaperdas, E. and Masoudi, M. (2001). "Inertial Contributions to the Pressure Drop of Diesel Particulate Filters". SAE 2001-01-0909

Kousoulidou, M., Fontaras, G., Ntziachristos, L., et al. (2009). "Evaluation of Biodiesel Blends on the Performance and Emissions of a Common-Rail Light-Duty Engine and Vehicle". SAE 2009-01-0692

Kumar, P. and Mohan, D. (2002). "Photochemical smog: mechanism, ill-effects, and control." Energy and Environment 1(3): 445-456.

Lee, K. O., Zhu, J., Ciatti, S., et al. (2003). "Sizes, graphitic structures and fractal geometry of light-duty diesel engine particulates". SAE 2003-01-3169

Levine, M. D. and GreshamIII, C. (2009). "Toxicity, Hydrocarbons". Emergency Medicine.

Li, X. and Wallace, J. S. (1995). "A phenomenological model for soot formation and oxidation in direct-injection diesel engines". SAE952428

Liu, Y. and Reitz, R. D. (2005). "Optimizing HSDI Diesel Combustion and Emissions Using Multiple Injection Strategies". SAE 2005-01-0212

MacMillan, D., Rocca, A. L. and Shayler, P. J. (2009). "Investigating the Effects of Multiple Pilot Injections on Stability at Cold Idle for a DI Diesel Engine". SAE 2009-01-0612

- Masahide, T. and Yoshio, T. (2004). "Study of Internal EGR Control Using Variable Valve Timing." Journal of the Japan Institution of Marine Engineering 39 (10).
- Mayer, A., Czerwinski, J., Wyser, M., et al. (2005). "Impact of RME/Diesel Blends on Particle Formation, Particle Filtration and PAH Emissions". SAE 2005-01-1728
- Mohammadi, A., Kee, S.-S., Ishiyama, T., et al. (2005). "Implementation of Ethanol Diesel Blend Fuels in PCCI Combustion". SAE 2005-01-3712
- Montajir, R. M., Kawai, T., Goto, Y., et al. (2005). "Thermal Conditioning of Exhaust Gas: Potential for Stabilizing Diesel Nano-Particles". SAE 2005-01-0187
- Montajir, R. M., Kusaka, T., Kaori, I., et al. (2007). "Soot Emission Behavior From Diverse Vehicles and Catalytic Technologies Measured by a Solid Particle Counting System". SAE 2007-01-0317
- Nagata, K., Tanaka, Y. and Yano, K. (2004). "Technologies of DENSO Common Rail for Diesel Engine and Consumer Values". SAE 2004-21-0075
- Najt, P. M. and Foster, D. E. (1983). "Compression-ignited homogeneous charge combustion". SAE 830264
- Nakajima, Y., Sugihara, K., Takagi, Y., et al. (1981). "Effects of exhaust gas recirculation on fuel consumption". SAE 814881
- Natti, K. C., Henein, N. A., Poonawala, Y., et al. (2008). "Particulate Matter Characterization Studies in an HSDI Diesel Engine Under Conventional and LTC Regime". SAE 2008-01-1086

- Neely, G. D., Sasaki, S. and Leet, J. A. (2004). "Experimental Investigation of PCCI-DI Combustion on Emissions in a Light-Duty Diesel Engine". SAE 2004-01-0121
- Nwafor, O. M. I. (2004). "Emission characteristics of diesel engine operating on rapeseed methyl ester." Renewable Energy. Vol 29 (2004), pp 119-129.
- Oetting, H. and Papez, S. (1979). "Reducing Diesel knock by means of exhaust gas recirculation". SAE 790268
- Oguma, M., Goto, S. and Chen, Z. (2004). "Fuel Characteristics Evaluation of GTL for DI Diesel Engine". SAE 2004-01-0088
- Ohara, E., Mizuno, Y., Miyairi, Y., et al. (2007). "Filtration Behavior of Diesel Particulate Filters (1)". SAE 2007-01-0921
- Ojeda, W. d., Zoldak, P., Espinosa, R., et al. (2008). "Development of a Fuel Injection Strategy for Diesel LTC". SAE 2008-01-0057
- Okude, K., Mori, K., Shiino, S., et al. (2004). "Premixed Compression Ignition (PCI) Combustion for Simultaneous Reduction of NOx and Soot in Diesel Engine". SAE 2004-01-1907
- Okude, K., Mori, K., Shiino, S., et al. (2007). "Effects of Multiple Injections on Diesel Emission and Combustion Characteristics". SAE 2007-01-4178
- Peckham, J. (2002). "GTL diesel companies urge U.S. Dept. of Energy to grant 'alternative fuel' status under 'EPAct'." from [http://findarticles.com/p/articles/mi\\_m0CYH/is\\_21\\_6/ai\\_94122823/?tag=content;col1](http://findarticles.com/p/articles/mi_m0CYH/is_21_6/ai_94122823/?tag=content;col1).

- Peterson, J. S., Miller, S. M. and Cairns, C. B. (2008). "Toxicity, Nitrous Dioxide". Emergency Medicine. <http://emedicine.medscape.com/article/820431-overview>.
- Roy, M. M. and Tsunemoto, H. (2002). "Effect of Injection Pressure and Split Injection on Exhaust Odor and Engine Noise in DI Diesel Engines". SAE 2002-01-2874
- Rubino, L., Phillips, P. R. and Twigg, M. V. (2005). "Measurements of Ultrafine Particle Number Emissions from a Light-Duty Diesel Engine Using SMPS, DMS, ELPI and EEPS". SAE 2005-24-015
- Sako, T., Furuhata, T. and Arai, M. (2007). "Nano-size PM Emission from Laminar Diffusion Flame of Diesel Fuel." JSAE 20077196.
- Santoro, R. J. (1987). "Soot Particle Formation in Diffusion Flames." Fuel Chemistry American Chemical Society 1987 Fall (NEW ORLEANS) 32(3).
- Santoro, R. J. and Miller, J. H. (1987). "Soot Particle Formation in Laminar Diffusion Flamed." Langmuir 3: 244-254.
- Schaberg, P., Botha, J., Schnell, M., et al. (2005). "Emissions Performance of GTL Diesel Fuel and Blends With Optimized Engine Calibrations". SAE 2005-01-2187
- Schuermann, D., Lies, K. H. and Klingenberg, H. (1990). "Unregulated motor vehicle exhaust gas components". SAE 902116
- Seiler, V., Boeckmann, E. and Eilts, P. (2008). "Performance of Undamaged and Damaged Diesel Particulate Filters". SAE 2008-01-0335
- Shochat, G. N. and Lucchesi, M. (2010). "Toxicity, Carbon Monoxide". Emergency Medicine.

- Stone, R. (1999). Introduction to Internal Combustion Engines. SAE International and Macmillan Press. ISBN: 978-0-7680-0495-3
- Stringer, V. L., Cheng, W. L., Lee, C.-f. F., et al. (2008). "Combustion and Emissions of Biodiesel and Diesel Fuels in Direct Injection Compression Ignition Engines Using Multiple Injection Strategies". SAE 2008-01-1388
- Sunderland, P. B. and Faeth, G. M. (1996). "Soot Formation in Hydrocarbon/Air Laminar Jet Diffusion Flames." Combustion and Flame. Vol 105, Issue 1-2, pp 132-146.
- Tan, P.-g., Hu, Z.-y., Lou, D.-m., et al. (2009). "Particle Number and Size Distribution from a Diesel Engine with Jatropha Biodiesel Fuel". SAE 2009-01-2726
- Tanaka, S. and Shimizu, T. (1999). "A study of composition and size distribution of particulate matter from DI diesel engine". SAE 1999-01-3487
- Tanaka, T., Ando, A. and Ishizaka, K. (2002). "Study on pilot injection of DI diesel engine using common-rail injection system." JSAE 20024248.
- Tao, F., Golovitchev, V. I. and Chomiak, J. (2004). "A phenomenological model for the prediction of soot formation in diesel spray combustion " Combustion and Flame. Vol 136, Issue 3, pp 270-282.
- Turner, J., Topaloglu, T. and Rideout, G. (1995). "A demonstration of transit bus particulate traps in Ottawa Ontario". SAE 952651
- Uchida, N., Daisho, Y., Saito, T., et al. (1993). "Combined effects of EGR and supercharging on diesel combustion and emissions". SAE 930601

US Energy Information Administration. (2009). "Biodiesel Supply and Consumption." from  
[http://www.eia.doe.gov/emeu/steo/pub/special/2009\\_sp\\_01.pdf](http://www.eia.doe.gov/emeu/steo/pub/special/2009_sp_01.pdf).

US Energy Information Administration. (2010). "US Fuel Supply Statistics Chart." from  
[http://www.eia.doe.gov/dnav/pet/pet\\_cons\\_psup\\_dc\\_nus\\_mbbl\\_m.htm](http://www.eia.doe.gov/dnav/pet/pet_cons_psup_dc_nus_mbbl_m.htm).

US Public Law 102-486 (1992). Energy Policy Act of 1992 (EPAct), the U.S. Environmental Protection Agency (EPA).

Vanegas, A., Won, H., Felsch, C., et al. (2008). "Experimental Investigation of the Effect of Multiple Injections on Pollutant Formation in a Common-Rail DI Diesel Engine". SAE 2008-01-1191

Vincent, M. W., Richards, P. J., Dementhon, J.-B., et al. (1999). "Improved Diesel Particulate Filter Regeneration Performance Using Fuel Soluble Additives". SAE 1999-01-3562

Weall, A. and Collings, N. (2007). "Highly Homogeneous Compression Ignition in a Direct Injection Diesel Engine Fuelled With Diesel and Biodiesel". SAE 2007-01-2020

Weiskirch, C. and Müller, E. (2007). "Advances in Diesel Engine Combustion: Split Combustion". SAE 2007-01-0178

Wilson, R. (1996). In Particles in Our Air- Concentrations and Health Effects. Harvard University Press. ISBN 0674240774

World Resources Institute, the United Nations Environment Programme and Nations, U. (1998). "Urban Air: Health Effects of Particulates, Sulphur Dioxide and Ozone". World Resources Institute

Yoon, C. S., Song, S. H. and Chun, K. M. (2007). "Measurement of Soot Mass and Pressure Drop Using a Single Channel DPF to Determine Soot Permeability and Density in the Wall Flow Filter". SAE 2007-01-0311

Yoro, K., Itsuaki, S., Saito, H., et al. (1998). "Diesel particulate filter made of porous metal". SAE 980187

Yoshida, K., Taniguchi, S., Kitano, K., et al. (2008). "Effects of RME30 on Exhaust Emissions and Combustion in a Diesel Engine". SAE 2008-01-2499

Zhan, R., Huang, Y. and Khair, M. (2006). "Methodologies to Control DPF Uncontrolled Regenerations". SAE 2006-01-1090

Zhang, L. (1999). "A study of pilot injection in a DI diesel engine". SAE 1999-01-3493

Zhang, X., Wang, H., Li, L., et al. (2008). "Characteristics of Particulates and Exhaust Gases Emissions of DI Diesel Engine Employing Common Rail Fuel System Fueled with Bio-diesel Blends". SAE 2008-01-1834

Zheng, M., Han, X., Tan, Y., et al. (2008). "Low Temperature Combustion of Neat Biodiesel Fuel on a Common-rail Diesel Engine". SAE 2008-01-1396

Zinola, S. and Lavy, J. (2009). "Detailed Particulate Characterization from HCCI Combustion for Future DPF Development". SAE 2009-01-1185